NATIONAL TECNHICAL UNIVERSITY OF ATHENS
SCHOOL OF APPLIED MATHEMATICS AND PHYSICAL SCIENCES

STUDY AND DISPERSION OF RADIONUCLIDES AND HEAVY METALS IN COASTAL AREAS OF GREECE, CHARACTERIZED BY ACTIVE AND PAST MINING ACTIVITIES

PhD THESIS

FILOTHEI PAPPA

Graduate of School of Applied Mathematics and Physical Sciences

Master graduate of Interdepartmental Postgraduate Studies Program "Physics and Technology Applications"

Research supervisor:

C. Tsabaris
Research Director of HCMR

Academic supervisor:

R. Vlastou,
Professor of NTUA

Athens, December 2018

NATIONAL TECNHICAL UNIVERSITY OF ATHENS
SCHOOL OF APPLIED MATHEMATICS AND PHYSICAL SCIENCES

STUDY AND DISPERSION OF RADIONUCLIDES AND HEAVY METALS IN COASTAL AREAS OF GREECE, CHARACTERIZED BY ACTIVE AND PAST MINING ACTIVITIES

PhD THESIS

FILOTHEI PAPPA

Graduate of School of Applied Mathematics and Physical Sciences

Master graduate of Interdepartmental Postgraduate Studies Program "Physics and Technology Applications"

Supervising committee:

C. Tsabaris (Research Director of HCMR)
R. Vlastou (Professor of NTUA)
M. Kokkoris (Associate Professor of NTUA)

Examination committee

A. Iurian (IAEA Officer)
A. Ioannidou (Associate Professor of AUTH)
H. Kaberi (Associate Researcher of HCMR)
T. Mertzimekis (Associate Professor of UoA)
M. Anagnostakis (Associate Professor of NTUA)

Athens, December 2018

ΕΘΝΙΚΟ ΜΕΤΣΟΒΙΟ ΠΟΛΥΤΕΧΝΕΙΟ
ΣΧΟΛΗ ΕΦΑΡΜΟΣΜΕΝΩΝ ΜΑΘΗΜΑΤΙΚΩΝ ΚΑΙ ΦΥΣΙΚΩΝ ΕΠΙΣΤΗΜΩΝ

ΜΕΛΕΤΗ ΚΑΙ ΔΙΑΣΠΟΡΑ ΡΑΔΙΟΝΟΥΚΛΙΔΙΩΝ ΚΑΙ ΒΑΡΕΩΝ ΜΕΤΑΛΛΩΝ ΣΕ ΠΑΡΑΚΤΙΕΣ ΠΕΡΙΟΧΕΣ ΤΗΣ ΕΛΛΑΔΟΣ, ΧΑΡΑΚΤΗΡΙΖΟΜΕΝΕΣ ΜΕ ΕΝΕΡΓΕΣ ΚΑΙ ΟΛΟΚΛΗΡΩΜΕΝΕΣ ΜΕΤΑΛΛΕΥΤΙΚΕΣ ΔΡΑΣΤΗΡΙΟΤΗΤΕΣ

ΔΙΔΑΚΤΟΡΙΚΗ ΔΙΑΤΡΙΒΗ

ΦΙΛΟΘΕΗ ΠΑΠΠΑ

Διπλωματούχος της Σχολής Εφαρμοσμένων Μαθηματικών και Φυσικών Επιστημών ΕΜΠ

Μεταπτυχιακό Δίπλωμα Ειδίκευσης «Φυσική και Τεχνολογικές Εφαρμογές» ΕΜΠ

Ερευνητικός επιβλέπων:

Χ. Τσαμπάρης
Ερευνητής Α' του ΕΛΚΕΘΕ

Ακαδημαϊκός υπεύθυνος:

Ρ. Βλαστού,
Καθηγήτρια του ΕΜΠ

Αθήνα, Δεκέμβριος 2018

To my family,

Kosmas, Vasiliki, Alexandros, Aglaia and Monica

…ὅτε ἤμην νήπιος, ἐλάλουν ὡς νήπιος, ἐφρόνουν ὡς νήπιος, ἐλογιζόμην ὡς νήπιος· ὅτε γέγονα ἀνήρ, κατήργηκα τὰ τοῦ νηπίου. βλέπομεν γὰρ ἄρτι δι᾽ ἐσόπτρου ἐν αἰνίγματι, τότε δὲ πρόσωπον πρὸς πρόσωπον· ἄρτι γινώσκω ἐκ μέρους, τότε δὲ ἐπιγνώσομαι καθὼς καὶ ἐπεγνώσθην. νυνὶ δὲ μένει πίστις, ἐλπίς, ἀγάπη, τὰ τρία ταῦτα· μείζων δὲ τούτων ἡ ἀγάπη.

Απόστολος Παύλος, Α᾽ προς Κορινθίους (Κεφ. 13)

Acknowledgments

This work was accomplished through an effort by the author, as well as the support of many people. First of all, I would like to express my gratitude to my Advisory Committee, Dr. Christos Tsabaris, Research Director at HCMR, Prof. Roza Vlastou, Professor at NTUA and Prof. Michael Kokkoris, Associate Professor at NTUA, for their guidance throughout the years.

I would like also to acknowledge Dr. Costas Kalfas for providing the gamma-ray analysis software and for the fruitful discussions regarding gamma-ray spectrometry. Additionally, I would like to thank the Handicraft and Industrial Education Museum of Lavrio and Mr. Costas Papathanasiou for the productive discussions concerning the interpretation of historical reconstruction of metal and metal flux profiles. Especially, I would like to express my sincere gratitude to Dr. Dionisis Patiris for his assistance and guidance in the experimental or theoretical aspects of this work, as well as for his warm encouragement during the doctoral dissertation. He was an invaluable co-supervisor and great advisor confronting all the arising obstacles. I would like to thank Dr. Georgios Eleftheriou, Dr. Effrosini Androulakaki and Stelios Alexakis for their consulting and support in the experimental and technical work.

I would like to thank the director Dr. Hildegarde Vandenhove and the researchers Dr. Talal Almahayni and Jordi Vives i Batlle of the Institute for Environment, Health and Safety of Belgian Nuclear Research Centre (SCK-CEN) for providing me the opportunity to perform radiological measurements at their laboratory, to study advection-convection models and train at ERICA Assessment Tool. I feel obliged to thank many member of HCMR such as Dr. Aris Karageorgis, and Dr. Eleni Kaberi, as well as Dr. Aristidis Prospathopoulos and Mr. Constantinos Sarantakos for their advices regarding the X-ray analysis and enrichment factor, as well as their ideas concerning the presentation of this work and the classification of metal enrichment, respectively. Additionally, the members of Nuclear Physics of NTUA improved the presentation work through their questions and ideas during the oral presentations of our group meetings.

A great source of support all these years were my friends Georgia Dapei, Konstantinos Preketes Sigalas, Athanasios Stamatopoulos, Dionisia Aravopoulou and Georgia Binou. Thus, I really thank them from the bottom of my heart.

I would like to thank the people who helped us in Stratoni during the sampling, especially Prof. Alexandra Ioannidou for her manual work and support in the whole sampling of the terrestrial region. Additionally, I would like to thank Mr. Alecos Dimitriades for providing technical reports from IGME regarding Lavrio. This work was partially supported financially by A.G. Leventis Foundation and the author acknowledge this assistance.

In the end, the individuals I would like to express my gratitude and respect are the members of my family, as they encouraged me, supported me and inspired me to be patient and persistent.

Table of Contents

Εκτεταμένη Ελληνική Περίληψη

Στην ενότητα αυτή θα παρουσιαστεί συνοπτικά η διδακτορική διατριβή, δίνοντας έμφαση στα αποτελέσματα και στα συμπεράσματα. Στην αρχή θα περιγραφεί το πρόβλημα που κλήθηκε να επιλύσει/προσεγγίσει η εργασία αυτή και εν συνεχεία το θεωρητικό υπόβαθρο και η μεθοδολογία βάσει των οποίων προσεγγίστηκε το πρόβλημα, καθώς και τα αποτελέσματα της μελέτης.

1. Εισαγωγή

Τα μέταλλα και τα φυσικά ραδιονουκλίδια, γνωστά ως NORM, είναι άφθονα στο περιβάλλον και οι συγκεντρώσεις τους εξαρτώνται από τη γεωλογία της περιοχής. Οι συγκεντρώσεις αυτές μπορούν να μεταβληθούν λόγω βιομηχανικών δραστηριοτήτων, όπως η εξόρυξη, η οποία επηρεάζει το περιβάλλον όχι μόνο τοπικά (έδαφος) αλλά και εκτεταμένα (υδάτινο οικοσύστημα). Για τον λόγο αυτό η βιβλιογραφία είναι πλούσια σε μελέτες που αφορούν στην επίδραση των μετάλλων λόγω της εκμετάλλευσης των ορυχείων. Από την άλλη πλευρά, η μελέτη της φυσικής ραδιενέργειας στα ορυχεία είναι σπανιότερη και εστιασμένη κυρίως σε ορυχεία άνθρακα, φωσφόρου, ουρανίου, πετρελαίου και χρυσού. Μία δεύτερη σημαντική έλλειψη που παρατηρείται στη διεθνή βιβλιογραφία, πέρα από την απουσία μελέτης της φυσικής ραδιενέργειας σε κάθε τύπο ορυχείου, είναι η απουσία μελέτης της επιβάρυνσης των εξορυκτικών διαδικασιών στο θαλάσσιο περιβάλλον.

Τα τελευταία χρόνια πραγματοποιείται μία πιο ολοκληρωμένη μελέτη σε διάφορους τύπους ορυχείων όπου συνδυάζεται η φυσική ραδιενέργεια και τα μέταλλα κυρίως στο έδαφος και σε ιζήματα. Η επιλογή των μητρών αυτών – εδάφους και ιζημάτων - δεν είναι τυχαία, αλλά βασίζεται στη φυσική τάση που εμφανίζουν τόσο τα μέταλλα όσο και τα ραδιονουκλίδια και προσροφώνται στις μήτρες αυτές. Ως εκ τούτου, τα ιζήματα μπορούν να χρησιμοποιηθούν για χωρικές και χρονολογικές μελέτες στις περιοχές ενδιαφέροντος. Οι χρονολογικές μελέτες βασίζονται στην χρήση χαρακτηριστικών ραδιονουκλιδίων (^{210}Pb, ^{137}Cs) προκειμένου να αντιστοιχηθεί το βάθος του ιζήματος στον πυρήνα με κάποια χρονική περίοδο. Με τον τρόπο αυτόν οι πυρήνες ιζήματος έχουν χρησιμοποιηθεί επιτυχώς για τον υπολογισμό του ρυθμού ιζηματογένεσης, την εκτίμηση της μόλυνσης και την ανοικοδόμηση ιστορικών γεγονότων επιβάρυνσης λόγω της μακροχρόνιας επίδρασης των ανθρωπίνων εργασιών.

Επιπροσθέτως, η χωρική και η χρονολογική μελέτη των περιοχών που χαρακτηρίζονται από εξορυκτικές διαδικασίες καθίσταται επιτακτική ειδικά σε περιπτώσεις παύσης λειτουργίας των διαδικασιών αυτών. Μετά τη ολοκλήρωση των εξορυκτικών διεργασιών οι τεράστιες εναπομείνασες ποσότητες των απορριμμάτων και των επηρεασμένων εδαφών (συμπεριλαμβανομένων και των ιζημάτων), καθώς και η μη σωστή διαχείριση αυτών οδηγούν στην ύπαρξη πηγών μόλυνσης και/ή επίδρασης του περιβάλλοντος για χρονικά διαστήματα που φτάνουν και τις χιλιετίες. Συμπληρωματικά αξίζει να σημειωθεί ότι τα ορυχεία εδράζονται κοντά σε δυνητικά ευαίσθητες περιοχές όπως ποτάμια, λίμνες και παράκτιες ζώνες, μιας και το υγρό στοιχείο είναι αναγκαίο σε διεργασίες όπως ο διαχωρισμός του μεταλλεύματος.

Οι περιοχές ενδιαφέροντος της παρούσας διδακτορικής διατριβής αφορούν στις παράκτιες ζώνες δύο κύριων εξορυκτικών περιοχών της Ελλάδος, το Στρατώνι και το

Λαύριο. Και οι δύο περιοχές είναι γνωστές για τις εξορυκτικές τους δραστηριότητες από αρχαιοτάτων χρόνων και την εκμετάλλευση των ορυκτών PBG (σιδηροπυρίτη, σφαλερίτη και γαληνίτη). Οι διεργασίες εξόρυξης στην πρώτη περιοχή συνεχίζονται ακόμα και σήμερα, ενώ στη δεύτερη έχουν παύσει εδώ και 30 χρόνια περίπου (αρχές της δεκαετίας του 1980). Και στις δύο περιπτώσεις υπήρχε σωλήνας διοχέτευσης των απορριμμάτων επίπλευσης στο θαλάσσιο περιβάλλον καθώς και εναπόθεση των στερεών απορριμμάτων της εξορυκτικής διεργασίας σε διάφορα σημεία της χερσαίας περιοχής και κατά μήκος των γειτνιαζόντων ποταμών (Stamatis et al. 2001; Kelepertsis et al. 2006; Alexakis 2011; Charalampides et al. 2013). Επιπλέον, ο Κόλπος της Ιερισσού, όπου βρίσκεται το Στρατώνι, όπως και το Λαύριο είναι γνωστά για δραστηριότητες όπως το ψάρεμα και ο τουρισμός, ενώ οι κατοικήσιμες περιοχές εδράζονται κοντά στις εξορυκτικές εγκαταστάσεις ή στα μεταλλευτικά απορρίμματα. Είναι χαρακτηριστική η περίπτωση της περιοχής του Λαυρίου, όπου ολόκληρη η πόλη έχει χτισθεί και αναπτυχθεί επάνω σε «βουνά» απορριμμάτων της εξορυκτικής διαδικασίας.

Με βάση τη βιβλιογραφία η μελέτη των δύο εξορυκτικών περιοχών έχει πραγματοποιηθεί κατά κύριο λόγο στο χερσαίο κομμάτι του περιβάλλοντος (έδαφος και ποτάμια), ενώ ελάχιστη πληροφορία είναι γνωστή για το παράκτιο και θαλάσσιο τμήμα. Η περιοχή του Λαυρίου έχει μελετηθεί σε βάθος μετά την εγκατάλειψη των εξορυκτικών διαδικασιών, ενώ η περιοχή του Στρατωνίου έχει μελετηθεί περιστασιακά και σποραδικά. Τόσο στην περίπτωση των ελληνικών ορυχείων όσο και των υπολοίπων παγκοσμίως, η μελέτη της επιβάρυνσης που αυτά προκαλούν αφορά κυρίως στα μέταλλα και δεν λαμβάνει υπόψιν τα φυσικά ραδιονουκλίδια τα οποία εμπεριέχονται στις ποσότητες των μεταλλευτικών απορριμμάτων, όπως αναφέρθηκε παραπάνω. Εν κατακλείδι, κίνητρο της διδακτορικής διατριβής ήταν να αναπτυχθεί μία μεθοδολογία για τη μελέτη παράκτιων περιοχών (ή θαλασσίου περιβάλλοντος γενικότερα) όσον αφορά σε συγκεντρώσεις μετάλλων και φυσικών ραδιονουκλιδίων. Αντικειμενικοί στόχοι της εργασίας ήταν τόσο η χωρική όσο και η χρονολογική μελέτη περιοχών που γειτνιάζουν με ορυχεία, οι οποίοι κινούνταν σε τρεις άξονες: (α) τον υπολογισμό της διασποράς των φυσικών ραδιονουκλιδίων στο θαλάσσιο περιβάλλον, (β) την ιστορική ανοικοδόμηση της ανθρωπογενούς δραστηριότητας της περιοχής και (γ) την εκτίμηση της μεταλλικής και ραδιολογικής επιβάρυνσης στο θαλάσσιο (και παράκτιο) περιβάλλον.

2. Θεωρητικό υπόβαθρο

Οι συγκεντρώσεις των ραδιονουκλιδίων και των μετάλλων μετρήθηκαν μέσω φασματοσκοπίας γάμμα και φθορισιμετρίας ακτίνων Χ. Οι μεθοδολογίες αυτές βασίζονται στην αλληλεπίδραση των ακτίνων γάμμα και Χ με την ύλη και την ανίχνευση αυτών με το κατάλληλο ανιχνευτικό σύστημα. Η εκπομπή ακτίνων γάμμα είναι πυρηνικής φύσεως, συμβαίνει όταν ένας πυρήνας χάνει την πλεονάζουσα ενέργεια διέγερσης και συνήθως η ακτινοβολία γάμμα ακολουθεί τις διεργασίες της αποδιέγερσης άλφα και βήτα όπως στις περιπτώσεις των φυσικών ραδιενεργών σειρών. Κατά την εκπομπή ακτίνων γάμμα ο πυρήνας μεταπίπτει από μια διεγερμένη κατάσταση σε μια κατάσταση χαμηλότερης ενέργειας και η ενεργειακή διαφορά μεταξύ των δύο καταστάσεων απελευθερώνεται με τη μορφή φωτονίων. Η

ακτινοβολία γάμμα ανιχνεύεται λόγω της αλληλεπίδρασής της με την ύλη μέσω του φωτοηλεκτρικού φαινομένου, του φαινομένου Compton και της δίδυμης γένεσης.

Η ακτινοβολία Χ είναι ατομικής φύσεως και οφείλεται στην αναδιάταξη των ατομικών ηλεκτρονίων που ακολουθούν φαινόμενα σύλληψης ηλεκτρονίων, εσωτερικής μετατροπής ή ατομικής διέγερσης με τεχνητό τρόπο όπως δέσμες φορτισμένων σωματιδίων υψηλής ενέργειας ή δέσμες ακτίνων Χ. Κατά τη διάρκεια τέτοιων φαινομένων κάποιο ηλεκτρόνιο αποκτά κινητική ενέργεια, αποδεσμεύεται από τη κατάσταση (στοιβάδα) ελάχιστης ενέργειας που βρίσκεται και αφήνει μία κενή θέση στην στοιβάδα. Στη συνέχεια, κάποιο ηλεκτρόνιο ανώτερης στάθμης θα κινηθεί σε καταστάσεις χαμηλότερης ενέργειας προκειμένου να καλύψει την κενή θέση εκπέμποντας έτσι ακτίνες Χ. Η ακτινοβολία Χ μπορεί να ανιχνευθεί μέσω της αλληλεπίδρασής της με την ύλη, με το φωτοηλεκτρικό φαινόμενο και το φαινόμενο Compton.

Προκειμένου να εκτιμηθεί το επίπεδο της μόλυνσης όσο αφορά στα μέταλλα έχουν διαμορφωθεί διάφοροι δείκτες όπως το φορτίο μόλυνσης (Pollution Load Index (PLI) και ο δείκτης εμπλουτισμού (Enrichment Factor (EF)), οι οποίοι επιλέχθηκαν και στην εργασία αυτή. Κάτι αντίστοιχο δεν υπάρχει όσο αφορά στα φυσικά ραδιονουκλίδια καθώς και στις τεχνητά επαυξημένες συγκεντρώσεις αυτών λόγω των ανθρωπογενών δραστηριοτήτων. Παρ' όλα ταύτα σε αυτή τη διδακτορική διατριβή επιλέχθηκαν ως προσεγγίσεις η σύγκριση με μία περιοχή που θεωρείται ανεπηρέαστη από τις ανθρώπινες δραστηριότητες, καθώς και η σύγκριση με τον παγκόσμιο μέσο όρο συγκεντρώσεων των φυσικών ραδιονουκλιδίων, προκειμένου να εκτιμηθεί ο εμπλουτισμός σε φυσικά ραδιονουκλίδια. Επίσης, χρησιμοποιήθηκε και το λογισμικό ERICA για τον υπολογισμό της ραδιενεργού δόσης σε έμβια - μη ανθρώπινα – όντα (βλ. πιο κάτω υποκεφάλαιο 3).

Ένα άλλο σημαντικό κομμάτι της εργασίας ήταν η χρονική αναδόμηση της ανθρώπινης επίδρασης στις περιοχές ενδιαφέροντος. Για τον λόγο αυτόν ήταν αναγκαία η χρονολόγηση των πυρήνων ιζήματος, εννοώντας την αντιστοίχηση του βάθους ιζήματος με κάποια χρονική περίοδο. Η χρονολόγηση μπορεί να πραγματοποιηθεί με τη χρήση ραδιονουκλιδίων που υπάρχουν στο περιβάλλον είτε φυσικών (π.χ. ^{210}Pb) είτε τεχνητών (^{137}Cs). Υπάρχουν διάφορα ραδιονουκλίδια που χρησιμοποιούνται σε εφαρμογές χρονολόγησης, οι διαφορετικοί χρόνοι ημιζωής τους όμως τα καθιστούν κατάλληλα για βραχυπρόθεσμες ή μακροπρόθεσμες χρονολογήσεις, οι οποίες μπορούν να κυμαίνονται από χρονικές περιόδους ημερών μέχρι και πολλών χρόνων. Μία άλλη προσέγγιση που υιοθετήθηκε στην παρούσα εργασία ήταν η χρήση της στατιστικής προκειμένου να αναδειχθούν τυχόν συσχετίσεις μεταξύ ραδιονουκλιδίων, μετάλλων και άλλων παραμέτρων όπως η κοκκομετρία.

3. Κώδικας ERICA

Ο κώδικας ERICA βασίστηκε στον κώδικα MCNP (MCNP4C) έτσι ώστε να περιλαμβάνει και να προσομοιώνει κάποιες βασικές ιδεατές γεωμετρίες έμβιων όντων και τις αλληλεπιδράσεις των ακτινοβολιών άλφα, βήτα και γάμμα μέσα ή γύρω από αυτά. Με τον κώδικα ERICA υπολογίζονται με συντηρητικό τρόπο οι ρυθμοί ραδιενεργού δόσης των έμβιων - μη ανθρώπινων – οργανισμών και να συγκρίνονται με κάποια όρια που έχουν υιοθετήσει διεθνείς οργανισμοί και αφορούν στη ραδιοπροστασία των έμβιων οργανισμών και του περιβάλλοντος γενικότερα (Brown

et al. 2008). Στον υπολογισμό των ρυθμών δόσεων λαμβάνονται υπόψιν μόνο οι ακτινοβολίες άλφα, βήτα και γάμμα, οι οποίες έχουν διαφορετικούς συντελεστές βαρύτητας στον υπολογισμό της δόσης, τα διάφορα στάδια ζωής ενός οργανισμού (π.χ. αυγό, ενήλικος οργανισμός), οι διάφορες μορφές ζωής (π.χ. ζώα, φυτά), το σχήμα του οργανισμού, η μάζα του οργανισμού και τα διάφορα είδη οικοσυστημάτων όπου ζουν οι οργανισμοί. Επίσης, στον υπολογισμό των ραδιενεργών δόσεων λαμβάνονται υπόψιν τόσο οι μητρικοί πυρήνες όσο και οι θυγατρικοί, στην περίπτωση που οι χρόνοι ημιζωής των δεύτερων είναι μικρότεροι των δέκα ημερών. Οι εξισώσεις που περιγράφουν τον εσωτερικό και εξωτερικό ρυθμό δόσης σε έναν οργανισμό είναι οι εξής:

$$D_{\text{int}} = \sum_{v}\left(\sum_{i} E_i Y_i \varphi_v(E_i) + \int N_v(E) E \varphi_v(E) dE \right) \qquad \text{(Εξ. 1)}$$

$$D_{ext} = \sum_{v}\left(\sum_{i} E_i Y_i (1-\varphi_v(E_i)) + \int N_v(E) E (1-\varphi_v(E)) dE \right) \qquad \text{(Εξ. 2)}$$

όπου,
ν αναφέρεται στο διαφορετικό είδος της ακτινοβολίας (άλφα, χαμηλής ενέργειας βήτα, υψηλής ενέργειας βήτα, φωτόνια), E_i αναφέρεται στην ενέργεια αποδιέγερσης του εκάστοτε ραδιονουκλιδίου (MeV), Yi αναφέρεται στο πλήθος των διακριτών εκπεμπόμενων ενεργειών ανά αποδιέγερση (αποδιέγερση^{-1}), $N_v(E)$ αναφέρεται στο ενεργειακό φάσμα ενόσω υπάρχει συνεχής εκπομπή ακτινοβολίας (αποδιέγερση^{-1} MeV^{-1}) και $\varphi_v(E)$ αναφέρεται στην ποσότητα της εναποτιθέμενης ενέργειας στον οργανισμό.

Εντούτοις, όπως μπορεί να έγινε σαφές από την παραπάνω συνοπτική περιγραφή του κώδικα ERICA, έχουν εισαχθεί πολλές παραδοχές στον κώδικα όσον αφορά στις ιδεατές προσομοιωμένες γεωμετρίες, στη θέση των παραγόμενων ραδιονουκλιδίων, στα χρησιμοποιούμενα ραδιονουκλίδια λαμβάνοντας υπόψιν την ραδιενεργό ισορροπία και τα ενσωματωμένα πειραματικά δεδομένα. Λόγω των πολλών παραδοχών αυτών, κρίθηκε σκόπιμο να δοκιμαστούν στην παρούσα εργασία οι κώδικες MCNP (MCNP-CP/MCNPX) και ERICA σε ένα υποθετικό σενάριο. Η συμφωνία μεταξύ των δύο κωδίκων ήταν ικανοποιητική – εντός 8% για τον εσωτερικό ρυθμό δόσης και εντός 12% για τον εξωτερικό ρυθμό δόσης- για τον έλεγχο των κωδίκων στο απλό υποθετικό σενάριο ενός σφαιρικού πελαγικού ψαριού που εξετάστηκε.

Επίσης, ο κώδικας ERICA έχει τη δυνατότητα να εκτιμήσει τις συγκεντρώσεις ραδιενέργειας σε διάφορες μήτρες (π.χ. νερό, ιζήματα) χρησιμοποιώντας απλά μοντέλα διασποράς ραδιονουκλιδίων βασισμένα σε εργασίες του Διεθνούς Οργανισμού Ατομικής Ενέργειας (IAEA, 2001). Αυτά τα μοντέλα είναι συντηρητικά και έχουν σχεδιαστεί ώστε να εκτιμούν τις συγκεντρώσεις των ραδιονουκλιδίων στην ατμόσφαιρα και το υδάτινο οικοσύστημα, προκειμένου οι εκτιμώμενοι ρυθμοί δόσεων να μην υποεκτιμούν την πραγματικότητα πάνω από ένα παράγοντα του 10. Τα μοντέλα διασποράς εκτιμούν τις συγκεντρώσεις ραδιενέργειας στο νερό ή τον αέρα, θεωρώντας μία σημειακή πηγή συνεχούς εκφόρτωσης και μία επικράτηση ισορροπίας ή ημί-ισορροπίας μεταξύ των απελευθερούμενων ραδιονουκλιδίων και των στοιχείων του περιβάλλοντος. Τα διαθέσιμα μοντέλα διασποράς συμπεριλαμβάνουν μικρή (< 400 km^2) και μεγάλη (≥400 km^2) λίμνη, εκβολή ποταμού, ποτάμι, παράκτια ζώνη και αέρα.

Πριν την ενσωμάτωση αυτών των μοντέλων στον κώδικα ERICA, τα αποτελέσματά τους ελέγχθηκαν με τα δημοσιευμένα παραδείγματα των εργασιών του IAEA.

4. Πειραματικές διατάξεις

Οι επιλεγμένες θαλάσσιες περιοχές του εν λειτουργία και του εγκαταλειμμένου ορυχείου βρίσκονται στη βόρεια και κεντρική Ελλάδα, στο Στρατώνι και στο Λαύριο, αντιστοίχως. Και οι δύο περιοχές χαρακτηρίζονται από δραστηριότητες εξόρυξης, από την αρχαιότητα μέχρι σήμερα. Τα επιφανειακά δείγματα και τα δείγματα πυρήνων ιζήματος που συλλέχθηκαν από τις δύο περιοχές μελέτης, προετοιμάστηκαν καταλλήλως για την μέτρηση του ποσοστού άμμου-ίλεως, την μέτρηση της συγκέντρωσης ενεργότητας και τη μέτρηση των συγκεντρώσεων ιχνοστοιχείων και βαρέων μετάλλων όπως έχουν περιγραφεί αναλυτικά αλλού (Eleftheriou, 2014; Pappa et al., 2016; Pappa et al., 2018). Οι μετρήσεις φασματοσκοπίας γάμμα για τον υπολογισμό των συγκεντρώσεων ενεργότητας πραγματοποιήθηκαν κυρίως στο Ελληνικό Κέντρο Θαλασσίων Ερευνών (ΕΛΚΕΘΕ) και στο Εθνικό Μετσόβιο Πολυτεχνείο (ΕΜΠ), ενώ χρησιμοποιήθηκαν και τα εργαστήρια του Αριστοτελείου Πανεπιστημίου Θεσσαλονίκης (ΑΠΘ) και του Εθνικού Κέντρου Έρευνας Φυσικών Επιστημών (ΕΚΕΦΕ) «Δημόκριτος». Από την άλλη πλευρά οι αναλύσεις κοκκομετρίας (ποσοστό άμμου-ίλεως), ιχνοστοιχείων και κύριων στοιχείων πραγματοποιήθηκαν στα εργαστήρια του ΕΛΚΕΘΕ.

Τα βασικά χαρακτηριστικά της πειραματικής διάταξης φασματοσκοπίας γάμμα φαίνονται στο κάτωθι σχήμα:

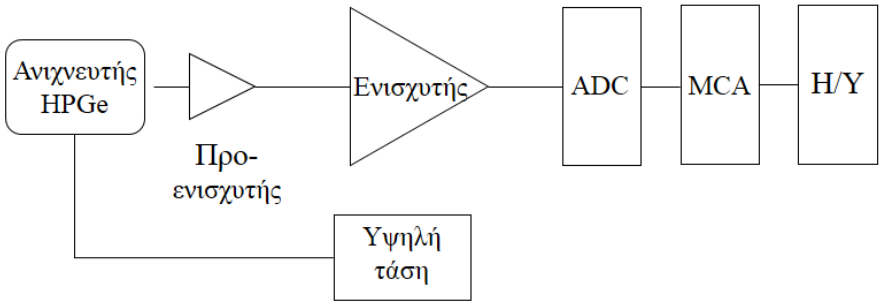

Εικ. 1 Τα βασικά χαρακτηριστικά του ανιχνευτικού συστήματος φασματοσκοπίας γάμμα (ADC: μετατροπέας σήματος αναλογικού σε ψηφιακό, MCA: πολυδιαυλικός αναλυτής)

Οι πειραματικές διατάξεις των εργαστηρίων στα οποία πραγματοποιήθηκαν οι μετρήσεις των συγκεντρώσεων ραδιενέργειας φαίνονται στην Εικ. 2:

α) Η πειραματική διάταξη του ΕΛΚΕΘΕ

β) Η θωράκιση του ανιχνευτή του ΕΛΚΕΘΕ

γ) Η πειραματική διάταξη του ΕΜΠ

δ) Η θωράκιση του ανιχνευτή του ΕΜΠ

ε) Η πειραματική διάταξη του ΑΠΘ

στ) Η θωράκιση του ανιχνευτή του ΑΠΘ

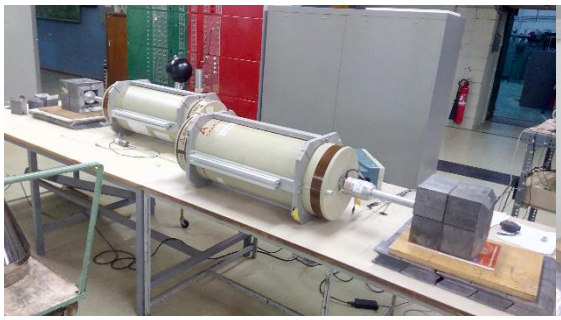

ζ) Η πειραματική διάταξη του of ΕΚΕΦΕ

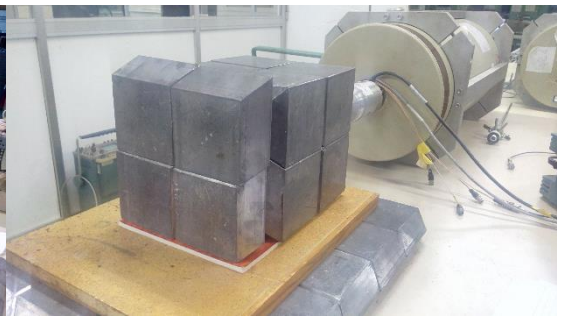

η) Η θωράκιση του ανιχνευτή του ΕΚΕΦΕ

Εικ. 2 Τα ερευνητικά εργαστήρια που χρησιμοποιήθηκαν στην παρούσα εργασία

Πριν την μέτρηση των δειγμάτων τα ανιχνευτικά συστήματα βαθμονομήθηκαν όσον αφορά στην ενεργειακή διακριτική ικανότητα και την απόλυτη απόδοση για εκτεταμένες γεωμετρίες μικρού και μεγάλου όγκου. Για να καλυφθεί ένα μεγάλο μέρος του ενεργειακού εύρους χρησιμοποιήθηκαν οι εκτεταμένες πηγές του ^{235,238}U για τις χαμηλές ενέργειες, του ^{152}Eu για τις μεσαίες ενέργειες και του ^{40}K για τις υψηλές ενέργειες. Οι παραγόμενες καμπύλες απόλυτης απόδοσης διορθώθηκαν επιπλέον για φαινόμενα πραγματικής σύμπτωσης και ενδοαπορρόφησης μέσω του λογισμικού EFFTRAN (Vidmar, 2005) προκειμένου να προσεγγίσουν την εσωτερική γεωμετρία (π.χ. πυκνότητα) των άγνωστων δειγμάτων. Η ποσοτική ανάλυση των δειγμάτων πραγματοποιείται χειροκίνητα μέσω του λογισμικού SPECTRW (Kalfas et al., 2016).

Για τη μέτρηση των μετάλλων χρησιμοποιήθηκε η φθορισιμετρία ακτίνων Χ και η πειραματική διάταξη που υλοποιήθηκαν οι μετρήσεις φαίνεται στο παρακάτω σχήμα:

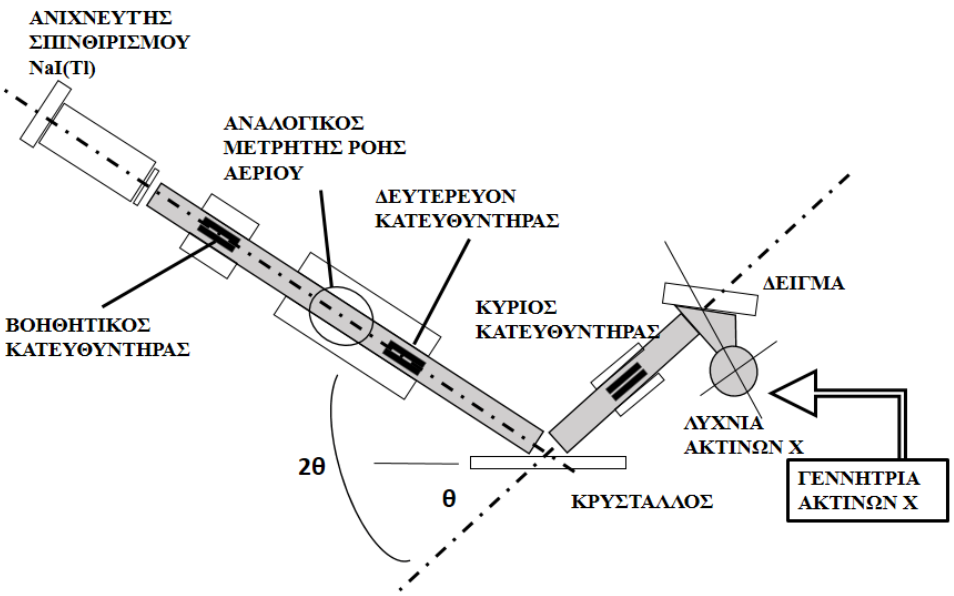

Εικ. 3 Το σχεδιάγραμμα του φθορισιόμετρου ακτίνων Χ (WDXRF PW-2400).

Οι καμπύλες βαθμονόμησης παρασκευάστηκαν για τον προσδιορισμό των κύριων στοιχείων, βασιζόμενες σε ένα μεγάλο σύνολο πιστοποιημένων υλικών αναφοράς. Επιπλέον, εφαρμόστηκαν διορθώσεις μήτρας για τη βελτίωση της ακρίβειας της μέτρησης. Μία παρόμοια διαδικασία διεξήχθη για τον προσδιορισμό των ιχνοστοιχείων χρησιμοποιώντας πρότυπα υλικά και το λογισμικό Pro-Trace. Το λογισμικό περιλαμβάνει (α) ένα σύνολο από 25 δείγματα ελέγχου στην ίδια γεωμετρία με τα άγνωστα προς μέτρηση δείγματα, (β) πρότυπα αναφοράς ενός ή πολλαπλών στοιχείων, (γ) διορθώσεις συντελεστών εξασθένησης μάζας και (δ) ένα εύρος συγκεντρώσεων 40 στοιχείων μεταξύ Be και U. Κάθε ένα από τα 40 ιχνοστοιχεία βαθμονομείται μεμονωμένα έναντι περισσότερων από 200 διεθνώς πιστοποιημένων υλικών αναφοράς. Η ανάλυση βασίζεται σε ευθείες βαθμονόμησης δύο σημείων χρησιμοποιώντας ένα πλήθος υλικών με αποτέλεσμα που χαρακτηρίζεται από υψηλή ακρίβεια. Η ποσοτικοποίηση των συγκεντρώσεων των μετάλλων καθώς και όλες οι διορθώσεις πραγματοποιούνται αυτοματοποιημένα μέσω του λογισμικού Pro-Trace.

5. Αποτελέσματα και Ερμηνεία

Στρατώνι

Για τη χρονολόγηση των πυρήνων ιζήματος εφαρμόστηκαν τα χρονολογικά μοντέλα βασιζόμενα στα ραδιονουκλίδια του ^{210}Pb και του ^{137}Cs, με τα οποία υπολογίστηκαν οι ρυθμοί ιζηματογένεσης στην περιοχή του Στρατωνίου ως **(0.26 ± 0.06) cm y^{-1}** και **(0.23 ± 0.01) cm y^{-1}**, αντιστοίχως. Επίσης, στην περιοχή του Κόλπου της Ιερισσού, ελήφθησαν 30 επιφανειακά δείγματα ιζήματος κατά μήκος του κόλπου προκειμένου να μελετηθεί η επίδραση των ανθρωπίνων μεταλλευτικών δραστηριοτήτων στην περιοχή όσο αφορά στις συγκεντρώσεις των ραδιονουκλιδίων και των μετάλλων. Ενδεικτικά θα αναφερθούν πιο κάτω κάποια από τα αποτελέσματα. Τα δείγματα οργανώθηκαν με βάση τις περιοχές δειγματοληψίας: (α) κοντά στην προβλήτα φορτοεκφόρτωσης στην περιοχή του Στρατωνίου, (β) στο υπόλοιπο λιμάνι του Στρατωνίου, (γ) στις μη παράκτιες περιοχές, στα ρέματα (δ) του Κοκκινόλακκα και (ε) του Καλατζή Λάκκου και (στ) στο λιμάνι της Ιερισσού. Επιπροσθέτως, τα αποτελέσματα κατηγοριοποιήθηκαν στα γραφήματα με βάση τις διαφορετικές μήτρες: (α) θαλάσσια ιζήματα (μπλε), (β) ιζήματα από τη διεπαφή θάλασσας-ακτής (σκούρο κίτρινο), (γ) δείγματα από την παραλία (καφέ), (δ) ιζήματα από τον πυθμένα των ρεμάτων (σκούρο πράσινο) και (ε) ιζήματα από την όχθη των ποταμών (ανοικτό πράσινο). Οι συγκεντρώσεις των ραδιονουκλιδίων της σειράς του ^{238}U (^{234}Th, ^{210}Pb, ^{226}Ra) έχουν ως εξής:

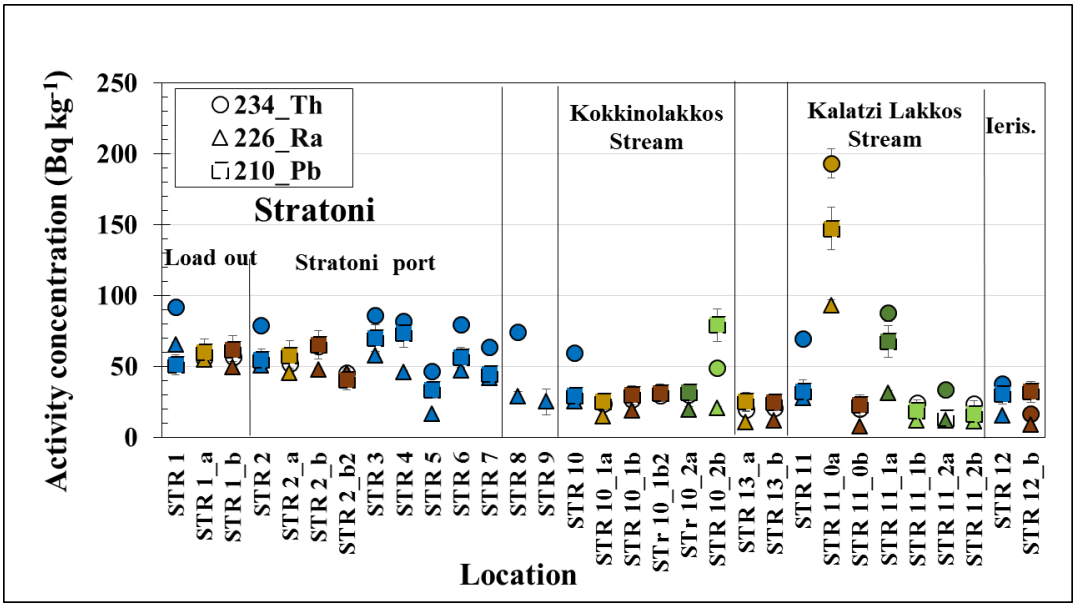

Εικ. 4 Τα αποτελέσματα της σειράς του ^{238}U όσον αφορά στα παράκτια και στα μη παράκτια (STR8, STR9) τμήματα του Κόλπου της Ιερισσού. Η συγκέντρωση ενεργότητας των ^{234}Th (κύκλος), ^{226}Ra (τρίγωνο) και ^{210}Pb (τετράγωνο) απεικονίζεται στο πιο πάνω γράφημα λαμβάνοντας υπόψιν τις διάφορες μήτρες (θαλάσσια ιζήματα (μπλε), ιζήματα από τη διεπαφή θάλασσας-ακτής (σκούρο κίτρινο), δείγματα από την παραλία (καφέ), ιζήματα από τον πυθμένα των ρεμάτων (σκούρο πράσινο) και ιζήματα από την όχθη των ποταμών (ανοικτό πράσινο).

Στην Εικόνα 4 απεικονίζονται οι συγκεντρώσεις ενεργότητας των ^{226}Ra, ^{210}Pb και ^{234}Th για όλες τις περιοχές (προβλήτα φορτοεκφόρτωσης του Στρατωνίου, λιμάνι Στρατωνίου, ρέματα Κοκκινόλακκα και Καλατζή Λάκκου και λιμάνι Ιερισσού). Οι

συγκεντρώσεις ενεργότητας των προαναφερθέντων ραδιονουκλιδίων κυμανθήκαν από (10-100) Bq kg^{-1}, (10-150) Bq kg^{-1} και (20-200) Bq kg^{-1}, αντιστοίχως. Οι μέγιστες συγκεντρώσεις ενεργότητας του ^{226}Ra ελήφθησαν κοντά στο Στρατώνι (αποβάθρα φορτοεκφόρτωσης και λιμάνι), ενώ οι ελάχιστες παρατηρήθηκαν κοντά στο ρέμα του Καλατζή Λάκκου και στο λιμάνι της Ιερισσού (δείγμα αναφοράς). Επίσης, οι συγκεντρώσεις ενεργότητας των μη παράκτιων δειγμάτων (STR8, STR9) βρέθηκαν στο ίδιο επίπεδο με εκείνες του λιμανιού της Ιερισσού. Οι συγκεντρώσεις ενεργότητας του ^{226}Ra στο θαλάσσιο πυθμένα ήταν παρόμοιες με εκείνες στην άμμο της παραλίας και στις εκβολές των ρεμάτων. Αυτή η παρατήρηση, υποδηλώνει ότι τόσο το θαλάσσιο όσο και το χερσαίο (παράκτιο) μέρος του Στρατωνίου έχουν επηρεαστεί εξίσου από τις εξορυκτικές δραστηριότητες λόγω της απόθεσης των αποβλήτων. Επιπλέον, η ισχυρή αλληλεπίδραση μεταξύ της ακτής και της παραλίας εξαιτίας των καιρικών συνθηκών μπορεί να οδήγησε σε ομογενοποίηση των συγκεντρώσεων στις αντίστοιχες μήτρες. Όσον αφορά στον πυθμένα του λιμένα του Στρατωνίου, παρατηρήθηκε η ελάχιστη τιμή για όλα τα ραδιονουκλίδια που εξετάστηκαν της σειράς του ^{238}U στη θέση STR5, η οποία θεωρείται τιμή υποβάθρου, καθώς είναι παρόμοια με αυτή του λιμένα της Ιερισσού (δείγμα αναφοράς). Οι χαμηλές συγκεντρώσεις ενεργότητας των υλικών NORM του δείγματος STR5 υποδεικνύουν ότι το βόρειο τμήμα της αποβάθρας φορτοεκφόρτωσης, δεν επηρεάστηκε από τις δραστηριότητες εξόρυξης όπως το νότιο τμήμα. Επιπλέον, οι συγκεντρώσεις ενεργότητας ^{226}Ra δεν μεταβλήθηκαν σημαντικά κατά μήκος των ποτάμιων δειγμάτων (STR10_ #, STR11_ #) γεγονός που υποδηλώνει την παρουσία φυσικών διεργασιών μεταφοράς υλικού. Οι συγκεντρώσεις ενεργότητας του ^{210}Pb εμφάνισαν υψηλότερες τιμές από εκείνες του ^{226}Ra στα δείγματα του θαλασσίου πυθμένα και των εκβολών των ρευμάτων, ενώ βρέθηκαν παρόμοιες - εντός αβεβαιότητας - με τις τιμές του ^{226}Ra στα δείγματα της άμμου της παραλίας και της όχθης των ρεμάτων. Οι υψηλότερες τιμές του ^{210}Pb σε σύγκριση με εκείνες του ^{226}Ra που παρατηρήθηκαν στον θαλάσσιο πυθμένα και στις εκβολές των ρεμάτων υποδεικνύουν δευτερεύουσες πηγές ^{210}Pb (π.χ. ατμοσφαιρική εναπόθεση) εκτός από την ύπαρξη του μητρικού ραδιονουκλιδίου (^{226}Ra). Η χωρική κατανομή του ^{234}Th ήταν παρόμοια με αυτή του ^{226}Ra, ενώ οι υψηλότερες συγκεντρώσεις ενεργότητας του ^{234}Th σε σύγκριση με εκείνες του ^{226}Ra, αναδεικνύουν την ανισορροπία εντός της σειράς του ^{238}U ίσως λόγω της πιο έντονης προσρόφησης του Th στα ιζήματα. Επομένως, οι χωρικές κατανομές των ^{226}Ra και ^{234}Th συνδέονται με τις εξορυκτικές δραστηριότητες κοντά στο λιμάνι του Στρατωνίου.

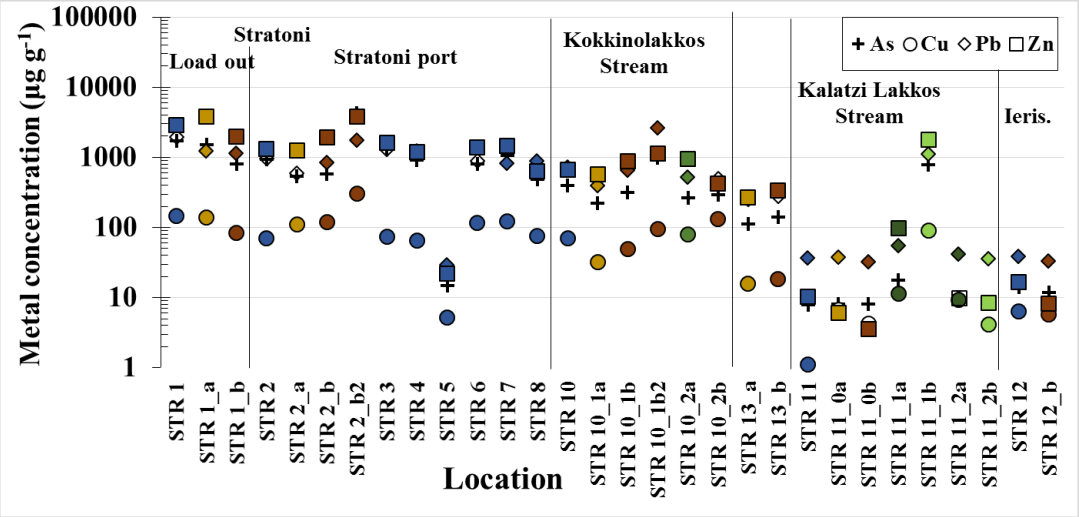

Εικ. 5 Οι συγκεντρώσεις των ιχνοστοιχείων (As, Cu, Pb και Zn) στις παράκτιες και μη παράκτιες περιοχές (STR8) του Κόλπου της Ιερισσού, όπου το As (σταυρός), ο Cu (κύκλος), ο Pb (ρόμβος) και ο Zn (τετράγωνο) απεικονίζονται λαμβάνοντας υπόψιν και τις διαφορετικές μήτρες (θαλάσσια ιζήματα (μπλε), ιζήματα από τη διεπαφή θάλασσας-ακτής (σκούρο κίτρινο), δείγματα από την παραλία (καφέ), ιζήματα από τον πυθμένα των ρεμάτων (σκούρο πράσινο) και ιζήματα από την όχθη των ποταμών (ανοικτό πράσινο).

Οι συγκεντρώσεις των As, Cu, Pb, Zn και Mn κυμάνθηκαν μεταξύ (10-4300) μg g^{-1}, (1-300) μg g^{-1}, (30-2500) μg g^{-1}, (5-4000) μg g^{-1}και (40-30000) μg g^{-1}, αντιστοίχως (Εικ. 5). Η χωρική κατανομή των ιχνοστοιχείων (As, Cu, Pb, Zn) και του Mn είναι παρόμοια με εκείνη του ^{226}Ra, όπου οι μέγιστες τιμές παρατηρήθηκαν στο λιμάνι του Στρατωνίου, ιδιαιτέρως κοντά στην αποβάθρα φορτοεκφόρτωσης. Οι τιμές των προαναφερθέντων μετάλλων μειώθηκαν κατά 50% στο ρέμα του Κοκκινόλακκα, ενώ οι ελάχιστες τιμές μετρήθηκαν στον Καλατζή Λάκκο και το λιμάνι της Ιερισσού. Στην περίπτωση των μετάλλων, οι συγκεντρώσεις μεταξύ των προαναφερθέντων περιοχών δειγματοληψίας διέφεραν μέχρι και 2 τάξεις μεγέθους και δεν μπορούν να αποδοθούν στα φυσικά χαρακτηριστικά των δειγμάτων όπως η κατανομή μεγέθους κόκκων, η οργανική ύλη ή η ορυκτολογία, αλλά στις δραστηριότητες εξόρυξης και στη διάθεση αποβλήτων (στερεών ή στερεών-υγρών μέσω του αγωγού). Οι συγκεντρώσεις των μετάλλων στο σημείο δειγματοληψίας STR5 παρουσίασαν επίσης τις ελάχιστες συγκεντρώσεις όπως στο λιμάνι της Ιερισσού, γεγονός που υποστηρίζει τα στοιχεία από τα δεδομένα του ^{226}Ra ότι το βόρειο τμήμα της αποβάθρας δεν επηρεάστηκε από τις ανθρωπογενείς δραστηριότητες όπως το νότιο τμήμα.

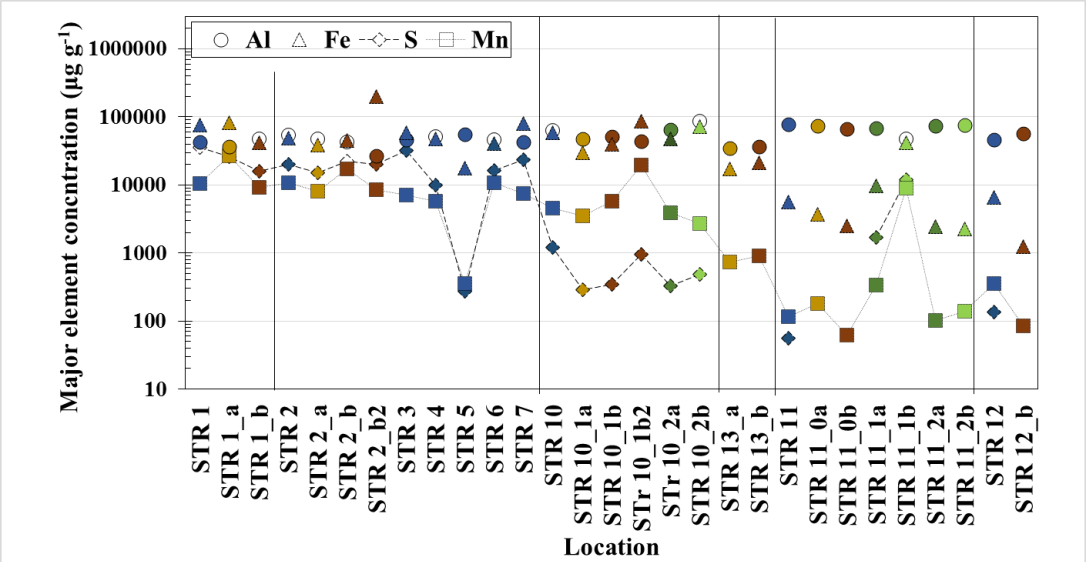

Εικ. 6 Οι συγκεντρώσεις των κύριων στοιχείων στις παράκτιες περιοχές του Κόλπου της Ιερισσού. Οι συγκεντρώσεις του S βρέθηκαν κάτω του ελαχίστου ορίου ανιχνευσιμότητας (LDM) και έτσι δεν απεικονίζονται στο γράφημα. Οι γραμμές μεταξύ των σημείων είναι για τη διευκόλυνση του αναγνώστη. Οι συγκεντρώσεις του Al (κύκλος), Fe (τρίγωνο), S (ρόμβος) and Mn (τετράγωνο) έχουν οργανωθεί λαμβάνοντας υπόψιν και τις διάφορες μήτρες (θαλάσσια ιζήματα (μπλε), ιζήματα από τη διεπαφή θάλασσας-ακτής (σκούρο κίτρινο), δείγματα από την παραλία (καφέ), ιζήματα από τον πυθμένα των ρεμάτων (σκούρο πράσινο) και ιζήματα από την όχθη των ποταμών (ανοικτό πράσινο)).

Η χωρική κατανομή των Fe, S και Mn είναι παρόμοια με εκείνη των ιχνοστοιχείων και του ^{226}Ra. Τα Fe και S είναι τα κύρια στοιχεία του σιδηροπυρίτη (FeS_2), ένα από τα βασικά εκμεταλλεύσιμα μεταλλεύματα, ενώ το Mn είναι μέρος του ροδοχρωσίτη ($MnCO_3$) ενός σύνδρομου - μη εκμεταλλεύσιμου - ορυκτού. Συνεπώς, υπάρχουν υψηλές συγκεντρώσεις αυτών των μετάλλων στα απορριπτόμενα απόβλητα είτε λόγω της απόδοσης της μεθόδου επίπλευσης (του FeS_2) είτε λόγω της απευθείας απόρριψης υλικών που δεν χρησιμοποιούνται εμπορικά ($MnCO_3$). Ως εκ τούτου, οι μέγιστες συγκεντρώσεις των Fe, S και Mn κατεγράφησαν στο Στρατώνι (αποβάθρα φορτοεκφόρτωσης και λιμένας) όπου είναι εγκατεστημένο και το εργοστάσιο επίπλευσης καθώς και άλλες εγκαταστάσεις (π.χ. αγωγός φόρτωσης εμπορεύματος, αγωγός απόρριψης απορριμμάτων επίπλευσης). Αυξημένες συγκεντρώσεις βρέθηκαν επίσης στο ρεύμα Κοκκινόλακκου, καθώς η απόθεση των αποβλήτων κατά μήκος του ρέματος πραγματοποιούνταν για πολλά χρόνια. Εντούτοις, οι απομακρυσμένες περιοχές από το Στρατώνι (ρέμα Καλατζή Λάκκου και λιμένας Ιερισσού) παρουσίαζαν ελάχιστες συγκεντρώσεις μετάλλων μέχρι 3 τάξεις μεγέθους χαμηλότερες από τις τιμές στο λιμάνι του Στρατωνίου και σε ορισμένες περιπτώσεις κάτω από το ελάχιστο όριο ανίχνευσης της μεθόδου (LDM) όπως S, υποδεικνύοντας μια μη επηρεασμένη περιοχή από τις δραστηριότητες εξόρυξης. Η χωρική κατανομή του Al είναι σχεδόν ομοιογενής μεταξύ των σημείων δειγματοληψίας, επομένως η συγκέντρωση αυτού του μετάλλου δεν έχει επηρεαστεί από τις ανθρωπογενείς δραστηριότητες.

Οι κατακόρυφες κατανομές των συγκεντρώσεων των ιχνοστοιχείων (As, Zn, Cu και Pb) και των κύριων στοιχείων (Al, Fe και Mn) καθώς και οι ροές εναπόθεσης μάζας αυτών για τον παράκτιο πυρήνα του Κόλπου της Ιερισσού απεικονίζονται στην Εικόνα

7. Σύμφωνα με αυτά τα προφίλ, ο πυρήνας των ιζημάτων μπορεί να χωριστεί σε δύο μέρη: το άνω (0-11 cm) και το κάτω (12-27 cm).

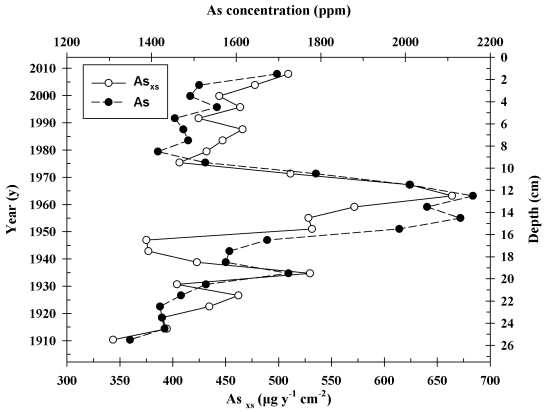

α) Κατακόρυφες κατανομές της συγκέντρωσης του As και της ροή εναπόθεσης μάζας (As_{xs})

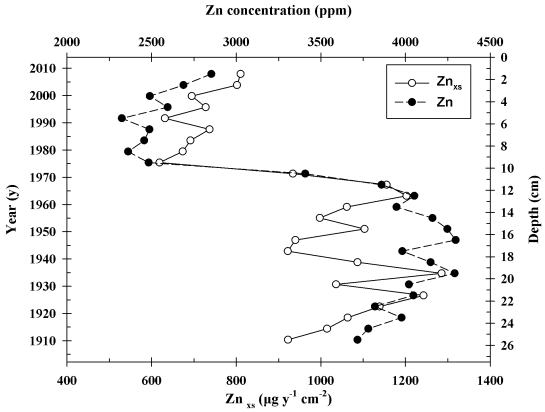

β) Κατακόρυφες κατανομές της συγκέντρωσης του Zn και της ροή εναπόθεσης μάζας (Zn_{xs})

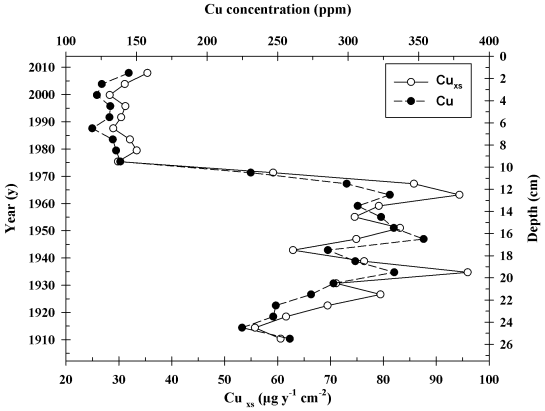

γ) Κατακόρυφες κατανομές της συγκέντρωσης του Cu και της ροή εναπόθεσης μάζας (Cu_{xs})

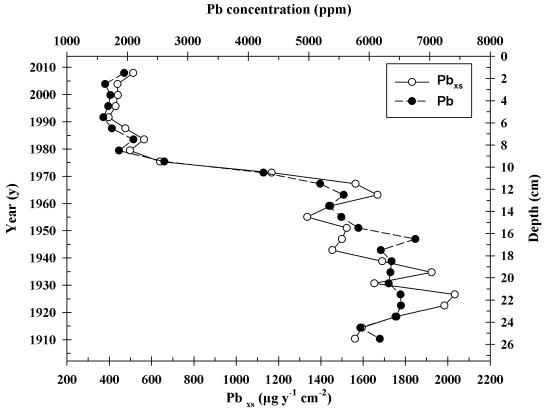

δ) Κατακόρυφες κατανομές της συγκέντρωσης του Pb και της ροή εναπόθεσης μάζας (Pb_{xs})

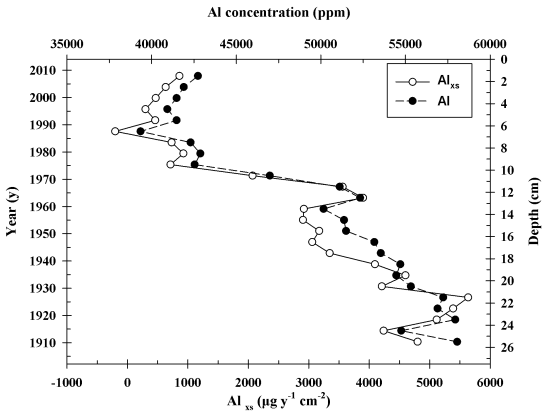

ε) Κατακόρυφες κατανομές της συγκέντρωσης του Al και της ροή εναπόθεσης μάζας (Al_{xs})

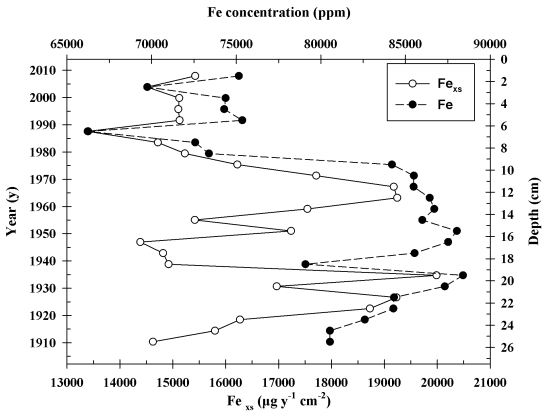

στ) Κατακόρυφες κατανομές της συγκέντρωσης του Fe και της ροή εναπόθεσης μάζας (Fe_{xs})

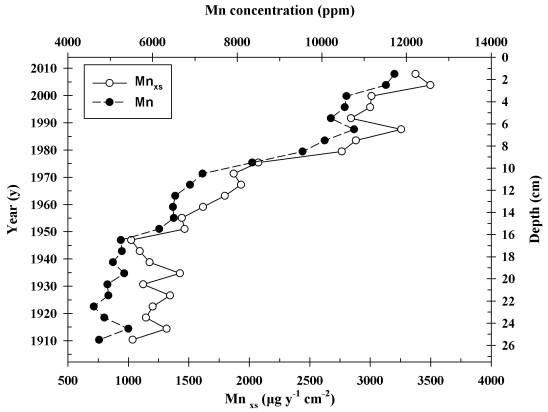

ζ) Κατακόρυφες κατανομές της συγκέντρωσης του Mn και της ροή εναπόθεσης μάζας (Mn_{xs})

Εικ. 7 Οι κατακόρυφες κατανομές των συγκεντρώσεων των ιχνοστοιχείων (As, Zn, Cu και Pb) και των κύριων στοιχείων (Al, Fe και Mn), καθώς και των ροών εναπόθεσης της μάζας αυτών για τον παράκτιο πυρήνα STR1 του Κόλπου της Ιερισσού.

Όσο αφορά στις κατακόρυφες κατανομές των ιχνοστοιχείων οι υψηλότερες συγκεντρώσεις των As, Cu, Zn και Pb βρέθηκαν στο κάτω τμήμα (12-27 cm) του πυρήνα ιζήματος και διέφεραν από το άνω τμήμα (0-11 cm) κατά έναν παράγοντα του 3. Παρόμοιες κατακόρυφες κατανομές παρατηρήθηκαν στις συγκεντρώσεις του Al και του Fe, όπως αυτές των ιχνοστοιχείων, μόνο που οι τιμές του κάτω τμήματος του πυρήνα ήταν 20-30% υψηλότερες από αυτές του άνω τμήματος. Αντίθετη κατακόρυφη κατανομή εμφάνισαν οι συγκεντρώσεις του Mn εν συγκρίσει με τις προαναφερθείσες, όπου οι τιμές στο άνω τμήμα του πυρήνα ήταν υψηλότερες από εκείνες του κάτω τμήματος κατά έναν παράγοντα του 4. Οι κατακόρυφες ροές της εναποτιθέμενης μάζας ακολούθησαν τις κατανομές των συγκεντρώσεων που χαρακτηρίζουν κάθε μέταλλο και έκαναν πιο ευκρινή τα τοπικά ακρότατα στις περιπτώσεις των As, Zn και Fe. Οι κατακόρυφες ροές των εναποτιθέμενων μαζών υπολογίστηκαν επίσης και για τα φυσικά ραδιονουκλίδια (^{226}Ra, ^{228}Ac, ^{235}U, ^{40}K) και εμφάνισαν παρόμοια μορφή με αυτές των ιχνοστοιχείων και των Al και Fe. Για λόγους συντομίας τα γραφήματα δεν παρουσιάζονται στο κομμάτι της εκτεταμένης περίληψης.

Οι συγκεντρώσεις των ραδιονουκλιδίων (^{226}Ra, ^{228}Ac, ^{235}U, ^{40}K) που μετρήθηκαν στο ίζημα του θαλασσίου πυθμένα χρησιμοποιήθηκαν για τον υπολογισμό του ρυθμού ραδιενεργών δόσεων στα έμβια - μη ανθρώπινα όντα- και στην εκτίμηση της διασποράς τους (^{226}Ra, ^{235}U) μέσω του κώδικα ERICA.

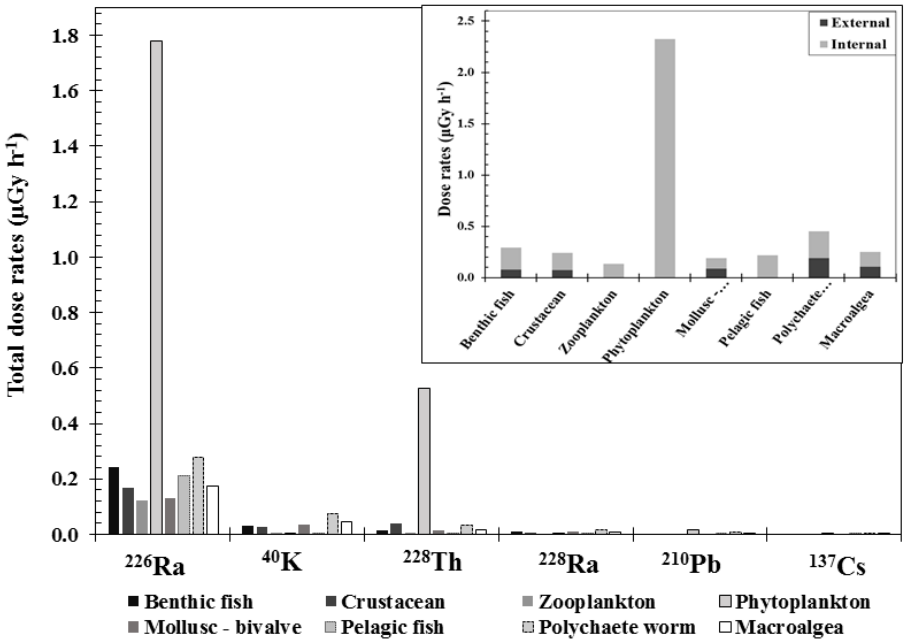

Εικ. 8 Ολικός, εσωτερικός και εξωτερικός ρυθμός δόσης για τα θαλάσσια έμβια όντα, όπως προέκυψαν από τις συγκεντρώσεις των φυσικών ραδιονουκλιδίων και του ^{137}Cs στα επιφανειακά ιζήματα του πυθμένα του λιμένα του Στρατωνίου (Κόλπος Ιερισσού).

Η επίδραση της ραδιενέργειας μπορεί να θεωρηθεί αμελητέα, καθώς σε όλες τις περιπτώσεις οι συνολικές δόσεις υπολογίστηκαν κατά δύο τάξεις μεγέθους χαμηλότερες από τις προτεινόμενες τιμές της IAEA (1992) και UNSCEAR (1996) για τους υδρόβιους οργανισμούς. Οι κύριοι συντελεστές των συνολικών ποσοστών δόσης βρέθηκαν να είναι ^{226}Ra (1.8 μGy h^{-1}) και ^{228}Th (5.3 10^{-1} μGy h^{-1}), καθώς τόσο αυτά τα ραδιονουκλίδια όσο και οι θυγατρικοί τους πυρήνες είναι άλφα εκπομποί και συνεισφέρουν σημαντικά στη ραδιενεργό δόση. Ο κώδικας ERICA θεωρεί ραδιενεργό ισορροπία μεταξύ του ^{226}Ra και των θυγατρικών του (^{222}Rn, ^{218}At, ^{218}Po, ^{214}Pb, ^{214}Bi, ^{214}Po), καθώς και μεταξύ του ^{228}Th και των θυγατέρων του (^{224}Ra, ^{220}Rn, ^{216}Po, ^{212}Pb, ^{212}Po, ^{212}Bi, ^{208}Tl) (Brown et al., 2008). Με βάση τους υπολογισμούς το φυτοπλαγκτόν έλαβε υψηλότερα ποσοστά ρυθμού δόσης από 9 έως 10 φορές υψηλότερες από τις δόσεις των άλλων οργανισμών. Ο κύριος συντελεστής στους συνολικούς ρυθμούς δόσης ήταν η εσωτερική δόση, λόγω των διασπώμενων άλφα πυρήνων όπως αναφέρθηκε προηγουμένως, ενώ η εξωτερική δόση για πολλές περιπτώσεις είναι αμελητέα σε σύγκριση με την εσωτερική. Η εξωτερική δόση καθίσταται σημαντική για τους οργανισμούς που ζουν κοντά ή πάνω στο ίζημα (π.χ. βενθικά ψάρια, δίθυρα, μακροφύκη). Οι λαμβανόμενοι εξωτερικοί ρυθμοί δόσης αποδίδονται κυρίως στο ^{40}K και κατά δεύτερον στο ^{226}Ra, συνεπώς, παρά τη μικρή συνεισφορά του ^{40}K στον υπολογισμό της συνολικής δόσης, θα πρέπει να λαμβάνεται υπόψη για τις περιπτώσεις οργανισμών που βρίσκονται κοντά στον θαλάσσιο πυθμένα.

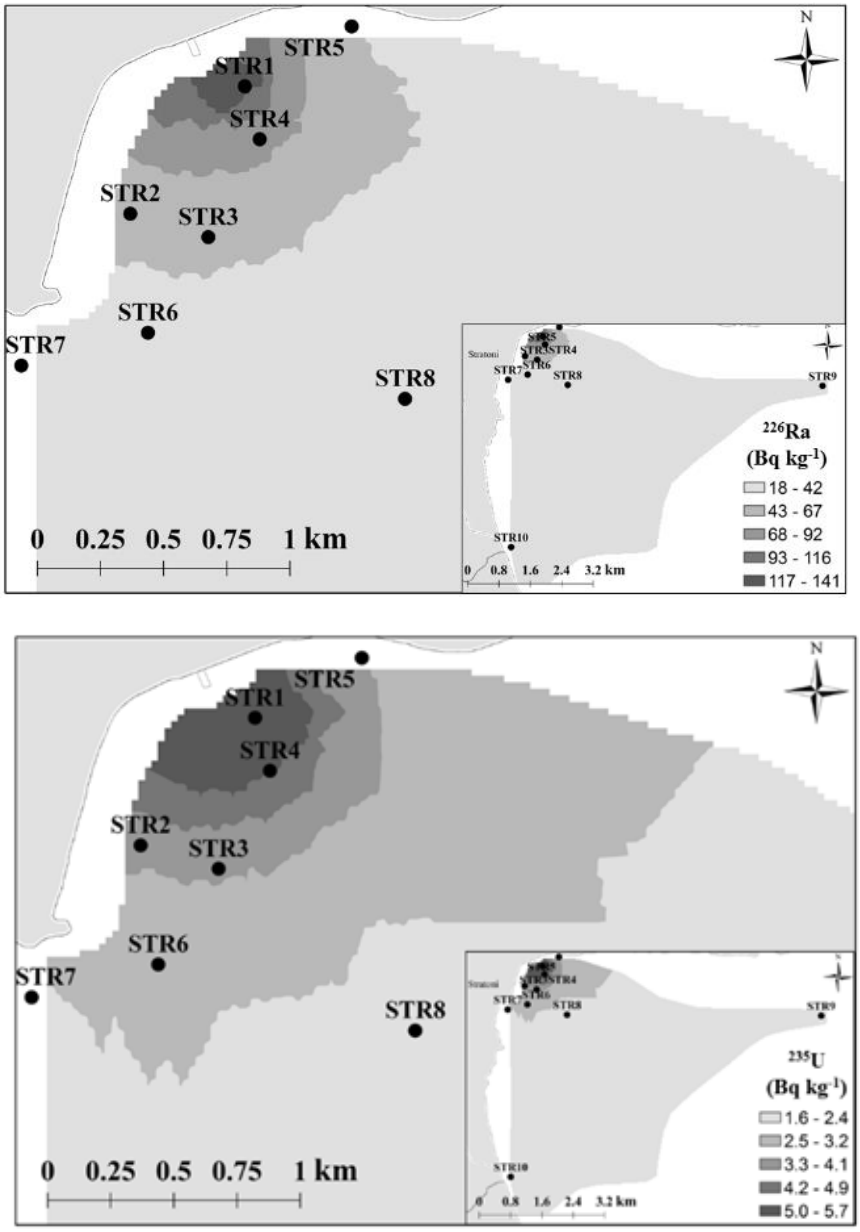

Εικ. 9 Η διασπορά του ^{226}Ra (άνω) και του ^{235}U (κάτω), καθώς και η εκτιμώμενη έκταση της επηρεασμένης περιοχής στον Κόλπο της Ιερισσού λόγω των μεταλλευτικών δραστηριοτήτων (ενσωματωμένη εικόνα).

Η διασπορά αυτών των ραδιονουκλιδίων εκτιμήθηκε για τα ραδιονουκλίδια των ^{226}Ra και ^{235}U, καθώς η χωρική τους κατανομή επηρεάζεται από τις δραστηριότητες εξόρυξης. Οι εκτιμώμενες και μετρημένες συγκεντρώσεις ενεργότητας των ^{226}Ra και ^{235}U, συμφωνούσαν ικανοποιητικά εντός 27% και 25% αντιστοίχως. Η βαθμονόμηση του μοντέλου με τη χρήση των πειραματικών δεδομένων παρείχε ρυθμούς απόρριψης 120 Bq s^{-1} και 14 Bq s^{-1} για τα ^{226}Ra και ^{235}U, αντιστοίχως. Η εκτιμώμενη διασπορά εμφάνισε μέγιστες συγκεντρώσεις ενεργότητας κοντά στην περιοχή της αποβάθρας φορτοεκφόρτωσης και για τα δύο ραδιονουκλίδια, οι οποίες μειώνονται με την απομάκρυνση από την αποβάθρα. Επιπλέον, οι τιμές της ακτογραμμής εμφάνισαν χαμηλότερα επίπεδα συγκριτικά με το κέντρο του λιμένα Στρατωνίου. Στους παραγόμενους χάρτες διασποράς χρησιμοποιήθηκαν μόνο τα εκτιμώμενα δεδομένα και για αυτό τα πειραματικά δεδομένα (π.χ. STR5, STR7) δεν περιλαμβάνονται σε

αυτούς. Τέλος, οι τιμές υποβάθρου που ελήφθησαν στις τοποθεσίες που βρίσκονται πολύ μακριά από το σημείο αποφόρτισης/απόρριψης (π.χ. STR9, STR10) χρησιμοποιήθηκαν για την εκτίμηση της επιφάνειας της επηρεασμένης περιοχής (ενσωματωμένες εικόνες). Η επηρεασμένη περιοχή και των δύο ραδιονουκλιδίων εμφανίζει ένα ημικυκλικό σχήμα γύρω από την αποβάθρα και εκτείνεται στα απομακρυσμένα σημεία δειγματοληψίας (STR9, STR10) αλλά όχι στην ακτογραμμή. Η αμελητέα επίδραση στα σημεία δειγματοληψίας της ακτογραμμής επιβεβαιώθηκε από τις χαμηλές τιμές που μετρήθηκαν στο ρέμα του Καλατζή Λάκκου (STR11) και στο λιμάνι της Ιερισσού (STR12). Με βάση τους χάρτες διασποράς έχει επηρεαστεί μόνο το βόρειο τμήμα του κόλπου της Ιερισσού λόγω των μεταλλευτικών δραστηριοτήτων και όχι το κεντρικό ή το νότιο τμήμα. Η επηρεασμένη περιοχή εκτείνεται σε επιφάνεια 21 km^2. Έτσι, η πόλη της Ιερισσού μπορεί να θεωρηθεί ασφαλής περιοχή για διαμονή, τουριστικές δραστηριότητες και ψάρεμα.

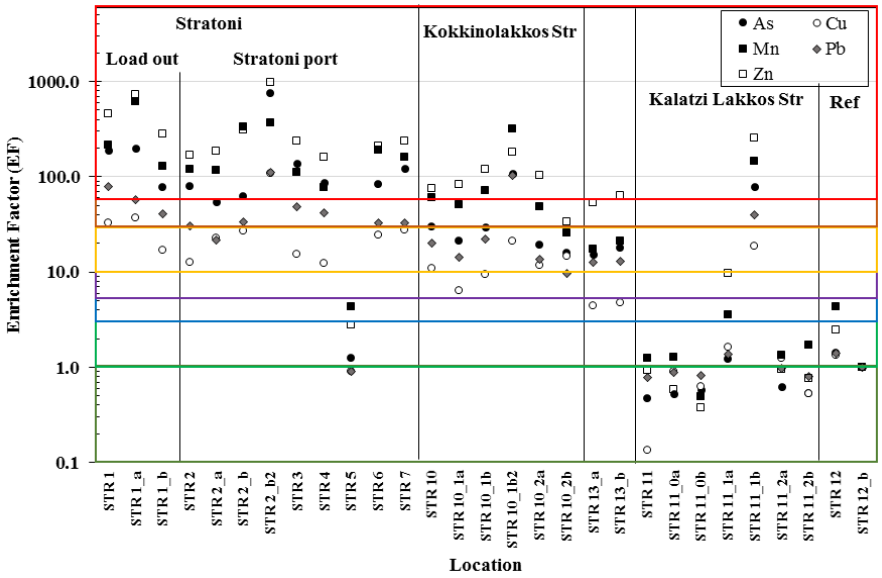

Εικ. 10 Η χωρική κατανομή των παραγόντων εμπλουτισμού για τα As, Cu, Zn, Pb and Mn. Ως συντηρητικό στοιχείο για τον υπολογισμό των παραγόντων εμπλουτισμού χρησιμοποιήθηκε το Al και ως περιοχή αναφοράς το λιμάνι της Ιερισσού. Η ταξινόμηση των παραγόντων εμπλουτισμού γίνεται με τη χρήση χρώματος, όπου το ανοικτό πράσινο αντιπροσωπεύει την απουσία εμπλουτισμού, το σκούρο πράσινο ελάχιστο εμπλουτισμό, το μπλε μέτριο εμπλουτισμό, το μωβ μέτριο προς σοβαρό εμπλουτισμό, το κίτρινο σοβαρό εμπλουτισμό, το πορτοκαλί πολύ σοβαρό εμπλουτισμό και το κόκκινο εξαιρετικά σοβαρό εμπλουτισμό.

Οι παράγοντες εμπλουτισμού (EFs) υπολογίστηκαν με βάση τις συγκεντρώσεις των ιχνοστοιχείων, του Mn και του Al που χαρακτηρίζουν την περιοχή μελέτης. Σύμφωνα με τους εκτιμώμενους EFs, οι περιοχές δειγματοληψίας μπορούν να κατηγοριοποιηθούν μεταξύ εξαιρετικά σοβαρού εμπλουτισμού και απουσίας εμπλουτισμού αναλόγως με τις τοποθεσίες δειγματοληψίας. Είναι προφανές ότι η πιο επηρεασμένη περιοχή είναι το Στρατώνι (τόσο θαλάσσια όσο και χερσαία) όσο αφορά στα Zn, As και το Mn, ειδικά η περιοχή κοντά στην αποβάθρα φορτοεκφόρτωσης καθώς και η άμμος της παραλία (STR2_b2). Ακόμη και αν τα Zn και As είναι ιχνοστοιχεία και το Mn είναι ένα κύριο στοιχείο, το δεύτερο εμφανίζει μικρότερο εμπλουτισμό σε σύγκριση με τα Zn και As. Αυτό αναδεικνύει ότι τα απορριπτόμενα απόβλητα που χαρακτηρίζουν αμφότερα τα περιβάλλοντα (θαλάσσια και χερσαία) οφείλονται στα εκμεταλλεύσιμα μεταλλεύματα (π.χ., P.B.G., πλούσια σε Zn και

ποσότητες από αρσενοπυρίτη (As)). Αυτό επιβεβαιώνεται και από τον πολύ σοβαρό εμπλουτισμό σε Pb στο Στρατώνι (επίσης μέταλλο πλούσιο στα μεταλλεύματα P.B.G.). Ο διαφορετικός τύπος εμπλουτισμού στο ρέμα του Κοκκινόλακκου π.χ. ο εξαιρετικά σοβαρός εμπλουτισμός σε Zn / Mn και ο πολύ σοβαρός εμπλουτισμός σε As μπορεί να αποδοθεί στις διαφορετικές συγκεντρώσεις μετάλλων που χαρακτηρίζουν τα απορριφθέντα υλικά. Το ρέμα του Καλατζή Λάκκου μπορεί να θεωρηθεί ως ανεπηρέαστο από τις δραστηριότητες εξόρυξης μιας και εμφάνισε χαμηλό ή / και καθόλου εμπλουτισμό, εκτός από ένα σημείο δειγματοληψίας (STR11_1b). Ο εξαιρετικά σοβαρός εμπλουτισμός του STR11_1b μπορεί να συσχετιστεί με την παρουσία αυξημένων τιμών Fe και S σε αυτό το δείγμα. Όσον αφορά στον εμπλουτισμό του Cu, το Στρατώνι και το ρέμα του Κοκκινόλακκα είναι σοβαρά εμπλουτισμένα, ενώ το ρέμα του Καλατζή Λάκκου και η παραλία της Ιερισσού εμφάνισαν τιμές που χαρακτηρίζουν το φυσικό υπόβαθρο της περιοχής. Για να συνοψίσουμε, η κατάταξη εμπλουτισμού των μετάλλων στο ίζημα βρέθηκε ως εξής: Zn> As> Mn> Pb> Cu.

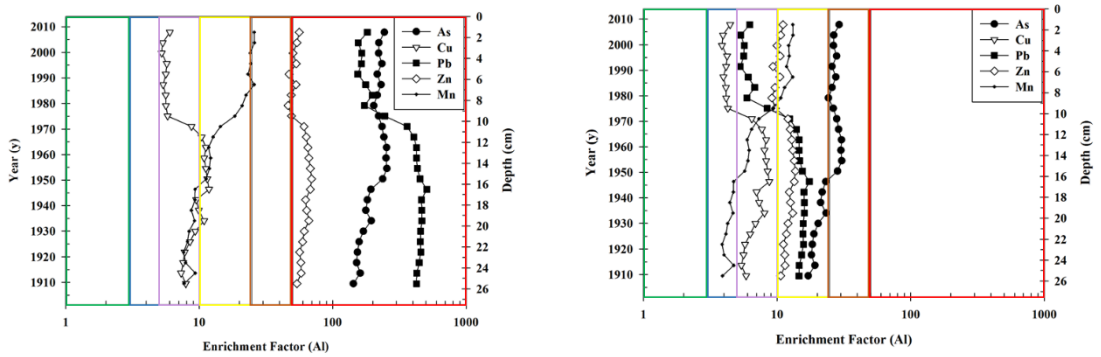

Εικ. 11 Οι κατακόρυφες κατανομές των παραγόντων εμπλουτισμού για τα As, Cu, Zn, Pb και Mn στον παράκτιο πυρήνα ιζήματος του Κόλπου της Ιερισσού. Ως συντηρητικό στοιχείο στους υπολογισμούς χρησιμοποιήθηκε το Al, ενώ οι συγκεντρώσεις των μετάλλων από τον σχιστόλιθο του φλοιού της Γης (Wedepohl, 1995) (αριστερά) και εκείνων του πιο βαθιού σημείου από τον μη παράκτιο πυρήνα (STR8) (δεξιά) χρησιμοποιήθηκαν επίσης στους υπολογισμούς. Η ταξινόμηση των παραγόντων εμπλουτισμού γίνεται με τη χρήση χρώματος, όπου το πράσινο αντιπροσωπεύει την απουσία εμπλουτισμού ή τον ελάχιστο εμπλουτισμό, το μπλε μέτριο εμπλουτισμό, το μωβ μέτριο προς σοβαρό εμπλουτισμό, το κίτρινο σοβαρό εμπλουτισμό, το πορτοκαλί πολύ σοβαρό εμπλουτισμό και το κόκκινο εξαιρετικά σοβαρό εμπλουτισμό.

Χρησιμοποιώντας ως συγκεντρώσεις αναφοράς εκείνες του σχιστόλιθου της Γης, ολόκληρος πυρήνας ιζήματος (STR1) χαρακτηρίστηκε ως εξαιρετικά αυστηρά εμπλουτισμένος (EF> 50) σε As, Pb και Zn κατά την ταξινόμηση Birch και Davies (2003). Ο εμπλουτισμός του άνω μέρους του πυρήνα (0-11cm) βρέθηκε σοβαρός και μετρίως σοβαρός για τα Mn και Cu, αντιστοίχως. Στο κάτω μέρος (12-27 cm) ο εμπλουτισμός ήταν κυρίως μετρίως σοβαρός και για τα δύο μέταλλα. Με βάση τις συγκεντρώσεις που μετρήθηκαν στον μη παράκτιο πυρήνα (STR8), ο εμπλουτισμός στο άνω τμήμα του παράκτιου πυρήνα STR1 βρέθηκε να είναι μέτριος, μετρίως σοβαρός, σοβαρός και πολύ σοβαρός για τα Cu, Pb, Zn και Mn / As, αντιστοίχως. Στο κάτω μέρος του πυρήνα ο εμπλουτισμός χαρακτηρίστηκε ως μέτριος, μετρίως σοβαρός και σοβαρός για Mn, Cu και As / Pb / Zn, αντιστοίχως. Η σειρά του εμπλουτισμού μετάλλου στο ίζημα χρησιμοποιώντας το σχιστόλιθο ως αναφορά ήταν Pb> As> Zn>

Mn> Cu, ενώ αυτή η κατάταξη άλλαξε σε As> Zn≥Pb> Mn> Cu χρησιμοποιώντας τον μη παράκτιο πυρήνα STR8 ως αναφορά. Εντούτοις, η κατηγοριοποίηση παρέμεινε σχεδόν η ίδια, ενώ κάποιες μικρές αλλαγές παρατηρήθηκαν για τα Cu και Mn. Για παράδειγμα, ο πυρήνας των ιζημάτων χαρακτηρίστηκε ως μετρίως έντονα εμπλουτισμένος σε Cu όταν χρησιμοποιήθηκαν οι τιμές του σχιστόλιθου, ενώ χαρακτηρίστηκε ως μετρίως εμπλουτισμένος στο Cu όταν χρησιμοποιήθηκαν τιμές του STR8. Από την άλλη πλευρά, η ταξινόμηση των As, Zn και Pb στον πυρήνα των ιζημάτων άλλαξε σημαντικά, υποδεικνύοντας ότι χρειάζεται μια ένα πιο βαθύ σημείο στο ίζημα του μη παράκτιου πυρήνα ή ένας πιο μακρινός πυρήνας για να εξακριβωθεί αν η επιλογή του χρησιμοποιούμενου δείγματος του πυρήνα STR8 αποτελεί καλό εκπρόσωπο του οικοσυστήματος ή απαιτείται η επιλογή ενός καλύτερου υποβάθρου.

Λαύριο

Παρόμοιες προσεγγίσεις υλοποιήθηκαν και για τη μελέτη της ανθρωπογενούς επίδρασης λόγω των μεταλλευτικών δραστηριοτήτων στην περιοχή του Λαυρίου. Από τις εξεταζόμενες παράκτιες περιοχές του Λαυρίου η πιο επιβαρυμένη από τις μεταλλευτικές δραστηριότητες ήταν ο κολπίσκος του Οξυγόνου, όπου ο ρυθμός ιζηματογένεσης υπολογίστηκε στα **(0.33 ± 0.03) cm y^{-1} από το ^{210}Pb.** Οι συγκεντρώσεις του ^{137}Cs ήταν αρκετά χαμηλές με αποτέλεσμα να μην είναι ευδιάκριτα τα τοπικά ακρότατα. Για λόγους συντομίας δεν θα παρουσιαστούν αναλυτικά τα αποτελέσματα της περιοχής του Οξυγόνου, αλλά μία μικρή αναφορά συγκριτικά με την περιοχή του Στρατωνίου. Όπως και στην περίπτωση του Στρατωνίου οι συγκεντρώσεις των φυσικών ραδιονουκλιδίων αυξήθηκαν λόγω των μεταλλευτικών δραστηριοτήτων και ακολουθούσαν την χωρική και κατακόρυφη κατανομή των ιχνοστοιχείων (As, Zn) και των κύριων στοιχείων (Fe, Mn). Παρ ‘όλα ταύτα οι συγκεντρώσεις των ραδιονουκλιδίων βρέθηκαν αρκετά χαμηλότερες εν συγκρίσει με εκείνες του Στρατωνίου, επομένως δεν υπάρχει κάποιος ραδιολογικός κίνδυνος. Από την άλλη πλευρά, οι συγκεντρώσεις των ιχνοστοιχείων (As, Cu, Pb, Zn) και του Mn βρέθηκαν στα ίδια επίπεδα με εκείνες του Στρατωνίου αναδεικνύοντας μία εξαιρετικά επηρεασμένη περιοχή, όπως επιβεβαιώθηκε και από τους παράγοντες εμπλουτισμού.

Το αξιοσημείωτο στην περιοχή του Οξυγόνου είναι ότι στις κατακόρυφες κατανομές των συγκεντρώσεων των μετάλλων δεν παρατηρείται κάποια μείωση, ακόμα και 30 χρόνια μετά την παύση των μεταλλευτικών δραστηριοτήτων στην περιοχή. Πιθανές αιτίες για τις ακόμα διατηρούμενες υψηλές συγκεντρώσεις των μετάλλων στον κολπίσκο του Οξυγόνου είναι η έκπλυση λόγω βροχών των μολυσμένων χερσαίων τμημάτων του Οξυγόνου ή η αλληλεπίδραση μέσω των θαλασσίων ρευμάτων με το μολυσμένο τμήμα του Κόλπου του Θορικού.

6. Συμπεράσματα

Στρατώνι

Συμπερασματικά, η χωρική μελέτη του κόλπου της Ιερισσού ανέδειξε την πιο επηρεασμένη περιοχή όσον αφορά στα ραδιονουκλίδια και τα μέταλλα το λιμάνι του Στρατωνίου. Σύμφωνα με τη χωρική μελέτη και το μοντέλο διασποράς οι δραστηριότητες εξόρυξης επηρέασαν το βόρειο τμήμα του κόλπου της Ιερισσού και έφθασαν μέχρι το μεσαίο τμήμα του κόλπου, ενώ η νότια περιοχή δεν επηρεάστηκε. Έτσι, η πόλη της Ιερισσού μπορεί να θεωρηθεί ασφαλής περιοχή για διαμονή, τουρισμό και ψάρεμα. Παρά τις αυξημένες συγκεντρώσεις ραδιονουκλιδίων εν συγκρίσει με το λιμάνι της Ιερισσού και τον παγκόσμιο μέσο όρο για το έδαφος, ο ραδιολογικός κίνδυνος για τους μη ανθρώπινους έμβιους οργανισμούς ήταν αμελητέος. Από την άλλη πλευρά, ο εμπλουτισμός μετάλλου βρέθηκε σοβαρός σε πολλά σημεία δειγματοληψίας και μια ενδεικτική κατάταξη εμπλουτισμού στα δείγματα επιφανείας ήταν η εξής: Zn> As> Mn> Pb> Cu.

Στη θαλάσσια περιοχή του Στρατωνίου δεν υπάρχουν δεδομένα μακροχρόνιας παρακολούθησης. Ως εκ τούτου, ο συλλεχθής παράκτιος πυρήνας ιζήματος χρησιμοποιήθηκε για την αναδόμηση της ανθρωπογενούς επίδρασης στην περιοχή. Οι μέγιστες συγκεντρώσεις ραδιονουκλιδίων και μετάλλων βρέθηκαν μεταξύ του 1908 και του 1970. Ωστόσο ο ραδιολογικός κίνδυνος ήταν επίσης αμελητέος, ενώ ο εμπλουτισμός βρέθηκε σοβαρός, ειδικά κατά την ίδια περίοδο (1908-1970). Μια ενδεικτική κατάταξη εμπλουτισμού μετάλλου στον πυρήνα ιζημάτων ήταν As> Zn≥Pb> Mn> Cu. Η αναδόμηση της ανθρωπογενούς επίδρασης ολοκληρώθηκε συνδυάζοντας τις συγκεντρώσεις ραδιονουκλιδίων και μετάλλων καθώς και τις εκτιμώμενες ροές εναποτιθέμενης μάζας. Οι περίοδοι των κύριων διεργασιών που αποτυπώθηκαν στους πυρήνες ιζήματος ήταν η εκμετάλλευση πυρίτη για την παραγωγή θειικού οξέος κατά την περίοδο 1912-1920, η μειωμένη εκμετάλλευση του μεταλλεύματος λόγω του Δευτέρου Παγκοσμίου Πολέμου κατά την περίοδο 1935-1945, η αλλαγή στη μέθοδο ανάκτησης του μεταλλεύματος λόγω διαφορετικών γεωλογικών χαρακτηριστικών των ορυκτών και η λειτουργία του εργοστασίου επίπλευσης της Ολυμπιάδας κατά τη διάρκεια του 1950-1970, και τέλος η παύση απόρριψης αποβλήτων στο θαλάσσιο περιβάλλον κατά την περίοδο του 1980-2010. Εν τέλει η ισχυρή συσχέτιση μεταξύ των ραδιονουκλιδίων (^{226}Ra, ^{235}U) και των μετάλλων (As, Cu, Pb, Zn, Mn) όπως εκτιμήθηκε μέσω της στατιστικής ανάλυσης και λαμβάνοντας υπόψη το μοντέλο διασποράς των ραδιονουκλιδίων μπορεί να αποτελέσουν μία ένδειξη για την διασπορά των μετάλλων στην περιοχή.

Λαύριο

Μια παρόμοια προσέγγιση, συμπεριλαμβανομένων των χωρικών και χρονολογικών κατανομών στο θαλάσσιο περιβάλλον, πραγματοποιήθηκε στο Λαύριο με επίκεντρο τον κολπίσκο του Οξυγόνου. Το Λαύριο βρίσκεται κοντά σε ένα εγκαταλελειμμένο ορυχείο και αντιμετωπίζει τον αντίκτυπο της εξόρυξης των μετάλλων, καθώς έχει αναπτυχθεί επάνω στα υπολείμματα και τα απόβλητα των εξορυκτικών δραστηριοτήτων. Ο αντίκτυπος αυτός είναι εμφανής και στο θαλάσσιο τμήμα του Λαυρίου. Όπως και στην περίπτωση του Στρατωνίου, οι συγκεντρώσεις ραδιονουκλιδίων αυξήθηκαν εξαιτίας της εξόρυξης, τόσο στο χώρο όσο και κατακόρυφα, ωστόσο αυτές οι τιμές βρέθηκαν πολύ χαμηλότερες από τις αντίστοιχες

στο Στρατώνι. Από την άλλη πλευρά, οι συγκεντρώσεις μετάλλων στον κολπίσκο του Οξυγόνου παρουσίασαν τιμές παρόμοιες με εκείνες του λιμένα του Στρατωνίου. Η κύρια διαφορά μεταξύ των δύο μελετούμενων περιοχών (Στρατώνι και Λαύριο), είναι ότι η επίδραση των μεταλλείων στο Στρατώνι είναι σημαντική κατά τη διάρκεια του 1908 - 1970, ενώ στο Λαύριο είναι σημαντική κατά τα τελευταία 100 χρόνια (1920-2014). Παρά την παύση της εξόρυξης, 30 χρόνια πριν, η παρουσία των μετάλλων εξακολουθεί να είναι εμφανής και αυτό οφείλεται σε απορρίμματα από τον περασμένο αιώνα στον όρμο του Θορικού. Το απόβλητο υλικό μεταφέρεται λόγω των διεργασιών θαλάσσιας κυκλοφορίας και της δυναμικής μεταφοράς ιζημάτων με αποτέλεσμα τη μόλυνση της χερσαίας περιοχής κοντά στον κολπίσκο του Οξυγόνου. Ομοίως όπως και στο Στρατώνι ο μεταλλικός εμπλουτισμός ήταν σοβαρός τόσο χωρικά όσο και χρονολογικά. Η πιο μολυσμένη περίοδος που αφορούσε στα στοιχεία Pb και Cu ήταν κατά την περίοδο του 1900-1930, ενώ όσον αφορά στα άλλα μέταλλα (As, Zn και Mn) η πιο μολυσμένη περίοδος ήταν τα τελευταία 100 χρόνια. Επιπρόσθετα, όπως και στην υπόθεση του Στρατωνίου, επηρεάστηκε για πολλά χρόνια και η μη παράκτια περιοχή του Λαυρίου, όπως φάνηκε από τις υψηλές τιμές μετάλλων στον μη παράκτιο πυρήνα. Οι χωρικές και κατακόρυφες μελέτες των μετάλλων αποκάλυψαν ότι η διαδρομή των μεταλλικών απορριμμάτων από τον Κόλπο του Θορικού κατευθύνεται στον κολπίσκο του Οξυγόνου καθώς και στη Μακρόνησο μέσω της θαλάσσιας κυκλοφορίας και της δυναμικής των ιζημάτων.

Στη χρονολογική αναδόμηση εντοπίστηκαν τέσσερις περίοδοι λειτουργίας: α) η περίοδος 1860-1900 όπου η απόδοση της εφαρμοζόμενης μεθόδου ήταν χαμηλή και οι αρχαίες σκωρίες χρησιμοποιήθηκαν ως πρώτες ύλες, β) η περίοδος 1900-1930 όπου η βελτίωση της μεθόδου ανάκτησης είχε ως αποτέλεσμα την αύξηση όλων των μετάλλων και των συγκεντρώσεων του ^{226}Ra, γ) την περίοδο 1930-1980 όπου καθιερώθηκε η μέθοδος ανάκτησης για τον Pb, ενώ τα As, Zn και Mn απορρίπτονταν καθώς δεν ήταν οικονομικά εκμεταλλεύσιμα εκείνη την περίοδο και δ) την περίοδο 1980-2014 όπου η μετα-εξορυκτική επίδραση είναι εμφανής είτε λόγω της κατανομής των αποβλήτων στο χερσαίο τμήμα ή / και λόγω μεταφοράς επιβαρυμένου νερού από τον γειτονικό Κόλπο του Θορικού.

Η μελέτη αυτή θα συμβάλει περαιτέρω στον εμπλουτισμό των υφιστάμενων πληροφοριών σχετικά με την ασφάλεια, την αποκατάσταση και την υποστήριξη των εθνικών και διεθνών οργανισμών όσον αφορά στην προστασία του περιβάλλοντος και, ενδεχομένως, τον σχεδιασμό μιας στρατηγικής παρακολούθησης για παρόμοιες περιοχές. Η μελέτη αυτή επίσης θα υποστηρίξει τις κοινωνίες στη λήψη αποφάσεων μιας και οι μελετούμενες περιοχές είναι γνωστές για τις κοινωνικές τους δραστηριότητες όπως ο τουρισμός. Η προτεινόμενη μεθοδολογία μπορεί να εφαρμοστεί σε άλλες ελληνικές (και όχι μόνο) παράκτιες περιοχές όπως η Καβάλα (βιομηχανία φωσφορικών λιπασμάτων, εγκαταστάσεις πετρελαίου), το Αλιβέρι (περιοχή εξόρυξης λιγνίτη, η βιομηχανία τσιμέντου) και η Ιτέα (βιομηχανία βωξίτη) ή στις παρθένες περιοχές που προβλέπονται για μελλοντικές δραστηριότητες εξόρυξης. Επιπλέον, το μοντέλο εκτίμησης της ραδιενεργού δόσης και διασποράς μπορεί να βελτιωθεί και να επικυρωθεί με τον πειραματικό προσδιορισμό των αναγκαίων παραμέτρων ή τη σύγκριση πειραματικών και εκτιμώμενων ρυθμών δόσεων σε έμβιους οργανισμούς (π.χ. μακροφύκη). Αυτή η μεθοδολογία μπορεί επίσης να εφαρμοστεί σε άλλες μήτρες, όπως οι βιο-συσσωρευτές (π.χ. φύκια, μύδια).

Abstract

In this PhD work the utilization of the NORM - metal association and the application of a radiological model (ERICA) to estimate radionuclide and metal dispersion in the marine sediment, was performed. Thus, the affected area due to the anthropogenic activities was determined. Except for the spatial investigation, the marine area was also studied in a temporal aspect. The combination of the estimated sedimentation rates with the mass flux determination, lead to a well-determined time scale. Therefore, the acquired data was verified by historical records of the area. To conclude, in this work a methodology has been established to study natural radioactivity (NORM) near metal mining areas, to assess the mining activities in the area and to verify their impact on coastal areas, using chronological records.

The established methodology was tested in two cases: an ongoing mining area (Stratoni, Ierissos Gulf) and an abandoned one (Oxygono Bay, Lavrio). The first has been for the last decades, a subject of investigation concerning environmental contamination due to the mining activities and waste deposits including mine tailings, flotation tailings, metallurgical slags, waste rock and pyrite concentrate stockpiles. The latter was influenced by the intensive mining and metallurgical activities over the past 100 years, which resulted in the production of huge volumes of wastes (e.g. slags, tailings) and their deposition in piles around Lavrio area, near the coastline or dumped into the sea.

For this reason surface seabed sediments, water samples and sediment cores were collected from the marine environment in order to investigate spatially and temporally the impact of the mining activities. A method for assessing the distribution of contamination due to the enrichment of metals and radionuclides in the sediment was introduced. In the spatial study surface sediments were collected for the determination of natural radioactivity, major elements and trace metals. Their measurements were held in the laboratory by means of gamma-ray spectrometry and X-ray spectroscopy, while the results were combined with *in situ* gamma-ray measurements in the seawater, using the NaI system KATERINA. The trace metals concentrations were used for the assessment of enrichment in the sediments. The radioactivity concentrations were utilized for the enhanced NORM study and the estimation of the sediment-water coefficient Kd, useful for the dose rate assessment in the biota incorporated in the ERICA Assessment Tool. Possible correlations between trace metals, radionuclides and other parameters such as granulometry and mineralogy, were also investigated using a standard statistical software package (SPSS). To complete the spatial investigation, the dispersion of natural radionuclides (^{226}Ra, ^{235}U) was estimated using a simplified generic model incorporated in ERICA and the affected area due to mining was determined.

The temporal study was applied in the sediment cores and included not only the statistical analysis and enrichment factor estimation, but also the radiochronology of the core and the excess mass fluxes estimations. The radiochronology was based on natural (^{210}Pb) and artificial (^{137}Cs) radionuclides, while the obtained trace metal profiles were verified by historical data. The estimated sedimentation rate (radiochronology), was utilized in the mass flux determination, which describes the surficial mass deposition per year and supported the unfolding of historical records included in the trace metal and radionuclide profiles. Therefore, the 100-year impact due to the anthropogenic activities was assessed.

Chapter 1

Introduction

Metals and natural radionuclides, known as NORM, are abundant in the environment and depending predominantly on the regional geology, their concentrations vary considerably. In addition, NORM concentrations can be altered due to various industrial activities, such as mining. According to the European Commission (European Commision (EC), 2003), fossil fuel power stations, mining and metal processing, extraction of oil and gas, phosphate industry, production of titanium oxide pigment, exploitation of zirconium, rare earth processes and production of cement, all contribute towards the alteration of NORM concentrations in the environment. Among the aforementioned industries, mining has a large impact on the environment not only locally (soil), near the mine location, but also at a larger scale (aquatic ecosystems) because of acid mine drainage, mining-milling operations, erosion of waste dumps, wastewaters, disposal of tailings and dust (Salomons, 1995; Allan, 1997; Razo et al., 2004; Li et al. 2006; Shukurov et al., 2014) and accidents (Riba, 2002).

Due to the known ecological impacts of mining, there are many long term studies (e.g. over decades) investigating metal concentrations (both trace and major) in different type of mines (e.g. copper, pyrite, lead, tungsten, manganese, antimony, Pb-Zn, Cu-Ag-Au-Zn, bauxite). On the other hand, the study of natural radioactivity in mines is poorer, due to the fact that the influence of the elevated activity concentrations to human and non-human health, was discovered much more recently. Thus, the published radionuclide investigation has been mainly focused on a much more limited variety of mines, such as coal, phosphate, uranium, oil and gold. Additionally, the time difference between metal and radionuclide investigations resulted in lack of data regarding the combined studies of these two parameters.

Due to the differences in scientific approaches for the study of mining impact different matrices have been studied for metals and radionuclides. For example, metal measurements have been performed in streams, lakes, groundwater, soils, plants and sediments (Li et al., 2006; Becker et al., 2001; Kerfoot et al., 2004; Yellishetty et al., 2009; Batista et al., 2007; Li et al., 2014; Rowan et al., 1995; Villa et al., 2011, Kusin et al., 2017), while solely NORM studies have been held in recent years, mainly in soil, water bodies (e.g. drainage basins, groundwater, river) and mussels (Njinga and Tshivhase, 2017; Jodlowski et al., 2017; Chalupnik et al., 2017; Saidu and Bala, 2018; Bezerra et al., 2018; Doering and Bollhofer, 2017).

Among the aforementioned matrices, those studied the most near mines, are soil and sediment, because both serve as a sink for contaminants and contain the depositional record of contamination. Therefore, surface and core sediments have been previously used to provide spatial and temporal information focusing mainly on metal concentrations, despite the fact that both metals and radionuclides are particle reactive and adsorbed by sediments. This is verified by the utilization of core sediments for metal accumulation and pollution assessment with regards to the description of past environmental conditions and history contamination investigation (Valette-Silver 1993) based on well-established radiological methods such as ^{210}Pb and/or ^{137}Cs (Vaalgamaa & Korhola, 2007; Ruiz-Fernandez & Hillaire-Marcel, 2009; Sanchez-Cabeza & Ruiz-Fernadez, 2012; Szarlowicz et al., 2013; Baskaran et al., 2014). However, as previously mentioned these studies have not been performed for

radioactivity. An effort has been attempted in recent years to fill the gap of combined metal-radionuclide studies, thus spatial investigations have been performed in soil media (Liang et al., 2017; Bai et al., 2017; Alashrah and El-Taher, 2018) and milk (Giri et al., 2011) amongst other matrices (Doering & Bollhofer, 2016). In additiona, vertical investigations have been applied in streams, river and lakes (Wennrich et al 2004; Pavlovic et al. 2005; Grygar et al. 2016; Noli & Tsamos 2018). However, the literature still lacks radionuclide and metal studies in marine environments, especially in response to multi-metallic mines.

Another aspect of the mining activities, is the remaining impact after the cessation of the industry, due to high radionuclide and metal concentrations accumulated in the affected sediments and wastes. Therefore, spatial and temporal investigation is important not only for ongoing but also for abandoned mines. For this reason, different matrices such as plant, biota, soil and sediment (surface and core) have been studied in abandoned metallic mines worldwide to investigate the post-mining effect (Komnitsas et al. 1995; Rowan et al. 1995; Larsen et al. 2001; Navarro et al. 2008; Bech et al. 2012; Gomez-Gonzales et al. 2015; Garcia-Ordiales et al. 2017), however focusing only on metal concentrations.

1.1 The status of coastal areas characterized with mining activities

According to the reasons mentioned above, mines are usually situated in the vicinity of rivers, lakes or coastal areas. Specifically, the latter acts as a receptor for both water transfer contaminants (river and drainage basin routes) and/or direct waste disposal. In this work two coastal areas of Greece, Stratoni and Lavrio, were studied, where mining activities occur (Stratoni) and have ceased (Lavrio). The status of both areas regarding wastes follows:

1.1.1 Coastal area of Stratoni

The wider area of Stratoni at Ierissos Gulf, is known for its ore deposits and long-term mining from ancient times (600 BC) until today. Stratoni is characterized by mixed sulphide and manganese ore deposits, which have been - and still are -exploited to extract different minerals such as pyrite (FeS_2), sphalerite (blende) (ZnS), galena (PbS), arsenopyrite (FeAsS), rhodochrosite ($MnCO_3$), chalcopyrite ($CuFeS_2$), bornite (Cu_5FeS_4) and magnetite (Fe_3O_4). The first three minerals are known as P.B.G. The mining activities resulted in affecting the area due to different type of wastes and waste disposals. For example, mine tailings, flotation tailings, metallurgical slags, waste rock and pyrite concentrated stockpiles (Kelepertzis et al., 2006; 2012), are some of the solid wastes produced. Part of the solid wastes (mine and flotation tailings) was and is still stored for future gold exploitation, while others (e.g. metallurgical processes) were disposed at various locations between Stratoni and Stratoniki, along the streams of Stratoni area (Charalampides et al., 2013; Kelepertzis et al. 2006). As far as the marine environment is concerned, both mine and flotation tailings were dispersed in it. The former were directly discharged into the nearshore environment until 1983 (Kelepertzis et al., 2013), while the latter were also directly discharged into marine environment through a pipeline. Flotation tailings are characterized as a slurry mixture of finely ground solids and process water, which is discharged daily. Other facilities, also located at Stratoni port, include a flotation plant, a load hoper and feeder and a transfer

and ship loader conveyor. Metal concentrations have been monitored for the terrestrial region (soil, rivers) by the exploration company (Kelepertzis et al., 2006, 2012; Lazaridou-Dimitriadou et al., 2004), and for the marine sediment by personal initiatives (Sakellariadou, 1987; Stamatis et al., 2002). Ierissos Gulf is a touristic region characterized by commercial fishing grounds, industrial and agricultural activities, it is thus of special interest to investigate the impact of those activities.

1.1.2 Coastal area of Lavrio

The wider area of Lavrio, located at Lavreotiki Peninsula, eastern Attica, bears mixed sulphide ore bodies which developed along contacts of schist with marble (Kontopoulos et al. 1995). More specifically, the P.B.G. massive sulfide mineralization of Lavrio is composed of Ag-bearing galena (PbS), pyrite (FeS_2), sphalerite (ZnS), arsenopyrite (FeAsS) and chalcopyrite ($CuFeS_2$). Lavrio is the area which hosted mining activities from ancient times (3000 B.C.) until the 1980s, producing silver and lead. A huge volume of wastes were produced due to the intensive mining and metallurgical activities, such as slags, tailings and low grade ore. These wastes were deposited in piles around Lavrio area, near the coastline or dumped into the sea. (Stamatis et al., 2001; Alexakis 2011). An extensive study and mapping of the disposed waste has been performed by the Institute of Geology and Mineral Exploration (IGME), was focused on the terrestrial region. The contamination in Lavrio has been also studied for different matrices such as mine wastes, soil, streams, groundwater, dust, animals, plants, urine, blood and teeth of children (Stamatis et al. 2001; Aberg et al. 2001; Xenidis et al. 2003; Alexakis 2011). Few data are known for the marine environment such as the geochemical studies of Lavrio port (Haralambides and Sakellariadou, 2008) and of the eastern marine part of Lavreotiki peninsula (Zotiadis and Kelepertzis, 1997). The focus on the terrestrial region is explained because Lavrio city expands from close to the waste stockpiles to on top of them, exposing the 10000 inhabitants to metal contamination. Additionally, Lavrio is also a touristic region, which attracts among others those who participate in wind-surfing.

1.2 Radionuclide and metals as environmental tracers for mining activities

In the beginning of this chapter, the occurring studies near mine areas regarding different matrices (e.g. soil, sediment, water) and parameters (metals and radionuclides) were presented. It became clear that the parameters are investigated separately depending on the type of the mine (e.g. bauxite, copper, uranium), while combined investigations of these parameters in the marine environment for on-going and abandoned mines are absent. Nevertheless, among the studies which combined the metal-radionuclide concentrations, some key elements are commonly measured, such as ^{226}Ra, ^{232}Th, As, Cu, Pb, Zn, Mn, Al and Fe (Giri et al., 2011; Wennrich et al. 2004; Doering &Bollhofer, 2016; Grygar et al. 2016; Bai et al., 2017; Liang et al., 2017; Alashrah & El-Taher, 2018; Noli &Tsamos, 2018), indicating a required investigation of these elements in different type of mines.

1.3 Motivation and objectives of this study

The impact of the mining activities, as well as the utilization of sediments to study the mining footprint became clear in this work. The sink-like behavior of the sediment was taken into consideration in the studies of mining impact near aquatic environments (e.g. rivers, lakes), however the analogous investigation in the marine environment is characterized by lack of published data. Additionally, the spatial studies in the marine environment have been performed spontaneously and not in for consistent monitoring purposes, thus the need to obtain retrospective information of past events due to the absence of long-term monitoring data arose. The utilization of both spatial and vertical studies in marine environment to estimate the affected area and to identify and assess previous impacts due to mining in a temporal manner, is a methodology developed in this work. Moreover, in this work the combination of radionuclides and metals as key elements has been implemented, so as to assess the radiological and metallic impact both spatially and temporally.

The spatial metal impact was estimated rapidly using pollution indices (e.g. enrichment factor, pollution load index), while the radioactive influence was achieved by applying a specified and simplified software for the radiological risk assessment and the radionuclide dispersion determination (ERICA). This way, the affected area based on NORM concentrations was determined and the statistical correlations among radionuclides and metals, indicated a possible metallic affected area. In the case where no strong correlations were observed or the dispersion model could not be applied, a spatial estimation was performed utilizing the experimental data and geostatistical methods via ArcGIS®.

Working in the same pattern, the vertical metal and radionuclide profiles were transformed to temporal profiles using radio-chronological models (^{210}Pb, ^{137}Cs). Then the temporal profiles were utilized for the reconstruction of pollution events and were validated with historical data. This way the metallic contamination was also assessed temporally. Moreover, the determination of the rate of the disposed mass assisted in further analysis of past event reconstruction. In the present work an indicative vertical assessment of mining impact was proposed in case of the absent parameters such as sedimentation rates and major element concentrations. This approach reveals the sediment core layers which correspond to pre-mining periods.

To summarize, in this work a multidisciplinary approach is proposed, combining nuclear (gamma ray spectrometry) and atomic physics (XRF spectroscopy), as well as geology and geochemistry, to study a multi-parametric problem: the impact of anthropogenic activities on radioactivity and metal concentrations in the marine environment near mining areas. The main objectives of the developed methodology is (a) to study the dispersion of radionuclides, (b) to reconstruct the contamination events and (c) to assess the contamination, spatially and temporally, for both radionuclides and metals. A well-organized sampling outline is required in order to secure precise geographic coordinates and undisturbed sediment cores, for the calibration and validation of the dispersion model, as well as the history reconstruction and verification of the chronological models.

Chapter 2

Theoretical background

The radionuclide and metal concentrations of the present work were obtained via gamma-ray and X-ray spectrometry, respectively. Thus, in this chapter the basic theory regarding the gamma-ray and X-ray emission and detection are presented. The radiological and metal assessment was also performed in this work, in a horizontal (spatial) and vertical manner, in which the time was incorporated. The process of the radiological assessment will be presented in chapter 3, while in this chapter the pollution indices are mentioned, which were utilized for the metal assessment. Additionally, chronological models which are based on radionuclides and are useful for integration of time in vertical radionuclide and metal profiles are presented. Lastly, the basic theory regarding the performed statistical analysis is also included in this chapter.

2.1 X-ray emission

The X-radiation is the result of atomic electron rearrangement, after electron capture, internal conversion or artificial atomic excitation using high-energy beams of charged particles (e.g. electrons, protons) or X-rays. The electron during e.g. the excitation process, is ejected from the bound state having a kinetic energy equal to the excitation energy minus electron's atomic binding energy. The excited atom or an electron from another state will move preferentially to the lowest possible energy state so as to fill the vacant spot (E_i), emitting X-rays. The electron transitions are characterized by the letters K, L, M, etc. which represent the final energy state (E_f). Therefore, transitions to the L state, from other initial state, are called L X-rays. These discrete characteristics X-rays, can be used as atom's fingerprints. The emitted electromagnetic radiation (X-ray) during an electron transition is characterized by the frequency:

$$v = \frac{E_i - E_f}{h} \qquad \text{(Eq. 2.1)}$$

where,

E_i is the energy of the initial orbit (state), E_f is the energy of the final orbit (state) and h is Planck's constant.

According to Moseley's law the energy of the X-ray depends on the atomic number and it may range from a few eV (light elements) to few hundreds of keV (heaviest elements).

$$E_x = hv = E_i - E_f = k\,(Z - a)^2 \qquad \text{(Eq. 2.2)}$$

where,

Z is the atomic number, k is a constant for a particular spectral series and α is a screening constant for the repulsion correction due to other electrons in the atoms (Van Grieken RE & Markowicz AA, 2002).

During the atomic electron rearrangement, the released energy can be either emitted through a photon (radioactive emission) or absorbed by a bound electron of a higher shell, causing its ejection. This radiationless transition is called Auger effect and the emitted electron is called Auger electron. The Auger effect increases with a

decrease between the energy states, while reaches a peak for low-Z elements. This effect is not in the scope of this work.

Additionally, X-rays can be emitted in a continuous (not discrete X-rays) spectrum when electrons or high-energy charged particles (e.g. protons, α-particles), lose energy in passing through the Coulomb field of a nucleus. During this interaction, the radiant energy (photons) lost by the electron is called Bremsstrahlung. The continuous spectrum can be produced by the acceleration of electrons in a voltage tube. However, the emission of continuous X-ray radiation is not in the scope of this work.

2.2 Gamma-ray emission

Gamma emission is the process where the nucleus loses its surplus excitation energy and it is usually a by-product of alpha and beta decay. In gamma emission, the nucleus goes from an excited state to a state of lower energy and the energy difference between the two states is released in the form of a photon. The gamma rays are monoenergetic and the gamma emission is described as:

$$ {}^{A}_{Z}X^{*} \rightarrow {}^{A}_{Z}X + \gamma \qquad \text{(Eq. 2.3)} $$

where,

X^{*} indicates the excited nucleus.

The half-lives of gamma emission range usually from 10^{-9} s to hours or days. A competing process to gamma emission is internal conversion, in which the nucleus de-excites by transferring its energy directly to an atomic electron. This process is one of the main processes which contribute to X-ray radiation as mentioned before (see 2.1), however this process is not studied in the present work.

Radioactivity is the process by which an unstable atomic nucleus loses energy by emitting radiation. It can be divided in two main categories, natural and artificial, depending on the origin of radioactivity, anthropogenic and non-anthropogenic, respectively. Natural or artificial radioactive nuclides with Z>82 (elements above ^{208}Pb) tend to gradually decay via alpha, beta and gamma emission. In this work, the latter emission process will be discussed in detail. The origin of radioactive nuclei can be Big Bang, cosmic processes (e.g. supernova), or nuclear reactions occurring on Earth due to natural or anthropogenic causes. Except from radioactive isotopes that are present in materials around us, such as rocks and minerals and were condensed with the Earth 4.5 10^{9} y ago, there are natural sources of radioactivity due to nuclear reactions occurring in the atmosphere (e.g. ^{3}H, ^{14}C). The natural radioactivity or naturally occurring radioactive materials (NORM) belonging to the first category can be divided into three groups: (a) ^{238}U, (b) ^{235}U and ^{232}Th series (Fig. 2.1).

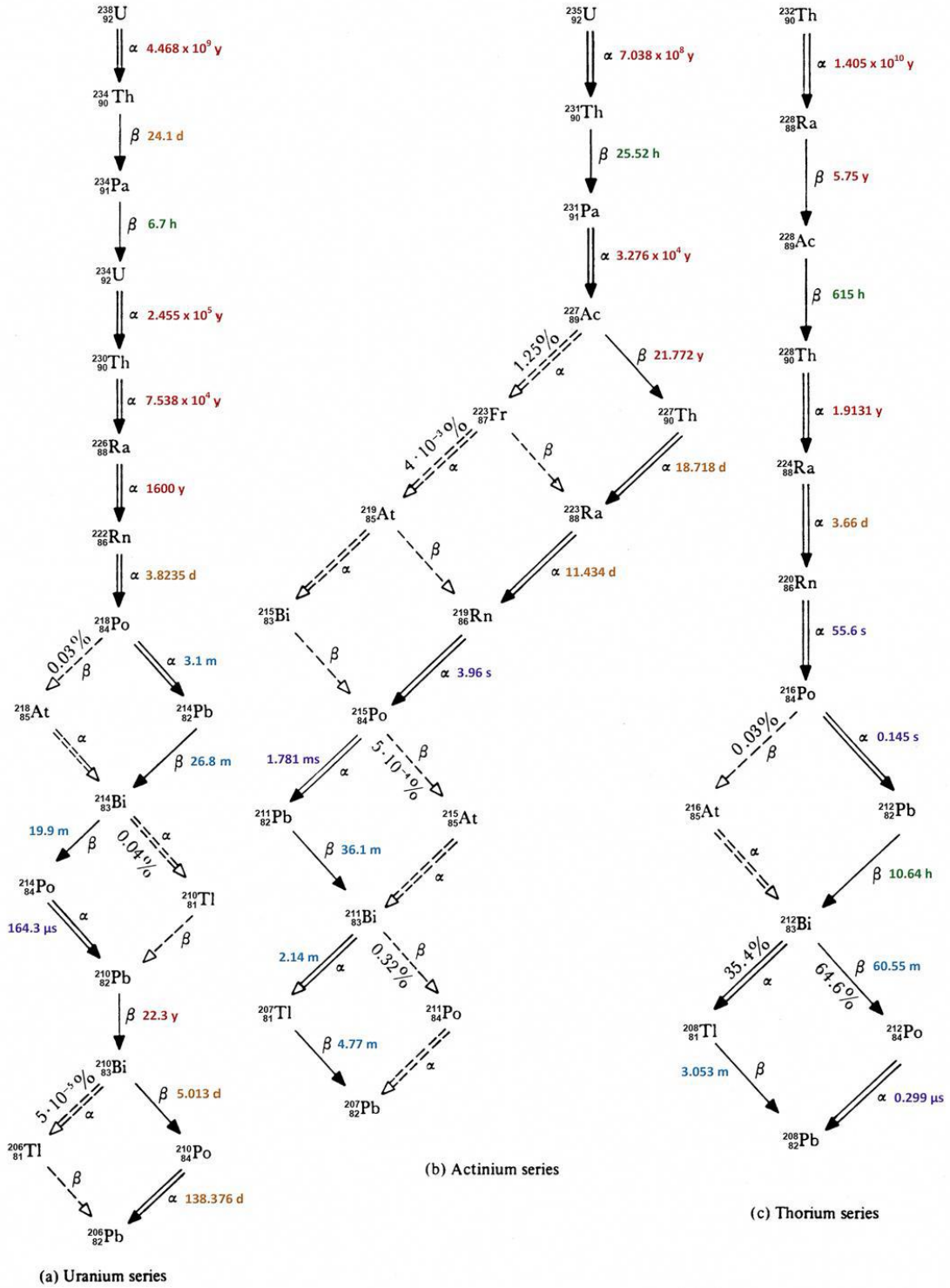

Fig. 2.1: The decay series of natural radioactivity **(Mermier & Seldon, 1969)**

Radioactive decay law

An unstable isotope decays exponentially in time, as stated by the radioactive decay law. The decay rate ($\frac{dN}{dt}$) is proportional to the present number of atoms (N) of radionuclide in the source, assuming that no new nuclei are introduced into the source.

$$A = -\frac{dN}{dt} = \lambda N \qquad \text{(Eq. 2.4)}$$

where,

A is the activity or rate of disintegration of the radionuclide (Bq) and λ is the disintegration or decay constant (s^{-1}). The units of activity are the Becquerel (Bq), which represents one decay per second or Curie (Ci) equal to 3.7 10^{10} Bq.

The decay constant (λ) represents the probability of a radionuclide to decay per unit time. The number of radionuclides N(t) follow the exponential behaviour (Eq. 2.5)

$$N(\mathrm{t}) = \mathrm{N}_0\, e^{-\lambda t} \qquad \text{(Eq. 2.5)}$$

where,

N_0 is the number of radionuclides at t=0 s. The decay equation describes also the radioactivity A(t), as it is proportional to the number of radionuclides.

If p(t) is the probability that a nucleus will decay between t and t+dt then the mean lifetime (τ) which represents the needed time for a sample of radionuclides to decay to 1/e of its initial activity is defined as:

$$\tau = \frac{\int_0^\infty t p(t) dt}{\int_0^\infty p(t) dt} = \frac{\int_0^\infty t e^{-\lambda t} \lambda dt}{\int_0^\infty e^{-\lambda t} \lambda dt} = \frac{1}{\lambda} \qquad \text{(Eq. 2.6)}$$

A more convenient magnitude is the half-life ($t_{1/2}$) of the radionuclide, representing the time during which radioactivity decreases to the half of its original value.

$$\frac{N(t_{1/2})}{N_0} = \frac{1}{2} \Rightarrow e^{-\lambda t_{1/2}} = \frac{1}{2} \Rightarrow \lambda = \frac{\ln 2}{t_{1/2}} \qquad \text{(Eq. 2.7)}$$

In the case of voluminous samples the term of specific activity is used to describe the activity of a radionuclide per unit mass (Bq kg^{-1}) or per unit volume (Bq m^3), assuming uniformity in activity distribution.

When a radioactive decay results in the production of a radioactive nucleus, which is also radioactive and decays to a third radioactive nucleus, a radioactive chain is generated. The original nucleus is called "parent" nuclide, while the produced radioactive products are referred as "daughters" or "progenies" of the parent nuclide. The Bateman's equation describes the number of atoms of the i^{th} isotope $N_i(t)$ of the series ($N_i(0)$) at time t=0 and $N_i(0)=0$ for i >1) (Tsoulfanidis & Landsberger, 2015).

$$N_i(t) = \lambda_1 \lambda_2 \cdots \lambda_{i-1} N_1(0) \sum_{j=1}^{i} \frac{e^{-\lambda_j t}}{\prod_{k \neq j} (\lambda_k - \lambda_j)} \qquad \text{(Eq. 2.8)}$$

There are three types of equilibrium

a) secular equilibrium ($\lambda_i << \lambda_{i+1}$): the daughter nuclide is decaying in the same rate at which it is produced
b) transient equilibrium ($\lambda_i < \lambda_{i+1}$): the daughter nuclide decays with the characteristic decay constant of its parent
c) non equilibrium ($\lambda_i > \lambda_{i+1}$): the parent nuclide decays quickly and the daughter activity rises to a maximum and then decays with its characteristic decay constant.

2.3 X-ray detection

The X-rays are also photons of lower energy than gamma rays, thus they can interact with matter through the main processes of photoelectric effect and Compton scattering. As mentioned above the emission of characteristic X-rays is preceded by ionization of inner atomic shells as a result of the photoelectric effect (see section 2.4.1) and Compton scattering (see section 2.4.2). The K shell electrons, as the most tightly bound to the atom orbit, are the most important for the photoelectric effect in the energy region considered in X-Ray spectrometry. However, the photoelectric effect cannot occur in the case of photon energy below the binding energy of a given shell. Another mechanism with which X-rays interact with matter is the elastic or coherent scattering called Rayleigh. During Rayleigh scattering the incident X-ray photon interacts with the whole atom and the electrons oscillate in the X-ray photon frequency, while the photon scatters without changing its energy and no energy is transferred to the atom.

2.4 Gamma-ray detection

The primary processes with which gamma rays interact with the matter are the photoelectric effect, Compton scattering and pair production. These processes are described briefly below.

2.4.1 Photoelectric effect

During the photoelectric effect (Fig. 2.2) a photon (gamma ray) interacts with a bound atomic electron, resulting in the disappearance of the photon and the ejection of the atomic electron from the atom. The free electron is called photoelectron and is characterized by a kinetic energy of

$$E_e = \mathrm{E}_\gamma - E_b \qquad \text{(Eq. 2.9)}$$

where,

E_e is the kinetic energy of the photoelectron, E_γ is the photon energy and E_b is the binding energy of the electron to the atomic orbit.

The photoelectric effect always occurs on bound electrons, so as to conserve momentum. Thus the nucleus absorbs the recoil momentum.

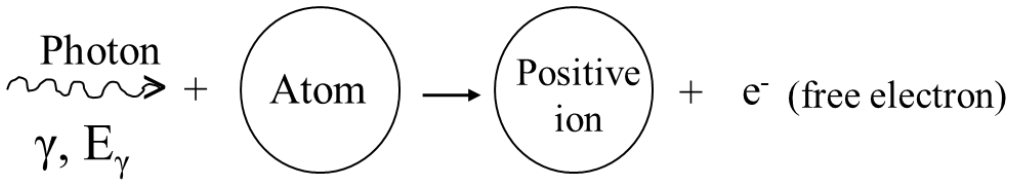

Fig. 2.2: The photoelectric effect

2.4.2 Compton scattering

During Compton scattering or Compton effect (Fig. 2.3) a photon scatters from a free or nearly free atomic electron, resulting in a less energetic photon and a scattered electron carrying the energy lost by the photon. The kinetic energy of the scattered electron is given by

$$E_e = \mathrm{E}_\gamma - E_{\gamma'} \qquad \text{(Eq. 2.10)}$$

where, E_e is the kinetic energy of the scattered electron, E_γ is the photon energy and $E_{\gamma'}$ is the energy of the scattered photon.

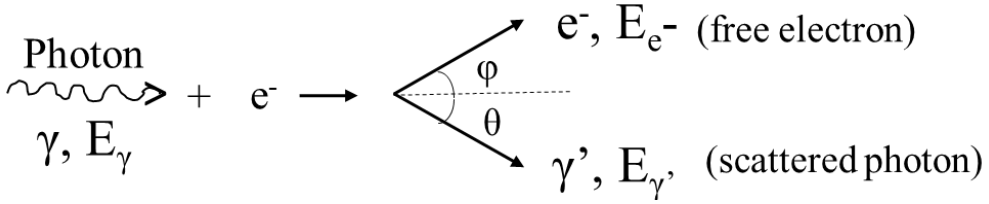

Fig. 2.3: The Compton scattering (or effect)

2.4.3 Pair production

In the pair production process (Fig. 2.4) a photon creates an electron-positron pair, while the photon disappears in this process. In order to conserve the momentum, this process occurs in the presence of a third body, usually a nucleus. Additionally, the photon energy must be at least 1.022 MeV, equals to the rest masses of electron-positron pair. According to the conservation of energy, the kinetic energy of the electron and the positron is given by

$$E_{e^-} + E_{e^+} = E_\gamma - (mc^2)_{e^-} - (mc^2)_{e^+} = E_\gamma - 1.022MeV \qquad \text{(Eq. 2.11)}$$

where,

E_e^- is the kinetic energy of the electron, E_e^+ is the kinetic energy of the positron, E_γ is the photon energy and mc^2 is the rest mass of electron or positron.

The electron and positron share the available kinetic energy

$$E_{e^-} = E_{e^+} = \frac{1}{2}(E_\gamma - 1.022MeV) \qquad \text{(Eq. 2.12)}$$

During pair production the original photon is eliminated, however two photons are created when the positron is annihilated.

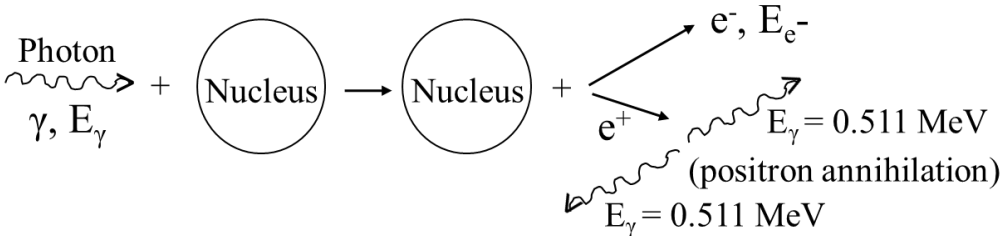

Fig. 2.4: The pair production. In this process the disappearance of the photon is followed by the positron-electron pair creation. After the positron annihilation, two 0.511 MeV photons are produced.

Upon completing the description of the main processes with which gamma rays interact with matter and thus can be detected, it is important to present the dominance of these processes as incident photon energy (E_γ) and the atomic number (Z) change. The dependence of the three main gamma ray interaction processes, with E_γ and Z, is depicted in Fig. 2.5.

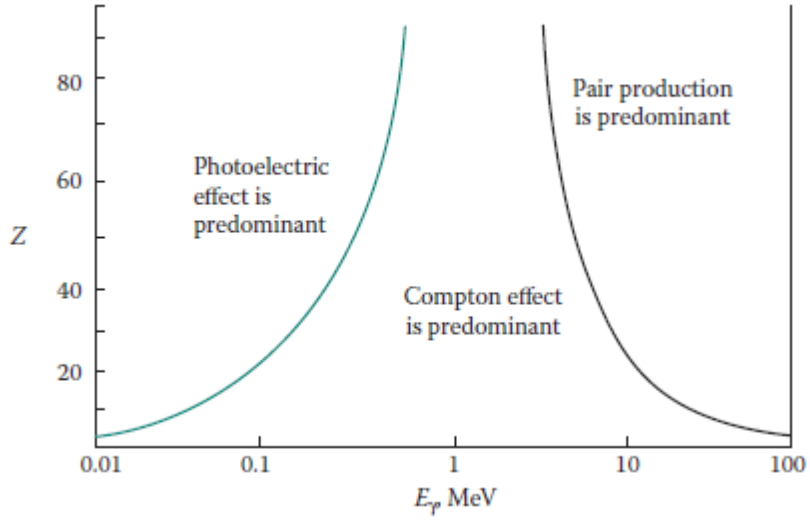

Fig. 2.5: The main gamma-ray interaction processes and their dominance regions **(Tsoulfanidis & Landsberger, 2015)**.

2.5 Sediment quality guidelines and indices

Contaminants such as metals and radionuclides, are characterized by their affinity to sediments. Thus, sediments can behave like sinks to the elements entering the aquatic environment. Nevertheless, the trapped elements can be recycled back to the water column, where they pose a threat to aquatic environments via the variation of the physico-chemical characteristics of the overlying water and sediment. In order to determine the extent of contamination in an aquatic system using the (heavy) metal load in the sediments, it is important to establish indicators of contamination and the natural level of these substances. The sources of metals in the aquatic system can be multiple, with the main ones being geochemical processes, agriculture, industrialization (e.g. mining, metallurgy) and waste disposal (e.g. leachates from landfills). Therefore, the input of metals in the aquatic environment can be atmospheric fallout, geological weathering, accidental leaks, dumping wastes and runoff of terrestrial systems (industrial and domestic effluents).

The contamination assessment of metals in the aquatic environment has been studied for many years and different approaches have been proposed. There are many established indicators used for the contamination assessment such as the geoaccumulation index (Igeo), contamination factor (CF), enrichment factor (EF), pollution load index (PLI), contamination degree (Cd), modified degree of contamination (mCd), potential ecological risk index (RI) and ecotoxicological sense of metals using sediment quality guidelines (SQG). The first four methods are the most common, however all the aforementioned methods are described briefly below. In this work EF, PLI and SQG have been applied. As it will be clear from the following description of the methods of contamination assessment, there are no indicators regarding the natural occurring radioactive materials (NORM) and the technically enhanced ones (TENORM), especially in the aquatic (UNSCEAR, 2000) environment. An approach to estimate sediment quality guidelines was attempted by Thompson et al. (2005), near an uranium mining in Canada, withougt satisfactory results. However,

an approach to assess TENORM, could be a comparison with a background area and the comparison with the world median concentration of natural radionuclides in the soil (UNSCEAR, 2000).

Geoaccumulation Index (Igeo)

The accumulation index was proposed by (Muller, 1979) so as to determine and define metal contamination in aquatic sediments by comparing current concentrations with background levels determined by

$$I_{geo} = \log_2 \frac{C_n}{1.5B_n} \qquad \text{(Eq. 2.13)}$$

where,

C_n is the concentration of the examined metal (n) in clay fraction (<2μm) of the sediment sample, B_n is the geochemical background values of the metal of interest (n) in fossil argillaceous sediment (e.g. average shale) and 1.5 is the background matrix correction factor due to lithogenic effects.

The accumulation index consists of seven grades and the highest grade (6) reflects 100-fold enrichment above the background values. The classification of the sediment contamination based on the grades of I_{geo} index are: Igeo ≤ 0 (grade 0) represents an unpolluted area, 0<Igeo ≤1 (grade 1) indicates an unpolluted to moderately polluted area, 1<Igeo ≤2 (grade 2) indicates a moderately polluted area, 2<Igeo ≤3 (grade 3) indicates a moderately polluted area to strongly polluted area, 3<Igeo ≤4 (grade 4) indicates a strongly polluted area, 4<Igeo ≤5 (grade 5) indicates a strongly to extremely polluted area and Igeo >5 (grade 6) indicates an extremely polluted area.

Contamination Factor (CF or C_f)

The contamination factor can be determined as the ratio between the metal concentration in the sediment and the background value of the metal.

$$CF = \frac{C_n}{B_n} \qquad \text{(Eq. 2.14)}$$

where,

C_n is the concentration of the examined metal (n) of the sediment sample (usually from surficial sediments) and B_n is the geochemical or preindustrial background values of the metal of interest (n).

In the case of $C_n > B_n$ the sample is contaminated or enriched in the examined element, while for $C_n < B_n$ the sample is not enriched. According to Hakanson (1980) CF<1 indicates low contamination; 1≤CF<3 moderate contamination; 3≤CF<6 considerable contamination and CF≥6 very high contamination. The substances Hakanson (1980) took into account for the estimation of contamination factor were PCB, Hg, Cd, As, Cu, Pb, Cr and Zn. The contamination factor was introduced mainly for lake systems, but it has been generalized in different aquatic systems (e.g. coastal areas).

Enrichment Factor (EF)

Another approximation to estimate any potential impact due to anthropogenic activities on marine sediments is the enrichment factor (EF) for metal concentrations above an uncontaminated background value (Salomons and Forstner, 1984). The EF represents the normalized metal concentration in the sample to a reference or background material free of contamination. This technique involves the metal

normalization to a conservative non-anthropogenic element, which also reduces the grain size effects in the sediment samples (Salomons and Forstner 1984). A variety of elements can be fitted for metal normalization, but Al and Fe are the most commonly used. For the selection of the proper normalizing element was adopted the methodology described by Karageorgis et al. (2009). Based on this methodology Al was selected as normalizing element, as it showed the minimum coefficient of variation (V). In this work Al was used as metal normalizer and the EF is given in:

$$EF = \frac{\frac{C_{sample}}{Al_{sample}}}{\frac{C_{bgr}}{Al_{bgr}}} \qquad \text{(Eq. 2.15)}$$

where,

C_{sample} is the concentration of the examined metal, Al_{sample} the concentration of the normalizer metal, $C_{bgr.}$ the concentration of the examined metal in the reference or background sample and Al_{bgr} the concentration of the normalizer metal in the reference sample.

Enrichment factor above a certain threshold indicates the level of contamination. The classification of enrichment is given according to (Birch and Davies (2003): where EF≤1 indicates no enrichment, EF≤3 a minor enrichment, 3<EF≤5 a moderate enrichment, 5<EF≤10 a moderately severe enrichment, 10<EF≤25 a severe enrichment, 25<EF≤50 a very severe enrichment, and EF>50 an extremely severe enrichment. Furthermore, according to Salomons and Forstner (1984) and using the continental crust concentrations if EF>4, then the enrichment is due to other sources except from weathering (e.g. anthropogenic).

Pollution Load Index (PLI)

The pollution load index was introduced by Tomlinson (1980) so as to classify the metal level in estuaries and it is based on the determination of the highest contamination factors (CF) according to the following equation. The main idea of PLI is to give an overall level of metal toxicity by estimating the number of times by which the metal concentrations in the sediment exceeded the background concentration.

$$PLI = \sqrt[n]{CF_1 \cdot CF_2 \cdots CF_n} \qquad \text{(Eq. 2.16)}$$

where,

CF_i is the concentration factor of the metals of interest for i=1, 2, … n

The classification of PLI can be divided into two levels: polluted (PLI>1) and unpolluted (PLI<1).

Contamination Degree (Cd)

To facilitate pollution control Hakanson (1980) proposed the degree of contamination by estimating the overall contamination:

$$C_d = \sum_{i=1}^{n} CF_i \qquad \text{(Eq. 2.17)}$$

where,

CF_i is the concentration factor of the metals of interest for i=1,2,..n.

The classification of contamination according to Hakanson (1980) is: Cd<8 low degree of contamination, 8≤ Cd<16 moderate degree of contamination, 16≤ Cd<32 considerable degree of contamination and Cd≥32 high degree of contamination

indicating serious anthropogenic impact. The substances Hakanson (1980) took into account for the estimation of the degree of contamination were PCB, Hg, Cd, As, Cu, Pb, Cr and Zn. Therefore, the C_d and its classification are restricted to only these substances and cannot be generalized.

Modified Degree of Contamination (mCd)

Due to the restrictions of the degree of contamination factor, Abrahim (2005) introduced a generalised form of Hakanson's C_d, achieving an overall average value for a range of contaminants at estuaries. The main modifications refer to the use of the mean concentration from at least three samples, there is no upper limit of the included metals and as baseline values can be utilized the concentrations of the lower part of the core or of similar nearby uncontaminated sediments. The modified equation is determined as:

$$mC_d = \frac{\sum_{i=1}^{n} CF_i}{n} \qquad \text{(Eq. 2.18)}$$

where,

CF is the contamination factor of the i^{th} element (or contaminant) and n is the number of the analysed elements.

The classification of mC_d is the following: $mC_d<1.5$ indicates nil or very low degree of contamination, $1.5\leq mC_d<2$ low degree of contamination, $2\leq mC_d<4$ moderate degree of contamination, $4\leq mC_d<8$ high degree of contamination, $8\leq mC_d<16$ very high degree of contamination, $16\leq mC_d<32$ extremely high degree of contamination and $mC_d\geq 2$ ultra high degree of contamination.

Potential Ecological Risk Index (RI)

The potential ecological risk index is calculated by the sum of the risk factors as proposed by Hakanson (1980) for lake ecosystems. It is a method to assess the characteristics and environmental behavior of metal contaminants in sediments.

$$RI = \sum_{i=1}^{8} Er_i = \sum_{i=1}^{8} Tr_i \cdot CF_i \qquad \text{(Eq. 2.19)}$$

where,

Er_i is the risk factor, Tr_i is the toxic-response factor for a given substance (PCB, Hg, Cd, As, Cu, Pb, Cr and Zn) and CF_i is the contamination factor of the examined substances. Tr_i is a function of the bioproduction index (BPI) and assuming an intermediate value of BPI=5 the TR_i values become PCB=40, Hg=40, Cd=30, As=10, Cu=5, Pb=5, Cr=2 and Zn=1.

The classification of RI is: $RI<150$ indicates low ecological risk for the lake or basin, $150\leq RI<300$ moderate ecological risk for the lake or basin, $300\leq RI<600$ considerable ecological risk for the lake or basin and $RI\geq 600$ very high ecological risk for the lake or basin.

Sediment Quality Guidelines (SQG)

The sediment quality guidelines are metal concentrations, that can be used in environmental risk assessment, so as to evaluate the potential of adverse impacts on aquatic organisms or can be utilized as environmental guidance and serve as national benchmarks. The SQG can be derived either mechanistically incorporating chemical and biological factors for the estimation of contaminant bioavailability or empirically using statistical analyses between sediment concentrations and biological effects.

Usually, they are characterized by two screening levels low and high (SEL or ISQG high). The low effect level (LEL or PEL or PEC or ISQG low) implies that adverse effects are not expected on the benthic life if the total trace element concentration is below this value, while the severe effect level (SEL) indicates that harmful effects are expected to occur in the benthic community if the concentration in the sediment is above this value. (Thompson et al., 2005).

As it has been clear in the description of the methods to assess contamination, the establishment of background or reference value is necessary for the determination of contamination. For the establishment of background values (pre-anthropogenic concentrations) different ideas have been proposed according to several empirical methods (e.g. use of global mean concentrations, pristine areas within the same ecosystem, pristine fluvial sediments, use of sedimentary cores of high depth), with the main ones being (Salomons and Forstner, 1984; Birch, 2017):

(a) the concentrations of the average shale composition (global mean concentrations)
(b) the utilization of fossil aquatic sediments by environments characterized as standards
(c) the values of recent deposits in relatively unpolluted areas and
(d) the utilization of short, dated sedimentary cores, which provide historical records of occurring events. Despite the estimation of the background levels, the core sampling may inform us of the element changes over an extended period of time. The study of sediment cores is suited for the distinction of natural metal enrichment in zones of mineralization and anthropogenic activities near mining and smelting processes.

2.6 Sediment chronological models

An important aspect of sediments is that behave as sink for contaminants, thus they can be used not only to assess the contamination level but also to record the impact of natural processes or anthropogenic activities. Sedimentary cores can be useful to provide retrospective information on the past characteristics of the aquatic environment and can be dated by means of certain granulometric characteristic, by pollen assemblages or by isotope measurements (Salomons and Forstner, 1984). During the last decades natural and artificial radionuclides have been used for chronological applications and the estimation of the sedimentation rates in the aquatic systems. The origin of the artificial radionuclides may be due to nuclear tests in the early 1960's, nuclear accidents (e.g. Chernobyl, Fukushima) and possible river runoff near nuclear power plants. In this work, some dating methods of sediments based either on natural or artificial radionuclides are going to be presented briefly. Among the radiodating methods those based on ^{210}Pb and ^{137}Cs have proved to be advantageous (Salomons and Forstner, 1984). The described methods will be focused on the marine environment.

Natural radionuclides:

^{7}Be ($t_{1/2}$=53.3 d) is a natural radionuclide produced in the upper atmosphere by cosmic ray spallation of nitrogen and oxygen.The dating method can be performed so as to estimate short-term accumulation rates in the near-shore and lake sediments for more than 200 days. The ^{7}Be is distributed by atmospheric deposition and thus can be useful for studying short-term and seasonal variation of sediment reworking (Krishnaswami et al., 1980).

^{234}Th ($t_{1/2}$=24.1 d) can be used so as to determine particle-mixing rates in near-shore sediments. The equilibrium between the parent (^{238}U) and the daughter (^{234}Th) nuclide results in the production of ^{234}Th at a constant rate in the water column. The parent nuclide is conservative element in the seawater, however ^{234}Th is very particle-reactive element and rapidly removes from the solution by binding with suspended particular matter. Thus the ^{234}Th/^{238}U disequilibrium (excess ^{234}Th) in the upper centimetres of the core can be utilized to determine rates of biogenic particle mixing and rapid diagenetic reactions near the sediment-water interface. The short half-life of ^{234}Th is sensitive to seasonal changes on at least a 100 day timescale. Additionally, the distribution of excess ^{234}Th can be proved useful in the study of transport-reaction processes, particulate sedimentation and resuspension (Aller et al., 1980; Rose et al., 1994).

^{210}Pb ($t_{1/2}$=22.3 y) is a natural radionuclide (^{238}U series) and has been used as radiotracer in many processes (e.g. ocean biochemistry, atmospheric deposition and contamination, sedimentary processes, sediment radiochronology). The excess ^{210}Pb is an additional portion of ^{210}Pb found in the sediment apart from the one produced in-situ by the parental ^{226}Ra. The excess ^{210}Pb supply in the near-shore zones can be atmospheric deposition, production from ^{226}Ra in the soil, riverine sediments and advective-diffusive inputs from circulating water masses (Radakovitch et al., 1999). The sedimentation rate can be determined from the slope of the least-square fit for the excess ^{210}Pb concentrations plotted versus depth or by various models whereby the radioactive decay correlates with mass flow rates. The proposed ^{210}Pb models incorporated in this work are presented in section 3.4.2. The ^{210}Pb method is suited for dating events occurring during the last 100-200 years.

^{32}Si ($t_{1/2}$=500 y) is a natural radionuclide produced in the atmosphere by interactions of cosmic ray particles with atmospheric argon nuclei. It can be used for chronology studies at a 2000 year timescale. According to Krishnaswamy et al. (1971) if the sediments are rich in biogenic skeletal remains, then the ^{32}Si dating method is analogous to ^{14}C and is based on the ^{32}Si/Si ratio. However, if the sediments are deficient in biogenic silica, a proposed method is the selective leaching of precipitated silica to obtain the ^{32}Si/Si ratio.

Artificial radionuclides:

^{55}Fe ($t_{1/2}$=2.7 y) is an artificial radionuclide produced by nuclear weapon testing and it can be utilized for a 10 year timescale. According to Krishnaswamy et al. (1971) using the known global fallouts of ^{55}Fe during 1963-1964 and finding these signals in the upper part of a core sediment, they can contribute to the estimation of sedimentation rates.

^{137}Cs ($t_{1/2}$=30.1 y) is an artificial radionuclide produced by atmospheric nuclear weapon testing and nuclear accident. The main fallout events were in the early 1950s and peaked in 1963 due to weapon testing, while in 1986 due to the Chernobyl Nuclear Power Plant accident. As in the case of ^{55}Fe, the correspondence of the fallout events to the measured signals in different depths of the core, can estimate the sedimentation rate. The ^{137}Cs method is suited for dating events occurring during the last 100-200 years.

^{239,240}Pu ($t_{1/2}$=24.1 y (^{239}Pu), $t_{1/2}$= 6561 y (^{240}Pu)) the plutonium isotopes have been introduced into the environment due to nuclear weapon testing. Assuming that

the nuclear fallout has been characterized by a constant average $^{239,240}Pu/^{90}Sr$ ratio, then the records of ^{90}Sr can define the time-dependence and latitude-dependence of Pu fallout (Krishnaswami et al., 1980). The plutonium isotopes are reactive and remove from the water column faster than the "typical soluble" fallout nuclides (e.g. ^{90}Sr, ^{137}Cs) by particulate materials, thus can be used as tracers to study sedimentation.

Stable isotopes:

The stable isotopes of organic carbon (^{13}C) and nitrogen (^{15}N) are natural source indicators of sedimentary particulate organic matter. These concentrations can be used complementary as geochemical information to unfold the interpretation of the radio-dating cores.

The application of the described radio-dating methods is restricted by other parameters such as low activity concentrations, presence of coarse sediments, post-depositional sediment mixing etc.

2.7 Statistical Models

Statistical methods can be useful in the planning, designing, data-collecting, analysing and interpreting the research findings. However, in order to not misuse statistical analysis, proper statistical tests must be performed and thus the basic parameters (e.g. sample size, power analysis, statistical errors) must be well understood. The data can be organized into two types of variables, quantitative and qualitative. A variable is any characteristic that can be measured or counted and its value varies between data units in a population and may change over time. Statistics try to describe the relationship between variables in a sample population, either by providing a summary of data of the sample and it is called descriptive statistics or by deducting inferences about the whole (or larger collection of the) population and it is called inferential statistics. Descriptive statistics can describe the shape, centre and spread of a dataset, using indices such as mean, median, mode, range, variance, standard deviation etc., however in this work we will focus on the inferential statistics.

As mentioned above, inferential statistics are a group of techniques to generalize an inference for the whole population based on the data collected from a sample. Therefore, they include estimation, associations within the data (correlation), modelling relationships within the data and hypothesis testing. Among the aforementioned inferences the associations within the data were examined in the present work. A hypothesis is proposed for the statistical relationship (e.g. data set associations) between two statistical data sets, or a data set and data determined by a model. This hypothesis is compared to an alternative idealized null hypothesis, which assumes no relationship between the two data sets. The rejection or approval of the null hypothesis is performed by hypothesis testing. The p value is the probability of the event or the relationship between the population variables to occur by chance if the null hypothesis is true. If p value is below the selected significant level of 0.01 or 0.05, then the result is highly significant (very probably true) or significant (probably true), respectively, and the null hypothesis can be rejected. In the case where the p value is higher than the significance level of 0.05, then the result is not significant and the null hypothesis cannot be rejected. The significance level indicates how likely a pattern of the data is due to chance and the most common used level is 95%. However, the statistical packages give the converse level (5% or 0.05) indicating that the result has

a 5% chance of not being true. The significance level can be affected by the sample size, as in small samples large differences between the samples can be non-significant and the opposite.

The numerical data (quantitative variables)-as the ones of this work- can be analysed using either parametric or non-parametric statistical analysis. The main difference among the two techniques is that the first assumes normal distributions and homogeneity of variances, while the latter does not require normal distributions (distribution-free). Nevertheless, non-parametric distributions may be useful when the assumptions of normality are not met, but have less power to detect the significant differences than the parametric ones. For multi-samples the common parametric tests are one-way or two-way analysis of variance (ANOVA) and Pearson correlation coefficient, while the non-parametric tests are Kruskal-Wallis test, Jonckheere test, Friedman test and Spearman rank order.

Non-parametric methods are more widely applied than the parametric ones, as they demand less assumptions and are simpler. They are more flexible as the model structure is not specified a priori, but it is determined by the data. In this work, a parametric (Pearson correlation coefficient) and a non-parametric (Spearman rank order) analysis were followed, using Statistical Package for the Social Sciences (SPSS). Pearson correlation coefficient (r) measures the linear correlation between two variables and ranges from -1 to 1, where -1 represents negative linear correlation, 0 no correlation and +1 positive linear correlation. The intermediate values (among -1 and +1) indicate the intensity of the linear correlation. Spearman's rank correlation coefficient (rho or ρ) measures the statistical dependence between two variables using a monotonic function. The correlation coefficient ranges from -1 to +1, where the intermediate values indicate the intensity of the monotonic dependence between the samples. Spearman's rho analysis represents a general correlation coefficient.

Chapter 3

Dose estimation and radionuclide dispersion using ERICA and MCNP5 codes

An important task of the present work was the estimation of dose rates in non-human biota due to natural and artificial radionuclides, as well as the dispersion of natural radionuclides near coastal areas. The software package used for this effort was the ERICA Assessment Tool. In the following sections some basic information regarding the theoretical background of ERICA and the incorporation of it in this work, will be described. Additionally, a small introduction regarding the general-purpose Monte Carlo Neutral Particle code (MCNP) will be presented, as the code was used as a check point of ERICA in a hypothetical scenario.

3.1 Theoretical background

In general, ERICA development was based on MCNP code (MCNP4C) so as to include and simulate some basic ideal geometries of biota and the interactions of alpha, beta and gamma radiations in the matter. However, many assumptions were introduced in ERICA regarding divergences from the ideal theoretical simulated geometries, the location of the generated radionuclide sources, the radionuclide inputs taking into account secular equilibrium hypotheses and the incorporated experimental datasets. Thus, despite the integration of MCNP in ERICA, it was considered appropriate to test the two codes in a hypothetical scenario, as mentioned before.

3.1.1 MCNP /MCNPX simulation code

MCNP is a general purpose Monte Carlo code for the transport of all kinds of particles and among its capabilities it can be applied for radiation protection and dosimetry purposes. The code was developed by Los Alamos National Laboratory, it is distributed by the Radiation Safety Information Computational Center for the United States and by the Nuclear Energy Agency internationally. MCNP code uses the Monte Carlo statistical method, which generates random numbers to solve problems that might be deterministic in principle. Thus, the code can simulate experimental cases so as to determine the interaction of neutrons, electrons and photons with the matter. The simulated interactions are established on data bases, incorporated in the system, which include cross-section data of these interactions. The experimental case such as geometry, materials, radioactive sources etc. must be described in detail.

In this work the MCNP5 code and the extensions of it (MCNP-CP, MCNPX) codes were used to simulate the non-human biota of the studied area, utilizing the measured activity concentrations of natural (e.g. ^{226}Ra, ^{40}K) and artificial (^{137}Cs) radionuclides. The MCNP-CP is an extension of MCNP5 and provides the capability to simulate the whole decay diagram, and not specific energies, of a gamma emitter. Therefore, it is useful to describe summing effects, which become critical in cases where the distances of the radioactive source and the detector are small (below 10 cm). The MCNPX code was also used to simulate ion (e.g. alpha particles) interactions with matter, as heavy ions are not included in MCNP5 code. The basic units of MCNP are centimeters (length), MeV (energy), sec (time), kT (temperature), atoms barn^{-1} cm^{-1}

(atomic densities), g cm^{-3} (mass densities) and MeV $collision^{-1}$ (heat number). In this work the energy deposition tally (F6) (MeV g^{-1}) was used and the description of the MCNP-ERICA test case will be presented in section 3.2.2.

3.1.2 ERICA Assessment Tool

The ERICA Assessment Tool is a software system to assess the radiological risk to biota and has been based on ERICA Integrated Approach, an objective of the EC-EURATOM 6^{th} Framework Programme (Brown et al., 2008). The main scope of this approach was to quantify the environmental risk firstly by combining environmental transfer and dosimetry data to estimate the exposure values and secondly by comparing these values with exposure levels of known detrimental effects.

ERICA adopts a tiered structure, whereby includes two generic screening tiers (Tier 1, 2) and a third site-specific tier. Tier 1 is a conservative tier, is based on the activity concentrations of the media and utilize pre-calculated environmental media activity concentration limits to estimate the risk quotients. Tier 2, is a more flexible tier, whereby the assessor may edit most of the parameters such as concentration ratios, distribution coefficients, dose conversion coefficient etc. and can calculate the dose rates. The last tier, Tier 3, is also flexible and provides the option of probabilistic assessment when the probability distribution functions are defined. In present work, the dose rates and the dispersion of radionuclides were estimated Tier 2 for the marine environment. Thus, many of the parameters, assumptions and calculations, which will be described in this chapter (ch. 3) will be focused on Tier 2 for an aquatic/marine environment case. For a more detailed and general description of the ERICA software please see Brown et al., (2008); Brown et al., (2016); Beresford et al., (2007); ERICA manual among all other literature regarding ERICA.

ERICA has been applied in various applications worldwide, after its release (Brown et al., 2016) such as (a) to estimate potential environmental impact in European countries due to geological disposal facilities, (b) to compare its results with newly introduced environmental regulations, (c) to quantify the environmental impact due to operating and planned nuclear power stations, (d) to derive radiological quality guidelines in uranium mines of Australia or (e) to assess the impact of uranium mining, (f) to evaluate the impact of surface deposited radioactive wastes in Europe and Australia, (g) to assess the impact of medical facility releases and (h) to estimate the exposure of biota after Fukushima accident. According to Beresford et al. (2007) the main structure of the ERICA Integrated Approach, incorporated in the ERICA Tool is:

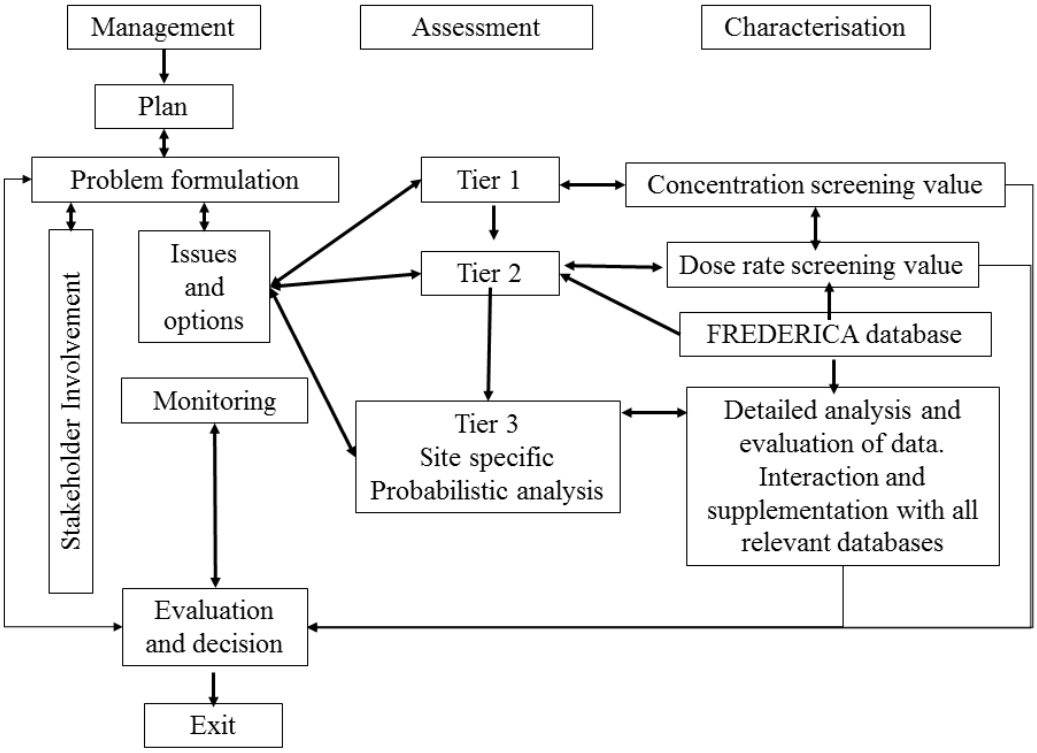

Fig. 3.1 The structure of the ERICA Integrated Approach. Management: refers to the decision make before, during and after an assessment, Assessment: refers to the estimation or measurement of activity concentration in environmental media and organisms, the definition of exposure conditions and the dose rate estimation, Characterization: refers to the estimation of the magnitude of adverse effects to biota by comparing the output data with existing effect analyses.

Dose concept

As absorbed dose (Gy), the energy absorbed per unit mass in a given organism or whole body is defined. The most important type of radiations which contribute to the absorbed dose in environmental conditions are alpha, beta and gamma radiation. The rest such as neutrons, heavy ions and fission fragments are of less relevance. It is known that different types of radiation cause different effects even in the case of similar absorber dose. The difference in the biological effect due to the different type of radiation, is expressed in the human dosimetry as equivalent dose (Sv), combines the absorbed dose with radiation weighting factors and has a stochastic nature. However, this approach cannot be applied in the case of non-human biota, where the radiation effects have a deterministic nature and usually refer to morbidity, mortality, reduced reproductive success and induced mutations (germ or somatic cells). Therefore, in ERICA, different default weighting factors for alpha, beta and gamma radiations have been included, which can be modified in Tier 2.

Reference organisms

Representative organisms of typical ecosystems (terrestrial, aquatic) have been chosen to represent (a) different life stages (e.g. egg fish, adult fish), (b) wide range of life forms, (c) organism's shape, (d) organism's masses, (e) ecosystems and (f) habitats. As "reference organism" is defined "a series of entities that provide a basis for the estimation of radiation dose rate to a range of organisms which are typical, or

representative, of a contaminated environment. These estimates, in turn, would provide a basis for assessing the likelihood and degree of radiation effects" according to Brown et al., 2016. The reference organisms of marine environment are phytoplankton, macroalgae, vascular plant, zooplankton, polychaete worm, benthic mollusk, benthic fish, pelagic fish, bird, mammal, reptile, sea anemones/true corals and colony of sea anemones/true corals.

General assumptions

In order for the dosimetric model to cover a wide range of exposure situations, it had to assume numerous simplifications regarding the variability of biota's sizes, shapes and habitats. The main simplifications accepted by the model are that (a) spheres and ellipsoids approximate the organisms' shape, (b) the radioactivity distribution is homogenized in the whole body for the internal dose rate calculation and not specific calculation is held for the different organs, (c) the radionuclide kinetic in the organism is not taken into account and equilibrium concentration in the whole body is assumed and (d) different source-target relationships are considered for the external dose rate calculation, so as to represent typical situations (e.g. the organism lives on or in the contaminated soil). Thus, ERICA estimates mean absorbed dose rates (internal or external) for the whole body of the organism.

Radiation types

In ERICA different radiation weighting factors (wf) have been implemented so as to assess the biological effectiveness. The types of radiation included in the dose calculations are: (a) alpha particles, (b) low-energy electrons (E_β < 10 keV) with discrete or continuous energy, (c) high-energy electrons ($E_\beta \geq 10$ keV) with discrete or continuous energy, (d) high-energy photons ($E_\gamma \geq 10$ keV). The default values of radiation weighting factors are 10 for alpha particles and fission fragments, 3 for low-energy electrons and 1 for all other types of radiation.

Radionuclide decay chains

For some radionuclides their radioactive daughters have been also accounted in the dosimetric model, when the half-lives of the latter are less than 10 days. Thus, secular equilibrium is assumed between parent and daughter nuclides.

Dose rate calculation

The dose rate (μGy h^{-1}) calculation is based on the activity concentration in the media or the organism, as well as on a set of parameters such as dose conversion coefficients (DCCs), distribution coefficients (K_ds), concentration ratios (CRs) etc. All these parameters will be described below, where special attention will be given to the most important parameter (DCC) in the dose rate calculation. The dose rate is divided in two fractions, internal and external, which are calculated separately and the sum of these components gives the total absorbed dose rate. The internal dose rate ($\dot{D}^b_{\text{int}}$) is given as:

$$\dot{D}^b_{\text{int}} = \sum_i C_i^b DCC^b_{\text{int},i} \qquad \text{(Eq. 3.1)}$$

where,

C_i^b is the average (whole body assumption) concentration of radionuclide i in the reference organism b (Bq kg^{-1} fresh weight), $DCC^b_{\text{int},i}$ is the internal dose conversion coefficient for the specific radionuclide (μGy h^{-1} per Bq kg^{-1} fresh weight) defined as

the ratio of the dose rate of the organism to the average activity concentration of the organism (see "Parameters" paragraph below for DCC full description).

The external dose rate ($\dot{D}_{ext}^{b}$) is calculated as:

$$\dot{D}_{ext}^{b} = \sum_{z} v_z \sum_{i} C_{zi}^{ref} DCC_{ext,zi}^{b} \qquad \text{(Eq. 3.2)}$$

where,

v_z is the occupancy factor (the time fraction that the organism b spends at a specified position z in its habitat), C_{zi}^{ref} is the average concentration of radionuclide i in the reference media of a given location z (Bq kg^{-1} in fresh weight of soil/sediment or Bq l^{-1} in water), $DCC_{ext,zi}^{b}$ is the external dose conversion coefficient for the specific radionuclide (μGy h^{-1} per Bq kg^{-1} fresh weight or Bq l^{-1}), defined as the ratio of the dose rate of the organism to the average activity concentration of the media.

Parameters

The main parameters of ERICA used for the dose rate calculations are concentration ratios (CRs), distribution coefficients (K_ds), percentage dry weight soil or sediment, dose conversion coefficients (DCCs), radiation weighting factors (wf) and occupancy factors. All these parameters cannot be changed in Tier 1, but can be altered in Tiers 2 and 3. A brief description of most parameters will be presented below, whereas special care will be held for the DCC, CR and K_d parameters.

Dose Conversion Coefficient (DCC)

As DCC is defined as the absorbed dose rate per specific source activity (μGy h^{-1} per Bq kg^{-1}) in organism or medium and can be expressed in terms of a key quantity for calculating **internal** doses, the absorbed fraction φ(E), which depends on the energy E. As φ(E), the fraction of energy emitted by a radiation source **within** the target tissue, organ or organism is defined. In the case of an aquatic reference organism, the organism is within a quasi-infinite homogeneous medium and the activity is assumed to be uniformly distributed in the whole body. The densities of the medium and the organism are the same. Taking all these into account the internal and external components of DCC for mono-energetic radiation can be expressed as a function of φ(E):

$$DCC_{\text{int}}(E) = E\varphi(\text{E}) \qquad \text{(Eq. 3.3)}$$

$$DCC_{ext}(E) = E(1-\varphi(E)) \qquad \text{(Eq. 3.4)}$$

As mentioned before the external DCC has a meaning only if the organism and the surrounding medium are of the same density and elemental composition. In an infinite homogeneous medium with uniform isotropic radiation sources, the DCC per unit source strength cannot exceed the full absorption limit, which is the adsorbed dose in uniform infinite media. Thus, for any given nuclide, the upper limit for the DCCs equals to:

$$DCC_{\infty}(E) \approx 5.76 \cdot 10^{-4} \overline{E} \qquad \text{(Eq. 3.5)}$$

where,

D_{∞} is the upper limit of DCCs in μGy h^{-1} Bq^{-1} Kg and $\overline{E}$ is the source energy in MeV average over the source emission spectrum (discrete and/or continuous):

$$\overline{E} = \sum_{v}\left(\sum_{i} E_i Y_i + \int N_v(E) E dE\right) \qquad \text{(Eq. 3.6)}$$

Therefore, the analytical equation describing the internal and external components of DCCs are:

$$D_{\text{int}} = \sum_{v}\left(\sum_{i} E_i Y_i \varphi_v(E_i) + \int N_v(E) E \varphi_v(E) dE\right) \qquad \text{(Eq. 3.7)}$$

$$D_{ext} = \sum_{v}\left(\sum_{i} E_i Y_i (1-\varphi_v(E_i)) + \int N_v(E) E (1-\varphi_v(E)) dE\right) \qquad \text{(Eq. 3.8)}$$

where,

v states the radiation types (alpha, low-beta, high-beta, photons and spontaneous fission fragments), E_i the decay energy of radionuclide in MeV, Y_i the yield of the discrete energy radiations per decay of the radionuclide in decay^{-1}, $N_v(E)$ the energy spectrum for continuous energy radiations of type v in decay^{-1} MeV^{-1}, $\varphi_v(E)$ the absorbed fraction.

According to Ulanovsky and Prohl, (2006) and Ulanovsky et al., (2008) if the organism (Hosseini et al., 2008) dimensions are much smaller than the radiation range in the medium then $DCC_{\text{int}} \rightarrow 0$ due to the escape of radiation from the body and $DCC_{ext} \rightarrow \infty$. On the other hand, when the size of the organism is much larger than the radiation range in the medium, then $DCC_{\text{int}} \rightarrow \infty$ and $DCC_{\text{ext}} \rightarrow 0$. The ranges of alpha particles and low-energy electrons are small (≤ 50-100 μm), so in many cases the practical relevance absorbed fractions are high $\varphi(E) \approx 1$. Therefore, according to equations 3.3 and 3.4, $DCC_{\text{int}} \approx DCC_{\infty}$ and $DCC_{\text{ext}} \approx 0$. On the contrary, for really small organisms and for longer range radiations (high-energy electrons and photons), $\varphi(E) \approx 0$, thus $DCC_{\text{int}} \approx 0$ and $DCC_{ext} \approx DCC_{\infty}$.

Weighted internal, external and total (sum of internal and external component) dose rates taking into account the radiation types are estimated by:

$$DCC_{\text{int}} = wf_{low\cdot\beta} DCC_{\text{int},low\cdot\beta} + wf_{\beta+\gamma} DCC_{\text{int},\beta+\gamma} + wf_{\alpha} DCC_{\text{int},\alpha} \qquad \text{(Eq. 3.9)}$$

$$DCC_{ext} = wf_{low\cdot\beta} DCC_{\text{ext},low\cdot\beta} + wf_{\beta+\gamma} DCC_{\text{ext},\beta+\gamma} \qquad \text{(Eq. 3.10)}$$

where,

wf are the radiation weighting factors, with default values of 10 for alpha particles and fission fragments, 3 for low-energy electrons and 1 for all other types of radiation (e.g. high-energy electrons and photons). If unweighted absorbed dose rates are required the default wf values can be altered by the assessor and set equal to unity.

Summarizing the theory regarding the DCC parameter it can be seen that the DCC data can be categorized according to (a) radionuclide, (b) reference organism, (c) internal irradiation, (d) external irradiation and (e) radiation types (DCC for alpha radiation, DCC for low beta radiation and DCC for high beta-gamma radiation). As mentioned above, in the case of radioactive chains, in the DCC calculation the daughter nuclides of a parent nuclide are also included assuming secular equilibrium, if they have half-lives shorter than 10 days. Special care was also given to the shapes, dimensions and masses of the reference organisms, in order to represent and include real cases.

Briefly, the absorbed fraction (φ(E)) and therefore DCC was estimated through Monte Carlo code (MCNP4C), assuming infinite water medium surrounding the organism, internal sources in the organism, homogeneous distributed for spheres and ellipsoids in the mass range of 10^{-6}-10^{3} kg for photon and electron sources with energies ranging from 10 keV to 5 MeV. The differences between absorbed fractions for spherical and non-spherical bodies depend on (a) mass of the body, (b) shape of the body, (c) type of the source particles and (d) energy of the source particles. Thus, in the φ(E) calculation the sphere geometry was simulated using MCNP4C and by producing a re-scaling factor RF(E,M,η), which depends on the energy (E), the mass (M) and the non-sphericity parameter (η), the ERICA team was able to produce DCC values for a wide range of organisms with an assumed ellipsoidal shape. This coefficient of variation following this approximation was determined for electron sources to be up to 10%, whereas for the majority of the studied energy and mass values did not exceed 3%. In the case of photon sources the uncertainties were up to 15%, where for most of the energy and mass values they were between 5 and 10%. According to Ulanovsky and Prohl, (2006) the DCC estimation can be extrapolated to body masses outside the studied range of 10^{-6}-10^{3} kg, but the limits and assumptions of ERICA must be taken into account.

Concentration Ratio (CR)

For the exposure assessment in the biota, the activity concentrations of environmental media and organisms are needed. If adequate measured data are unavailable, the activity concentrations of radionuclides in biota can be calculated indirectly by multiplying the corresponding media activity concentrations (water for aquatic ecosystems) by equilibrium concentration ratios (CRs) and vice versa. For Tiers 2 and 3 the activity concentrations of the media can be estimated by dividing the activity concentrations of the biota by the corresponding CR. For aquatic ecosystems the concentration ratio (or concentration factor or bioaccumulation factor) is defined as:

$$CR_{j,i} = \frac{C_{j,i}}{C_i^{aq}} \qquad \text{(Eq. 3.11)}$$

where,

$CR_{j,i}$ is the concentration ratio for the j organism and i radionuclide (dimensionless or l kg^{-1}), $C_{j,i}$ is the activity concentration of i radionuclide in the whole body of j organism (Bq kg^{-1} fresh weight) and C_i^{aq} is the activity concentration of i radionuclide in aqueous phase (Bq l^{-1}), typically filtered water.

The CR method usually assumes that an organism is in biochemical equilibrium with its surroundings. However, the required time for the equilibrium to be attained depends on the physical half-life of the radionuclide and the biological half-life of the element in the organism, thus the assumption of instant equilibrium adopted by ERICA, may result in poor predictions regarding the concentrations in organisms in some cases (Hosseini et al., 2008). The core problem of these poor predictions is that in reality radionuclides are retained in some organisms and then are returned to the medium surrounding them after days or years and not instantly. Furthermore, according to Hosseini et al. (2008) the influence of physical and chemical reasons on uptake and depuration at different trophic levels is needed for a long-term and robust prognoses taking into account the contaminant behavior and fate. For example, the changing

conditions in an aquatic environment may influence the contaminant transfer and affect the water-organism radionuclide concentration. This will lead to different radionuclide concentrations in high trophic-level organisms, where the main contaminant source will be the ingested food. In such a case the accumulation of contaminants in high trophic-level organisms cannot be assumed as a linear process.

Ideally, CR data must refer to the whole organism as the DCC and the dose rate calculations refer to the whole body. However, in some cases the available data refer to tissue types (soft/edible/muscle/hard tissues) and/or organs. Thus, the conversion of partial CRs to whole-body CRs were needed and were calculated as:

$$C_{MtoW} = \frac{\sum_i f_i CR_i}{CR_M} \qquad \text{(Eq. 3.12)}$$

where,

C_{MtoW} is the conversion factor so as to convert a muscle CR to a whole-bofy equivalent CR, f_i is the fractional mass of the organ/body part i, CR_i is the concentration ratio of the organ/body part and CR_M is the concentration ratio of muscle or flesh.

In the marine environment conversion factors were not calculated for photoautotrophic reference organisms (i.e. phytoplankton, macroalgae and vascular plant) as the CR data of these organisms either already refer to the whole body or the sampled tissues were not specified. For the heterotrophic reference organisms if the registered CR data were specified for the different tissue/organ part, the conversion factors were estimated.

Default CR values are incorporated in ERICA for each default element and reference organism. These values have derived from reviews of original publications (such as (International Atomic Energy Agency (IAEA), 2004)). Nevertheless, in many cases, no empirical data were available, therefore the gaps in the CR database were filled by various methods such as taxonomic/similar species analogues, biochemical analogues and transfer modelling approaches (Hosseini et al., 2008). Due to these approximations, ERICA provides the assessor with information of the origin of the derived CRs.

Distribution coefficient (K_d)

The water-sediment distribution (or partition) coefficient (K_d) is an important parameter used in estimating the migration potential of contaminants present in aqueous solutions in contact with surface, subsurface and suspended solids (United States Environmental Protection Agency (USEPA), 1999). The K_d value is a direct measure of the partitioning of a contaminant between the solid and aqueous phases, it is an empirical metric to account for various chemical and physical retardation mechanisms (e.g. surface adsorption, absorption into the solid structure, precipitation, physical filtration of colloids), it varies greatly between contaminants and it is a function of aqueous and solid phase chemistry. K_ds also vary significantly depending on the location, thus, if possible, site specific data must be acquired. K_d is used in aquatic environments to derive activity concentrations in sediment from water concentrations and vice versa, assuming equilibrium between the media. The K_d is defined as:

$$K_d = \frac{C_{s,i}}{C_{w,i}} \qquad \text{(Eq. 3.13)}$$

where,

K_d is the distribution coefficient (l kg^{-1}), $C_{s,i}$ is the activity concentration in the sediment (Bq kg^{-1} dry weight) of the radionuclide i and $C_{w,i}$ is the activity concentration in the water (Bq l^{-1} usually filtered water) of the radionuclide i.

Percentage dry weight soil/sediment

The estimated activity concentrations in biota and water, through CRs and K_ds require activity concentrations in dry weight portion of sediment. On the other hand, the external dose rate estimation requires fresh weight activity concentrations. To enable the conversion from dry weight to fresh weight activity concentrations, the percentage of dry weight in sediment is needed. If this value is not given, ERICA assumes 100% dry matter, which leads to conservative (overestimated) dose rates.

Radiation weighting factors (wf)

The radiation weighting factors have been already mentioned in the DCC section and they are used in order to assess the different biological effect in the organism due to different types of radiation. The wf default values in ERICA are 10 for alpha particles and fission fragments, 3 for low-energy electrons and 1 for all other types of radiation (e.g. high-energy electrons and photons)

Occupancy factors

Occupancy factor is the fraction of time that an organism spends at a specified location in its habitat. The maximum percentage of occupancy is 100%, it can be divided in other percentages if the organism resides in more than on media, it is not necessary the sum of the occupancy factors to be 100% in case where the radius of the organism's residing region is larger than the radius of the contaminated area and it can be modified by the assessor. The default occupancy factors of ERICA have been selected to estimate conservative dose rates, meaning to maximize the dose. The occupancy options according to ERICA manual in aquatic ecosystems are:

1. water-surface (when an organism spends time on the surface of the water (e.g. duck))
2. water when an organism spends time swimming through the water column (e.g. pelagic fish)
3. sediment-surface (when an organism spends time near the bottom of the water column (e.g. benthic fish) or lives on the surface of the sediment (e.g. macrophytes)
4. sediment (when an organism spends time in the sediment (e.g. marine polychaete worm) and actually is buried in the sediment).

Tier 2 and dosimetric module description

This work will be focused on Tier 2 and not on the other tiers (1 and 3). More details regarding Tiers 1 and 3 can be found in Beresford et al. (2007), Brown et al. (2008) and ERICA manual. The dosimetric relationships (DCC calculations) have been implemented in a dosimetric module, which has been integrated into ERICA Tool. The dosimetric module refers to a uniform isotropic model (Eqs 3.3 and 3.4) applied for aquatic organisms (this work) to estimate their external and internal exposure, for mass ranges from 10^{-6} kg to 10^{3} kg based on pre-calculated absorbed fraction values and linked with the electronic database with the decay properties of 838 radionuclides

(nearly any known radionuclides) (Ulanovsky et al., 2008). The flowchart of this dosimetric module is shown in Fig. 3.2.

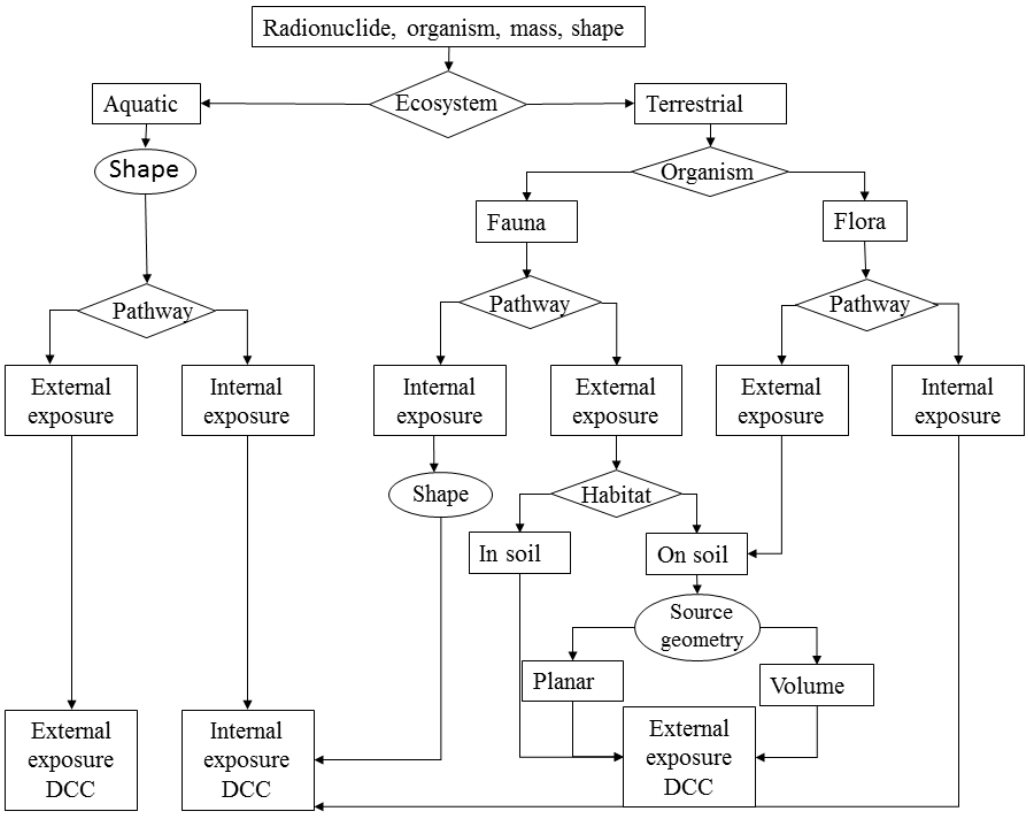

Fig. 3.2 The flowchart of the dosimetric module integrated in the ERICA Tool (aquatic and terrestrial ecosystems)

At Tier 2 the total (internal and external) weighted estimated dose rates for each reference organism included in the assessment are compared with dose rate screening values that were selected by the user to assess the situation. The screening dose rate values included in ERICA (Tier 1, 2 and 3), which can be selected by the assessor are two: (a) 10 μGy h^{-1} for all ecosystems and (b) 40 μGy h^{-1} and/or 400 μGy h^{-1} depending on the ecosystem. ERICA's default incremental screening value (10 μGy h^{-1}) applies to all ecosystems and was derived by a deliverable of ERICA project (ERICA manual, see section 10.12). This screening dose rate was calculated so that generic ecosystems (freshwater, marine and terrestrial) be protected from effects on structure and function under chronic exposure to radionuclides. Additionally, it was the result of a chronic exposure analysis of 26000 data. The 40 μGy h^{-1} screening value is set for terrestrial animals and aquatic species of aquatic mammals, reptiles, amphibians and birds, while the 400 μGy h^{-1} value is set for terrestrial plants and all other aquatic species not mentioned above (e.g. fish, worms). These values were derived from the IAEA (1992) and UNSCEAR (1996) reports and are real benchmarks below which populations are unlikely to be significantly harmed based on reviews of scientific literature. In the case where the assessor use his/hers own screening values, they must be justified as these values are used for comparison reasons to assess the exposure and produce risk quotients:

$$RQ_{org} = \frac{DR_{org}}{SDR} \qquad \text{(Eq. 3.14)}$$

where,

RQ_{org} is the risk quotient for reference organism, DR_{org} is the estimated total dose rate ($\mu Gy\ h^{-1}$) and SDR is the screening dose rate ($\mu Gy\ h^{-1}$) selected by the user at the assessment context stage.

As have already been mentioned, Tier 2 is a flexible tier, where activity concentrations of organisms and media (water and/or sediment) can be inserted, many parameters (K_ds, CRs, wf, occupancy factors and percentage dry weight in sediment) can be altered and new organisms or isotopes can be inserted, taking into account the necessary data for their descriptions (e.g. mass, shape, K_d, CR, etc.). Additionally, the objective of Tier 2 is to identify situations where there is a very low probability (e.g. few percent) that the dose to any selected reference organism exceeds the adopted screening dose rate. Thus, this screening test uses two RQ values, the expected one and the conservative one. The former is calculated using the expected values for input data (assessor) and the parameters. The latter is calculated by multiplying the expected RQs with uncertainty factors (UFs).

The uncertainty factor is an approximation applied to account for uncertainty in the dose-rate estimation. According to ERICA manual "The uncertainty factor is defined as the ratio between the 95th, 99th or any other percentile (above the expected value) and the expected value of the probability distribution of the dose rate (and RQ). To estimate the UF, it is assumed that the dose rate and the RQ, follow exponential distributions with means equal to the estimated expected values. In this case the UFs corresponding to the 95th and 99th percentiles are equal to 3 and 5 respectively. Under these assumptions and selecting a UF = 3, if the estimated expected value multiplied by the UF is equal to or lower than one, then the probability that the RQ exceeds 1 is equal to or lower than 5%. This is the same as saying that the probability of the estimated dose rate exceeding the screening dose rate is equal to or lower that 5%".

In Tier 2 the expected (RQ_{exp}) and conservative RQ (RQ_{cons}) values are reported for every organism selected in the assessment. Depending on the RQ_{exp} and RQ_{cons} values a concluding assessment or having to conduct a more detailed assessment is decided by the assessor (ERICA provides a colored index to assess the exposure according to the RQ_{exp} and RQ_{cons} values):

1. if $RQ_{cons} < 1$ (green cells) for all organisms then the probability that the screening dose-rate has been exceeded is low, the environmental risk is arguably negligible and the risk assessment can be terminated.
2. if $RQ_{exp} < 1$and $RQ_{cons} \geq 1$ (amber cells) for any organism then the probability that the screening dose-rate has been exceeded is substantial and further work is needed either to reduce the uncertainties in the dose-rate estimation, thus possibly RQ_{cons} will fall below 1 or to check the results with available effect data or background dose rates, therefore the risk will be proved minimal.
3. if $RQ_{cons} \geq 1$ (red cells) for any organism then the screening value has been exceeded and further assessment must be conducted e.g. by using Tier 3.

Tier 2 also contains an effect tab, which consist of a series of tables for each reference organism group for the ecosystem under assessment. This information is provided so as to compare the predicted dose rates for the selected organisms with a

summary of information about the known biological effects in ionizing radiation on non-human biota included in FREDERICA database (Copplestone et al., 2008). Through this comparison an idea regarding the expected radiation effects may support the assessor to decision making. The flowchart of Tier 2 incorporated in ERICA Tool is shown in Fig. 3.3.

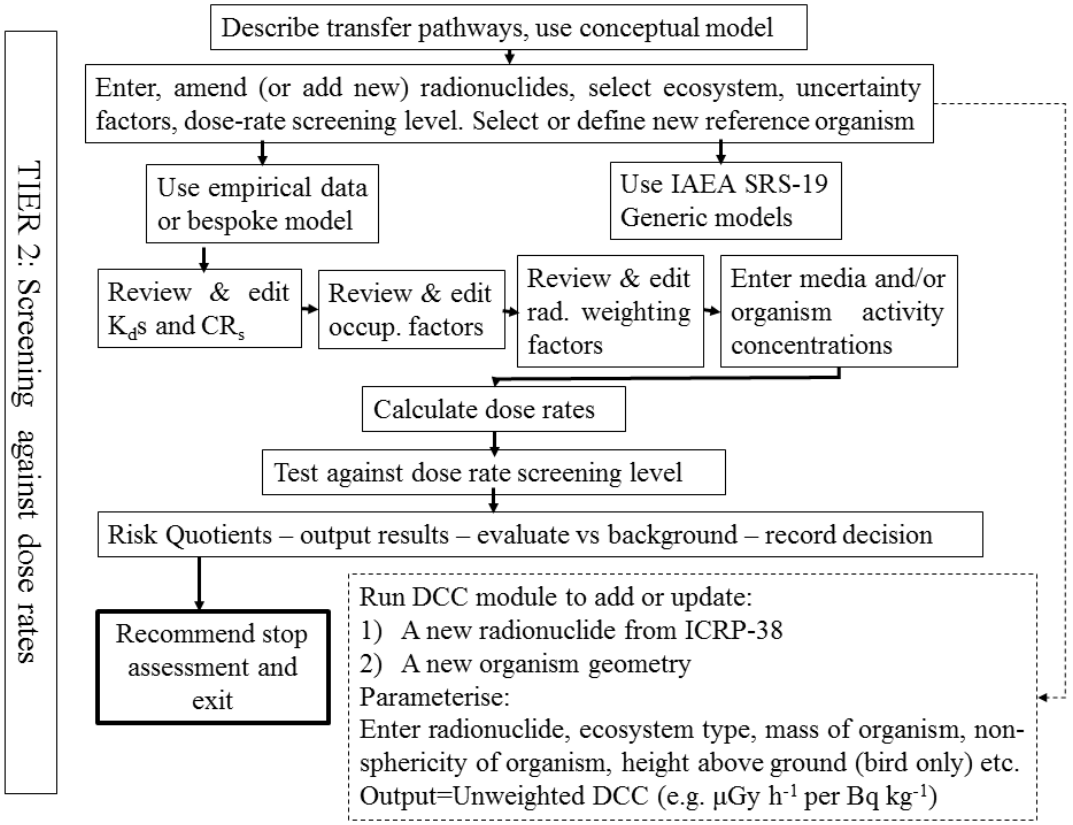

Fig. 3.3 The flowchart of Tier 2 incorporated in ERICA Tool (Beresford et al., 2007; Brown et al, 2008)

Dispersion model

ERICA Tool and specifically Tiers 1 and 2, enable the assessors to estimate the media activity concentrations from discharge data using "transport" models based upon IAEA Safety Report Series (SRS) 19 (IAEA, 2001). These models are screening ones, designed to estimate levels of radionuclides in atmospheric and aquatic systems, and simultaneously try to minimize the possibility that the calculated results would underestimate real doses by more than a factor of 10. The dispersion models estimate activity concentrations in water or air assuming a single source of continuous release and an equilibrium or quasi-equilibrium has been established among the released radionuclides and the relevant components of the environment. The available transport models in ERICA are (a) small lake (< 400 km^2), (b) large lake (≥400 km^2), (c) estuarine, (d) river, (e) coastal and (f) air. According to Brown et al. (2008) the implementation of these models in ERICA has been tested by comparing their results with those of IAEA examples (original publication) and those of other codes which implement SPR-19 models. This work refers to coastal marine regions, thus the detailed description of the coastal model will follow bellow.

The coastal generic model is based on a steady state and vertically averaged advection-diffusion equation.

$$U\frac{\partial C_{w,tot}}{\partial x}=\varepsilon_y\frac{\partial^2 C_{w,tot}}{\partial y^2}-\lambda_i C_{w,tot} \qquad \text{(Eq. 3.15)}$$

where,

$C_{w,\,tot}$ is the concentration of the radionuclide of interest (Bq m^{-3}), U is the velocity of flow in the x (longitudinal) direction (m s^{-1}) (0.1 m s^{-1} as a default), ε_y is the (lateral) dispersion coefficient in the y axis (m^2 s^{-1}), λ_i is the radionuclide decay constant (s^{-1}).

The scale of the mixing length becomes larger as the radionuclide plume spreads further in coastal waters, therefore the lateral dispersion coefficient is assumed to be a function of the longitudinal distance (Eq. 3.16) (IAEA, 2001):

$$\varepsilon_y=3.44\ 10^{-7}\left(\frac{x}{U}\right)^{1.34} \qquad \text{(Eq. 3.16)}$$

The solution of the advection-diffusion equation is calculated as:

$$C_{w,tot}=\frac{962\ U^{0.17}Q_i e^{-\frac{7.28\ 10^5 U^{2.34}(y-y_0)^2}{x^{2.34}}-\frac{\lambda_i x}{U}}}{D\ x^{1.17}} \qquad \text{(Eq. 3.17)}$$

where,

Q_i is the discharge rate of the selected radionuclide (Bq s^{-1}), D is the water depth at the radionuclide discharge effluent outfall (m), y_0 is the longitudinal distance between the release point and the shore (m), y is the location of the receptor (along the shoreline or in the sea), x is the longitudinal distance (along the coastal current direction) between the release point and a potential receptor (m). The rest of the notation is as in Eq. 3.15.

The coastal model has some limitations or requires some assumptions, whereby the main ones are: (a) the shoreline is straight along the x axis (y = 0), (b) the water depth (D) is constant, (c) the coastal current (U) is constant and is parallel to the shoreline and (d) the longitudinal dispersion is not important. These limitations are described by the following equations:

$$7D < x < 8\cdot 10^7 \text{ m} \qquad \text{(Eq. 3.18)}$$

$$\left|\frac{y-y_0}{x}\right| << 3.7 \qquad \text{(Eq. 3.19)}$$

According to equation 3.18 the coastal model can be applied for distances up to 100 km from the discharge point.

3.2 Materials and Methods

After the description of ERICA and Tier 2 especially, the application of ERICA in the study areas is presented in this section. In order to estimate the dose rates (Stratoni, Oxygono Bay) and the radionuclide dispersion (Stratoni) some features of ERICA were altered, some assumptions were adopted and some default parameter values were used. Additionally, as mentioned before in section 3.1.1, even if ERICA is based on MCNP code (MCNP4C), a test case (dose rate estimation in a hypothetical organism) was examined in present work using ERICA and MCNP5/MCNPX codes, so as to better understand ERICA and test the assumption of full absorption limit (according to the external dose rate definition, the sources must be around the

organisms, while ERICA assumes internal sources in the organisms and the remaining energy fraction "escaping" from the organism equals to external exposure).

3.2.1 Radionuclide dispersion (Stratoni)

Implementation field

The followed procedure to apply the coastal dispersion model at the study area of Stratoni (Ierissos Gulf), is presented in Fig. 3.4. The Ierissos Gulf was parameterized in two different grid distances using the ArcGIS 10.2 software®: (a) a dense grid of 160 points (receptors) every 100 m (Fig. 3.4b), close to the Stratoni port; and (b) a less dense one of 230 points (receptors) every 1000 m (Fig. 3.4a), covering the remaining region of the gulf . As potential discharge source, eleven (11) release points (Fig. 3.4c) in the vicinity of the load out pier area of Stratoni port were tested, including the STR1 sampling point which exhibited the highest activity concentrations (see chapter 5-chapter of results). For each one of these points the coastal model was properly altered so as to adjust the depth of the source (D), the release point to shore distance (y) and the release point to receptor distances (x) according to the source coordinates. The bathymetry of the region is known, with a mean seabed slope of approximately 5%. Therefore, the inserted distance to the model, between the release point and the receptor considering the bathymetry, remains almost the same. For the coastal current velocity (U), the results of a 2D-hydrodynamic-model applied in the Ierissos Gulf were utilized (Chantzi, 2012). This model estimates the current velocities taking into consideration the physical characteristics of the gulf (e.g. bathymetry, river discharges, wind direction, wind force). The map of the estimated current velocities (mean values and directions) for an Eastward wind of 5 bft (Beaufort) was utilized in this work as this combination of wind direction and wind force represents the prevailing wind in the area. The radionuclide discharge rate (Q) was thus the only free parameter that had to be determined with respect to the experimental data. The activity concentration in the sediment is derived from the activity concentration in the water using the distribution coefficient (K_d).

The model was calibrated regarding the discharge rates (Q) of selected radionuclides by using the radionuclide activity concentrations measured in the surface sediment samples. With the aim of obtaining the optimum Q for each one of the 11 release scenarios, a number of successive runs of the model were executed using different Q values until the difference between the estimated and experimental activity concentrations was minimized for all the sampling points. The total activity concentration estimated at the sampling points was assumed to be the sum of the transferred activity and the background activity concentrations. The transferred activity was estimated via the coastal generic model, while the background activity was set equal to the one of the reference sample collected at Ierissos port (site STR12). This sampling point, which was the most distant site from the point source, exhibited the minimum observed concentration values of radionuclides (and major/minor elements), and therefore was considered less affected by anthropogenic activities (see chapter 5-chapter of results). The release scenario that exhibited minimum deviation from the experimental data for the radionuclides of interest (^{226}Ra and ^{235}U) was finally selected as the most realistic. The boundaries of the affected region due to the discharge area in the inner part of the gulf derived from the points for which the estimated activity

concentrations became similar (within uncertainties) to the background values. Mapping

In order to estimate the activity concentration in the (whole) surface of the affected area, without running the ERICA Tool, three interpolation methods were tested. These methods were the Inverse Distance Weighting (IDW) (Shepard, 1968), the Empirical Bayesian Kriging (Gribov & Krivoruchko, 2012) and the Spline (Franke, 1982; Mitas and Mitasova, 1988) interpolation method. Different numbers (e.g. 4, 6, 8, 10, 12) of neighboring points, necessary for the interpolation, were tested for the Kriging method and the IDW method. The IDW method provided the same results (saturation) taking into account more than 4 neighboring points, while for the Kriging method the difference in the interpolation between the minimum (4) and the maximum (12) neighboring points was up to 28%. Additionally, the estimated values (ERICA Tool) were grouped in classes and were compared with the grouped interpolated data, keeping the same number of classes. This comparison revealed no difference between the mean value of the classes of ERICA estimation and the classes of the IDW interpolation. However, the mean value of the classes of ERICA estimation differed from the classes of the Kriging interpolated data up to 10 % or 40 %, considering four (4) or twelve (12) neighboring points, respectively. Therefore, 4 points were selected as neighbors for the interpolation, in order to minimize the computational time. The aforementioned methodology was also implemented using four (4) points in the same area for the Spline interpolation method. The differences between the mean values of the five classes of ERICA estimated data and the mean value of the classes of Spline interpolation were much higher (up to 60%), therefore this method was not used. In the end, the results of the IDW method and the Kriging method were compared with ten randomly selected ERICA estimated points. Although the IDW method was independent from the number of neighboring points and the mean values of IDW classification did not differ from the estimated value classification, the Kriging method reproduced satisfactorily the random estimated data (difference up to 14% for most points, except one 26%) from the ERICA tool.

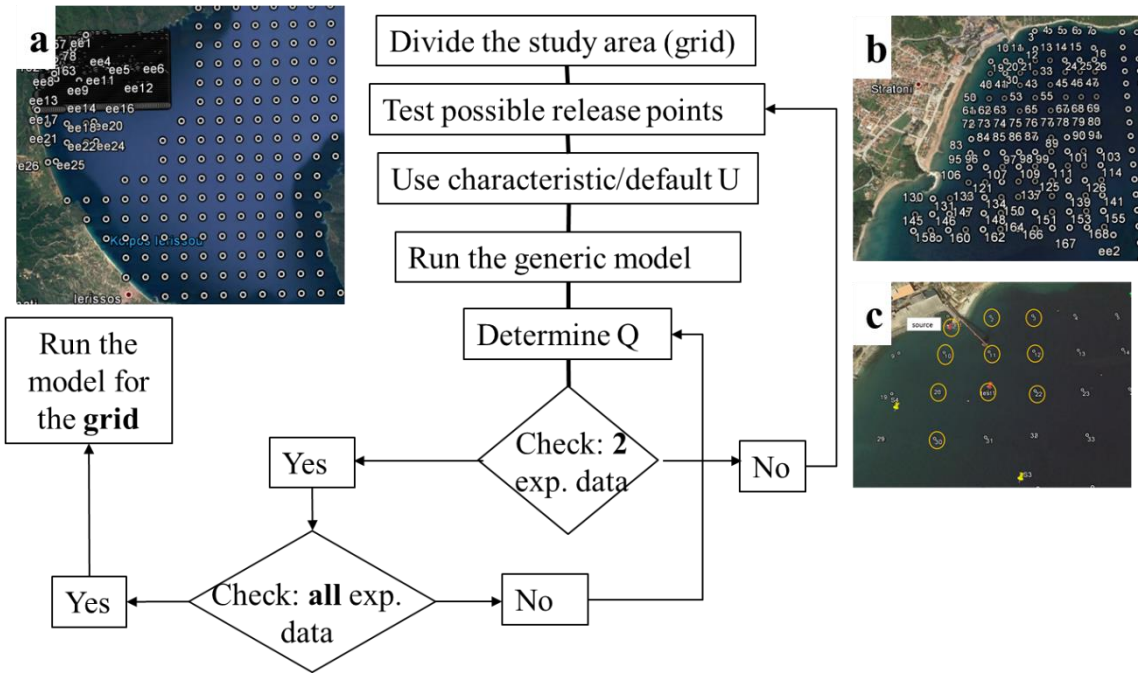

Fig. 3.4 The flowchart of the dispersion model application in Stratoni (Ierissos Gulf).

3.2.2 MCNP5 and ERICA comparison at a hypothetical case

The scope of this work was to compare the internal and external dose rates obtained by two codes (MCNP-CP code and the ERICA Assessment Tool), in an unreal simple case scenario – a spherical pelagic fish – for some radionuclides (pure alpha/beta/gamma emitters or/and beta and gamma emitters). Some of the studied radionuclides are observed in marine environments. MCNP/ MCNPX is a general purpose Monte Carlo code for the particle transport of all kinds, while ERICA is a more specified software tool for assessing the radiological risk to non-human biota (terrestrial, freshwater and marine environments). A spherical pelagic fish was created in both codes bearing the same characteristics (radius 5.130 cm, density 1 g cm^{-3}, mass 0.566 kg) while the activity concentration of all radionuclides in the water medium was assumed to be 1Bq l^{-1}.

The assumptions and parameters used by ERICA for the dose rate estimations, were included in the dose rate calculations by the MCNP-CP code. The dose rates (in μG h^{-1}) of seventeen radionuclides (^{40}K, ^{137}Cs, ^{210}Pb, ^{210}Bi, ^{208}Tl, ^{57}Co, ^{134}Cs, ^{131}I, ^{132}I, ^{140}La, ^{59}Ni, ^{210}Po, ^{242}Cm, ^{231}Pa, ^{90}Sr, ^{90}Y and ^{3}H), some of which are also included as default radionuclides in the ERICA database, were estimated by the two codes. The ^{40}K and ^{208}Tl radionuclides are not included in ERICA and were inserted as explained below.

ERICA case

In the ERICA whole-body-dose-rate calculations the important parameters of a marine organism to be inserted are:(a) the characteristics of the organism (radius (in cm), density (in g cm^{-3}), mass (in kg)), if a new organism is created, (b) the concentration ratio (CR) of the radionuclide of interest, (c) the distribution coefficients (K_d) of the radionuclide of interest if the organism resides in the seabed and (d) the

activity concentrations of the media (sediment and water for aquatic environments) where the organism resides. Moreover, ERICA includes default marine organisms (e.g. pelagic fish) of ellipsoidal geometry. In this work the pelagic fish geometry was altered from ellipsoid to sphere, to facilitate the MCNP geometries, while the default CRs of pelagic fish, were inserted in the new geometry. For the dose rate estimation of ^{210}Pb and ^{90}Sr, the contribution of ^{210}Bi and ^{90}Y were also taken into account by default in ERICA, respectively, as the half-lives of daughter nuclides (^{210}Bi, ^{90}Y) are less than 10 days (in ^{208}Tl case this assumption of ERICA is not valid as it decays in a stable isotope (^{208}Pb)). Additionally, weighted total dose rates are estimated by ERICA through the application of weighting factors (dimensionless) (see "Radiation weighting factors (wf)" in section 3.1.2).

The ^{40}K and ^{208}Tl isotopes are not included in the default-radionuclides database of the ERICA Tool, however they were added as described in ERICA manual and briefly mentioned in Brown et al. (2008). The CR and K_d parameters of ^{208}Tl were inserted from the IAEA Technical report (IAEA, 2004) for the cases of marine organisms and ocean margin, accordingly. Due to the lack of literature data regarding ^{40}K, potassium was inserted in the ERICA Tool using the CR of Na (IAEA, 2004), while the K_d was calculated by measured data of ^{40}K activity concentration in sediment and water of Stratoni port (Ierissos Gulf) and Oxygono Bay (see 3.2.3 section and Pappa et al., 2016).

Monte Carlo case geometry

The MCNP-CP code, instead of older MCNP versions (e.g. MCNP5) takes into account the whole cascade scheme of a radionuclide. Two different geometry cases were simulated with the Monte Carlo. The first where the particles (histories) were generated inside the fish volume and the energy deposited in the fish volume (internal) and in the water volume around the fish (external) were recorded using the energy pulse height *F8 tally (Fig.3.5a). The second where the histories were generated in the water volume (around the fish) and the energy deposited inside the fish was also recorded using the *F8 tally (Fig. 3.5b). The second geometry was tested only for five (^{40}K, ^{137}C, ^{210}Pb and ^{208}Tl) from the seventeen radionuclides, as it requires more computational time so as to keep the density of generated particles in the two geometries (see below) the same. With the first geometry the calculation of both internal and external dose rates is feasible, while in the second geometry only the external dose rate was calculated. The first geometry approximated the external dose rate calculation of ERICA, while the second one corresponds to (the definition of) the external dose rate concept. With the aim of associating the external dose rates of the two geometries, it was crucial to keep the (density of) histories that escape the water volume and reach the fish volume in the second geometry to be the same as the (density of) histories that escape the fish volume and deposit their energy in the water volume in the first geometry. Thus, the ratio of generated histories to the volume of interest (fish volume in the first geometry and water volume in the second geometry) was kept the same in the two geometry cases.

The effective (spherical) water volume – a quasi-infinite homogeneous medium volume, where the organism resides - was calculated using as radius the length attenuation of the highest gamma-ray of the isotope, assuming the loss of 10000 to 1

gamma-ray photons. In the cases of radionuclides with high photon energies of low intensities, the effective volume was calculated using the attenuation length of the maximum gamma energy with intensity 0.1% at least (higher energies with lower intensities were excluded). In the case of pure beta or alpha emitters, the effective volume was calculated by lengthening the fish effective radius with the endpoint beta-decay-energy range or the alphas' range. The histories generated in the fish volume were 10^5. The energy cutoffs in MCNP-CP for photons were the default ones (1 keV) and for electrons, 10 keV or 3 keV to match the ERICA Tool assumptions. The activity concentration in the water was assumed to be 1 Bq l^{-1} for all radionuclides. The activity concentration in the fish –for the first geometry case- (calculated using the CRs of the ERICA Tool) was 1 Bq kg^{-1}, 84 Bq kg^{-1}, 33000 Bq kg^{-1}, 33000 Bq kg^{-1}, 5000 Bq kg^{-1}, 5300 Bq kg^{-1}, 84 Bq kg^{-1}, 9 Bq kg^{-1}, 9 Bq kg^{-1}, 11263.5 Bq kg^{-1}, 250 Bq kg^{-1}, 80000 Bq kg^{-1}, 1400 Bq kg^{-1}, 50 Bq kg^{-1}, 25 Bq kg^{-1}, 25 Bq kg^{-1}, 1 Bq kg^{-1} and for ^{40}K, ^{137}Cs, ^{210}Pb, ^{210}Bi, ^{208}Tl, ^{57}Co, ^{134}Cs, ^{131}I, ^{132}I, ^{140}La, ^{59}Ni, ^{210}Po, ^{242}Cm, ^{231}Pa, ^{90}Sr, ^{90}Y and ^{3}H, respectively. As mentioned before, the ERICA Tool assumes secular equilibrium between the parent and the daughter nuclides, if the half-life of the latter is less than 10 days, as in the cases of ^{210}Pb- ^{210}Bi and ^{90}Sr-^{90}Y. Therefore, in the MCNP-CP code these radionuclides were simulated separately.

a) 1st geometry b) 2nd geometry

Fig. 3.5 The simulated geometries executed by MCNP code (the gray color represents the generated histories).

The external dose rates in μGy h^{-1} of ^{40}K, ^{137}C, ^{210}Pb and ^{208}Tl radionuclides for the first geometry and second geometry cases are presented in Table 1. In the table are presented: (a) the radionuclide of interest, (b) the estimated dose rate with the ERICA Tool and the Monte Carlo code, (c) the ratio of the dose rate estimated by the Tool to the one calculated using the MCNP-CP code and (d) the statistical error of the Monte Carlo simulations (in %). The major contribution in the external dose rates, was observed for the ^{137}Cs and ^{208}Tl radionuclides compared to the one of ^{40}K and ^{210}Pb, for both geometries (Table 1). The ^{137}Cs and ^{208}Tl radionuclides are characterized by medium and high energy gamma-ray photons, thus the energy deposition of these radionuclides is higher than the energy deposition due to ^{210}Pb. The external dose rate of ^{40}K was also lower than the one of ^{137}Cs and ^{208}Tl, even though ^{40}K is characterized by a high energy gamma-ray (1460 keV) emission. This difference is explained through the decay scheme of ^{40}K, as only a branching ratio of 10.7% is followed by the 1460 keV gamma-ray photon. The external dose rate results obtained by both codes were in good agreement – up to 12% - for all radionuclides. The external dose rate results obtained by both codes (ERICA and MCNP-CP) for the second geometry were in good agreement – within 6 % - for all radionuclides. In both geometry cases the external dose rate calculations (using the MCNP-CP code) were in good agreement with the ERICA Tool estimations, therefore the external dose rate calculation using these two

alternative ways (ERICA approximation (1st geometry) and external dose rate concept (2nd geometry) proved to be equivalent. The great advantage of the ERICA approximation was naturally the much reduced computational time. Thus for the remaining twelve studied radionuclides, the approximation of ERICA (1st geometry) was selected in order to test other decay types (e.g. pure beta, pure alpha, beta-gamma).

Table 1 External dose rates in calculation in μGy h^{-1} using ERICA and MCNP-CP code (for two different geometries).

		1st geometry			2nd geometry		
Radionuclide	ERICA	MCNP-CP	D.R	Error (%)	MCNP-CP	D.R	Error (%)
^{40}K	$8.87\ 10^{-5}$	$8.77\ 10^{-5}$	1.01	0.88	$9.45\ 10^{-5}$	0.94	7
^{137}Cs	$2.88\ 10^{-4}$	$2.87\ 10^{-4}$	1.00	0.16	$2.72\ 10^{-4}$	1.06	2
^{210}Pb	$4.81\ 10^{-6}$	$9.35\ 10^{-7}$	0.88	1.56	$7.59\ 10^{-7}$	1.01	2
^{210}Bi		$4.53\ 10^{-6}$		2.41	$3.99\ 10^{-6}$		3
^{208}Tl	$1.78\ 10^{-3}$	$1.78\ 10^{-3}$	1.00	0.07	$1.80\ 10^{-3}$	0.99	6

D.R. : the difference ratio between ERICA and MCNP-CP
Error is the statistical error of the Monte Carlo simulations

In Table 2, the results of the external dose rate calculation using ERICA and MCNP/MCNPX codes for all studied (seventeen) radionuclides are summarized. The error in the second geometry is higher due to the small number of generated histories for the given volume. The external dose rates were in good agreement (up to 12%), in all cases of (high) beta-gamma decays (^{40}K, ^{137}Cs, ^{210}Pb+^{210}Bi, ^{208}Tl, ^{134}Cs, ^{131}I, ^{132}I, ^{140}La), as well as (up to 6%) in the cases of pure high-beta emitters (^{90}Sr, ^{90}Y). The case of low energy beta radiation was tested (^{3}H), where the external dose rate has no physical meaning as the number of electrons expected to escape the fish volume and deposit their energy in the water volume were insignificant. This fact was verified by the MCNP simulation, as the external dose rate was 9 orders of magnitude lower than the internal one and it was not included in Table 2. The low energy beta radiation was also verified for the ^{59}Ni nuclide, which decays with electron capture mode and emits only X-ray photons up to 7 keV. The external dose rate was not included in Table 2, for the same reason as ^{3}H. Finally, the alpha radiation (^{210}Po, ^{242}Cm, ^{231}Pa) case was also tested. Even if the alpha decay radiation does not contribute in the external dose rate estimation (see ^{210}Po and ^{242}Cm cases not included in Table 2), the calculated external dose rate of ^{231}Pa (alpha, beta and gamma emitter) was found 23% higher than the one calculated by the MCNP-CP code.

Table 2 The external dose rate results in μGy h^{-1} using ERICA and MCNP-CP/MCPX codes for different decay procedures.

	ERICA	MCNP-CP	D.R.	Error (%)	comment
^{40}K	8.87 10^{-5}	8.77 10^{-5}	1.01	0.88	beta-gamma
^{137}Cs	2.88 10^{-4}	2.87 10^{-4}	1.00	0.16	beta-gamma
^{210}Pb	4.81 10^{-6}	9.35 10^{-7}	0.88	1.56	beta-gamma
^{210}Bi		4.53 10^{-6}		2.41	
^{208}Tl	1.78 10^{-3}	1.78 10^{-3}	1.00	0.07	beta-gamma
^{134}Cs	7.92 10^{-4}	7.91 10^{-4}	1.00	0.08	beta-gamma
^{131}I	1.93 10^{-4}	1.92 10^{-4}	1.00	0.12	beta-gamma
^{132}I	1.17 10^{-3}	1.16 10^{-3}	1.01	0.09	beta-gamma
^{140}La	1.21 10^{-3}	1.21 10^{-3}	1.00	0.07	beta-gamma
alpha decay (pure alpha (^{210}Po, ^{242}Cm), alpha-gamma (^{231}Pa)					
^{210}Po	-	-	-	13.91	pure alpha (MCNPX)
^{242}Cm	-	-	-	14.13	pure alpha (MCNPX)
^{231}Pa	1.92 10^{-5}	7.09 10^{-7}	-	16.65	mcnp-x (only alpha)
^{231}Pa		1.49 10^{-5}	1.23	0.93	mcnp-cp (only gamma & beta), 3keV cutoff
beta decay (pure high (>10keV) beta (^{90}Sr+^{90}Y), pure low (<10keV) beta (^{3}H)					
^{90}Sr	2.48 10^{-5}	7.58 10^{-7}	0.99	4.34	endpoint beta energy range
^{90}Y		2.44 10^{-5}		1.50	
^{3}H	-	-	-	10.19	~ mean energy, 1keV cutoff
beta-gamma decay (low gamma or only X-ray photons)					
^{57}Co	6.09 10^{-5}	6.07 10^{-5}	1.00	0.11	3keV cutoff
^{59}Ni	-	-	-	5.36	x-ray range, 3 keV cutoff

D.R. : the difference ratio between ERICA and MCNP-CP
Error is the statistical error of the Monte Carlo simulations

As shown in Table 3, the internal dose rates were higher than the external ones, as many radionuclides are characterized by alpha decay, beta decay and emit high energy electrons, X-ray and gamma-ray photons. Additionally, the alpha and beta-electron ranges are shorter than the X-ray and gamma-ray photon ranges and the radius of fish geometry, therefore all the alpha decay particles and beta decay electrons deposit practically their whole energy inside the fish volume, while the X-ray and gamma-ray photons only partially. The ERICA and MCNP-CP estimated internal dose rates were in good agreement (up to 8%), in all cases of (high) beta-gamma decays (^{40}K, ^{137}Cs, ^{210}Pb+^{210}Bi, ^{208}Tl, ^{134}Cs, ^{131}I, ^{132}I, ^{140}La), as well as (4%). in the cases of pure high-beta emitters (^{90}Sr, ^{90}Y). In the case of low energy beta radiation (^{3}H) the estimated internal dose rates of ERICA and MCNP code differed by a factor of 3, due to the weighting factors assumption of the ERICA Tool. The weighting factor assumption was also verified for the ^{59}Ni nuclide (low-beta radiation), which decays with electron capture mode and emits only X-ray photons up to 7 keV. The low X-ray photons produce low beta electrons, therefore ^{59}Ni can be thought as "pure" low beta emitter for the estimation of the internal dose rate (in ERICA). In the alpha radiation case for the internal dose rate estimation, the energy deposited due to alpha radiation must be weighted by a factor of 10 in the **total** internal dose rate estimation. The factor of 10 difference between ERICA and MCNPX code, is verified in the cases of pure

alpha (^{210}Po, ^{242}Cm) and alpha-gamma decays (^{231}Pa). If this factor is taken into account the internal dose rates calculated by both codes were in good agreement (up to 2%).

Table 3 The internal dose rate results in μGy h^{-1} using ERICA and MCNP-CP/MCPX codes for different decay procedures

	ERICA	MCNP-CP	D.R.	Error (%)	comment
^{40}K	3.03 10^{-4}	2.80 10^{-4}	1.08	-	beta-gamma
^{137}Cs	1.53 10^{-2}	1.58 10^{-2}	0.97	-	beta-gamma
^{210}Pb	8.35	4.66 10^{-1}	1.00	0.12	beta-gamma
^{210}Bi		7.90		0.19	
^{208}Tl	2.55	2.66	0.96	0.08	beta-gamma
^{134}Cs	1.68 10^{-2}	1.69 10^{-2}	0.99	0.07	beta-gamma
^{131}I	1.24 10^{-3}	1.26 10^{-3}	0.99	0.09	beta-gamma
^{132}I	3.87 10^{-3}	3.91 10^{-3}	0.99	0.00	beta-gamma
^{140}La	4.95	5.05	0.98	0.00	beta-gamma
alpha decay (pure alpha (^{210}Po, ^{242}Cm), alpha-gamma (^{231}Pa)					
^{210}Po	2.44 10^{3}	2.44 10^{2}	10.00	-	pure alpha (mcnp-x)
^{242}Cm	4.93 10^{1}	4.92	10.02	-	pure alpha (mcnp-x)
^{231}Pa	1.44	1.43 10^{-1}	9.98	-	mcnp-x (only alpha)
^{231}Pa		9.01 10^{-4}		-	mcnp-cp (gamma & beta), 3keV
beta decay (pure high (>10keV) beta (^{90}Sr+^{90}Y), pure low (<10keV) beta (^{3}H)					
^{90}Sr	1.57 10^{-2}	2.93 10-^{3}	0.96	-	endpoint beta energy range
^{90}Y		1.33 10^{-2}		-	
^{3}H	8.23 10^{-6}	3.26 10^{-6}	2.53	-	~ mean en.,1keV
beta-gamma decay (low gamma or only x-ray photons)					
^{57}Co	1.98 10^{-1}	1.08 10^{-1}	1.83	0.14	3keV
^{59}Ni	2.31 10^{-3}	8.28 10^{-4}	2.79	0.12	x-ray range, 3 keV

D.R. : the difference ratio between ERICA and MCNP-CP
Error is the statistical error of the Monte Carlo simulations

To conclude, in this work the internal and external dose rates for a marine organism (pelagic fish) were calculated using two different codes, a general purpose MC code (MCNP-CP/MCNPX) and a more specialized one (ERICA Tool). A good agreement of the calculated dose rates – up to 8% for the internal dose rate and up to 12% for the external dose rate - using the two codes for a simple case scenario was obtained. Additionally, two different geometry cases were tested for the external dose rate calculation using MCNP, the first geometry case approximated the ERICA Tool external dose rate estimation and the second one was the external dose rate as routinely defined in physics. In both cases the agreement was satisfactory (up to 6%), therefore the ERICA approximation is well established for the pelagic fish case.

3.2.3 Dose rate estimation

Tier 2 of the ERICA Assessment Tool was used to calculate dose-rates for a number of marine organisms which are common in near shore marine environments such as the study areas (Stratoni, Oxygono Bay) of this work. The maximum values of activity concentration in the sediment of ^{226}Ra, ^{228}Ra, ^{224}Ra, ^{210}Pb, ^{235}U and ^{137}Cs were utilized in the dose rate estimations. The default values of dose conversion coefficients (DCCs), concentration ratios (CRs) and sediment-water distribution coefficient (K_ds) were used.

Additionally, as the contribution of ^{40}K in the marine environment cannot be considered negligible, the radionuclide was added to the radiological model. All the parameters were added prior to the calculations according to the following procedures and assumptions: (a) the dose conversion coefficients were calculated via a dosimetric module (Ulanovksy and Prohl, 2006; Ulanovsky et al., 2008), (b) the K_d values are highly depended on environmental factors and (c) the CR of ^{40}K is not available in the database of the tool neither in recent bibliography. Regarding (b), K_d data of ^{40}K are not available for marine environments and thus an estimated value of ^{40}K activity concentration in the seawater based on the salinity was used (the ^{40}K activity concentration in the sediment was determined via the gamma-ray measurement of itself in a HPGe detector). The activity concentration of ^{40}K in seawater was calculated by converting a representative salinity value to activity concentration (Tsabaris & Ballas, 2005). Concerning (c), the similarities of the chemical properties between potassium and sodium were taken into account and the values for the latter were used as obtained from the IAEA technical report (IAEA, 2004). It is also mentioned that for the case of polychaete worms the CR value of crustaceans was used, considering them similar reference organisms living in and/or so close to the seabed.

Especially for the case of Oxygono Bay, salinity measurements were not available. Therefore, an approximation was followed where the K_d value of ^{40}K was obtained as the ratio of sediment activity concentration to seawater activity concentration (Pappa et al., 2018). The latter value was measured via the KATERINA underwater in-situ detector system (Tsabaris et al., 2008). However, this approximation could not be applied for the other natural radionuclides (^{238}U and ^{232}Th daughters), as their activity concentrations in the seawater were below the minimum detectable activity (MDA) of the KATERINA system and thus, the default K_d values of these elements were used for the dose rate calculation.

The main uncertainty of the aforementioned approximation in Oxygono Bay, is that the seawater ^{40}K activity concentration resulted from ^{40}K measurement in the seawater column, 1 m above the sediment and not in the seawater-sediment interface, where the equilibrium among the two phases (liquid and solid) is assumed and K_d is defined. Two ERICA runs were executed using the site specific K_d values of Stratoni and Oxygono. The former is closer to K_d definition as the ^{40}K value in the seawater was measured indirectly via a salinity meter located in the seawater-sediment interface. Comparing the total dose rates of each reference organism inserted in ERICA, based on the two K_d values, the differences were below 2% except from zooplankton where the differences are 9%, thus this procedure (using KATERINA system for ^{40}K seawater measurements) was considered a good first approximation if site specific data do not exist.

Chapter 4

Materials and Methods

In this chapter the following topics are described: the characteristics of the studied areas (Stratoni, Lavrio), the sampling procedures, the sample preparation, the measurement methodologies, the chronological models and the approach of the mass flux estimation.

4.1 Sampling and field work

This work is focused on marine areas near mining locations, which have been affected by anthropogenic activities. Generally, naturally occurring radioactive material (NORM) measurements have been held near mining areas of e.g. gold, coal, uranium etc., as the NORM concentrations of the residual masses after the mineral exploitation were expected to increase. However, these studies have been performed in other type of mines, like those mentioned before, and not in multi-metallic mines, as well as they have been focalized on the terrestrial areas (soil, river and lake matrices) and not in the marine ones. To summarize, the NORM study regarding the marine environment of mines is scarce. Thus, in the present work two marine areas near multi-metallic mines, an operating and an abandoned one, were studied for their environmental status through processes that produce NORMs and metals. In both cases samples from the coastal area (marine and terrestrial) were collected to study the interaction between the marine and terrestrial coastal areas.

4.1.1 Study area

The selected marine areas of the operating and the abandoned mine are located in the north and central Greece, in Stratoni and Lavrio, respectively. Both areas are characterized by mining activities, since ancient times until nowadays.

4.1.1.1 Stratoni

Stratoni is located in Ierissos Gulf, in Chalkidiki Peninsula in northern Greece. The gulf is characterized by a surface of 116 km^2 and a volume of 8.30 x 10^9 m^3, is one of the larger semi-enclosed water bodies in the Thracian Sea and is considered important nursery and fishing ground of North Aegean Sea for pelagic species (Sylaios et al., 2006). Ierissos Gulf has an elliptical shape with a northwest-southeast orientation. The bottom is steep near the coast and the isobaths increase away from the coast, whereby the 50-m isobaths is lying very close to shore. Moving seawards (northeast) the slope diminishes and reaches a maximum depth of 80 m at the central part of the gulf. The mouth of the gulf is closed by a southeast-sloping sill with a depth of 65-70 m (Perissoratis et al., 1989; Sylaios et al., 2006).

Stratoni lies between latitudes 40º 30’ and 40º 23.9’ and longitudes 23º 49’ and 23º 53.10’. For the sake of completeness a brief description of the geology and mineralization, as well as the physiography and hydrology of the terrestrial part of the study area follow.

Geology and mineralization

Stratoni is part of the mining area, well known as Kassandra mining district, (Mavres Petres, Madem Lakkos and Stratoniki deposits) which is characterized by polymetallic mineralization. Kassandra mining district is part of the Serbo-Macedonian Massif (SMM), characterized by Paleozoic or older age geotectonic units (Kerdilion, Vertsikos) and various chronologically younger (Tertiary) post-orogenic granitoids. The SMM is divided into two lithostratigraphic and tectonic units, the lower Kerdilion Formation in the eastern part and the upper Vertsikos Formation in the western part (Gilg and Frei, 1994), which are separated by the Stratoni-Varvera fault. The Kerdilion formation consists of migmatitic biotite gneisses, hornblende gneisses, amphibolite lenses and two phlogopite-bearing marble horizons and the Vertsikos Formation is composed of two mica gneisses, garnet-, staurolite- and kyanite-bearing mica schists, amphibolites, metagabbros and ultramafic bodies (Gilg and Frei, 1994). Additionally, Kassandra mining district is composed from metamorphic host rocks, igneous rocks, hydrothermal minerals (Cu skarn, porphyry Cu mineralization, carbonate-hosted Pb-Zn-Ag-Au replacement ores). The Mavres Petres, Madem Lakkos and Stratoniki deposits are controlled by the northwest-southeast trending Varvara- Stratoni fault. The primary minerals in these deposits are pyrite (FeS_2), galena (PbS), sphalerite/zinc blende (ZnS), while secondary ones are arsenopyrite (FeAsS), rhodochrosite ($MnCO_3$), chalcopyrite ($CuFeS_2$), bornite (Cu_5FeS_4) and magnetite ($Fe^{2+}Fe^{3+}{}_2O_4$) (Kelepertsis et al., 2006; Kelepertzis et al., 2012). Some of the gangue minerals - meaning commercially worthless material that surrounds, or is closely mixed with, a wanted mineral in an ore deposit - are quartz (SiO_2), rhodochrosite ($MnCO_3$) and calcite ($CaCO_3$).

Physiography and hydrology of terrestrial area

Kassandra mining district belongs to the catchment region of the wider area of Stratoni. The streams (Piavitsa, Kerasia and Kokkinolakkos) of the drainage basin have their source in the foothills of Stratonikon Mountain, are located northward of Stratoni–Varvara fault, follow a general north–south direction and discharge in Asprolakkas stream. Asprolakkas stream has a west–east direction, flowing toward the north part of Ierissos Gulf. The wider area of Stratoni is characterized by mountainous relief with approximately 92% of the surface covered by deciduous forest, and by a well-developed dendritic style drainage network (Kelepertzis at al., 2012). The elevation reach 600 m in the west part of Stratoni's wider area and gradually decrease towards the sea. Stratoni is characterized by typical Mediterranean climate, with rainy winters and dry-warm summers. The average pluviometry of the area is 650 mm, whereby the 50% of the annual rainfall occurs between November and February. The area is classified as mining concessions, however it is adjacent in the north to a protected area of NATURA 2000 (Kelepetsis et al., 2006) and thus the mining activities have raised environmental pollution concerns in recent years.

4.1.1.2 Lavrio

Lavrio (municipality of Lavreotiki) is a town of south-east of Athens at Lavreotiki Peninsula. The region runs along the western coast of the Aegean Sea. The study area is the coastal part of Lavrio and lies between latitudes 37º 45.6' and 37º 41.9' and longitudes 24º 3.6' and 24º 53.5'. Additionally, includes the bays of

Thorikos, Delenia, Perdika and Oxygono, whereby emphasizing in the latter. Again, for the sake of completeness a brief description of the geology and mineralization, as well as the physiography and hydrology of the terrestrial part of the study area follow.

Geology and mineralization

The Lavreotiki area belongs to the Attico-Cycladic gaotectnic zone and its rock formations can be subdivided into two distinct units: (a) the autochthonous Attica unit and (b) the overthrust cover or Lavrion unit. The former consists of marble (often dolomitized), mica schist and mafic-ultramafic rocks. The latter is a allochthonous formation, trust on top of the metamorphosed Attica unit and it costists of phyllite, quartzite, sericite-chlorite schist, metamorphosed mafic rocks and marble intercalations (Demetriades & Vergou-Vichou, 1999). Lavreotiki Peninsula is rich in mixed sulfide (galena (PbS), sphalerite (ZnS), pyrite (FeS_2)) and iron-manganese ores (manganese bears ankerite ($Ca(Fe,Mg,Mn)(CO_3)_2$) or rhodochrosite ($MnCO_3$) with baryte ($BaSO_4$), fluorite (CaF_2), quartz (SiO_2)). Except from these primary minerals, in the Lavretoki Peninsula have been identified many secondary minerals, mainly sulphides, arsenates, carbonates, chlorides, fluorides, phosphates, hydroxides, molybdates, oxides, silicates, sulphates, sulphosalts, vanadates and native metallic elements (Demetriades & Vergou-Vichou, 1999). In the primary minerals of mixed sulphides, exist minerals associated with other elements such as As, Ag, Au, Bi, Cu, Ni, Co etc. Accessory -secondary mineral which is present in small amounts in a rock, but is not characteristic of the rock - and gangue minerals of the mixed sulphides are fluorite (CaF_2), barite ($BaSO_4$), ankerite ($Ca(Fe,Mg,Mn)(CO_3)_2$), quartz (SiO_2), chalcedony (SiO_2), calcite ($CaCO_3$), kaolinite ($Al_2Si_2O_5(OH)_4$), etc.

Physiography and hydrology of terrestrial area

The landscape of Lavrio is hilly or semi-hilly and the elevation reaches 373 m. Intense parts of the relief appear in some parts of the basin where ravines exist (Stamatis et al., 2002). The climate of Lavrio is a typical Attica Mediterranean type, with long, dry periods (May to October) mainly in the summer and a short, wet period in the winter, when the highest precipitation is experienced. The average annual rainfall is 385 mm.

4.1.2 Sampling methodology

In this subsection the field work performed in both studies areas (Stratoni, Lavrio) is described. In both cases, two sampling surveys were held, a preliminary and a more extended. The matrices studied were sediment (beach sand, seafloor) in both areas and seawater in Stratoni case. Especially for Stratoni, sediments (streambed, streambank) from the two main streams discharging in Ierissos Gulf were also collected as the scope of this work was to perform a thorough study regarding the coastal area. Stratoni is located near or at a mining district where the mining operation is still on-going. Little data are published regarding the impact of these activities in metal concentrations, while no data are available concerning NORM concentrations at the terrestrial and marine region. On the other hand, in Lavrio, an extended study has been performed mainly from the Institute of Geology and Mineral Exploration (IGME) and the literature is rich in studies held in the area regarding mainly the mining anthropogenic impact to the terrestrial part. Nevertheless, no data are available

concerning NORM concentrations at the terrestrial and marine region. All this work has been published or held after the cessation of the mining activities in the late 1980's, therefore in the present work the rivers or streams discharging in Lavrio coastal area were excluded.

Stratoni

Two sampling campaigns (July 2012, June 2014) and a complemental one (July 2015) were held in the coastal and offshore area of Ierissos Gulf, respectively. During the preliminary study (July 2012) 9 surface sediments were collected from the upper seabed layer (approximately 2 cm) by a diver, so as to estimate the seafloor's current status (sample code S#). In the same locations oceanographic measurements (e.g. salinity, temperature) were performed using a portable CTD (Conductivity-Temperature-Density) instrument. The sampling locations were organized to represent the status of the area near Stratoni's flotation plant (load out pier area of Stratoni port, the adjacent area of Stratoni port), the estuary of the main stream (Kokkinolakkos) affected by the mining activities and the reference site. The selected reference site was Ierissos port as it is located in the middle of the coastline of Ierissos Gulf, at a distance of approximately 13 km from Stratoni area and approximately 9 km from Kokkinolakkos estuary.

The second sampling survey (June 2014) was more detailed, wherein samples were collected from the marine and the terrestrial area (sample code STR#). The marine samples included sediment (surface, core) and seawater samples, while the terrestrial ones included only surface sediments. The surface-sediment marine samples were collected from the seafloor and the sea-coast interface and the water marine samples were collected from the sediment-seawater interface keeping in mind the locations and the scope of the preliminary survey. The terrestrial samples were collected from the beach sand of Ierissos Gulf and the riverbed and river bank of the two main streams (Kokkinolakos, Kalatzi Lakkos). In total 30 sediment and 8 water samples were collected. Additionally, a sediment core (code CS, approximately 30 cm depth) was also collected near the load out pier area of Stratoni port (point STR1 in the map), so as to study the anthropogenic impact of previous years. In all the marine locations CTD measurements were conducted. The surface seafloor sediments, sediment core and seawater samples were collected by a diver. The sample collected at the sea-coast interface (STR12_a) of Ierissos port was discarded, due to its coarse nature (grain size above 3 mm).

The complemental sampling was held by the crew of research vessel "Aegeao" of HCMR in July 2015, wherein a core sediment (approximately 30 cm depth) and a surface sediment sample were collected using box-corer (code STR#). These sites were located offshore of Stratoni port. The surface sample of the core (STR8) (1.5 km distant from the load out pier) and of site (STR9) (6.0 km distant from the load out pier) were used as input for the dispersion model estimation while the maximum depth of STR8 core was used as background to estimate the metal flux profiles. The sampling locations of all campaigns are shown in Fig. 4.1 and the performed field work, the site coordinates (in decimal degrees) and site oceanographic measurements are presented in Table 4.

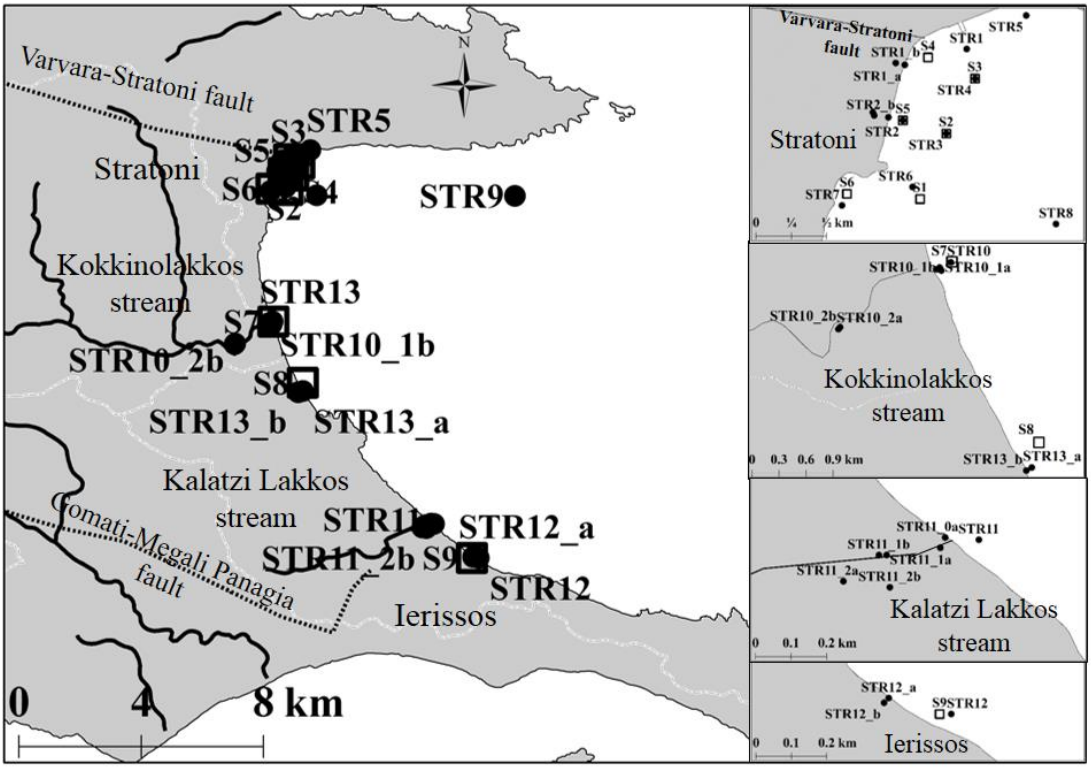

Fig. 4.1 The map of sampling points for preliminary (squares) and extended (black dots) surveys. The preliminary survey was held in July 2012 (code S#), the second survey took place in June 2014 (code STR#) and the complemental sampling occurred in July 2015 (STR8 and STR9 sites).

Table 4 The sampling data of Ierissos Gulf. The types of samples (s.w.: seawater, s.s.: sediment, c.s.: core sediment) collected in each station for all sampling campaigns (July 2012_code S#, June 2014_code STR#, complemental sampling July 2015_STR8 and STR9) followed by oceanographic parameters are summarized below. The "s.s." sample includes sediment from seafloor (code STR#_a), sea-coast interface (STR#_b), riverbed (code STR#_a) and/or riverbank (STR#_b). Beside the name of samples coded STR# (second sampling) the name of the samples of the preliminary sampling is given inside the parenthesis.

Station	**Latitude**	**Longitude**	**Depth (m)**	**Temp* (°C)**	**Salinity (‰)**	**DO** (mg L^{-1})**	**s.w.**	**s.s.**	**c.s.**
S1	40.506500	23.830667	0	26.9	34.20	-			
			20	21.4	35.90	-		√	
S2	40.510667	23.832333	0	26.7	34.40	-			
			20	19.6	26.40	-		√	
S3	40.514157	23.834162	8	26.5	28.80	-			
			22	20.5	29.60	-		√	
S4	40.515500	23.831167	-	-	-	-		√	
S5	40.511500	23.829558	6	-	-	-		√	
S6	40.506833	23.826000	4.8	27.2	22.70	-		√	
S7	40.467833	23.826500	2.4	27.2	34.50	-		√	
S8	40.449833	23.835167	2.3	26.9	34.00	-		√	
S9	40.398334	23.885033	3.4	26.8	34.60	-		√	
STR1 (near S4)	40.516033	23.833638	0.0	25.1	30.20	7.56			
			5.0	24.8	30.60	7.53			
			10.3	24.6	30.24	7.33	√	√	√
STR1_a	40.515028	23.829287	-	-	-	-		√	
STR1_b	40.515147	23.829116	-	-	-	-		√	

Table 4 Continue…

Station	Latitude	Longitude	Depth (m)	Temp* (ºC)	Salinity (‰)	DO** (mg L^{-1})	s.w.	s.s.	c.s.
STR2 (S5)	40.511500	23.829558	0.0	25.3	25.76	7.79			
			5.2	25.3	25.96	7.60			
			9.2	26.3	25.60	7.30	√	√	
STR2_a	40.511694	23.828106	-	-	-	-		√	
STR2_b	40.511809	23.827742	-	-	-	-		√	
STR2_b2	40.512011	23.827652	-	-	-	-		√	
STR3 (S2)	40.510667	23.832333	0.0	23.9	26.00	8.07			
			6.4	23.9	27.40	8.04			
			13.5	22.3	26.85	8.44	√	√	
STR4 (S3)	40.514150	23.834167	0.0	24.5	25.30	7.88			
			11.1	22.3	25.80	7.91			
			20.4	28.7	27.57	8.19	√	√	
STR5	40.518162	23.837434	-	-	-	-		√	
STR6 (near S1)	40.507267	23.830183	0.0	25.9	25.99	7.58			
			4.5	25.7	25.06	7.62			
			8.5	-	-	-		√	
STR7 (S6)	40.506100	23.825683	0.0	25.6	25.03	7.78			
			4.5	25.9	25.34	7.61	√	√	
STR8	40.504917	23.839333	58.8	-	-	-			√
STR9	40.504675	23.897715	79.6	-	-	-		√	
STR10 (S7)	40.467783	23.826383	5.8	26.0	24.14	7.59	√	√	
STR10_1a	40.466967	23.825442	-	-	-	-		√	
STR10_1b	40.467258	23.825268	-	-	-	-		√	
STR10_1b2	40.467084	23.824939	-	-	-	-		√	
STR10_2a	40.461122	23.815165	-	-	-	-		√	
STR10_2b	40.461312	23.815333	-	-	-	-		√	
STR11	40.408333	23.872500	0.0	25.2	28.04	7.72			
			2.3	25.1	28.32	7.69	√	√	
STR11_0a	40.408393	23.871782	-	-	-	-		√	
STR11_0b	40.408129	23.871660	-	-	-	-		√	
STR11_1a	40.407949	23.871512	-	-	-	-		√	
STR11_1b	40.407944	23.871318	-	-	-	-		√	
STR11_2a	40.407279	23.870420	-	-	-	-		√	
STR11_2b	40.407127	23.870056	-	-	-	-		√	
STR12 (S9)	40.398333	23.885550	0.0	24.7	30.07	7.76			
			1.8	25.0	30.70	7.59			
			3.3	25.8	28.88	7.30	√	√	
STR12_a	40.398744	23.883957	-	-	-	-		√	
STR12_b	40.398621	23.883838	-	-	-	-		√	
STR13_a	40.447330	23.834449	-	-	-	-		√	
STR13_b	40.447026	23.833905	-	-	-	-		√	

*Temp: Temperature ** DO: Dissolved Oxygen

Lavrio

Two sampling surveys were held along the east part of Lavreotiki Peninsula in 2014 (January and April) and 2016 (October). The preliminary survey was held in January 2014, where surficial samples of beach sand (code P#) and coastal marine sediments (code I#) were selected at four bays Delenia, Oxygono, Thorikos and Perdika to determine the most affected area due to mining activities in the adjacent

region of the remediated site of Thorikos. Among those bays, Oxygono was selected for further investigation as the maximum concentrations were observed in this region. Therefore, two sediment cores, one near the coast (core 1) and the other in the offshore (core 2), were selected in April 2014 for the history reconstruction of the study area. The length of each core was about 52 cm. The coastal core was collected by a diver at 4.5 m depth and was located 50 m from the coast. The offshore core was collected by the HCMR's research vessel "Aegaeo" at 45 m depth (using a core sampler) and it was located at a distance of approximately 1880 m from the coast (between Lavreotiki Peninsula and Makronisos Island). The deep slice of the offshore core was selected to define the background level of the area, as it exhibited the minimum observed concentrations for the studied trace metals. Additionally, in October 2016 a more detailed study, focused on Oxygono Bay occurred, where five surficial coastal sediments (code N#) of approximately 2 cm depth were collected by a diver, so as to determine the spatial distribution of radionuclides and metals. A total of 14 samples (beach sand and coastal sediment) were collected during all sampling surveys. The sampling locations are shown in Fig. 4.2 and their coordinates (in decimal degrees) and sampling dates are presented in Table 5.

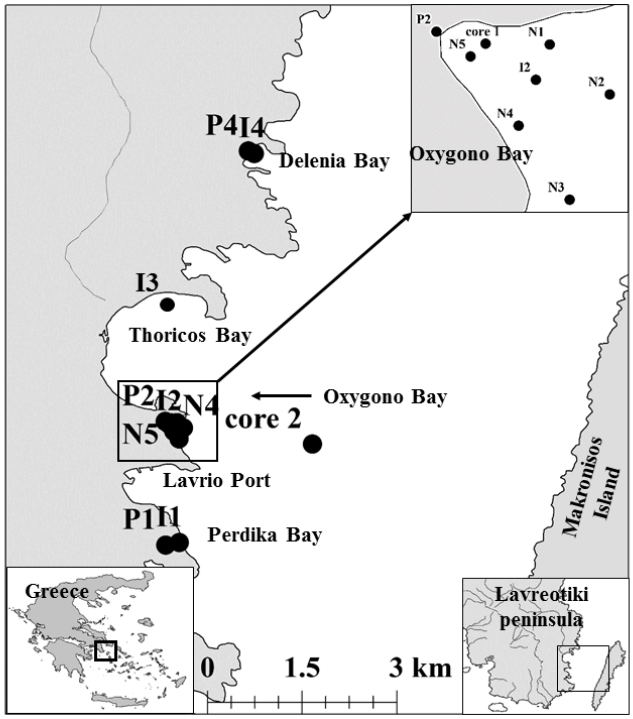

Fig. 4.2 The map of sampling points for all surveys. The preliminary survey of the eastern coastal area of Lavretoki Peninsula was held in January and April 2012 (code I#, P#, core 1 and core 2) and the second sampling survey was focused on Oxygono Bay and took place in October 2016 (code N#).

Table 5 The sampling data in decimal degrees of Lavreotiki Peninsula.				
Sample	**Latitude**	**Longitude**	**Sampling date**	**Comment**
core 1	37.719556	24.062874	April 2014	52 cm length
core 2	37.716500	24.083167		52 cm length
I1	37.702418	24.064149	January 2014	seafloor
P1	37.702026	24.062229		beach sand
I2	37.719021	24.063628		seafloor
P2	37.719744	24.062137		beach sand
I3	37.737820	24.061029		seafloor
I4	37.757983	24.074870		seafloor
P4	37.758369	24.074017		beach sand
N1	37.719550	24.063833	October 2016	seafloor
N2	37.718800	24.064733		seafloor
N3	37.717217	24.064133		seafloor
N4	37.718333	24.063367		seafloor
N5	37.719367	24.062650		seafloor

4.2 Sampling preparation

The sediment cores were sliced every 1 cm and with the surface sediments (e.g. seafloor, riverbed) were treated appropriately, using a standard procedure prior to radioactivity (gamma-ray spectrometry) and trace metal/major element measurements (X-ray fluorescence spectrometry). During this process (IAEA, 2003; Tsabaris et al., 2012a) the sediment samples were cleaned of stones, shells and algae, grains of size greater than 2 mm were discarded and finally the remaining sample (< 2 mm) was dried (105 ^{o}C for 24 h at least) and pulverized via a twin mill with agate mortars in a fine grain powder (< 63 μm). Before and after the drying, the wet and dry density, respectively, of the samples were measured. Additionally, before and after the pulverization, grain size distribution analysis or granulometry (see section 4.7) via sieving and density determination of the obtained homogenized powder were performed, respectively. The dry density measurement is important in the mass flux estimation (see section 4.5), the grain size distribution may be associated with discrepancies of NORM and trace metal/major element concentrations, and the density value of the pulverized sample is necessary for the self-attenuation corrections of low energy (< 100 keV) radioactivity measurements. During all these processes the used equipment (e.g. agate mortars, cylindrical containers) is cleaned in every step with deionized water, to avoid contamination among samples. The sample preparation was held in the sedimentology lab of HCMR.

4.2.1 X-Ray Fluorescence spectrometry (trace metals/major elements)

X-ray fluorescence (XRF) spectrometry can be applied for qualitative analysis as it can recognize a majority of elements between beryllium and uranium and it can be implemented for quantitative analysis (from μg g^{-1} to 100%). The main principle of XRF analysis is that the irradiated surface using primary X-rays, represents the whole sample and the preparation of the samples and the standards should ensure this condition. The XRF technique is very sensitive and requests clean samples, e.g. fingerprints on a sample can affect the result of the analysis. Thus, the preparation of

samples for the trace metal/major element measurement via X-ray fluorescence (Karageorgis et al. 2005), provides a smooth surface for irradiations and ensures a reproducible geometry. According to this methodology, 5 g of the sediment-powder were mixed with 1.25 g of wax powder and pressed (20 tn for 20 s) in a pellet (standard aluminum cup of 31 mm diameter), so as to determine trace metal concentrations. The pellet's surface must be free from cracks and wrinkles before the trace metal analysis. For the major element measurement, 0.6 g of the pulverized sample were fused with 5.4 g of flux (50:50 Lithium Meta- Borate, Lithium Tetra-Borate) and 0.5 g of Lithium Nitrate with 5.4 g of flux (50:50 Lithium Meta- Borate, Lithium Tetra-Borate) and 0.5 g of Lithium Nitrate, wherein a few drops of LiBr were used as non-wetting agent. The major elements are determined as oxides (Na_2O, MgO, Al_2O_3, SiO_2, TiO_2, Fe_2O_3, K_2O, CaO, P_2O_5 and MnO), thus the loss on ignition (LOI) must be measured to verify the correct preparation of the fused samples. The LOI determination is obtained by heating 1 g of dry sediment in a muffle furnace for 1 h at 1000^{o}C and by weighting the samples before and after heating.

LOI is an empirical parameter, used for the assessment of the content of non-volatile organic matter in the sample. It expresses the mass change as a result of heating a sample under specific conditions and it is given as a weight percentage of the dry mass. It should be noted that generally inorganic substances (e.g. H_2O, SO_2, O_2) can be released or absorbed, among them some are volatile under the reaction conditions, thus the loss of volatile inorganic substances can occur and give high values in the results. Possible causes wherein inorganic substances volatilize are (a) chemically bound water which is released during heating, (b) iron or other present metals in the sample in metallic state which can be oxidized during heating and produce lower results, (c) sulphides present in the sample which can be oxidized to sulphate during heating and produce lower results, (d) explosive ignition wherein the residue from the crucible is lost and this contributes to the LOI and (e) calcium hydroxide or calcium oxide present in large amounts which can be combined with sulphuric oxides liberated during ignition or with carbon dioxide formed during ignition producing lower results.

4.2.2 Gamma-ray spectrometry (radionuclides)

In order to obtain NORM concentrations by gamma-ray spectrometry technique, the pulverized samples were air-tightly sealed to standard cylindrical containers for 20 days to achieve secular equilibrium between radium ^{226}Ra and radon daughters (^{214}Pb, ^{214}Bi). Cylindrical containers of different volumes, made by polyethylen with thickness of 0.5 mm from the side and 1 mm at the top and bottom part were utilized depending of the available sample quantity. The air-tight sealing, in order to verify possible radon escape, was determined experimentaly. A few samples were measured in different time periods of 0, 20, 30 and 40 days and the activity concentrations of ^{214}Pb and ^{214}Bi were determined. In all cases the values of ^{214}Pb and ^{214}Bi were found the same – within uncertainties- for all time periods, verifying negligible radon escape. For the standard geometry of 68 mm inner diameter and 18 mm inner height (volume: 65 cm^3), a mass of 50 g to 100 g is needed depending on the grain size distribution of the samples. If the mass sample is not enough to fill the "big" standard geometry, the remaining volume is filled with a non-radioactive material (usually talcum powder), so as to all the prepared samples have the same geometry. This step is important for the self-

attenuation corrections among the samples and the calibration sources (standards). Additionally, in order not to change the matrix composition and sample homogeneity, a thin film is added between the sample and the non-radioactive material (e.g. talcum powder). This geometry is described in detail in EFFTRAN code and appropriate correction factors are produced for each sample separately. These correction factors are inserted in the equation of determining the activity concentration (see ET parameter in section 4.2.2). In case of samples wherein the usable mass is very little (< 30 g), mainly in the case of cores, such as the offshore core (core 2) of Lavrio study area, a different standard "small" geometry of 36 mm inner diameter and 5 mm inner height (volume: 5.7 cm^3) of a plexiglass container is used, filled with 5 g to 9 g of the fine pulverized powder. A part of samples (coastal sediment core of Lavrio) were re-measured for ^{210}Pb in a germanium planar detector (see section 4.3.1), thus these samples were put in cylindrical containers of polyethylene of 59 mm inner diameter and 18 mm inner height (volume: 49 cm^3).

4.3 Spectrometry systems

The main methods used in present work were gamma-ray and X-ray spectrometry for the determination of radioactivity (mostly NORM) and trace metal/major element concentrations, respectively. In the following subsections a succinct description regarding the gamma-ray detectors and X-ray spectrometer, the experimental set-up and the performed calibrations for both systems (gamma-ray, X-ray) is presented.

4.3.1 X-Ray spectrometer

X-ray fluorescence spectrometry has been an irreplaceable technique for elemental qualitative and quantitative analysis. Different type of spectrometers are commercially available such as wavelength-dispersive (WDXRF), energy-dispersive (EDXRF) or total reflection (TRXRF). In this work a brief presentation of a WDXRF instrument will be presented. Generally, WDXRF spectrometers are typically employed for both routine and non-routine analyses of a wide range of products such as ores and minerals, oils, glasses, powders, solutions. This type of spectrometer was obtained by the Biogeochemical laboratory of the Institute of Oceanography (HCMR), mainly for its application in geological research.

4.3.1.1 Spectrometer characteristics

The WDXRF system of HCMR includes the Phillips PW-2400 XRF spectrometer, employing a 3 kW rhodium (Rh) tube and a set of 8 crystals capable of measuring all elements from beryllium (Be) to uranium (U) in a non-destructive manner. Two detectors are used: (a) a gas flow proportional counter using argon and (b) a scintillator. The system may determine chemical elements in solids, powders as well as liquids and is accompanied by a 30-position robotic sample changer. All operations are computer controlled and the software is running under Microsoft Windows. The software (e.g. Panalytical's Pro-Trace) can perform a qualitative and semi-quantitative analysis of the unknown sample. The latter is a first approximation of the sample composition. A full quantitative analysis can be also carried out, using known standards e.g. certified materials or self-made standards for the calibration. The

accuracy and precision of the analysis depends on the quality of the samples and the standards.

4.3.1.2 Experimental set-up

Basically, the experimental set-up incorporated in the WDXRF spectrometer that was briefly presented above, is shown in Fig. 4.3. More specifically, the spectrometer consists of: (a) a high voltage supply, (b) an X-ray tube, (c) 8 diffraction crystals, (d) 2 collimators, (e) 2 detectors, (f) a multi-channel analyzer (g) a sample handling system and (f) control electronics. The X-ray tube is supplied with a super sharp end-window Rh target and is characterized by thin window, as well as by a short distance between the sample and the anode. The emitted photons from the X-ray tube excite simultaneously all the elements in the sample. The Rh target, incorporated in the X-ray tube, is a general purpose target proper for heavy metal excitation (medium performance) and light element analysis (high performance). Additionally, the operation of the tube remains constant at 3kW, so as to enhance the life of the tube. The spectrometer includes also primary beam filters to remove characteristic tube lines or to improve the peak to background ratio, which are placed between the X-ray source and the sample. The provided filters are: (a) brass (100, 300 μm), (b) Al (200,750 μm) and (c) Pb (1000 μm). The selection of the filters can be performed via the analytical software.

Additionally, the WDXRF system of HCMR consists of 8 analyzing/ diffraction crystals (or monochrometers). The crystal is a stack of thin layers of similar thickness, wherein each layer reflects the different energies of the characteristic radiation emitted from the sample into different directions. The reflected X-rays, emitted from the excited sample and obeying the Bragg's law, are those of interest which must be measured by the detectors. However, others with slightly different energy (wavelength) are also reflected and interfere with the energy measured by the detectors. Thus, the collimators (primary and secondary) are utilized to obtain parallel X-rays and exclude those which do not fall exactly at the required angle on the analyzing crystal. The NaI(Tl) scintillation counter is used for the detection of K_α radiation (for measurement of elements between Cu and U), while the proportional counter is used for the L_α radiation (for measurement of elements between Be and Cu). Both detectors produce an electrical pulse when an X-ray photon enters the detector. The pulse height is analog to the incoming photon energy, is amplified and counted by a multi-channel analyzer. As mentioned above, the WDXRF system consists of a 30-position robotic sample changer and all the operations, including calibration and analysis, are computer controlled.

4.3.1.3 Calibrations and LDM

Calibration curves were prepared for the major element determination, based on a large set of certified reference materials. Additionally, matrix corrections were applied to improve accuracy. A similar procedure was performed for the minor and trace metal determination using standards and Pro-Trace software. The software includes (a) a set of 25 high purity blanks, in the same geometry as the unknown samples, (b) single- or multi-element reference standards, (c) mass attenuation coefficient corrections and (d) concentration standards for 40 elements ranging among

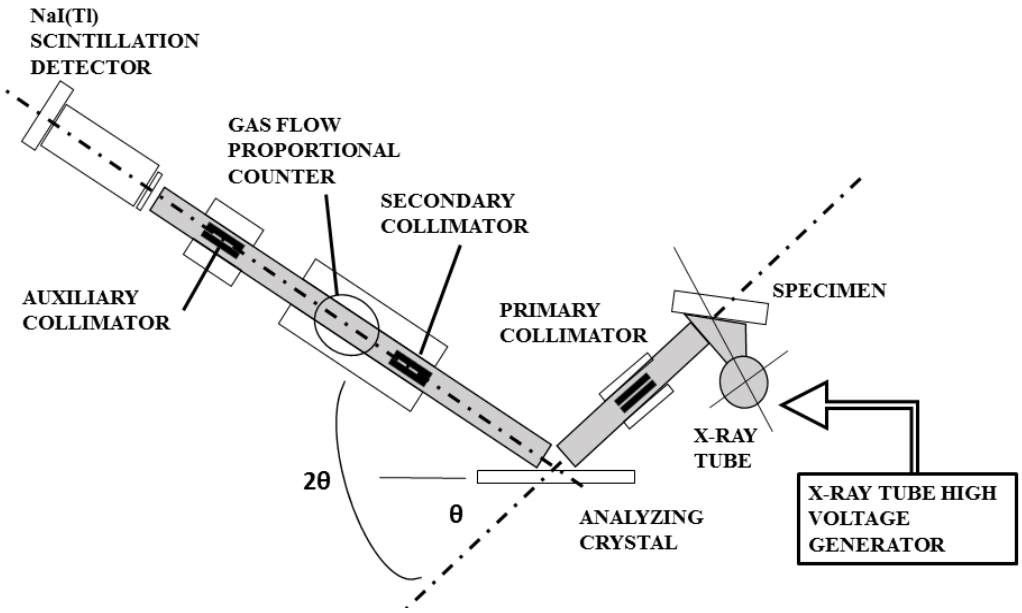

Fig. 4.3 The schematics of the wavelength-dispersive PW-2400 X-ray spectrometer

Be to U. Each one of the 40 minor and trace elements is calibrated individually against more than 200 internationally certified reference materials. The analysis is based on two-point calibration lines forced through the origin, thus the overall performance can be characterized by high accuracy and precision.

The stability of the WDXRF system is controlled periodically, by checking the temperature and the instrument drift over time. Regarding the temperature control, a synthetic multi-element sample is scanned (approximately 10 times) prior to analysis of unknown samples until stable conditions are achieved for all subsystems (e.g. X-ray tube, detectors, analytical crystals). Concerning the second control parameter (instrument analytical drifting), another synthetic multi-element sample is scanned in a monitoring base (e.g. every week) or in cases of a change in the WDXRF subsystems (e.g. new gas detector windows). Using the differences in the measured intensities, the software generates correction factors, which applies automatically in the following measurements of the unknown samples. During calibration, the analytical accuracy is also checked, prior and after every batch of unknown samples, using certified reference materials as unknown samples. The continuous comparison between the measured certified materials and the assigned ones ensures the reproducibility and accuracy of the measurements, achieving measurements with 95% confidence level. The quality control of the determination of metal concentrations (trace metal and major elements) was verified via the reference materials of MESS-2 and PACS-2 provided by the National Research Council of Canada. More information regarding the uncertainty of the metals of interest as well as the difference among the reference and the measured values are presented in Annexes V and I, respectively.

The low detection limit (LLD) is a minimum theoretical estimation of the smallest analyte amount that can be detected in a specimen, however it is not representative of true experimental results. Therefore, the limit of determination of the method (LDM) is determined for the XRF spectrometry, which is defined as the concentration of an element equivalent to two standard deviations of the same

representative concentration. LDM takes into account the uncertainties of sample preparation, instrument statistics and counting statistics. The LDM of the XRF method was calculated using a series of 6 to 10 replicate international certificate samples, measured in the same experimental conditions:

$$LDM = 2\sqrt{\frac{\sum_{m=1}^{n}\left(C_m - \overline{C}\right)^2}{n-1}} \qquad \text{(Eq. 4.1)}$$

where,
C_m is the sample concentration, n is the number of the sample produced by the same certified material and $\overline{C}$ is the mean concentration value, which is calculated as:

$$\overline{C} = \frac{\sum_{m=1}^{n} C_m}{n} \qquad \text{(Eq. 4.2)}$$

4.3.2 HPGe detectors

The gamma-ray spectrometry was performed via high purity Germanium detectors (HPGe). As their name suggests, HPGe detectors are semiconductor detectors manufactured by germanium (Ge). The higher atomic number of Ge comparing to Si (other type of semiconductor detectors), results in larger linear attenuation coefficient, which leads to a shorter mean free path. Therefore, Ge is preferred for hard X-ray or gamma-ray detection to achieve higher detection efficiency.

4.3.2.1 Detector characteristics

The radioactivity measurements are characterized for their high energy resolution. Four HPGe detectors were utilized of four different laboratories. The detectors were: (a) Ortec GEM-FX8530P4 (50%), (b) Canberra GC5021 (50%), (c) Canberra GL2020R and (d) Canberra GMX-90-220-S (100%) of the laboratories: (a) Marine Environmental Radioactivity Laboratory (MERL) at HCMR, (b) Nuclear Laboratory of Physics Department of National Technical University of Athens (NTUA), (c) Department of Physics of the Aristotle University of Thessaloniki (AUTH) and (d) Institute of Nuclear and Particle Physics of National Center for Scientific Research (NCSR) “Demokritos”. Most of the samples were measured at laboratories (a) and (b). The basic characteristics of the used gamma-ray detectors are presented in Table 6. More information regarding the operation of HPGe detector and the gamma-ray detection system are included in section 4.3.1.2 (Experimental set-up).

Table 6 The basic characteristics of the used gamma-ray detectors

	HCMR	**NTUA**	**AUTH**	**NCSR**
Company	Ortec	Canberra	Canberra	Canberra
Detector code	GEM-FX8530P4	GC5021	GL2020R	GMX-90-220-S
Detector type	p-type coaxial	p-type coaxial	p-type planar	n-type coaxial
Nom. rel. eff. [a]	50%	50%	-	100%
Energy range (keV)	0-1800	50-1800	0-200	0-1800
Detector's window	C-fiber	Al	Be	Mg
Window's thickness (mm)	0.8	1.8	0.5 mm	1.5
Detector diameter (mm)	84.8	63.5	50.5	75.6
Detector length (mm)	32.1	63.5	20	91.9
Useful surface (cm^2)	56.5	31.7	20	44
Useful volume (cm^3)	275	233	40	400
Operational voltage (V)	+4800[b]	+3500	+3100	-5000
FWHM (keV), 1.33 MeV	1.77 [b]	2.1	0.7[c]	2.05

a) Nom. rel. eff.: nominal relative efficiency
b) The detector of HCMR has been repaired, the new operational voltage is +2700 V and the FWHM is 1.72 keV at 1.33 MeV. During samples' (code S#) measurement period the detector operated in a lower voltage (+3700 V) than the optimum one.
c) The detector of AUTH is specialized for low energy measurements, thus the FWHM value of 0.7 keV corresponds to energy of 0.12 MeV.

In many cases, re-measurements were performed to determine ^{210}Pb concentrations, useful for the sedimentation rate and the mass flux estimations, in detectors appropriate of low-energy measurements (< 45keV) (see the "energy range" characteristic of Table 6). For convenience reasons a summarizing table (Table 7) shows the realized measurement for each gamma-ray spectrometry laboratory.

Table 7 The information of the performed radioactivity measurements for every gamma-ray laboratory

Code	**Location**	**Geometry** [a]	**Sample type** [b]	**HCMR**	**NTUA**	**AUTH**	**NCSR**
S#	Stratoni-Ierissos Gulf	big	surface (9)	R+^{210}Pb [c]			
STR#		big	surface (29)				R+^{210}Pb
STR 1		big	core (27 cm)	^{210}Pb	R		
STR8		big	core (27 cm)	R+^{210}Pb			
I#,P#	Oxygono - Lavrio	big	surface (7)		R		
N#		big	surface (5)	R+^{210}Pb			
core 1		big	core (52 cm)		R	^{210}Pb	
core 2		small	core (52 cm)		R		

a) The geometry column describes the geometry of the cylindrical boxes used in the measurements. "Big" geometry is referring to those of 65 cm^3 volume (and 49 cm^3 volume for AUTH laboratory) and the "small" geometry to those of 5.7 cm^3 volume).
b) The parenthesis beside the sample-type characteristic (surface or core sediments) represents the number of samples. In the core sediment case, the core was sliced every 1 cm, thus the length of the core indicates the number of samples.
c) The letter "R" describes radionuclide measurements (natural or artificial (^{137}Cs), not ^{210}Pb). When, ^{210}Pb measurements are also performed, then the indication "+^{210}Pb" is added.

An additional detection system was also applied in both sites of Stratoni port and Oxygono Bay to measure the natural radioactivity in the seawater and contribute to the determination of a K_d-parameter approximation as mentioned in section 3.2.3. The applied detection system was KATERINA, which is an underwater in-situ low resolution spectrometer (Tsabaris et al., 2008). This system is designed for qualitative

and quantitative (Bq m^{-3}) radionuclide detection in marine environment. However, it was used only for the estimation of ^{40}K K_d parameter as the activity concentrations of other natural radionuclides (^{238}U and ^{232}Th daughters) in the seawater, were below the minimum detectable activity (MDA).

4.3.2.2 Experimental set-up

The main characteristics of the detection system are (a) the HPGe detector, (b) the detector's preamplifier (pre-AMP), (c) the high voltage supply (HV), (d) the amplifier (AMP), (e) the analog-to-digital converter (ADC), (f) the multi-channel analyzer (MCA), (g) the uninterruptible power supply (UPS) and (j) the computer (PC). These characteristics are presented in Fig. 4.3:

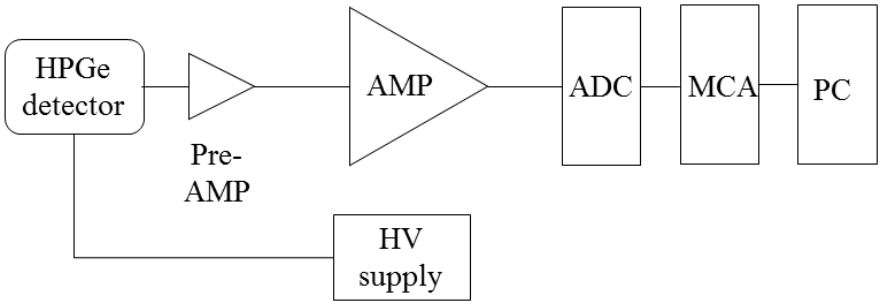

Fig. 4.4: The basic characteristics of the detection system, applied for gamma ray spectroscopy.

The high voltage supplies the p-n junction of the detector so as to form and expand the depletion region, with the depletion depth given by:

$$d \cong \sqrt{\frac{2\varepsilon V_0}{eN}} \qquad \text{(Eq. 4.3)}$$

where,
V_0 is the reverse bias voltage, ε is the dielectric constant of the semiconductor, e is the elementary charge ($1.6\ 10^{-19}$ C) and N is the net impurity concentration of the initial semiconductor material.

When fully depleted the electric field inside the crystal is almost uniform and charge carriers drift under a constant electric field. The signal is extracted from the detector via the preamplifier, without significantly degrading the intrinsic signal-to noise ratio. Moreover, the preamplifier is installed in the cryostat package, as close as possible to HPGe crystal, so as to minimize the overall capacitance. At the next step, the signal is processed through the amplifier for counting and pulse-amplitude (energy) spectroscopy applications. During this step, all the pulse-shaping controls are performed, needed to optimize the performance of the analog electronics, such as the pulse-height shaping where the amplitude of the preamplifier is increased from millivolt range into the 0.1-10 V range or the energy resolution optimization, where the overlap between successive pulses is minimized. Additionally, spectroscopy amplifiers incorporate a circuit of pole-zero cancellation to eliminate the produced amplified-pulse undershoot, produced by the long exponential decay on the

preamplifier output pulse. The amplified analog signal is converted, through a mathematical function, into a digital one, via the analog-to-digital converter. Firstly, the signal is sampled, secondly is quantized and finally is digitally coded. The multi-channel analyzer uses the ADC output to record incoming pulses and stores the pulse information based on amplitude. The counted different amplitudes are stored in a range of few thousand channels (usually 4096 channels) and thus a histogram of frequency against pulse amplitude is produced and sent to the computer. This mode is applied in gamma spectroscopy to analyze the energy distribution of various nuclear processes (e.g. nuclear decay). The recorded spectrum can be further analyzed by gamma spectroscopy software, like SPECTRW (Kalfas et al., 2016). An important aspect of the detector system is the shielding surrounding the HPGe detector crystal. The used detectors and their shielding, for the different nuclear laboratories, are shown below, in Fig. 4.5:

a) The experimental set-up of HCMR

b) The shielding of HCMR's detector

c) The experimental set-up of NTUA

d) The shielding of NTUA's detector

e) The experimental set-up of AUTH

f) The shielding of AUTH's detector

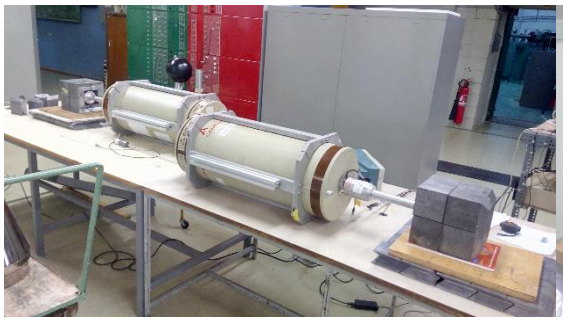

g) The experimental set-up of NCSR

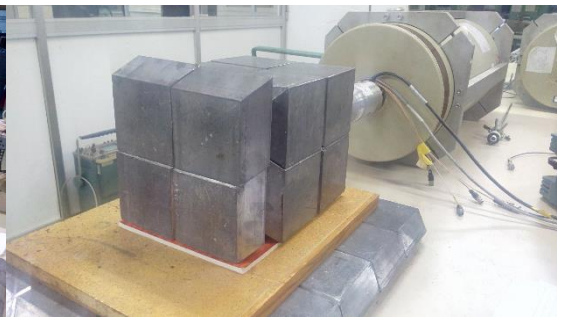

h) The shielding of NCSR's detector

Fig. 4.5 The experimental laboratories utilized in this work

The different shielding results in different radiation backgrounds due to the contribution of ambient natural radioactivity. This contribution depends on the

thickness of the Pb shielding, the detector's location (e.g. subsurface, surface), the building materials of the laboratory and possibly the distance from the sea (the HCMR lab is located near the sea).

4.3.2.3 Calibrations and MDA

The basic calibration needed for the radioactivity quantification, is the determination of the detector's full-energy peak efficiency (FEPE). Additionally, the energy calibration of the detection system and the energy resolution calibration, are important for the analysis of the unknown samples and the control of detector's linearity. The energy calibration consists of the experimental function determination (first or second order polynomial), describing the energy dependence of the channel number in the spectrum. It can be applied manually or automatically by the software using calibrated sources and it can be used to check the linearity of detection system (preamplifier-amplifier-ADC-MCA):

$$E_\gamma = a + b \cdot ch + c \cdot ch^2 \qquad \text{(Eq. 4.4)}$$

where,
E_γ is the gamma-ray energy, ch is the channel number for the peak center corresponding to E_γ, and a, b, and c are the calibration determined constants.

The resolution calibration, known as Full-Width at Half Maximum (FWHM) calibration, describes the peak width versus the spectral energy. This parameter characterizes the system performance in separating different photon emissions in a narrow energy range. The energy resolution depends on: (a) the statistical fluctuations of charge carries produced in the detector, (b) the electronic noise in detector itself, the preamplifier and the amplifier and (c) the incomplete collection of the charge produced in the detector (Tsoulfanidis & Landsberger, 2015). The total FWHM is calculated by the quadrature sum of the FWHM values for each individual source of fluctuation:

$$(FWHM)^2_{total} = (FWHM)^2_{statistical} + (FWHM)^2_{noise} + (FWHM)^2_{collection} \qquad \text{(Eq. 4.5)}$$

The most frequently types-of-efficiency used are: (a) the total detector efficiency and (b) the full-energy peak efficiency. These efficiencies can be either (a) intrinsic, (b) absolute or (c) relative. As intrinsic total detector efficiency is defined the probability of an incident gamma with a specific energy will be recorded by the detector. As absolute total detector efficiency is defined the probability of a gamma which is emitted from a specific source will be recorded in the detector. The intrinsic efficiency depends on the gamma radiation energy and the length of the detector, while the absolute total efficiency also depends on the radius of the detector and the source-detector distance (or practically the solid angle). The relative efficiency can be determined as the ratio of the absolute efficiency (total or full-energy peak) to the efficiency of a standard. For quantitative measurements the absolute full-energy peak efficiency (or absolute efficiency for simplicity) of the detector is usually used, as the number of the full energy events is not sensitive to perturbing effects e.g. scattering from surrounding objects or spurious noise.

For the determination of the absolute efficiency of the unknown sample, the absolute FEPE of the detector must be known. Therefore, a function describing the

FEPE versus the gamma-ray energy (E_γ) must be produced using radioactive standard sources. These sources are characterized by a wide energy range, can contain a number of monoenergetic (e.g. ^{40}K) or multienergetic radionuclides (e.g. ^{152}Eu) or mixtures of several radionuclides. In this work the used standard sources of extended geometry are presented in Table 8:

Table 8 The used standard sources for the absolute full-energy peak efficiency (FEPE) calibration

Source		**Activity (Bq)**	**Production date**	**Energy range (keV)**	**Density (g cm^{-3})**
Big geometry (V= 65 cm^3)	^{238,235}U*	730±34/34±1	6/12/2011	25-300	1.45±0.01
	^{152}Eu	6700±200	20/2/2001	120-1400	0.020±0.008
	^{40}K	1133±1	1/6/2008	1460	0.700±0.008
Small** geometry (V=5.7 cm^3)	^{238,235}U*	69±6/3.2±0.3	10/6/2015	25-300	1.45±0.01
	^{152}Eu	1380±30	14/10/2009	120-1400	1.465±0.008
	^{40}K	142±16	1/6/2008	1460	1.070±0.008

*Natural soil sample collected from the mountainous Epirus region near Perivleptos village was calibrated based on ^{152}Eu to determine the low energy FEPE values (Eleftheriou, 2014)
**The absolute efficiency calibration with source standards of small geometry was performed only for the NTUA detector for the samples of core 2 of Lavreotiki Peninsula (see Table 7 section 4.3.2.1).

The FEPE values were determined by:

$$\varepsilon_{\exp}(E_\gamma) = \frac{counts}{t \cdot I_\gamma \cdot A_{std}} \qquad \text{(Eq. 4.6)}$$

where,
counts are the recorded incident gammas, t is the acquisition time, I_γ is the intensity of the gamma-ray of energy E_γ and A_{std} is the absolute activity (in Bq) of the standard source.

The fitting functions applied in the FEPE values so as to reproduce via interpolation a whole energy range efficiency curve of the present work was either an empirical (Eq. 4.7) (Kalfas et al., 2016) or a polynomial one (Eq. 4.8). The FEPE functions were selected to reproduce satisfactorily the efficiency of the measured extended geometry samples. The uncertainty budget of the absolute efficiency was determined taking into account the uncertainties of the experimental values, the mean uncertainty of the parameters and the divergence from the experimental values, and ranged between 2% and 5% depending on the energy region. In the quantitative calculations of the sample's absolute activity, the efficiency value of 5% was used for the whole energy range.

$$\varepsilon(E_\gamma) = \frac{a \cdot E_\gamma^b}{1000c + E_\gamma^d} \qquad \text{(Eq. 4.7)}$$

$$\varepsilon(E_\gamma) = a + \frac{b}{E_\gamma} + \frac{c}{E_\gamma^2} + \frac{d}{E_\gamma^3} \qquad \text{(Eq. 4.8)}$$

where,
$\varepsilon(E_\gamma)$ is the interpolated FEPE, E_γ is the energy of the gamma-ray and a, b, c and d are the fitting parameters.

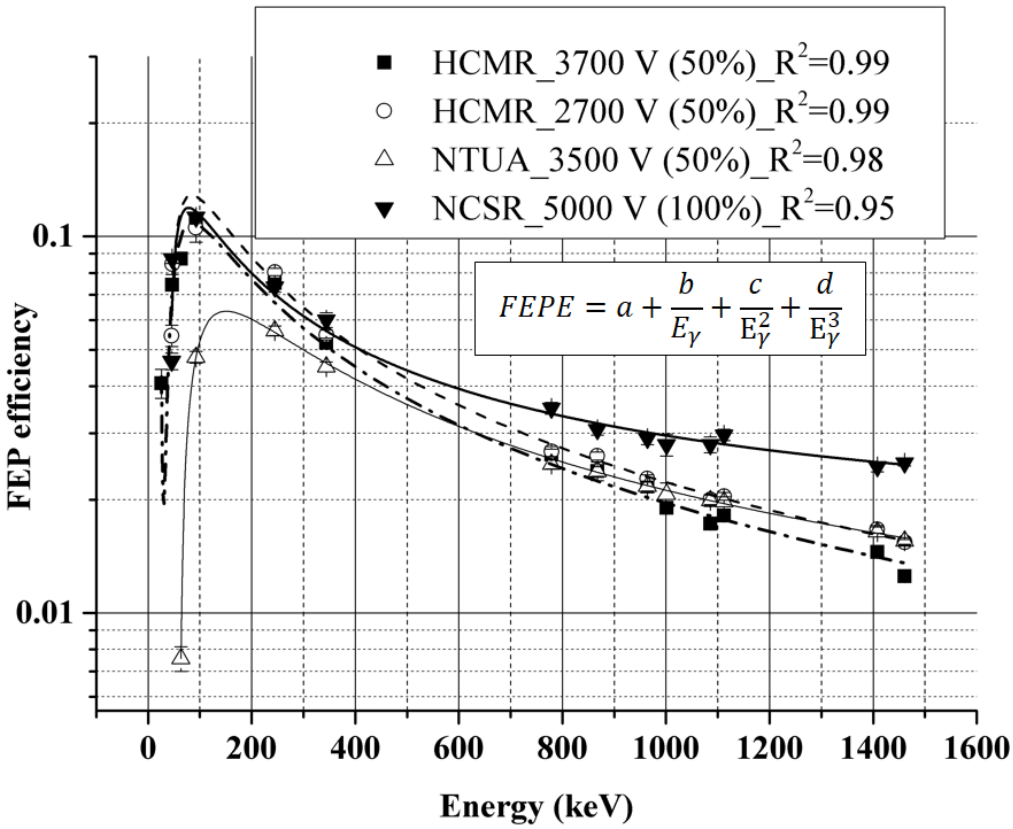

Fig. 4.6 The full energy photopeak efficiencies (FEPE) of the used detectors from the three laboratories of HCMR, NTUA and NCSR. The efficiency of AUTH's detector is not presented, as its energy range was 0-200 keV. During samples' (code S#) measurement period the HCMR detector operated in a lower voltage (+3700 V) than the optimum one (+4800 V). The detector was fixed and its new optimum operational voltage is + 2700 V.

The standard sources used at the absolute full-energy peak efficiency calibration, as well as all the unknown-to-be-measured samples are placed on the detector's window (practically in touch geometry). The final step of the FEPE calibration includes corrections regarding (a) true coincidence summing effects (TCS) especially for the ^{152}Eu source, as well as (b) self-absorption corrections. The latter is important for analyzed peaks of energy below 100 keV and depends mainly on the source's density and source/sample intrinsic geometry. Thus, self-absorption corrections of all sources are referred to a hypothetical sample with a specific density (1.2 g cm^{-3}) similar to the unknown samples which will be measured. The corrected FEPE values regarding TCS and self-attenuation effects are presented in Table II-2 (see Annex II) for all the utilized detection systems. The two type of corrections (a and b) have been also performed during the quantification of the absolute activity of the unknown samples, as many natural radionuclides (e.g. ^{214}Pb, ^{214}Bi) are multi-energy gamma-ray emitters and are characterized by TCS effects, and the density of the sediment samples varies from region to region due to many reasons such as the geology of the area and the distance from the shore (coast, offshore). The corrections regarding TCS and self-attenuation, both during the FEPE determination and radionuclide quantification in the collected samples, were realized via EFFTRAN code (Vidmar et al., 2005; 2011). The contribution of the ambient natural radioactivity was recorded periodically and was subtracted by the source spectrum, using a non-radioactive sample

(e.g. talcum powder), with the same geometry (volume: 65 cm^3 or 5.7 cm^3) as that of the standard sources and the unknown samples.

The quality control and quality assurance of radionuclide determination for HCMR laboratory was validated via the certified reference material IAEA-385. For all the measured radionuclides the mean |z| score was calculated to be 1.1, while in all cases no outliers (|z|>3) were found. More information regarding the calibration are presented in Annex III. Additionally, intercomparison exercises were performed among the laboratories of HCMR, NTUA and NCSR. The calculated activity concentrations of the radionuclides of interest were found in good agreement – within uncertainties- which verify the reliability of the obtained results. Moreover, an additional intercomparison exercise was realized between the laboratory of HCMR and SCK-CEN, where the activity concentration of ^{210}Pb was calculated via gamma- and alpha- spectrometry, respectively. The ^{210}Pb determined at SCK-CEN was systematically lower (up to 40%) than the one determined at HCMR. Nevertheless, the agreement between the two laboratories is acceptable, due to the high uncertainties of alpha-spectrometry methodology (up to 38%).

The minimum detectable activity (MDA) for each HPGe detector of the laboratories (HCMR, NTUA, NCSR, AUTH) is presented below. MDA is defined as the minimum quantity of a radionuclide that can be detected, taking into account the experimental set-up and the geometry. In the present work, the MDA was determined for the whole energy spectrum, using the background of the ambient activity concentration - of each laboratory - as the lower limit above which the measured values can be accepted. The MDA was calculated as:

$$MDA = \frac{2.71 + 4.65\sqrt{B}}{\varepsilon \cdot t \cdot m \cdot I_\gamma} \qquad \text{(Eq. 4.9)}$$

where,
B is the number of background counts in the area of interest, ε is the FEP efficiency, t is the acquisition time and I_γ is the intensity of the gamma-rays

The number of background counts (B) is calculated as:

$$B = \frac{(B_1 + B_2) \cdot N}{2} \qquad \text{(Eq. 4.10)}$$

where,
B_1 and B_2 are the sum of the counts left and right of the area of interest and N is the number of channels of the area of interest.

The MDA*I_γ spectra were determined for all the used HPGe detectors and (a) the different type of shielding or (b) the different characteristics of each detector (e.g. relative efficiency, detector window) or (c) the optimum operational voltage (HCMR detector) are depicted in them. More specifically, part of the sample measurements was held in the detector of HCMR, which was not operating in the optimum voltage (+4800 V) but in a lower one (+3700 V), thus the higher MDA values are observed for this system, especially for the higher energies. Additionally, the different types of shielding between the laboratory of HCMR and NTUA, result in higher values of MDA regarding the first laboratory (see energy range from 400 keV to 1400 keV). Lastly, the highest relative efficiency of the NCSR's detector, leads to lowest MDA values

comparing with all the other systems. The MDA*I_γ spectra are presented in Fig. 4.6. The MDA*I_γ spectrum of AUTH laboratory is presented separately, as this detection system was used for low energy (< 200 keV) measurements only. The scripts for the production of MDA*I_γ spectra are presented in Annex IV.

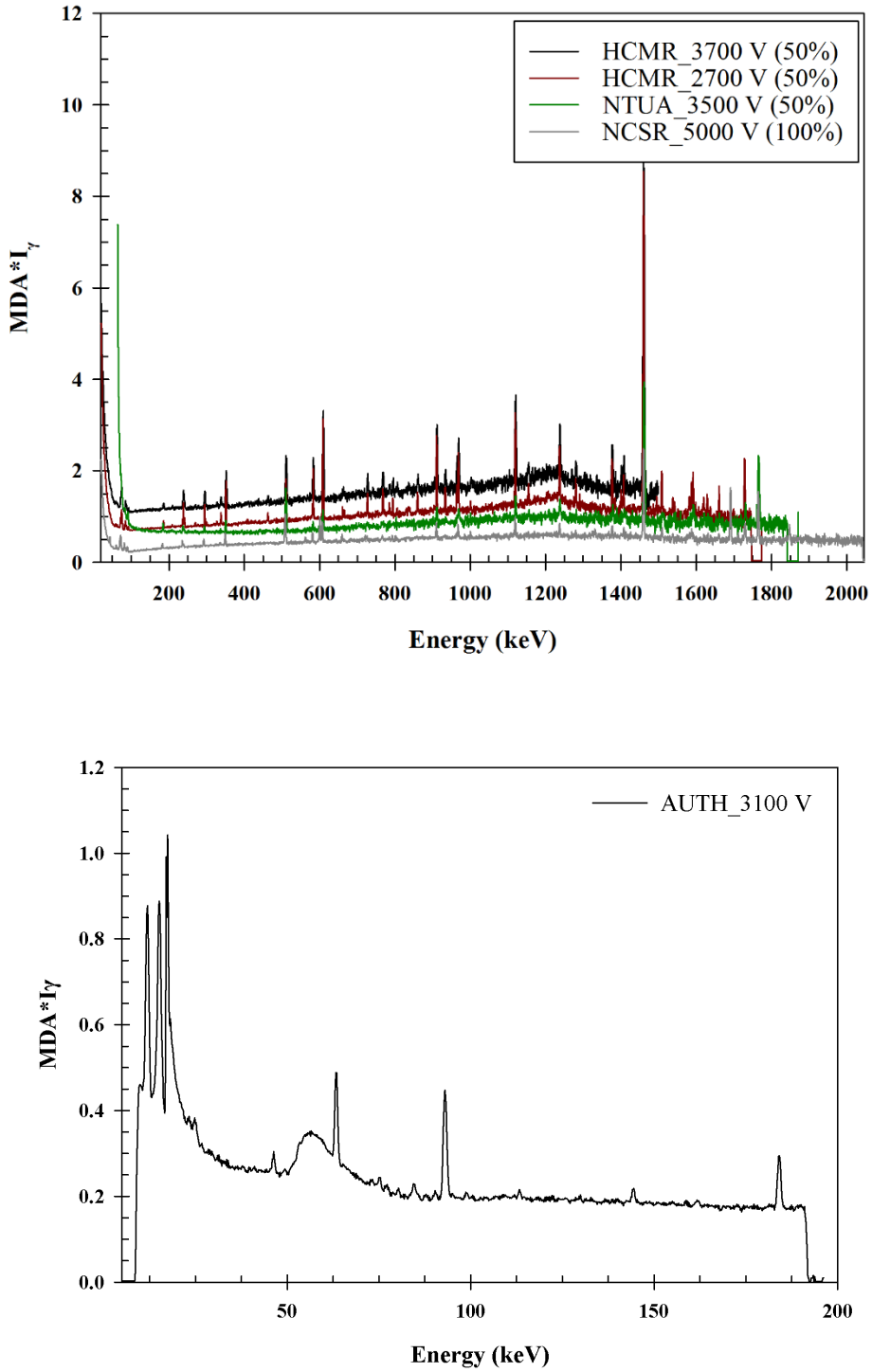

Fig. 4.7 The minimum detectable activity (MDA) multiplied by the intensity (I_γ) of the gamma-ray emission for the detection systems of HCMR, NTUA and NSCR (above) and AUTH (below). These spectra offer the MDA values for the photopeaks of interest.

4.4 Quantification

After the sample preparation, the applied calibrations and the sample measurements, the sample analysis follows. The latter can be realized in two steps, the first is the qualitative analysis and the second is the quantification one. In this chapter, the quantification process of radionuclide, trace metal and major element analysis are presented, as well as the calculation of the uncertainty budget. This process is the final step before obtaining the results and it is strongly depended on the determined calibration curve, as well as the spectra analysis. In the case of trace metal and major element analysis, the quantification is realized through a commercialized WDXRF detection system, thus the required procedures (e.g. re-calibration of the system, attenuation corrections) are applied automatically. On the other hand, the radioactivity quantification and every step included in it, have been carried out manually.

4.4.1 Heavy metal concentration

The commercialized WDXRF system may determine chemical elements in solids, powders as well as liquids and is accompanied by a 30-position robotic sample changer. All operations are computer controlled and the software is running under Microsoft Windows. The software (e.g. Panalytical's Pro-Trace) can perform a qualitative and semi-quantitative analysis of the unknown sample. The latter is a first approximation of the sample composition. A full quantitative analysis can be also carried out, using known standards e.g. certified materials or self-made standards for the calibration. The qualitative and quantitative analysis method of the WDXRF system is based on the height of the peak. This height is used to identify the elements present in the sample, as well as to measure the intensities (practically the peak top). This is possible as the peak positions are known. Thus, by measuring only the height (intensity) of the peak, the analysis is complete in an accurate and fast way. The net intensities are used in the quantification, meaning that background (under the peak) must be subtracted from the spectrum. The determination of the background is achieved by measuring a few background positions close to the peak, which are clean from other peaks, and by interpolating the measured intensities at these positions.

The obtained net intensities can be converted into concentrations, using calibration curves. These curves are produced by measuring one or more reference materials, thus they describe the relationship between the concentrations and the intensities of elements. When this relationship is determined, the concentrations of unknown elements are calculated by adjusting the measured intensities of the unknown elements to those of the calibration curve. In theory, the intensity of an analytical line is linearly proportional to the concentration of the analyzing element. In practice the intensity can be either attenuated or enhanced due to the presence and concentrations of other elements in the unknown sample. This problem is called matrix effect and many matrix models have been proposed to solve it. The main equation these models are called to solve is:

$$C_i = D_i + E_i R_i M_i \qquad \text{(Eq. 4.11)}$$

where,

C_i is the concentration of analyzing element i, R_i is the intensity of analyzing element i, D_i and E_i are parameters determined by linear regression and M_i is the matrix

correction factor. Two standards are required to calculate the D and E parameters, while M is calculated for each individual standard when D and E are determined for all elements.

The solutions of the aforementioned equations are realized using fundamental parameter method, which calculate accurately the matrix correction factors by describing fully the matrix. The main hypothesis of the fundamental parameter is that the sum of all concentrations in the sample must be 1, thus one element can be eliminated from the system of equations. Usually, that element is a major component such as Fe. Before the sample analysis, two standards are utilized to determine D and E. Knowing these factors and using iterative methods until convergence is achieved between the calibration intensities and sample intensities, the element concentrations of the sample can be obtained.

4.4.2 Radioactivity concentration

The methodology of the photo-peak analysis is described in detail in Pappa et al., (2016); Patiris et al., (2016). In brief, prior to measurement the unknown samples are kept shielded for 20 days (see section 4.2.1) to achieve secular equilibrium between radium ^{226}Ra and radon daughters (^{214}Pb, ^{214}Bi). The shielded days are calculated as five times the half life of radon ($t_{1/2}$= 3.8 d). The quantification of the sample's activity concentration is determined by:

$$A = \frac{counts \cdot TCS \cdot ET}{\varepsilon \cdot t \cdot I_{\gamma} \cdot m} \qquad \text{(Eq. 4.12)}$$

where,
A is the absolute or specific activity concentration (in Bq kg^{-1}), counts is the number of the recorded gamma-rays of a specific photo-peak with energy (E_γ), TCS is the correction of the true coincidence summing effect for the specific photo-peak of energy (E_γ), ET is the self-absorption correction between the geometry of the calculated absolute FEPE and that of the unknown sample, ε is the absolute full energy peak efficiency (FEPE) of the analyzed peak, t is the acquisition time (in sec), I_γ is the intensity of the recorded gamma-ray and m is the (net) dry mass of the pulverized sample (in kg).

In case of determining activity concentration from more than one photo-peaks then of the weighted average is calculated as:

$$\overline{A} = \frac{\sum_{i=1}^{k} A_i w_i}{\sum_{i=1}^{k} w_i} \qquad \text{(Eq. 4.13)}$$

where,
$\overline{A}$ is the weighted average of the activity concentration, A_i is the activity concentration calculated by the i photo-peak and w_i is the weight of each photo-peak, defined as the inverse square of the activity concentration uncertainty.

The contribution of the ambient natural radioactivity is recorded periodically and subtracted from the sample's spectrum using the sample of the talcum powder as mentioned before. In case where the activity concentration of a radionuclide can be determined by more than one photo-peak, then the final activity concentration results from the weighted average of the activity concentrations of the different photo-peaks. The analyzed photo-peaks from an unknown spectrum of natural radioactivity are presented below. The methodology of the photopeak analysis is described in Patiris et al. (2016). All the analysed photopeaks were corrected for TCS and self-attenuation effects (see section 4.3.2.3).

Table 9 Characteristic analyzed peaks.

Radionuclide series	**Isotope**	**Energy (keV) (Intensity)**
^{238}U	^{234}Th	**63.3** (3.8%), **92.6** (5.4%)
	^{234}Pa	**1001** (0.84%)
	^{226}Ra	**186.2** (3.5%)
	^{214}Bi	**609.3** (46.1%), **1120.3** (15%), **1238.1** (5.9%), **1764.5** (15.9%),
	^{214}Pb	**295.2** (19.2%), **351.9** (37.1%)
	^{210}Pb	**46.5** (4.1%)
^{235}U	^{235}U	**143.8** (11.0 %), **185.7** (57.2%)
^{232}Th	^{228}Ac	**338.4** (11.3%)**, 911.2** (26.6%), **964.6** (5.05%), **969.0** (16.2%)
	^{212}Pb	**238.6** (43.5%), **300.1** (3.3 %)
	^{212}Bi	**727.3** (6.64 %), **1620.7** (1.5 %)
	^{208}Tl	**583.2** (30.36%), **860.6** (4.5 %)
-	^{137}Cs	**661.7** (85.2%)
-	^{40}K	**1460.8** (10.67%)

4.5 Uncertainty estimation

The results derived during the quantification process are followed by an uncertainty, which includes the uncertainties of the method and laboratory. In the next subsections the uncertainty calculation regarding the gamma-ray and XRF measurements, is described. For both measurements the calculated uncertainty include the 95 % of confidence level. The calculated relative uncertainties of radionuclides, trace metals and major elements are included in Annex V.

4.5.1 Heavy metal uncertainty concentration

The total uncertainty of trace metal and major element concentration is determined as:

$$U_{XRF} = k\sqrt{u\left(R_w\right)^2 + RMS_{bias}^2 + u\left(C_{ref}\right)^2} \qquad \text{(Eq. 4.14)}$$

where,

k is a coverage factor, receiving a value of 2 for 95% confidence level, $u(R_w)$ is the standard deviation of the laboratory reproducibility, RMS_{bias} is the square root of the bias values (practically the divergence between the measured and the assigned values of the certified materials), $u(C_{ref})$ is the average uncertainty of the assigned values.

The RMS uncertainty is calculated as:

$$RMS_{bias} = \sqrt{\frac{\sum\left(bias_i\right)^2}{l}} \qquad \text{(Eq. 4.15)}$$

where,

bias is the bias of compound i (the divergence between the measured and the assigned value of the certified materials) and l is the number of the used certified materials.

4.5.2 Radioactivity uncertainty estimation

The uncertainty budget is determined taking into account the photopeak-counts statistical uncertainty, the intensity of the gamma-rays, the efficiency of the detector and the sample mass:

$$\frac{\sigma_{\mathrm{A}}}{\mathrm{A}} = \sqrt{\left(\frac{\sigma_{cps}}{cps}\right)^2 + \left(\frac{\sigma_{\mathrm{I}_\gamma}}{\mathrm{I}_\gamma}\right)^2 + \left(\frac{\sigma_\varepsilon}{\varepsilon}\right)^2 + \left(\frac{\sigma_m}{m}\right)^2} \qquad \text{(Eq. 4.16)}$$

where,

A is the activity concentration (in Bq kg^{-1}), cps is the number of photopeak-counts per acquition time, I_γ is the intensity, ε is the detector's FEPE efficiency, m is the sample mass and σ_i is the uncertainty of every i (A, I_γ, ε, m) parameter.

In the case of determining an activity concentration from more than one photo-peaks then the uncertainty of the weighted average is calculated as:

$$\sigma_{\bar{\mathrm{A}}} = \frac{\sum_{i=1}^{k} w_i\left(A_i - \bar{A}\right)^2}{\sum_{i=1}^{k} w_i} \qquad \text{(Eq. 4.17)}$$

where,

$\sigma_{\bar{\mathrm{A}}}$ is the uncertainty of the weighted average of the activity concentration, A_i is the activity concentration calculated by the i photo-peak and w_i is the weight of each photo-peak, defined as the inverse square of the activity concentration uncertainty.

4.6 Proposed chronological models

The radiochronology of a sediment core can be achieved by estimating the sedimentation rate (SR). Among other radionuclides, in the present work, two radionuclides, a natural (^{210}Pb) (Appleby & Oldfield, 1978) and an artificial (^{137}Cs) (Tsabaris et al., 2012b) were selected for the SR estimation. The different origins,

meaning the different physical processes contributing to these radionuclides, provide two independent methodologies to SR calculation, where usually the ^{137}Cs methodology is utilized to verify the SR estimated via ^{210}Pb measurements. The vertical profiles of the aforementioned radionuclides were utilized in the radiometric dating. A brief description of the applied models follows.

4.6.1 ^{210}Pb tracer

The total activity concentration of ^{210}Pb consists of a supported and an unsupported part (excess). The first is due to ^{226}Ra presence in the sediment of the sampling location, while the latter is due to the transfer of ^{222}Rn to the sampling location and subsequent sedimentation of aerosols containing also long-lived ^{222}Rn daughter products. Therefore, the unsupported portion ($^{210}Pb_{ex}$) can be determined by subtracting the activity concentration of ^{226}Ra (average value of ^{226}Ra progenies) from the total activity of ^{210}Pb so as to remove the supported portion. In the present work three ^{210}Pb-based radio geochronological models (CF:CS, CIC and CRS) were tested, while the CF:CS was applied in the sampling areas of interest, as it provided more consistent sedimentation rate (SR) values. The main assumptions of these models are (a) the non-disturbance of the sediment, (b) the ideal deposition of $^{210}Pb_{ex}$ fluxes and (c) the non-depositional redistribution of sediment. In brief, the Constant Flux: Constant Sedimentation model (CF:CS) assumes a constant SR, which can be estimated by the slope of the logarithmized $^{210}Pb_{ex}$ activity concentration:

$$\ln\frac{A_0}{A_i} = \frac{\lambda}{\overline{SR}} z_i \qquad \text{(Eq. 4.18)}$$

where,
A_0 and A_i are the unsupported activity concentrations in the sediment core surface and the remaining ith slice of the sediment core (Bq kg^{-1}), respectively, λ is the ^{210}Pb radioactive decay constant (0.03114 y^{-1}), z_i is the depth (cm) of the ith slice and $\overline{SR}$ is the mean sedimentation rate of the sediment core (cm y^{-1}).

The Constant Initial Concentration (CIC) model assumes that the initial $^{210}Pb_{ex}$ concentration must be constant when each sediment layer is formed. Therefore the time is estimated as:

$$t_i = \frac{1}{\lambda}\ln\frac{A_0}{A_i} \qquad \text{(Eq. 4.19)}$$

where,
A_0 and A_i are the unsupported activity concentrations in the sediment core surface and the remaining ith slice of the sediment core (Bq kg^{-1}), respectively and λ is the ^{210}Pb radioactive decay constant (0.03114 y^{-1}).

The Constant Rate of Supply (CRS) model assumes that the $^{210}Pb_{ex}$ flux is constant in the sediment surface. Thus the time can be estimated by the accumulated deposit of $^{210}Pb_{ex}$ activity AD, which practically is the activity inventory:

$$t_i = \frac{1}{\lambda}\ln\frac{A_0}{A_i} = \frac{1}{\lambda}\ln\frac{\int_{m_0}^{\infty} AD_0\,dm}{\int_{m_i}^{\infty} AD_i\,dm} \qquad \text{(Eq. 4.20)}$$

where,
AD_0 and AD_i are the unsupported activity inventories in the sediment core surface and the remaining i^{th} mass depth of the sediment core (Bq m^{-2}),

4.6.2 ^{137}Cs tracer

The ^{137}Cs radiodating is based on the ^{137}Cs peaks due to nuclear tests (1963) and Chernobyl accident (1986). These peaks can be observed in the ^{137}Cs profile and thus allow the estimation of the mean sedimentation rate according to:

$$SR = \frac{z_i}{t - i} \qquad \text{(Eq. 4.21)}$$

where,
t is the year of the collected sediment core and z_i is the depth where the ^{137}Cs peaks corresponding to nuclear incidents (i= 1963, 1986) were found.

4.7 Mass fluxes, Grain size analysis, Statistical analysis, Trace metals in seawater

Mass fluxes

The evaluation of both geochemical and industrial input of metals into aquatic sediments is established by means of mass flux (MF) calculations. A necessary requirement is the application of this method in undisturbed sediment core samples combined with accurate dating methodology (Salomons and Forstner, 1984). The excess flux was calculated in the sediment cores with well estimated sedimentation rate, for trace metals, major elements and long-lived radionuclides using the following formula (Cochran et al., 1998; Spencer et al., 2003):

$$MF_i = (M_{xs})_i \cdot SR_i \cdot \rho_i \qquad \text{(Eq. 4.22)}$$

where,
MF_i is the excess metal flux for the i^{th} depth interval (μg y^{-1} cm^{-2}), M_{xs} the excess metal concentration for the i^{th} depth interval (μg g^{-1}), SR_i the mean sedimentation rate at the i^{th} depth interval (cm y^{-1}) and ρ_i the sediment dry bulk density (g cm^{-3}).

In the present study, as baseline elemental concentration was considered the maximum depths of the offshore cores at each study area. The excess metal flux (MF_i) was determined by subtracting the elemental concentration of the i^{th} depth from this baseline elemental concentration.

Grain size analysis

Particle size determination characterizes the physical properties of the sediment and effects also the chemical composition of the material, as fine grain particles have high active surfaces and adsorb or absorb contaminants (e.g. radionuclides and metals). In many cases, the observed variations of contaminant concentrations may be attributed to the grain size distribution in the sediment sample. Thus, in order to verify if the elevated radionuclide and metal concentrations obtained in this work are mainly attributed in the physical properties of sediments and/or to other causes, such as mining, this parameter should be determined. A rough estimation of the grain size distribution was performed in the samples. The core sediment subsamples were split into sand and mud fractions by wet and/or dry sieving through a 63 μm mesh. The sand-mud separation was conducted, in order to investigate the grain size effect in the radionuclide and trace metal/major element concentrations.

Statistical analysis

In this work, a parametric (Pearson correlation coefficient) and a non-parametric (Spearman rank order) analysis were followed, using Statistical Package for the Social Sciences (SPSS) for the surface and core sediments (see section 2.7 regarding statistical analysis theory). The first statistical analysis (Pearson) measures the linear correlation between two variables, thus due to this restriction (linearity) it was applied for a small part of the data and was abandoned. The latter statistical analysis (Spearman) measures the statistical dependence between two variables using a monotonic function. Therefore, this general correlation was estimated in the majority of the data sets. The statistical analysis may reveal possible associations between radionuclides and metals, as well as among the contaminants and sediment physical properties, indicating the origin of these contaminants and the composition of disposed wastes.

Trace metals in seawater

In order to investigate possible metal impact in the seawater of Ierissos Gulf, water samples were collected in the sediment - seawater interface. The seawater work was realized in a smaller scale, comparing to the sediment study, and can be used only as complementary tool. The seawater samples were appropriately treated for trace element concentration measurements (ICP-MS). The trace metal measurement in the seawater was held at the Trace Metal Laboratory of HCMR as described in Kalantzi et al. (2016). Briefly, about 15 mL of seawater sample passed through the ion-exchange resin via a peristaltic pump. The trace metals were held in the column and then eluted with 1M HNO3. The seawater sample was pre-concentrated to 3 mL of 1M HNO3 and then measured using ICP-MS analysis. The trace metal determination in the eluates of the seawater samples was conducted using ICP-MS (Thermo- XSeries II). The accuracy of the trace metal analysis was tested against the CASS certified reference material provided by the National Research Council of Canada with z scores indicating satisfactory performance ($|z| < 2$) for all metals studied (Kalantzi et al. 2016).

Chapter 5

Results

In this section the results are presented for each study area. More specifically, the following results include (a) the sedimentation rate, (b) the activity concentrations of key radionuclides, (c) the trace metal and major element concentrations, (d) the mass fluxes of metals and radionuclides of interest, (f) the dose rates for non-human biota, as well as (g) the grain size distribution of sediments. All these parameters contribute to investigate the areas of interest in a spatial and a temporal basis.

5.1 Stratoni

Stratoni is the area that hosted, hosts and will be hosting metal mining activities. As mentioned before in the sampling and study area description (section 4.1) two main surveys took place in 2012 and 2014. During first sampling seafloor sediments were collected, while during the second sampling surface (seafloor, river, beach sand) and core sediment samples were collected. Both the spatial and vertical distributions of the results of second sampling will be presented in the same subsection, if the title of the subsection does not refer differently. The results of 2014campaign will be presented in this section, while those of 2012 survey will be used for comparison as discussed in section 6.3.

5.1.1 Sedimentation rate

The sedimentation rate (SR) of Stratoni marine region, was estimated near the load out pier area (STR1), implementing two independent radiochronological methods based on ^{137}Cs and ^{210}Pb activity concentration profiles. The first radionuclide is artificial, while the latter is natural. The vertical profile of ^{137}Cs and the correspondence of the ^{137}Cs-peak maxima to historical nuclear accidents (e.g. nuclear tests in 1963, Chernobyl accident in 1986), as well as the logarithmized excess ^{210}Pb versus depth are depicted in the following figures (Fig. 5.1):

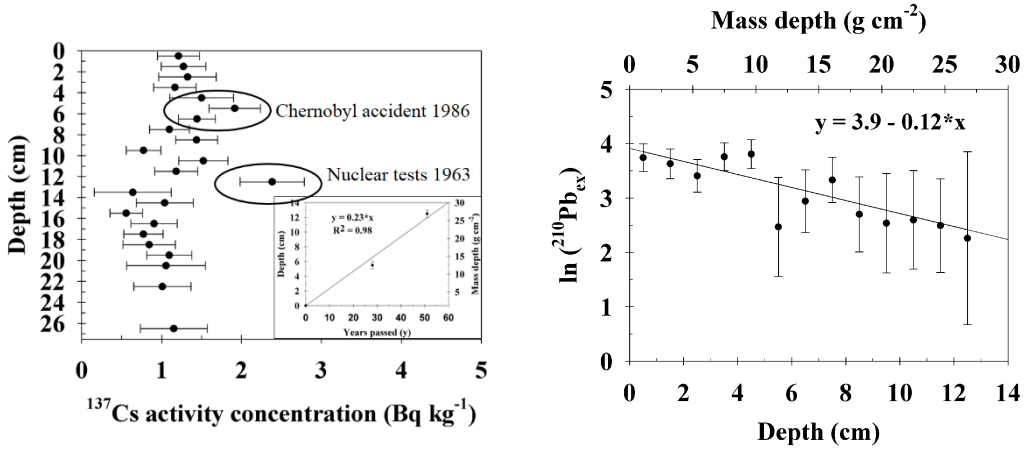

a) the ^{137}Cs method (MDA = 0.6 Bq kg^{-1})

b) the ^{210}Pb method, utilizing the constant flux : constant sedimentation (CF:CS) model

Fig. 5.1 The two sedimentation rate estimation methods applied in location STR1 (load out pier area) of Stratoni port

The ^{137}Cs activity concentrations corresponding to the nuclear incidents were found above the MDA values (0.6 Bq kg^{-1}). Among the aforementioned proposed ^{210}Pb chronological models (section 4.4.1), in Stratoni area was utilized the constant flux: constant sedimentation (CF:CS) model. This model was selected as it can be satisfactorily applied in a wide range of environments (Eleftheriou et al., 2018), since in long term basis the flux and sedimentation process can be assumed constant. The SRs utilizing independently the maxima of ^{137}Cs, which correspond to the incidents of 1963 and 1986, were calculated at (0.21 ± 0.02) cm y^{-1} and (0.24 ± 0.01) cm y^{-1}, respectively. The estimated sedimentation rates are consistent within uncertainties and the produced differences in sediment ages ranged from <1 to 16 y among the surface and the deepest layers of the core (110 y before), respectively. Thus the mean value (0.23 ± 0.01 cm y^{-1}) of these SRs was utilized for the validation of ^{210}Pb radiometric model. The SR, applying the **^{137}Cs and ^{210}Pb** methods, was estimated to be **(0.23 ± 0.01) cm y^{-1}** and **(0.26 ± 0.06) cm y^{-1}**, respectively, revealing a satisfactory agreement within uncertainties. The validation of ^{210}Pb radiometric model was performed via ^{137}Cs sedimentation model. The difference of the ages produced by the two calculated sedimentations rates was up to 10 years. The uncertainties of both sedimentation rates were estimated via the slope of the graphs (Fig 5.1) and include an age uncertainty ranging from 1 to 50 years for ^{210}Pb and from 1 to 10 years for ^{137}Cs among the surface and the deepest layers of the core, respectively. Theefore, the mean sedimentation rate was used in the historical reconstruction of metal and radionuclide observed values at Stratoni port (STR1). Near Stratoni port a core (STR8) was also collected, however the SR calculation was not performed due to the little amount of sample mass, despite the sampling per 2 cm.

5.1.2 Radioactivity and trace metal/major element spatial distribution

Thirty (30) samples were collected in the marine and terrestrial coastal environment of Ierissos Gulf. The results are presented according to the sampling regions, as well as the different matrices. The regions are (a) the load out pier area of Stratoni port, (b) the Stratoni port, (c) the offshore region (STR8, STTR9), (d) Kokkinolakkos stream, (e) Kalatzi Lakkos stream and (f) the Ierissos port, and are indicated by a title in the graphs (Fig. 5.2-5.8). The sampling was organized in this way so as to describe the affected region due to anthropogenic activities (cases a and b), the main streams of the drainage basins (cases d and e) and a reference region (case f), which was located far enough from the occurring mining activities of Stratoni. The results are also classified for the different matrices, which are indicated using colors. The used colors are: a) blue for marine sediments, b) dark yellow for sea-coast interface samples, c) brown for the beach sand samples, d) dark green for the streambed samples and e) light green for the streambank samples.

Another reference sample is the deep sediment slice of the offshore core (STR8), since the content of such slice corresponds to past years of the last century, before the beginning of the industrial mining. This sample will be used for the enrichment factor and mass flux estimations, described in 6.1.4, of the coastal core. The activity concentrations of key NORMs and ^{137}Cs, as well as the concentrations of trace metals (As, Cu, Pb, Zn) and major elements (Mn, Al, Fe) are described in detail. The variability concentrations of the selected metals (e.g. As, Cu, Pb, Zn, Mn, Al, Fe) and

radionuclides (e.g. ^{226}Ra, ^{235}U) were found to be key indicators of the mining-activities impact to marine and terrestrial coastal environment.

The activity concentrations of the ^{238}U series (^{234}Th, ^{210}Pb, ^{226}Ra), ^{228}Ac, ^{235}U, ^{40}K and ^{137}Cs, as well as of trace metals and major elements are presented below. The ^{226}Ra is assumed to be in secular equilibrium with radon progenies (^{214}Pb, ^{214}Bi) and the concentrations of ^{228}Ac represent the whole ^{232}Th decay series since similar concentrations - within uncertainties - were obtained among ^{228}Ac, ^{212}Pb, ^{212}Bi and ^{208}Tl. The calculated relative uncertainties of radionuclides, trace metals and major elements are included in Annex V. All the other measured trace metals and major elements are presented in Annex VI.

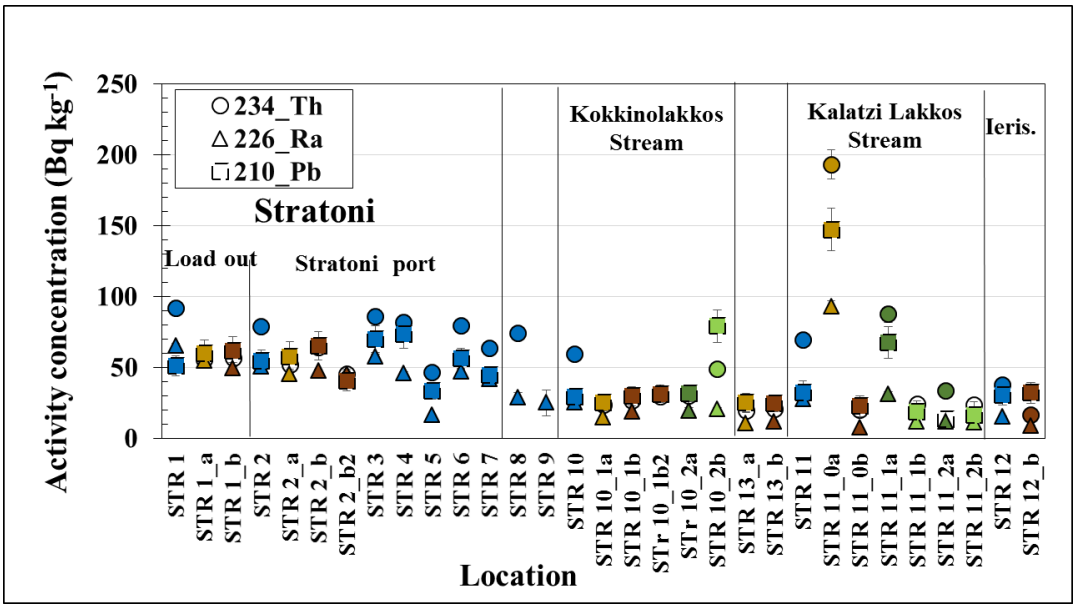

Fig. 5.2 The ^{238}U series activity concentration results regarding the coastal and offshore (STR8, STR9) parts of Ierissos Gulf. The activity concentrations of ^{234}Th (circle), ^{226}Ra (triangle) and ^{210}Pb (square) are depicted corresponding to the different matrices (blue for marine sediments, dark yellow for sea-coast interface samples, brown for the beach sand samples, dark green for the streambed samples and e) light green for the streambank samples).

In Fig. 5.2., the activity concentrations of ^{226}Ra, ^{210}Pb and ^{234}Th are depicted for all regions (load out pier area of Stratoni, Stratoni port, Kokkinolakkos stream, Kalatzi Lakkos stream and Ierissos port). The activity concentrations of the aforementioned radionuclides ranged from (10 - 100) Bq kg^{-1}, (10 - 150) Bq kg^{-1} and (20-200) Bq kg^{-1}, respectively. The maximum activity concentrations of ^{226}Ra were obtained near Stratoni (load out pier and port), while the minimum ones were observed near Kalatzi Lakkos stream and Ierissos port (reference sample). The activity concentrations of the offshore samples (STR8, STR9) were also found in the same level as those of Ierissos port. The activity concentrations of ^{226}Ra in the seafloor were similar to those at the beach sand and stream estuaries. This observation, especially for Stratoni seafloor and beach sand, may indicate that both the marine and terrestrial (coastal) part have been affected equally by the mining activities due to waste disposals. Additionally, the strong interaction between the coast and the beach due to weather conditions, may resulted in homogenizing the content of materials in the corresponding matrices. Regarding seafloor of Stratoni port, a minimum value is observed for all the studied

radionuclides of ^{238}U series at STR5 site, which is considered a background value as it is similar to the one of Ierissos port. The low activity concentration of NORMs of STR5 sample indicate the north part of the load out pier area, has not been affected by the mining activities as the south part of the load out pier area. Additionally, ^{226}Ra activity concentrations did not change significantly along the stream samples (STR10_#, STR11_#) implying the presence of natural transport processes. The activity concentrations of ^{210}Pb exhibited higher values than those of ^{226}Ra at the seafloor samples and stream estuaries, while they were found similar - within uncertainties - to ^{226}Ra values at the beach sand and streambank samples. The higher values of ^{210}Pb comparing to those of ^{226}Ra at seafloor samples and stream estuaries, may indicate secondary sources of ^{210}Pb (e.g. atmospheric deposition) except from its parent radionuclide (^{226}Ra). The spatial distribution of ^{234}Th was similar to the one of ^{226}Ra and the higher activity concentrations of ^{234}Th comparing to those of ^{226}Ra, reveal a disequilibrium within ^{238}U series maybe due to Th affinity to sediments. The spatial distribution of ^{226}Ra and ^{234}Th are associated with the mining activities near Stratoni port.

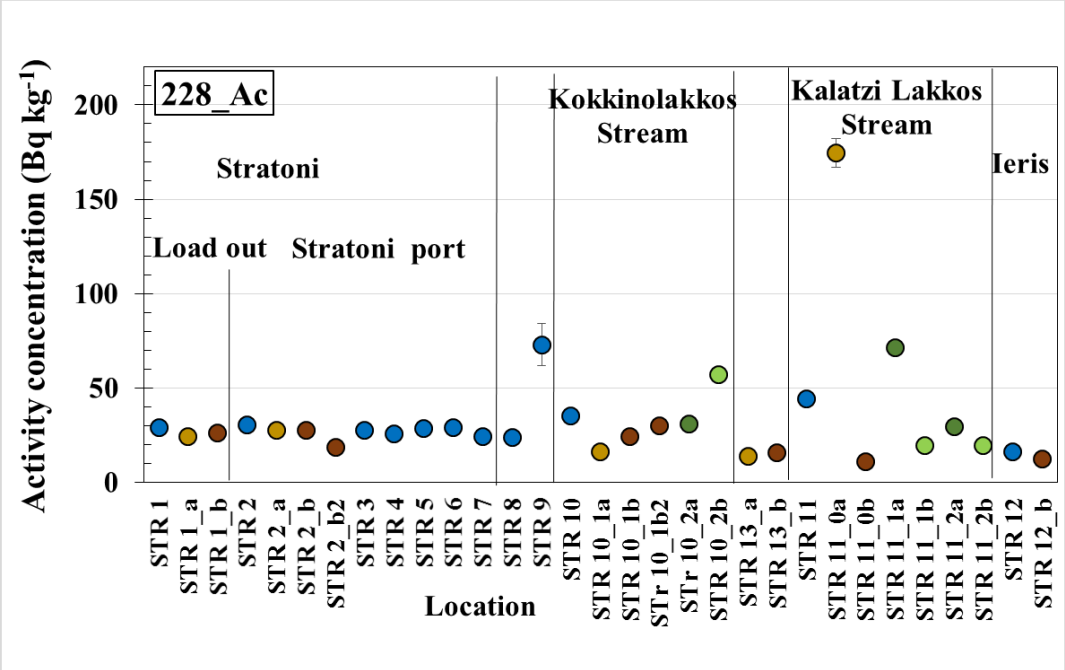

Fig. 5.3 The ^{232}Th series activity concentration results regarding the coastal and offshore (STR8, STR9) parts of Ierissos Gulf. The activity concentrations of ^{228}Ac represent the whole ^{232}Th decay series, as similar concentrations were obtained - within uncertainties - among ^{228}Ac, ^{212}Pb, ^{212}Bi and ^{208}Tl. The activity concentrations are depicted corresponding to the different matrices (blue for marine sediments, dark yellow for sea-coast interface samples, brown for the beach sand samples, dark green for the streambed samples and e) light green for the streambank samples).

The activity concentration of ^{232}Th decay series ranged between (10 ±2) Bq kg^{-1} and (180± 7) Bq kg^{-1} (Fig. 5.3). Almost all samples exhibited a mean value of (30 ± 2) Bq kg^{-1}, while at some specific sites the activity concentrations of ^{232}Th decay series were found elevated compared to the mean value. The elevated concentrations may be associated with the physical (e.g. organic matter content) or geological (e.g. presence of oxides) characteristics of the samples. The almost homogeneous spatial distribution

of ^{228}Ac, as well as the studied daughter radionuclides of ^{232}Th series, indicate that the activity concentration of this decay series is not affected by the occurring mining activities.

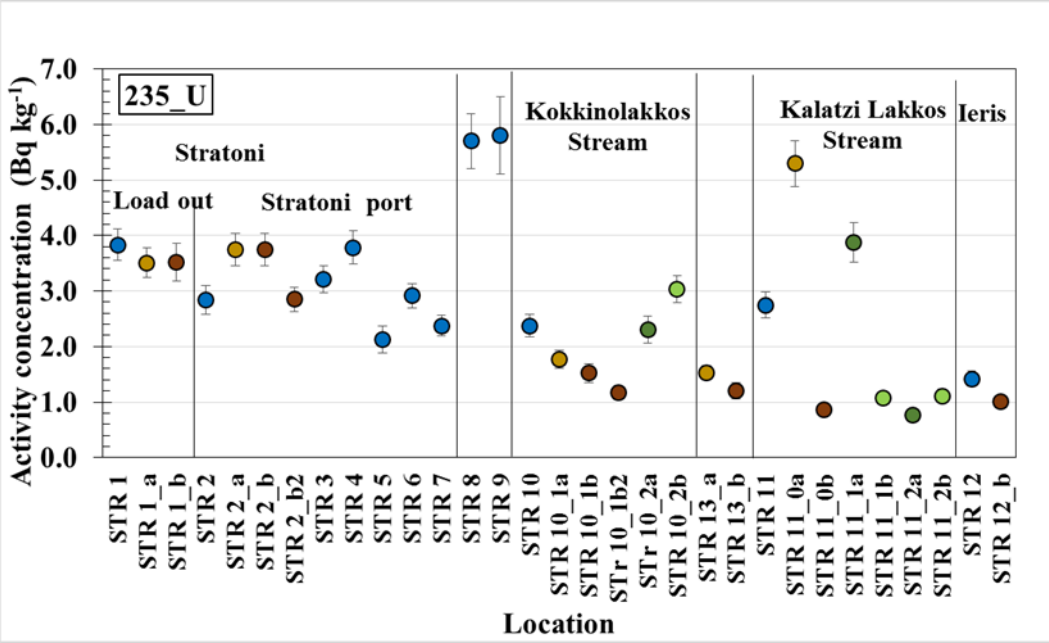

Fig. 5.4 The ^{235}U activity concentration results regarding the coastal and offshore (STR8, STR9) parts of Ierissos Gulf. The activity concentrations are depicted corresponding to the different matrices (blue for marine sediments, dark yellow for sea-coast interface samples, brown for the beach sand samples, dark green for the streambed samples and e) light green for the streambank samples).

The activity concentrations of ^{235}U ranged from (0.8 ± 0.1) Bq kg^{-1} to (5.8± 0.7) Bq kg^{-1} (Fig. 5.4). The spatial distribution of ^{235}U was similar with the one of ^{226}Ra, where the maximum activity concentrations were observed at Stratoni port, especially near the load out pier area and decreased when the distance from the load out and the beach increase. The minimum activity concentrations were found at Ierissos port and this area is defined as background area. Additionally, elevated values of ^{235}U were found in the offshore samples (STR8, STR9) maybe due to the higher mud content, while the elevated values of ^{235}U obtained at Kalatzi Lakkos stream may be associated with other physical characteristics such as the content of organic matter into the sample.

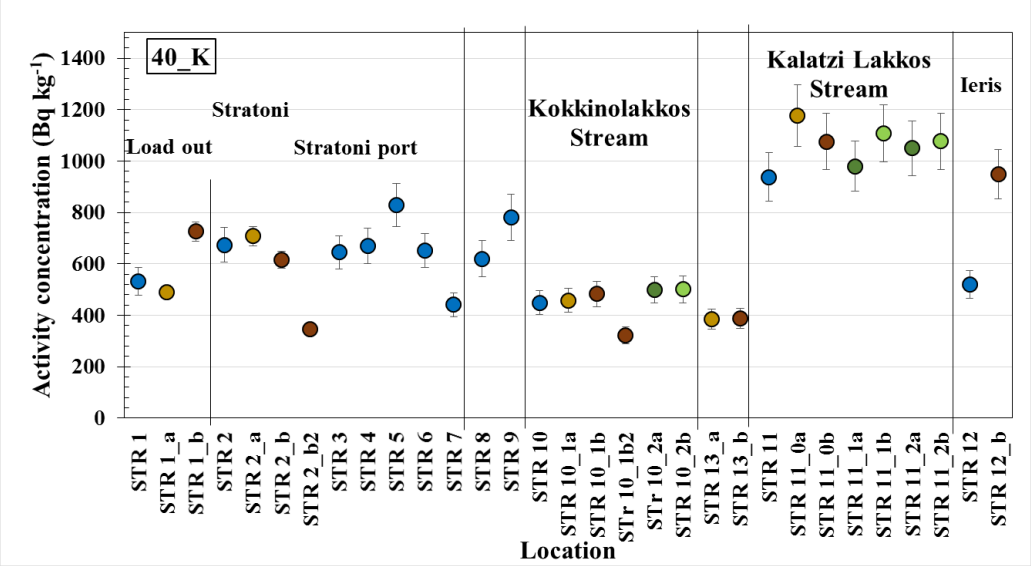

Fig. 5.5 The ^{40}K activity concentration results regarding the coastal and offshore (STR8, STR9) parts of Ierissos Gulf. The activity concentrations are depicted corresponding to the different matrices (blue for marine sediments, dark yellow for sea-coast interface samples, brown for the beach sand samples, dark green for the streambed samples and e) light green for the streambank samples).

The activity concentration of ^{40}K ranged from (350 ± 20) Bq kg^{-1} to (1200 ± 120) Bq kg^{-1} (Fig. 5.5). The ^{40}K spatial distribution can be classified in 3 main regions: (a) Stratoni port and offshore samples (STR8, STR9), (b) load out pier area, Kokkinolakkos Stream and Ierissos port seafloor and (c) Kalatzi Lakkos Stream and Ierissos port beach sand. The activity concentration of ^{40}K at the three aforementioned regions exhibited a mean value of (630 ± 50) Bq kg^{-1}, (420 ± 40) Bq kg^{-1} and (1050 ± 105) Bq kg^{-1}, respectively. The observed differences among regions may be associated with the mineralogy of the area.

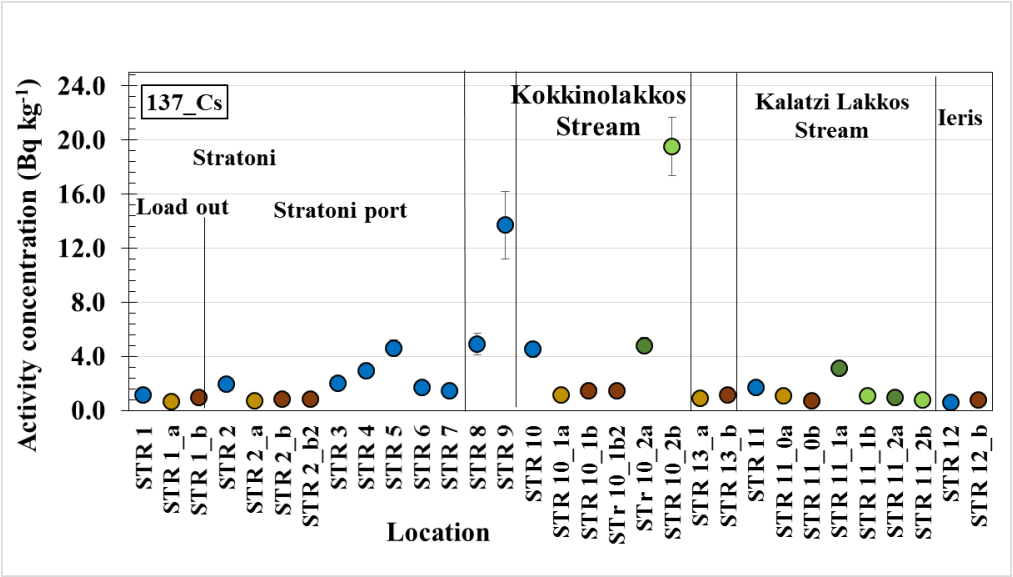

Fig. 5.6 The ^{137}Cs activity concentration results regarding the coastal and offshore (STR8, STR9) parts of Ierissos Gulf. The activity concentrations are depicted corresponding to the different matrices (blue for marine sediments, dark yellow for sea-coast interface samples, brown for the beach sand samples, dark green for the streambed samples and e) light green for the streambank samples).

The activity concentration of ^{137}Cs was found to be (0.8 – 20) Bq kg^{-1} (Fig. 5.6). For most sampling points ^{137}Cs exhibited values below 2.4 Bq kg^{-1}, while in the cases where elevated levels were observed, such as the offshore sample STR9 and the riverbank sample STR10_2b, they may be attributed to a combination of physical characteristics like organic matter and grain size distribution.

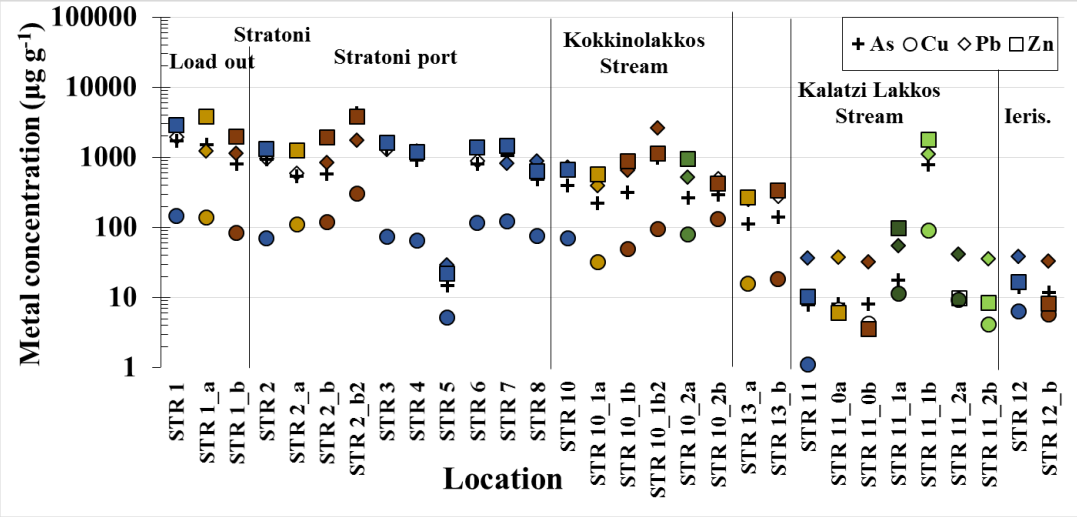

Fig. 5.7 The trace metal (As, Cu, Pb and Zn) concentration results regarding the coastal and offshore (STR8) parts of Ierissos Gulf. At the offshore sample (STR9) only radioactivity measurements have been performed for the application of the dispersion model incorporated in ERICA Tool. The metal concentrations of As (cross), Cu (circle), Pb (rhombus) and Zn (square) are depicted corresponding to the different matrices (blue for marine sediments, dark yellow for sea-coast interface samples, brown for the beach sand samples, dark green for the streambed samples and e) light green for the streambank samples).

The concentrations of As, Cu, Pb, Zn and Mn ranged among (10-4300) μg g^{-1}, (1-300) μg g^{-1}, (30-2500) μg g^{-1}, (5-4000) μg g^{-1} and (40-30000) μg g^{-1}, respectively (Fig. 5.7). The spatial distribution of trace metals (As, Cu, Pb, Zn) and Mn (Fig. 5.7) is similar to the ones of ^{226}Ra and ^{235}U, where the maximum values were observed at Stratoni port, especially near the load out pier area. The values of the aforementioned metals were reduced by 50% at Kokkinolakkos stream, while the minimum values were found at Kalatzi Lakkos and Ierissos Port. However, in the case of metals, the concentrations among the aforementioned sampling regions differed by up to 2 orders of magnitude. It is evident that these great differences cannot be attributed to physical characteristics of the samples such as grain size distribution, organic matter or mineralogy, but the main contributor are the mining activities occurring in the area and the disposal of wastes (solid or solid-liquids through the pipeline). The concentrations of metals at sampling point STR5 exhibited the minimum concentrations like at Ierissos port, which supports the evidence from ^{226}Ra data that the north part of the load out pier area has not been affected by the anthropogenic activities as the south part. All the other measured trace metals and major elements are presented in Annex VI.

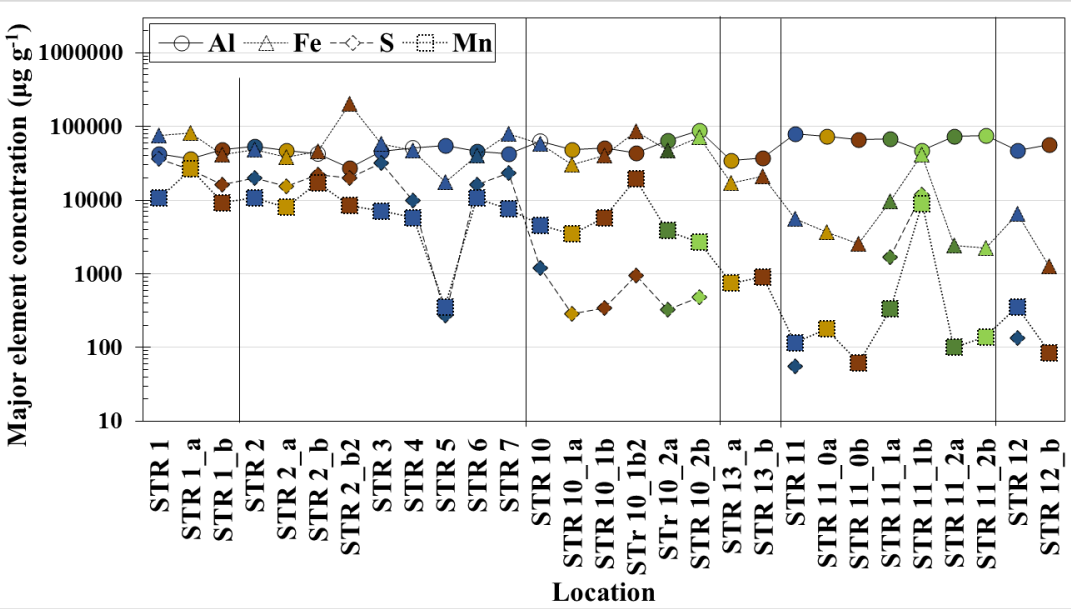

Fig. 5.8 The major elements (Al, Fe, S and Mn) concentration results regarding the coastal part of Ierissos Gulf. At the offshore samples (STR8, STR9) only radioactivity measurements have been performed for the application of the dispersion model incorporated in ERICA Tool, thus this sites are not included in the figure. The concentration of S in some sampling point was below the LDM (Limit of determination of the method), therefore they are not depicted in the graph. The lines between the points (e.g. solid, dashed) are used only for convenience so as to guide the eye. The metal concentrations of Al (circle), Fe (triangle), S (rhombus) and Mn (square) are depicted corresponding to the different matrices (blue for marine sediments, dark yellow for sea-coast interface samples, brown for the beach sand samples, dark green for the streambed samples and e) light green for the streambank samples).

The spatial distribution of Fe, S and Mn are similar to those of trace metals, ^{226}Ra and ^{235}U. Fe and S are the main metals of pyrite (FeS_2), one of the basic exploited ores, while Mn is part of rhodochrosite ($MnCO_3$) a gangue mineral which surrounds the mineral of interest. Therefore, high concentrations of these elements are present in the disposed waste, either due to the flotation method efficiency (FeS_2) or to direct discharge of minerals not commercially exploited ($MnCO_3$). Hence, the maximum concentrations of Fe, S and Mn were obtained at Stratoni (load out pier and port) where the flotation plant and other facilities (e.g. load hoper, flotation tailing pipeline) are established. Elevated concentrations were also found in Kokkinolakkos Stream, since waste disposals took place for many years. However, the distant areas from Stratoni (Kalatzi Lakkos Stream and Ierissos port) exhibited minimum concentrations of metals up to 3 orders of magnitude lower than the values at Stratoni port and in some cases below the LDM (Limit of Determination of the Method) such as S, indicating a non-affected area by mining activities. The spatial distribution of Al is almost homogenized among the sampling points, hence it is not strongly affected by anthropogenic activities at the regions of study. All the other measured trace metals and major elements are presented in Annex VI.

5.1.3 Trace metal/major element and mass flux vertical distribution

The concentrations and mass fluxes of some trace metals and major elements for the coastal core (STR1) are presented below in Figs. 5.9 and 5.10. The radioactivity,

trace metal and Mn measurements are also presented for the offshore core (STR8) and are depicted in Figs. 5.11 and 5.13. The results of trace metal and Mn of the offshore core will be presented in correspondence to those of the coastal core (STR1). The calculated relative uncertainties of radionuclides, trace metals and major elements are included in Annex V.

STR1 coastal core results

The results of trace metal (As, Zn, Cu and Pb) concentrations and mass fluxes are shown in Fig. 5.9. According to these profiles, the sediment core can be divided into two parts: the upper (0-11 cm) and the lower (12-27 cm).

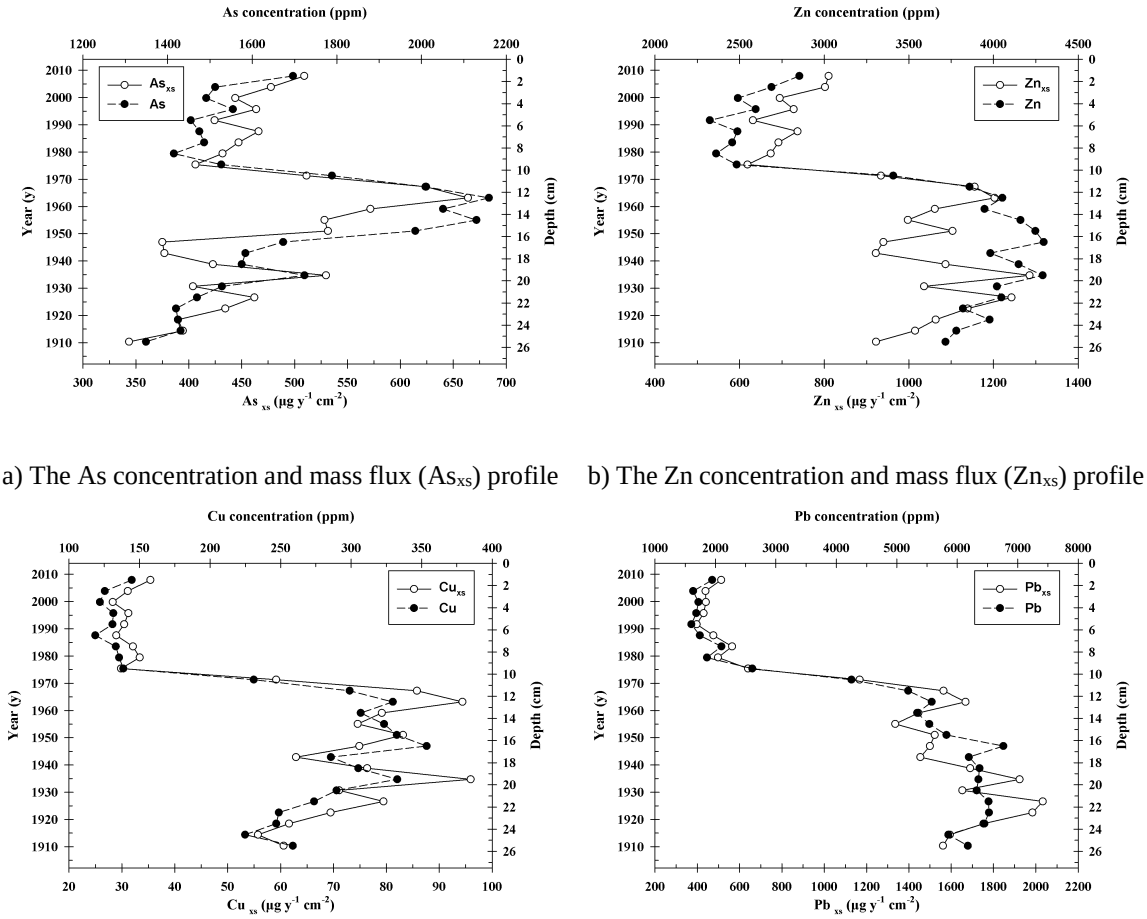

a) The As concentration and mass flux (As_{xs}) profile b) The Zn concentration and mass flux (Zn_{xs}) profile

c) The Cu concentration and mass flux (Cu_{xs}) profile d) The Pb concentration and mass flux (Pb_{xs}) profile

Fig. 5.9 The metal concentration and mass flux profiles of trace elements (As, Zn, Cu and Pb) in STR1 (coastal) core.

The concentrations of As, Zn, Cu, and Pb in the sediment core ranged between $(1.4\text{-}2.2)\cdot10^3$ μg g^{-1}, $(2\text{-}6)\cdot10^3$ μg g^{-1}, (100-250) μg g^{-1} and $(2.5\text{-}4.0)\cdot10^3$ μg g^{-1}, respectively. The maximum values were found in the lower part of the core and were up to 3 times higher than those obtained in the upper part. In concentration profile of As the maximum concentration was found at 12 cm sediment depth, which was followed by a linear gradual decrease to values similar to those of the upper core part. Furthermore, the concentrations of Mn, Al and Fe are depicted in Fig. 5.10 and exhibited values of $(4 – 12)\cdot10^3$ μg g^{-1}, $(40 - 60)\cdot10^3$ μg g^{-1} and $(70 - 85)\cdot10^3$ μg g^{-1},

respectively. The maximum values of Fe and Al were measured at 12-27 cm (lower part) of the core and were 20-30% higher than those observed at 0-11 cm (upper part). On the other hand, the highest concentrations of Mn were obtained in the upper part of the core exhibiting values up to 4 times higher than those of the lower part.

The excess fluxes of Al and Fe ranged between $(0 - 5)\cdot 10^3$ μg y^{-1} cm^{-2} and $(14 - 20)\cdot 10^3$ μg y^{-1} cm^{-2}, respectively. The maximum values of the Fe excess flux were observed at 12 cm and 20 cm depth, as As and Zn excess flux profiles. The maximum values of Al excess flux were found at the lower part of the core (11 - 27 cm), as those of Cu and Pb excess flux profiles.

The excess metal fluxes were calculated for the aforementioned trace metals based on the satisfactory agreement of the sedimentation rates using the ^{210}Pb and ^{137}Cs dating methods. The method of the calculation of metal fluxes is described in detail in chapter 4. The As excess flux ranged between (350 – 650) μg y^{-1} cm^{-2}. Additionally, two local maxima of 650 μg y^{-1} cm^{-2} and 550 μg y^{-1} cm^{-2} were observed at 12 cm and at 20 cm, respectively. The Cu and Pb metal fluxes ranged between (30 – 95) μg y^{-1} cm^{-2} and $(0.4 – 2)\cdot 10^3$ μg y^{-1} cm^{-2}, respectively, wherein the maximum values were obtained in the lower part of the core (11-27 cm). The metal flux profile of Zn exhibited values of $(0.6\cdot - 1.2)\cdot 10^3$ μg y^{-1} cm^{-2} and two local maxima were also found at 12 cm and 20 cm.

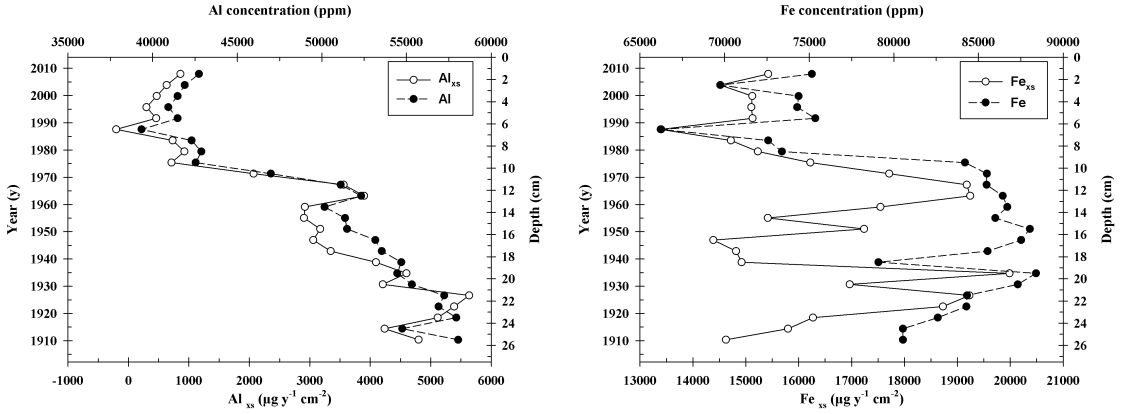

a) The Al concentration and mass flux (Al_{xs}) profile b) The Fe concentration and mass flux (Fe_{xs}) profile

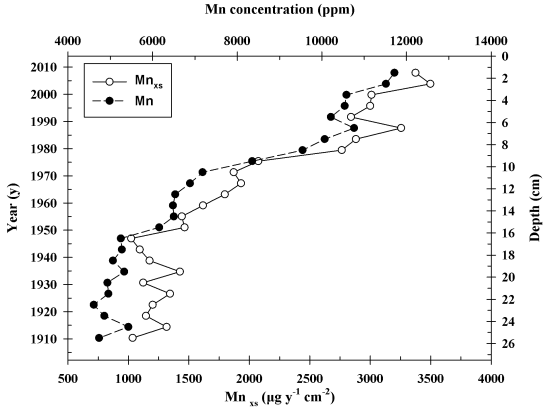

c) The Mn concentration and mass flux (Mn_{xs}) profile

Fig. 5.10 The metal concentration and mass flux profiles of major elements (Al, Fe and Mn) in STR1 (coastal) core.

STR8 offshore core results

The trace metal and Mn concentrations of the STR8 offshore core (white points) exhibited elevated values at the first 12 cm, which decrease in deeper layers (Fig. 5.11). The concentrations of As, Zn, Cu, Pb and Mn of the offshore core were found to range between (50-480) μg g^{-1}, (240-630) μg g^{-1}, (30-80) μg g^{-1}, (300-900) μg g^{-1} and (0.9-2.2)·10^3 μg g^{-1}, respectively. The calculated relative uncertainties of trace metals and major elements are included in Annex V.

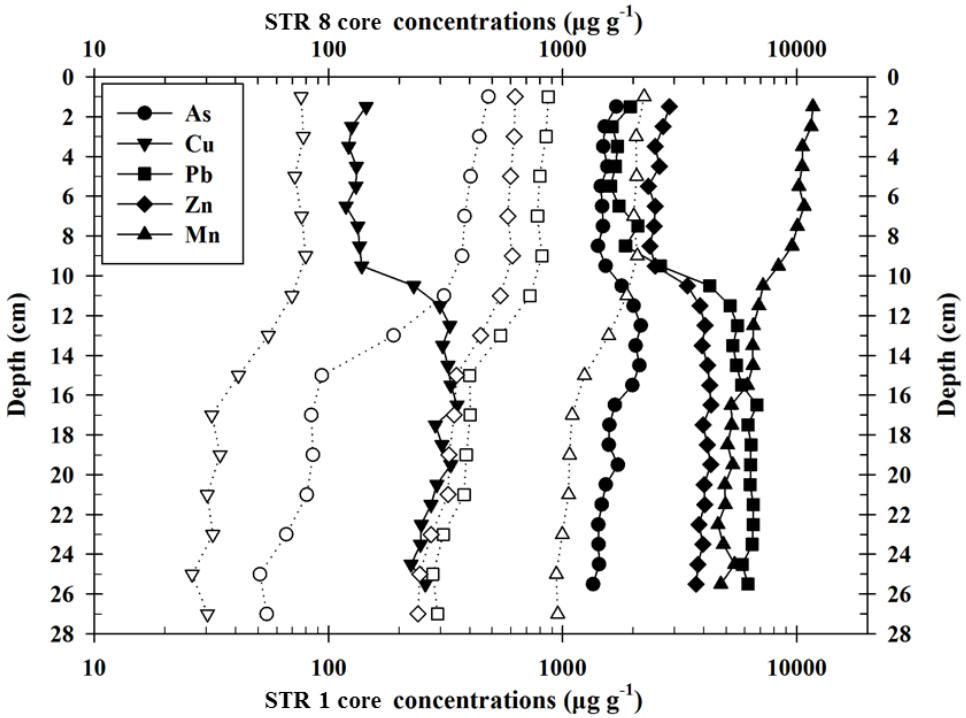

Fig. 5.11 The concentration profiles of trace metals (As, Cu, Pb, Zn) and Mn of the coastal core (STR1_black points) and the offshore core (STR8_white points).

These elevated values cannot be attributed solely to the fine grain fraction of STR8 core, as the sand-mud vertical distribution changes slightly between the upper part (0-12 cm) and the lower part (13-27 cm) of the core (see section 5.3.1.6). The vertical distribution among cores, the coastal (STR1) and the offshore (STR8), indicate that both have been affected by the anthropogenic activities, wherein STR8 core in a lesser extent, as it is evident by the one-order-of-magnitude lower values of trace metal and Mn concentrations comparing to STR1 core. The mining activities have affected the coastal area for many years, as shown by the high concentrations of trace metals and Mn in STR1 profile. Additionally, this impact reached the offshore area (STR8), however for fewer years, as indicated by the elevated values, were found only in the first 12 cm.

5.1.4 Radioactivity and mass flux vertical distribution

STR1 coastal core results

According to the metal profiles presented above, the sediment core STR1 can be divided in two parts: the upper (0-11 cm) and the lower (12-27 cm). The same trend show the radioactivity measurements of ^{226}Ra, ^{235}U and ^{40}K. The radionuclides of ^{226}Ra, ^{235}U, ^{228}Ac and ^{40}K exhibited values of (75-120) Bq kg^{-1}, (4.8-13.4) Bq kg^{-1}, (30-40) Bq kg^{-1} and (570-860) Bq kg^{-1}, respectively (see Fig. 5.12 a-d). The activity concentrations of ^{228}Ac represent the whole ^{232}Th series, as similar values were obtained for ^{212}Pb, ^{212}Bi and ^{208}Tl.

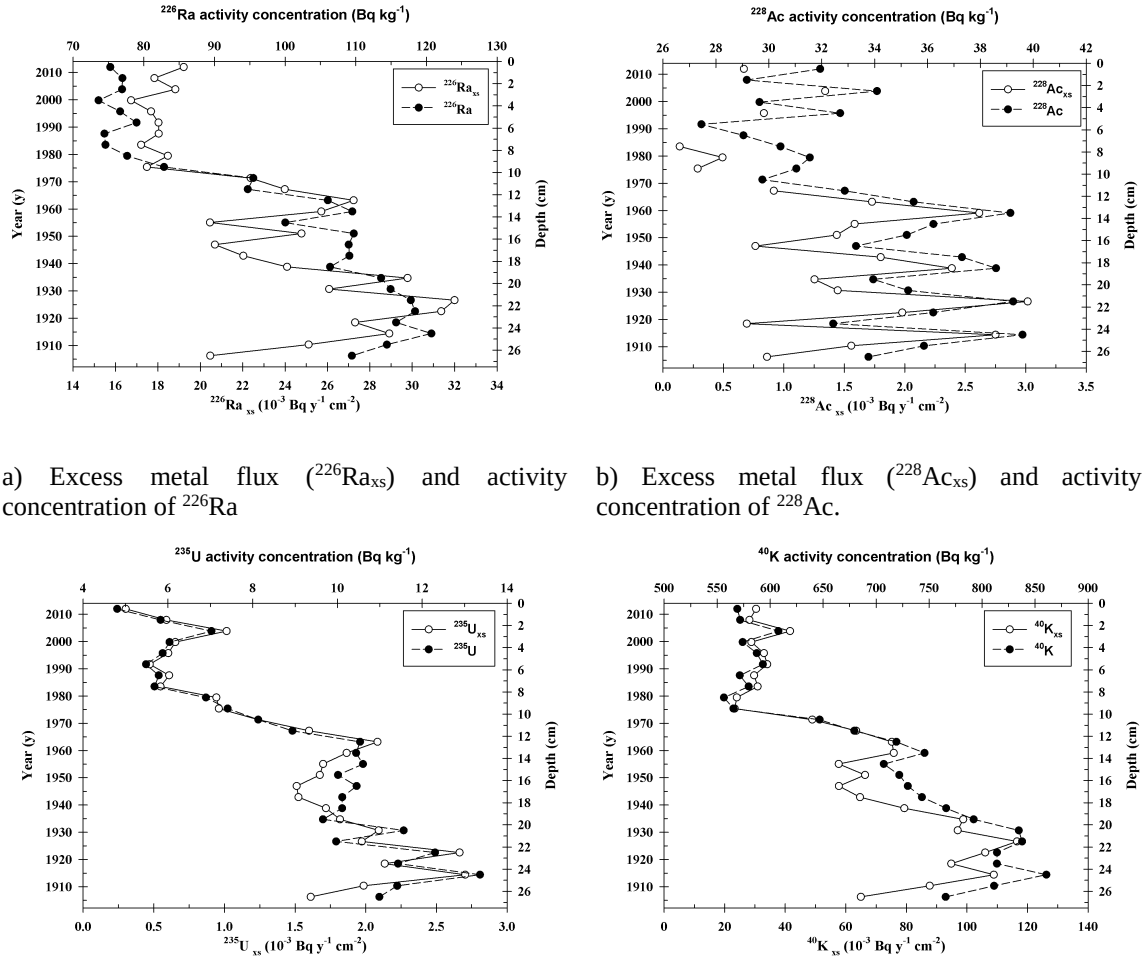

a) Excess metal flux ($^{226}Ra_{xs}$) and activity concentration of ^{226}Ra

b) Excess metal flux ($^{228}Ac_{xs}$) and activity concentration of ^{228}Ac.

c) Excess metal flux ($^{235}U_{xs}$) and activity concentration of ^{235}U.

d) Excess metal flux ($^{40}K_{xs}$) and activity concentration of ^{40}K.

Fig. 5.12 The excess metal flux and activity concentrations of the long-lived radionuclides, as well as ^{228}Ac, assuming secular equilibrium with its parent nuclide. in STR1 (coastal) core of Ierissos Gulf.

At the upper part, the activity concentrations of ^{226}Ra, ^{235}U and ^{40}K were 2 times less than those of the lower part of the core. However, a homogeneous profile, within uncertainties, was observed for ^{228}Ac, exhibiting a mean value of (30 ± 3) Bq kg^{-1}. The excess metal flux (in 10-3 Bq y^{-1} cm^{-2}) was also calculated for the long-lived natural radionuclides and ^{228}Ac, assuming it is in secular equilibrium with its parent nuclide ^{232}Th. The mass flux values of ^{226}Ra ($^{226}Ra_{xs}$), ^{228}Ac ($^{228}Ac_{xs}$), ^{235}U ($^{235}U_{xs}$) and ^{40}K

($^{40}K_{xs}$), exhibited values of (18 - 32)·10^{-3} Bq y^{-1} cm^{-2}, (0.3-3.0) 10^{-3} Bq y^{-1} cm^{-2}, (0.3 to 2.7) 10^{-3} Bq y^{-1} cm^{-2} and (20-120) 10^{-3} Bq y^{-1} cm^{-2}, respectively. In the activity concentration and mass flux profiles of ^{226}Ra, ^{235}U and ^{40}K the lower values were found in the upper part of the core (0-10 cm), compared to the deeper layers. Two local maxima (see excess metal profiles of Fe, As and Zn) were also obtained at 12 cm and 21 cm.

STR8 offshore core results

The activity profiles of ^{226}Ra, ^{235}U, ^{228}Ac and ^{40}K of the offshore core are presented below. The activity concentrations of the aforementioned radionuclides exhibited values of (13-30) Bq kg^{-1}, (2.7-4.1) Bq kg^{-1}, (25-35) Bq kg^{-1} and (460-650) Bq kg^{-1}, respectively. For the offshore core the excess metal flux estimation was not performed, as the sedimentation rate calculation was not possible.

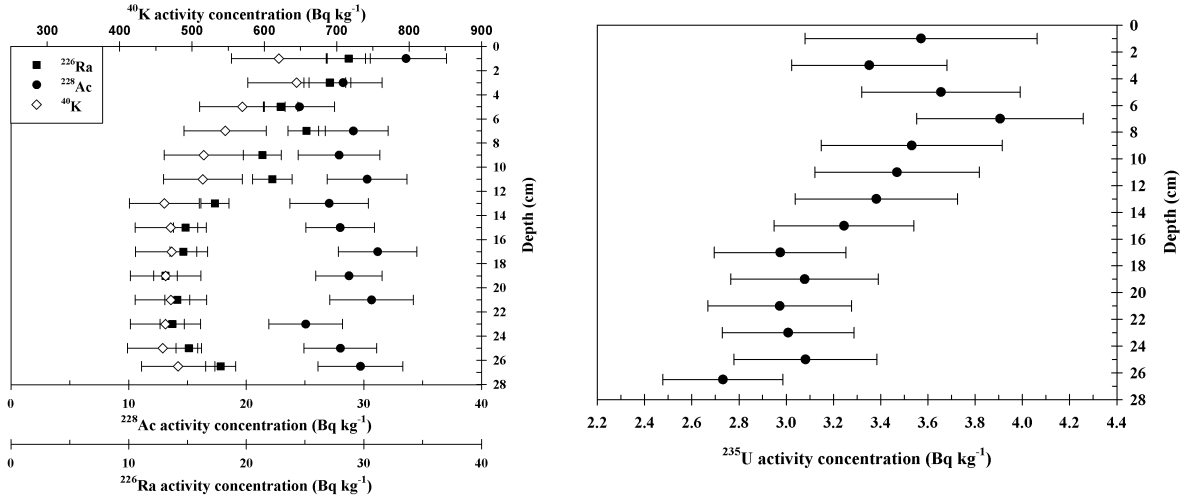

a) The activity concentration profile of ^{226}Ra, ^{228}Ac, ^{40}K.

b) The activity concentration profile of ^{235}U

Fig. 5.13 The radionuclide activity concentration profiles of the offshore core (STR8). ^{228}Ac represents the ^{232}Th series as similar values were found for ^{212}Pb, ^{212}Bi and ^{208}Tl.

At the upper part of the core (0-11cm), the values of ^{226}Ra, ^{40}K and ^{235}U were found higher than those of the lower part (12-27 cm), while ^{228}Ac was characterized by a homogeneous profile. The different values of these radionuclides between the upper and the lower part indicate that the concentrations of ^{226}Ra, ^{40}K and ^{235}U have been affected by the mining activities occurring in the area. However, the anthropogenic impact at the offshore core is lesser as the radionuclide profiles exhibited lower values in it (STR8) comparing with those of the coastal core (STR 1). Additionally, the impact of the mining activities reached the offshore core (STR8) and lasted for quite some time as it can be identified by the enhanced radionuclide concentrations of the upper layer (till 11 cm), compared to background values (deepest slice). Finally, comparing the ^{228}Ac profiles for both cores, it is safe to assume that this radionuclide is not affected by the mining activities. This assumption supports the first hint originated by the spatial distribution of ^{228}Ac discussed in section 5.1.2.

5.1.5 Dose rate assessment

The average measured values of activity concentrations of ^{226}Ra, ^{40}K, ^{228}Th, ^{228}Ra, ^{210}Pb, ^{137}Cs and ^{235}U in the seafloor sediments were used for the dose rate estimation implemented by ERICA Assessment Tool. The radionuclides of ^{228}Th and ^{228}Ra are assumed to be in secular equilibrium with their daughters ^{228}Ac and ^{210}Pb, ^{212}Bi and ^{208}Tl, respectively. The total dose rates, as well as the external and internal fractions, absorbed by the reference organisms are depicted in Fig. 5.14.

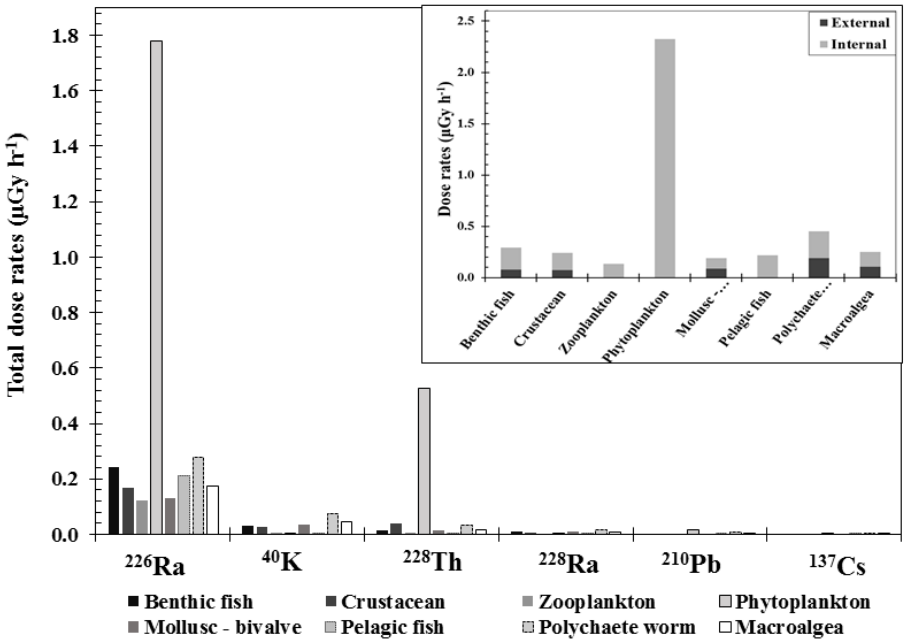

Fig. 5.14 Total, internal and external dose rates of marine biota based on the measured activity concentrations of natural and ^{137}Cs radionuclides in the seafloor sediment of Stratoni port.

The radiation effect can be considered negligible possessing no significant risks, as in all cases the total dose rates were calculated to be two orders of magnitude lower than the proposed screening values by IAEA (1992) and UNSCEAR (1996) for aquatic biota. The main contributors to the total dose rates were found to be ^{226}Ra (1.8 μGy h^{-1}) and ^{228}Th (5.3 10^{-1} μGy h^{-1}), as both radionuclides and their progenies are alpha emitters resulting in a significant radiological impact due to alpha particle nature (energies of several MeVs, strong interaction with matter). The ERICA Tool assumes secular equilibrium among ^{226}Ra and its progenies (^{222}Rn, ^{218}At, ^{218}Po, ^{214}Pb, ^{214}Bi, ^{214}Po), as well as among ^{228}Th and its daughters (^{224}Ra, ^{220}Rn, ^{216}Po, ^{212}Pb, ^{212}Po, ^{212}Bi, ^{208}Tl) (Brown et al., 2008). The reference organism of phytoplankton received the major dose rates exhibiting values 9 to 10 times higher than the dose rates received by other organisms. The main contributor to the total dose rates was the internal fraction, due to the alpha emitters as mentioned before, while the external fraction for many cases is negligible comparing to the internal one. The external fraction becomes significant for the organisms living close to or in the sediment (e.g. benthic fish, crustacean, mollusk-bivalve, polychaete worm, macroalgae). The received external dose rates are attributed mainly to ^{40}K and secondly to ^{226}Ra, thus despite the minor contribution of ^{40}K to the total dose rate calculation, it should be taken into account for the cases of organisms which reside close to or in the seafloor.

5.1.6 Grain size analysis

Spatial distribution

Grain size distribution measurement were performed in detail for the samples of the first survey in 2012. According to this work (Pappa et al., 2016) all the samples can be considered to have comparable to the reference site (Ierissos port) grain size distribution. Meaning that the grain size effect, the affinity of metals and radionuclides to different grain sizes, is similar among the sampling points and the observed differences of radionuclides and metals cannot be attributed to different sediment textures. Thus, the grain size measurement was not held for the surface samples of the second survey in 2014.

Vertical distribution

A rough estimation of the grain size distribution was performed in the samples, determining the mud-sand portions. The sand-mud vertical distribution for both cores, coastal (STR1) and offshore (STR8) are depicted below.

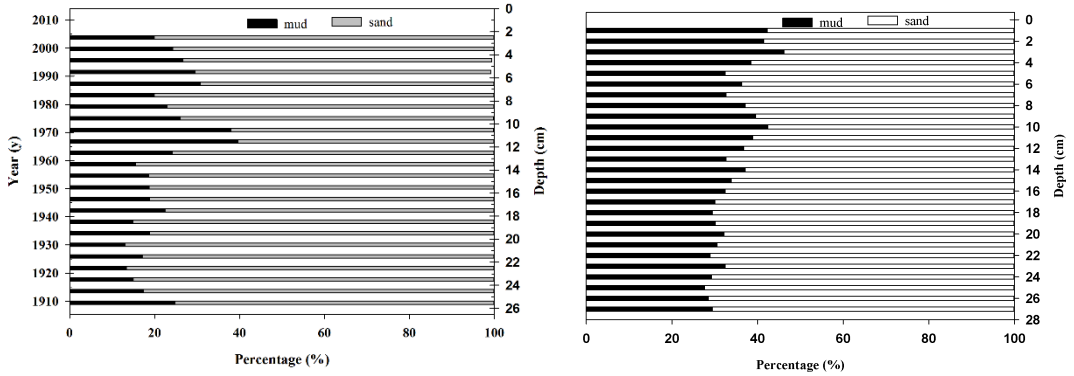

Fig. 5.15 Mud-sand vertical distribution of the STR1 coastal core (left) and the STR8 offshore core (right) at Ierissos Gulf.

STR1 core is characterized as muddy sand, while the offshore core (STR8) is characterized as sandy mud according to Folk's classification (Folk 1954). The coastal core can be slightly divided into two parts: the upper part (0-11 cm), which consists of 60-70% sand and 40-30% mud and the lower part (12-27 cm), which consists of 80% sand and 20% mud. The offshore core can be also slightly divided into two parts: the upper (0-12 cm), which consists of 60% sand and 40% mud and the lower one (13-27 cm), which consists of 70% sand and 30% mud. The elevated concentrations of radionuclides and metals in both cores, and especially in the coastal core, cannot be solely attributed to the grain size distribution.

5.1.7 Trace metal measurements in seawater

In order to investigate possible metal impact in the seawater of Ierissos Gulf, water samples were collected in the sediment- seawater interface. The metal concentrations of Cu, Pb, Zn, Ni and Cd are presented below, in Table 10.

Table 10 Trace elements concentration in seawater.					
Station	**Cu**	**Pb**	**Zn**	**Ni**	**Cd**
	(μg L^{-1})				
STR1	0.36	6.80	3.34	0.19	0.095
STR2	<LDM	0.13	0.44	0.14	0.013
STR3	1.22	22.71	1.08	0.31	0.091
STR4	0.15	1.51	0.52	0.18	0.016
STR7	0.11	0.23	1.47	0.18	0.008
STR10	<LDM	0.23	0.57	0.20	0.011
STR11	<LDM	0.14	0.50	0.22	0.011
STR12	0.16	0.14	0.61	0.22	0.012
LDM: Limit of Detection of the Method					

The concentrations of Cu, Pb, Zn, Ni and Cd ranged within the Limit of Detection of the Method (LDM) - 1.22 μg L^{-1}, 0.14 -22.71 μg L^{-1}, 0.44 – 3.34 μg L^{-1}, 0.14-0.31 μg L^{-1} and 0.008 – 0.095 μg L^{-1}, respectively. The maximum values of almost all metals were observed at the sampling points of the load out pier area (STR1) and the adjacent site (STR3). The Cu, Pb, Zn, Ni and Cd concentrations at STR1 and STR3 sampling points were up to 8, 161, 5, 1.4 and 8 times higher than the values at Ierissos port (STR12). The minimum values of metals were obtained for Pb, Zn and Ni at STR2 and for Cd at STR7. The Pb, Zn and Ni concentrations at STR2 were 5%, 28% and 37% lower than the values at Ierissos port. The concentration of Cd at STR7 was 33% lower than the one at Ierissos port, while the measured metal concentrations at Kokkinolakos (STR10) and Kalatzi Lakkos (STR11) estuaries were the same as those at Ierissos port.

5.2 Lavrio

Two sampling surveys were also held along the east part of Lavreotiki Peninsula in 2014 and 2016, where surface sediments, a coastal (core 1) and an offshore (core 2) sediment cores were collected. The area hosted for many years mining activities, however the last 30 years all mining activities are ceased. In this work surficial samples were collected in different bays, focusing on Oxygono Bay, to study the mining impact spatially. In the same bay the coastal core was sampled to investigate the anthropogenic impact of previous years (temporal study). Additionally, the second core was utilized to investigate the mining impact at the offshore part of Lavreotiki Peninsula. Both results of the spatial and vertical distributions will be presented in the same subsection.

5.2.1 Sedimentation rate

Coastal core (core 1) results

The aforementioned proposed ^{210}Pb chronological models (section 4.6.1), were applied in Oxygono Bay (core 1) and the results are presented below, in Fig. 5.16:

9

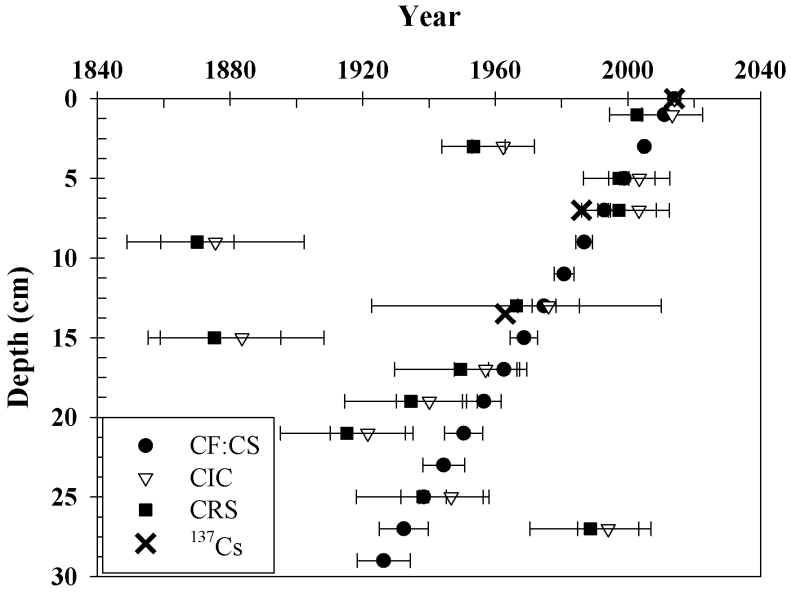

Fig. 5.16 The applied radiochronological models in Oxygono Bay based on ^{210}Pb (CF:CS, CIC, CRS) and ^{137}Cs. CF:CS –Constant Flux:Constant Sedimentation, CIC- Constant Initial Concentration, CRS - Constant Rate of Supply.

Among the proposed models based on ^{210}Pb excess concentrations, great discrepancies were observed for CIC and CRS models, while a good agreement was obtained between CF:CS model and the sedimentation estimations utilizing ^{137}Cs. The observed discrepancies are due to the hypotheses incorporated in each model. This investigation of applying appropriate models for the sedimentation rate estimation, suggests the implementation of CF:CS and ^{137}Cs models. Thus, The vertical profile of ^{137}Cs and the correspondence of the ^{137}Cs-peak maxima to historical nuclear events (e.g. nuclear test in 1963, Chernobyl accident in 1986), as well as the logarithmized excess of ^{210}Pb versus depth are depicted in the following figures:

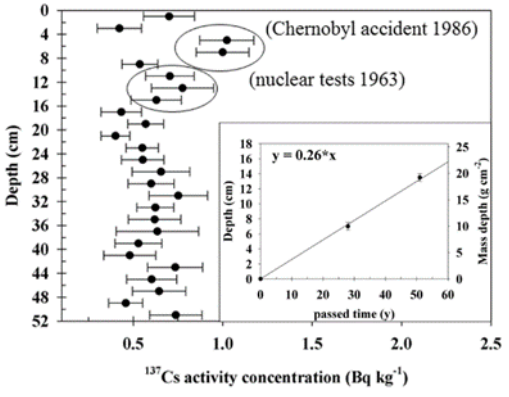

a) the ^{137}Cs method (MDA = 0.6 Bq kg^{-1})

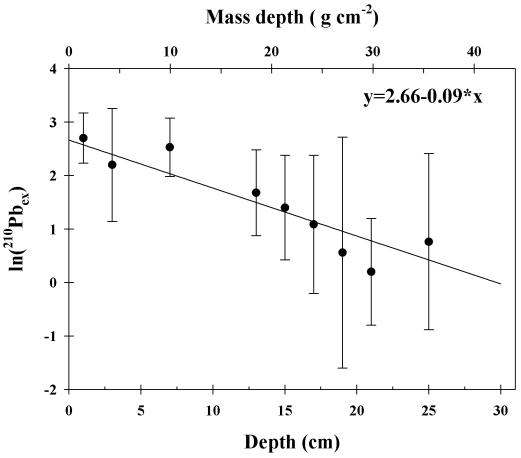

b) the ^{210}Pb method, utilizing the constant flux : constant sedimentation (CF:CS) model.

Fig. 5.17 The two sedimentation rate estimation methods applied in coastal core (core 1) of Oxygono Bay.

The SRs utilizing independently the maxima of ^{137}Cs, which correspond to the incidents of 1963 and 1986, were found (0.26 ± 0.01) cm y^{-1} and (0.25 ± 0.01) cm y^{-1}, respectively. The estimated sedimentation rates are consistent within uncertainties and

the produced differences in sediment ages ranged from <1 to 8 y among the surface and the deepest layers of the core (200 y before), respectively. The radiodating methods based on ^{137}Cs and ^{210}Pb, revealed similar **sedimentation rates of (0.26 ± 0.01) cmy^{-1} and (0.33 ± 0.03) cm y^{-1}**, respectively. However, the sedimentation rate determined by the ^{137}Cs method was not used for the reconstruction of historical levels of metals and radionuclides at Oxygono Bay, as the signals of Chernobyl accident and nuclear tests were not clearly distinguished in ^{137}Cs profile. Additionally, the counting statistics were low and the activity concentrations of ^{137}Cs were near the MDA values (0.6 Bq kg^{-1}) for the whole core.

Offshore core (core 2) results

The radioactivity measurements were determined with large uncertainty due to the small quantity of mass sample and the low values of activity concentrations (the gravel nature of the sediments samples characterize the offshore area of Lavrio). Furthermore, the exponential decrease of ^{210}Pb activity concentration, as well as ^{137}C values were not distinct and the sedimentation rate estimation for this core was not applicable.

5.2.2 Radioactivity and trace metal/major element spatial distribution

The presented results refer to the work held mainly during the main surveys (April 2016, October 2016), including the surface and sediment core samples at Oxygono Bay, as well as the sediment core located offshore of Oxygono Bay. The results of the preliminary survey (January 2014), including surface samples from Oxygono and neighbouring bays (Thorikos, Delenia, Perdika) have already been discussed in the master thesis of Michalopoulou, (2014) and presented in a conference Michalopoulou et al., (2015). Thus, the latter will be only used in the interpretation section of next chapter (chapter 6).

The activity concentrations of natural radionuclides (^{210}Pb, ^{226}Ra, ^{234}Th, ^{228}Ac, ^{235}U and ^{40}K) and ^{137}Cs at the surface sediments of Oxygono Bay are presented in Table 11. The ^{210}Pb activity concentration ranged among (42-112) Bq kg^{-1} and the maximum value was obtained at N5 station, the nearest sampling point to the coast. The spatial distribution of the activity concentrations of the other radionuclides (^{226}Ra, ^{228}Ac, ^{235}U, ^{40}K and ^{137}Cs) was almost homogeneous, exhibiting mean values of 9, 13, 2.3, 159 and 1.3 Bq kg^{-1}, respectively. The minimum values of ^{226}Ra and ^{228}Ac were observed in the south part of Oxygono Bay (N3, N4). ^{234}Th was also determined and ranged among (30-47) Bq kg^{-1} exhibiting up to 4 times higher values compared to those of ^{226}Ra. Hence, secular equilibrium between ^{234}Th and ^{226}Ra cannot be assumed. This difference may be attributed to the particle-reactive nature of thorium (Rose et al., 1994) or to the metal post-mining impact (Abril et al., 2018). The calculated relative uncertainties of radionuclides, trace metals and major elements are included in Annex V.

Table 11 Activity concentration of ^{210}Pb, $^{210}Pb_{ex}$, ^{234}Th, ^{226}Ra, ^{228}Ac, ^{235}U, ^{40}K and artificial radionuclide ^{137}Cs in the surface sediments. The MDA values are given in Fig. 4.7 for each detection system.								
Station	**$^{210}Pb_{tot}$**	**$^{210}Pb_{ex}$**	**^{234}Th**	**^{226}Ra**	**^{228}Ac**	**^{235}U**	**^{40}K**	**^{137}Cs**
	Bq kg^{-1}							
N1	42 ± 5	30 ± 5	30 ± 4	11.4 ± 0.6	14.0 ± 1.1	2.4 ± 0.3	184 ± 12	1.2 ± 0.2
N2	94 ± 8	84 ± 8	47 ± 6	9.5 ± 1.1	17.0 ± 1.2	1.3 ± 0.2	175 ± 11	1.2 ± 0.2
N3	50 ± 4	46 ± 4	32 ± 3	4.7 ± 0.3	10.2 ± 0.9	2.7 ± 0.2	136 ± 9	1.3 ± 0.4
N4	53 ± 6	47 ± 6	31 ± 3	6.6 ± 0.5	10.5 ± 1.5	3.0 ± 0.6	191 ± 12	1.2 ± 0.3
N5	112 ± 10	101 ± 10	29 ± 5	11.9 ± 0.5	13.2 ± 1.1	2.3 ± 0.3	111 ± 8	1.5 ± 0.4

The concentrations of trace metals (As, Cu, Pb, Zn) are presented in Table 12 and their values ranged among (2.1-8.6)·10^3 μg g^{-1}, (46-102) μg g^{-1}, (2.3-3.9)·10^3 μg $g^{-1}$and (4.9-12.5)·10^3 μg g^{-1}, respectively. The spatial distribution of trace metals exhibited maximum concentrations at the nearest station to the coast, N5, and minimum values at the south part of Oxygono Bay (N3, N4), like ^{226}Ra and ^{228}Ac activity concentrations. All the other measured trace metals and major elements are presented in Annex VI.

Table 12 Trace metal (As, Zn, Cu, Pb) and major element (Mn, Al, Fe) concentrations in the surface sediments of Oxygono Bay.							
Station	As (·10^3)	Cu	Pb (·10^3)	Zn (·10^3)	Mn (·10^3)	Fe (·10^4)	Al (·10^3)
	(μg g^{-1})						
N1	4.2±0.5	70±4	2.52±0.12	7.2±0.7	9.3±0.5	12.7±0.6	23.3±1.2
N2	4.3±0.5	74±4	2.94±0.14	7.4±0.7	7.5±0.4	12.4±0.6	17.2±0.9
N3	2.1±0.3	46±2	3.00±0.14	5.7±0.5	4.2±0.2	7.8±0.4	20.5±1.0
N4	2.1±0.3	50±3	2.30±0.11	4.9±0.4	5.0±0.2	8.0±0.4	21.6±1.1
N5	8.6±1.1	102±5	3.91±0.18	12.5±1.1	11.3±0.6	20.6±1.0	14.4±0.7

Additionally, large variations were also observed in the spatial distribution of Mn and Fe, wherein they exhibited values of (4 to 11)·10^3 μg g^{-1} and (8 to 21)·10^3 μg g^{-1}, respectively. The maximum concentrations were also observed at station N5. The spatial distribution of Al was almost homogeneous, exhibiting a mean value of 19·10^3 μg g^{-1}.

5.2.3 Trace metal/major element and mass flux vertical distribution

Coastal core (core 1) results

The concentrations and mass fluxes of some trace metals and major elements for the coastal core (core 1) are presented below. Regarding the offshore core (core 2), only radioactivity, trace metal and Mn measurements were performed. The results of the trace metals and Mn of the offshore core will be presented in correspondence to those in the coastal core (STR1).

According to radionuclide and metal profiles the sediment core can be divided in three parts: the upper (0-28 cm), the middle (28-38 cm) and the lower (38-52 cm). The calculated relative uncertainties of radionuclides, trace metals and major elements are included in Annex V.

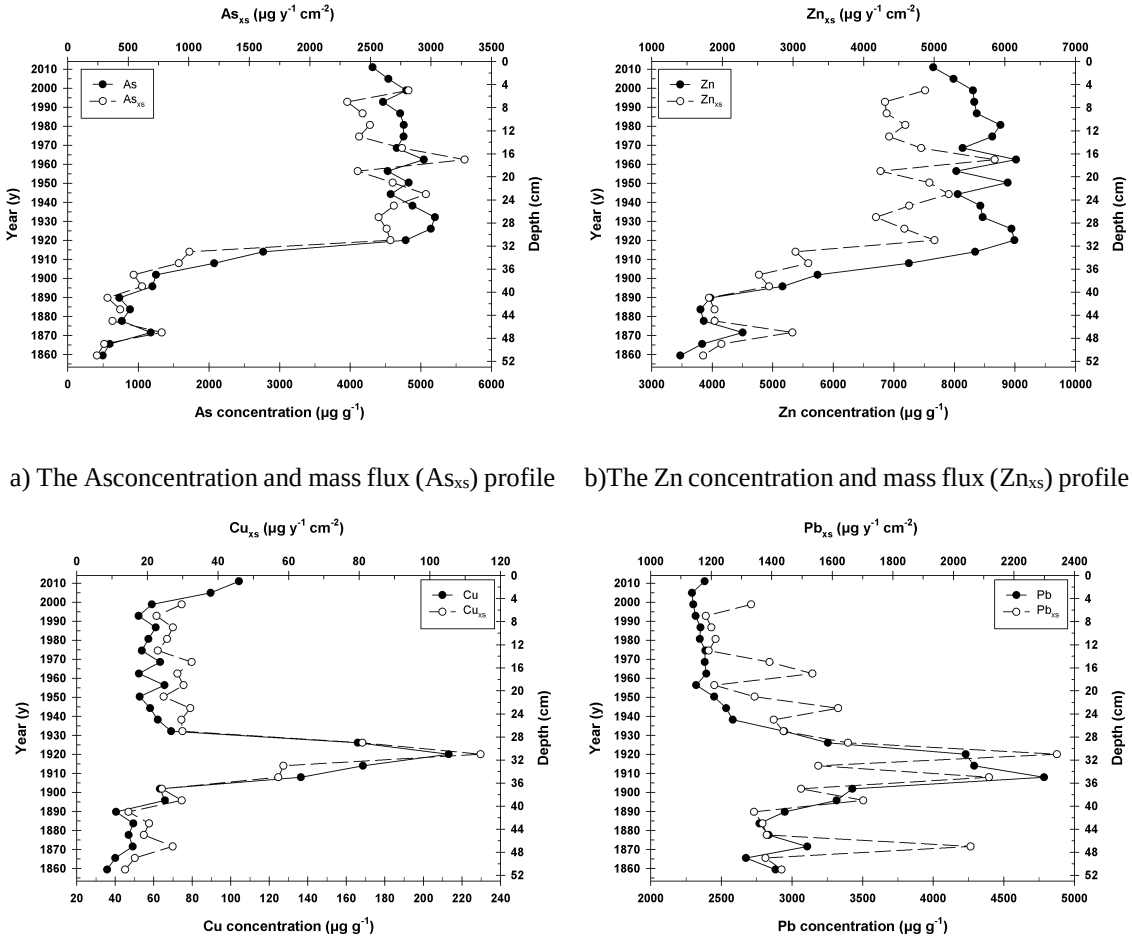

a) The Asconcentration and mass flux (As_{xs}) profile b)The Zn concentration and mass flux (Zn_{xs}) profile

c) The Cu concentration and mass flux (Cu_{xs}) profile d) The Pb concentration and mass flux (Pb_{xs}) profile

Fig. 5.18 The metal concentration and mass flux profiles of trace elements (As, Zn, Cu and Pb).

The As, Zn, Cu and Pb concentrations exhibited values of $(0.5\text{-}5.5)\cdot10^3$ µg g^{-1}, $(3.5\text{-}9.0)\cdot10^3$ µg g^{-1}, (40-210) µg g^{-1} and $(2.4\text{-}4.8)\cdot10^3$ µg g^{-1}, respectively. The vertical distribution of As and Zn revealed higher concentrations in the upper part of the core, approximately 6 and 2 times, with respect to those of the lower part. However, in the Cu and Pb vertical distribution, a peak was observed in the middle part of the coastal core (28-38 cm). In this peak, Cu and Pb concentrations were found 3 and 2 times higher, with respect to those in the upper and lower part of the core. The trace metal excess mass fluxes were determined in the coastal core, taking into account the sedimentation rate value. The excess mass fluxes of As, Zn, Cu and Pb ranged between $(0.3\text{-}3.3)\cdot10^3$ µg y^{-1} cm^{-2}, $(1.5\text{-}5.5)\cdot10^3$ µg y^{-1} cm^{-2}, (10-110) µg y^{-1} cm^{-2} and $(1.2\text{-}2.3)\cdot10^3$ µg y^{-1} cm^{-2}, respectively. For all trace metal vertical distributions, the mass flux profiles exhibited similar trend as the concentration profiles.

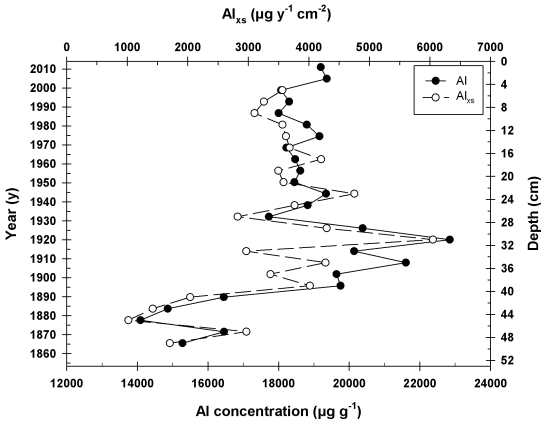

a) The Al concentration and mass flux (Al_{xs}) profile

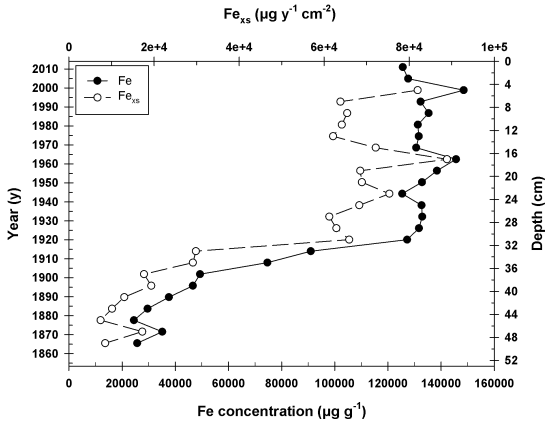

b) The Fe concentration and mass flux (Fe_{xs}) profile

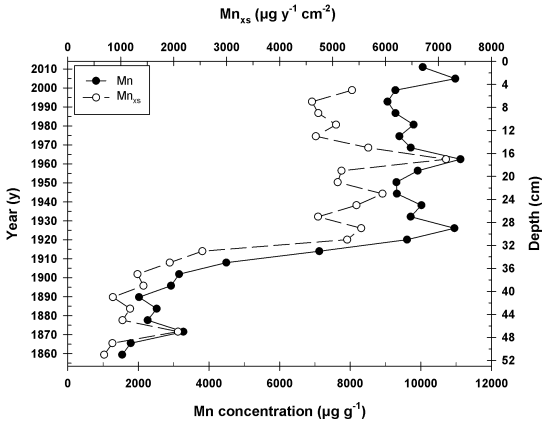

c) The Mn concentration and mass flux (Mn_{xs}) profile

Fig. 5.19 The metal concentration and mass flux profiles of major elements (Al, Fe and Mn).

The Al, Fe and Mn concentrations ranged between $(1.4\text{-}2.3)\cdot10^4$ μg g^{-1}, $(2\text{-}15)\cdot10^4$ μg g^{-1}, and $(1.5\text{-}11.0)\cdot10^3$ μg g^{-1}, respectively. As in trace metal profiles, the Fe and Mn concentrations in the upper part of the core, were 4 times, for both elements, higher than those of the lower part. The values of Mn in the middle part increased linearly between the concentrations of the lower part and those of the upper one. Al profile exhibited a peak with a maximum value during 1910-1930 (28-34 cm), as in Cu and Pb profiles, which was 1.5 times higher than those of the lower part, respectively. The Al concentrations varied in a lesser extent and were found at the upper part higher by up to 20% than those of the lower part of the core. The excess mass fluxes of Al, Fe, and Mn exhibited values of $(1\text{-}6)\cdot10^3$ μg y^{-1} cm^{-2}, $(1\text{ -}9)\cdot10^4$ μg y^{-1} cm^{-2}, and $(1\text{-}7)\cdot10^3$ μg y^{-1} cm^{-2}, respectively. In all major element vertical distributions, the mass flux profiles exhibited a similar trend as the concentration profiles.

Offshore core (core 2) results

At the offshore core only trace metal (and radioactivity) measurements were performed. Additionally, the metal flux estimation was not applied as the sedimentation rate determination was not possible due to the gravel nature of the sediment samples. The trace metal and Mn results of core 2 are presented in correspondence with those of core 1.

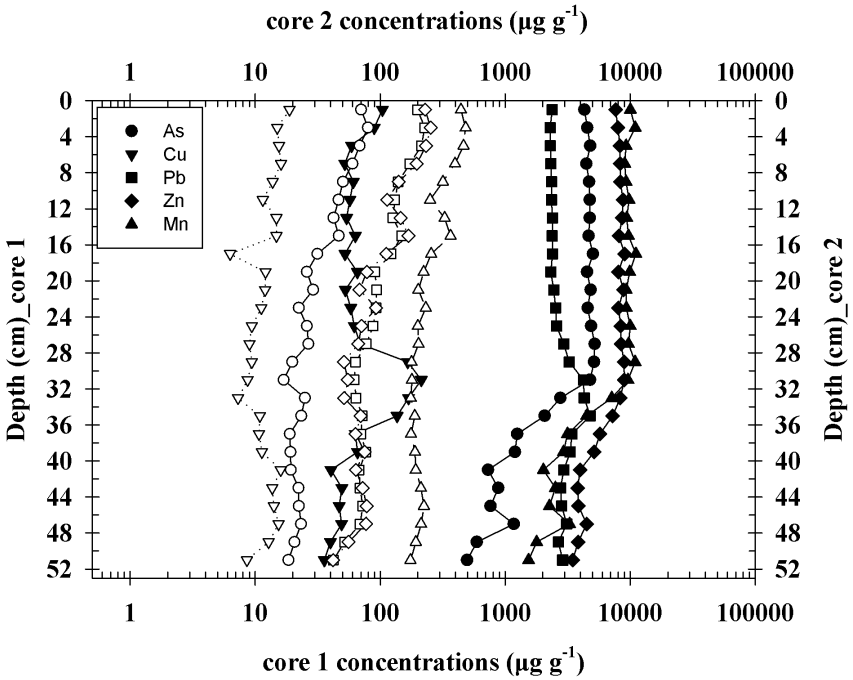

Fig. 5.20 The concentration profiles of trace metals (As, Cu, Pb, Zn) and Mn of the coastal core (core 1_black points) and the offshore core (core 2_white points).

The profiles of As, Cu, Pb, Zn and Mn at the offshore core exhibited values of (20-80) μg g^{-1}, (8-20) μg g^{-1}, (40-200) μg g^{-1}, (40-200) μg g^{-1}, (150-500) μg g^{-1}, respectively. Based on the measured concentrations, the core consists of two distinct parts: upper (0-18 cm) and lower (18-52 cm), wherein in the former part the values were up to 3 times higher than in the latter part. Additionally, comparing the concentrations of the offshore core with those of the coastal core, they were found to be up to 2 orders of magnitude lower, indicating an influenced area in a lesser extent due to past anthropogenic activities. All the other measured trace metals and major elements are presented in Annex VI.

5.2.4 Radioactivity and mass flux vertical distribution

Coastal core (core 1) results

According to radionuclide profiles the sediment core can be divided in three parts: the upper (0-28 cm), the middle (28-38 cm) and the lower (38-52 cm), as mentioned above. The activity concentrations of ^{226}Ra, ^{235}U, ^{228}Ac and ^{40}K exhibited values of (4-16) Bq kg^{-1}, (8-16) Bq kg^{-1}, (1.5-3.5) Bq kg^{-1} and (130-200) Bq kg^{-1}, respectively. At the upper part the values of ^{226}Ra and ^{228}Ac were found 2 times higher than those of the lower part, while in the middle part they increased linearly between these values. However, the profiles of ^{235}U and ^{40}K were homogeneous, within uncertainties, exhibiting mean values of 2.5 Bq kg^{-1} and 180 Bq kg^{-1}, respectively.

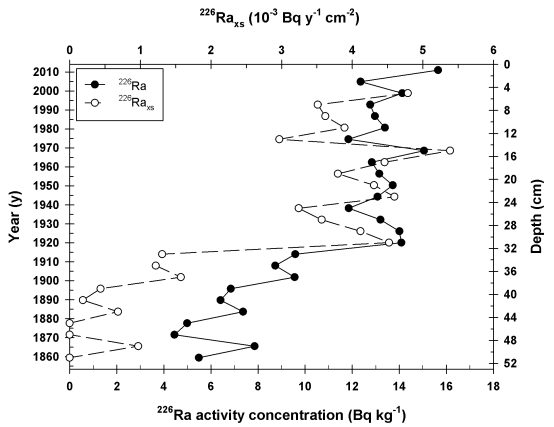

a) Excess metal flux ($^{226}Ra_{xs}$) and activity concentration of ^{226}Ra.

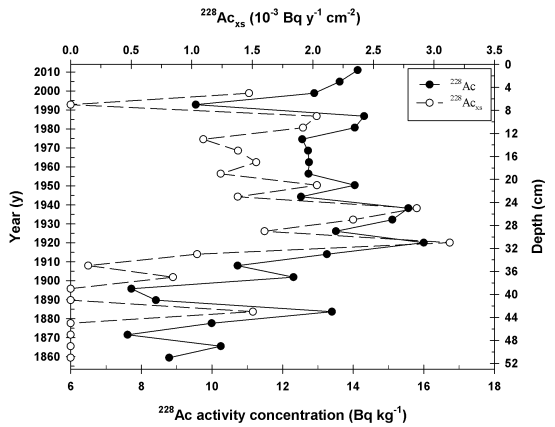

b) Excess metal flux ($^{228}Ac_{xs}$) and activity concentration of ^{228}Ac.

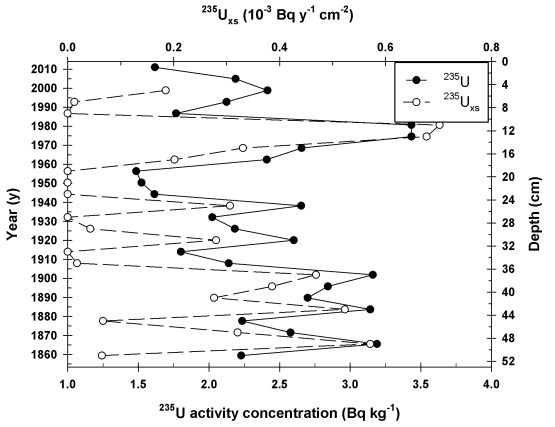

c) Excess metal flux ($^{235}U_{xs}$) and activity concentration of ^{235}U.

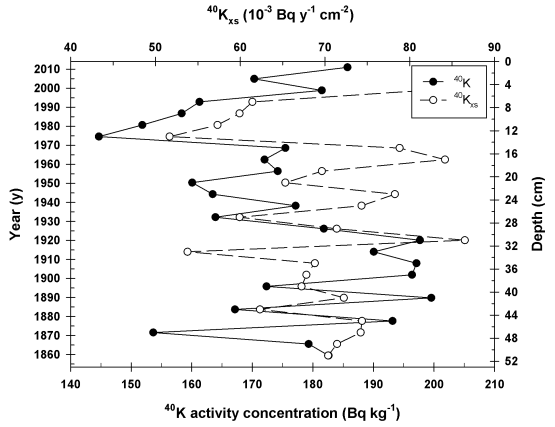

d) Excess metal flux ($^{40}K_{xs}$) and activity concentration of ^{40}K.

Fig. 5.21 The excess metal flux and activity concentrations of the long-lived radionuclides, as well as ^{228}Ac, assuming secular equilibrium with its parent nuclide.

The excess mass flux was also calculated for the long-lived natural radionuclides and their results are depicted above. Although ^{228}Ac is not a long-lived radionuclide, the mass flux estimation can be considered as ^{232}Th mass flux estimation, assuming secular equilibrium between them. The mass fluxes of $^{226}Ra_{xs}$, $^{228}Ac_{xs}$, $^{235}U_{xs}$ and $^{40}K_{xs}$ exhibited values of (0-5.5)·10^{-3} Bq y^{-1} cm^{-2}, (0-3)·10^{-3} Bq y^{-1} cm^{-2}, (0-0.7)·10^{-3} Bq y^{-1} cm^{-2} and (50-85)·10^{-3} Bq y^{-1} cm^{-2}, respectively. Similarly, as in metal mass flux profiles, the radionuclide mass flux profiles exhibited the same trend as the concentration profiles.

Offshore core (core 2) results

The excess mass fluxes of natural radionuclides were not determined for the offshore core, because the sedimentation rate models based on ^{210}Pb and ^{137}Cs were not applicable as mentioned in section 5.2.1. Despite the analysis of the low-statistics spectra, radionuclide profiles were not obtained due to activity concentration large discrepancies. Thus, the ranges of activity concentrations are given below, wherein

^{226}Ra, ^{235}U, ^{228}Ac and ^{40}K exhibited values of among detector's system MDA and 18 Bq kg^{-1}, 6.7 Bq kg^{-1}, 18 Bq kg^{-1} and 300 Bq kg^{-1}, respectively. The activity concentration of ^{137}Cs was below the detection system's MDA. These values were similar to the activity concentrations of the coastal core.

Table 13 The activity concentrations of natural radionuclides measured in the offshore core (core 2) of Lavrio offshore marine area.

		^{226}Ra	**^{228}Ac**	**^{235}U**	**^{40}K**
		(Bq kg^{-1})			
core 2	min	MDA	MDA	MDA	MDA
	max	18	18	6.7	300

5.2.5 Dose rate assessment

For the dose rate assessment, the maximum activity concentrations of ^{210}Pb, ^{226}Ra, ^{228}Th, ^{228}Ra, ^{235}U, ^{40}K and ^{137}Cs, measured in the surface sediment of Oxygono Bay, were utilized. The total dose rate was calculated, which can be divided into the internal and external fractions. Additionally, the total dose rate of each radionuclide per organism was determined and the results are shown below.

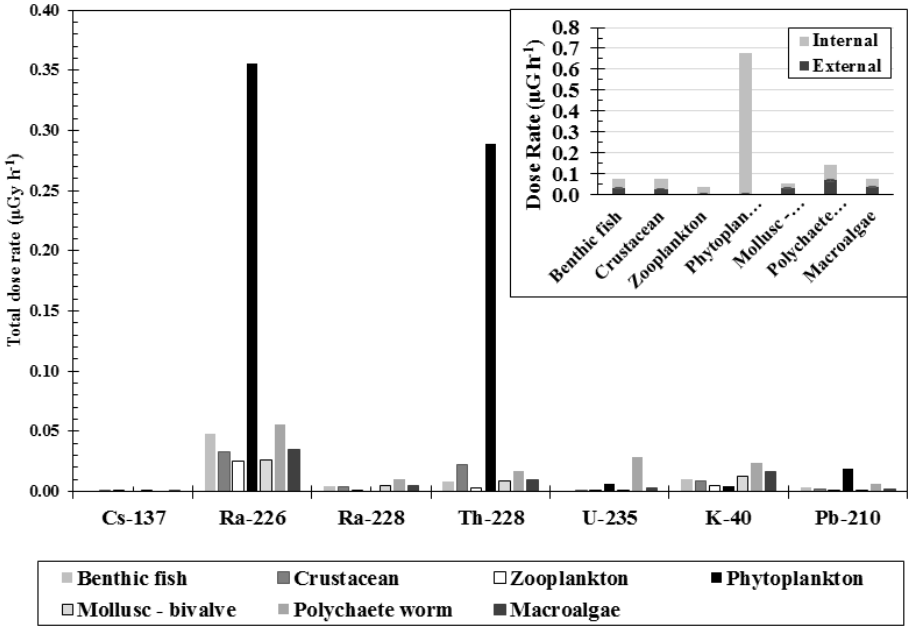

Fig. 5.22 Total, internal and external dose rates of marine biota based on the measured activity concentrations of natural and ^{137}Cs radionuclides in the seafloor sediment of Oxygono Bay.

The radiological risk was found to be negligible, as all the estimated dose rates were more than two orders of magnitude lower compared to the proposed screening levels for aquatic biota (400 µGy h^{-1}) (IAEA, 1992; UNSCEAR, 1996). Among the studied organisms, Phytoplankton received the maximum total dose rate (0.65µGyh^{-1}). The major contributor to the total dose rate was the internal fraction as discussed in section 5.3.1.5, while the external fraction contribution became noticeable for the habitants of the seafloor (e.g. crustacean, polychaete worm) due to sediment activity concentrations.

5.2.6 Grain size analysis

The vertical distribution of the grain size analysis was implemented to support the data interpretation. This analysis was conducted roughly determining the sand-mud or gravel-sand-mud portion. The spatial study regarding the grain size distribution (surface samples) was not performed since the grain size distribution results during the preliminary survey, as well as the surface samples of the coastal sediment core (core 1) revealed that the samples are characterized by highly sandy content. Additionally, all the samples collected in Oxygono Bay are close to the shore, not exceeding 150-m distance. Thus, the surface sediments were assumed to be sandy and the small differences of grain size distribution that may be observed among them are not the main contributor to the spatial distribution of radionuclide, trace metal and major element concentrations.

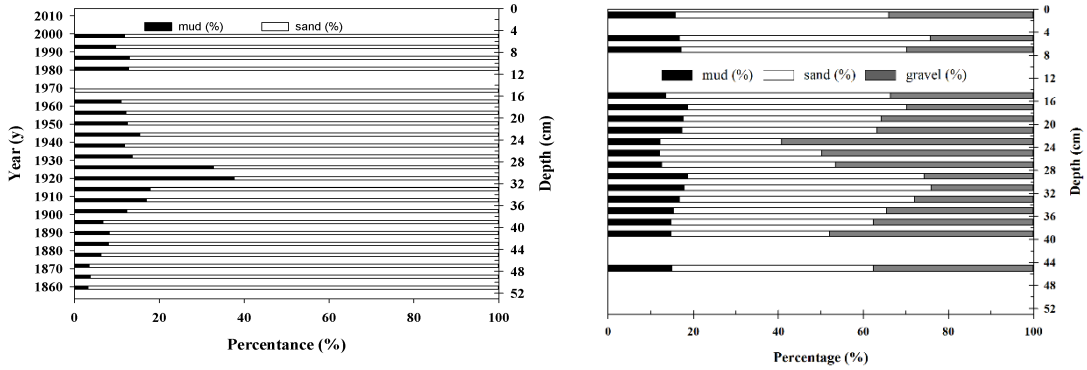

Fig. 5.23 Mud-sand-(gravel) vertical distribution of the core 1 coastal core (left) and the core 2 offshore core (right) at Oxygono Bay and Lavrio offshore area, respectively.

Both the coastal (core 1) and offshore (core 2) sediment cores were sliced per 2 cm and grain size distribution analysis was performed for each sample. According to Folk's classification (Folk, 1974) core 1 was characterized as muddy sand, while core 2 as muddy sandy gravel. The percentages of sand and mud in core 1 were 80-100% and 0-20%, respectively, while in core 2 the percentages of gravel, sand and mud ranged among 25-60%, 20-55% and 15-20%, respectively. Especially in core 1 a distinct area is observed in the middle part of the core, at 28-32 cm, wherein the mud portion reached 40%.

Chapter 6

Data interpretation

In this chapter the interpretation of the obtained results, using other processes such as the enrichment factor estimation and assessment, the reconstruction of past events, the statistical analysis and the comparison with previous data or neighbouring-area values or Mediterranean data will follow. The results will be interpreted according to the area of study, combining all measured parameters performed in this work.

6.1 Stratoni

The elaboration of results oriented to study the processes of potential contamination in a spatial and temporal basis. The spatial study, which is related to the area affected by the mining activities, was performed through the dispersion models, while the temporal study was implemented by using the vertical profiles of the measured data (radionuclides, trace metals, major elements and grain size distribution).

6.1.1 Estimated dispersion area

The dispersion of natural radionuclides was performed by ERICA Tool, which incorporates a generic transport model proposed by IAEA, as described in section 3.2.1. The measured activity concentrations of ^{226}Ra and ^{235}U in the surface seafloor sediments were utilized. The dispersion of these radionuclides was estimated, as their spatial distribution (see section 5.1.2) indicated an affinity with the occurring mining activities. The measured data of the preliminary study (in 2012) were used for the calibration of the generic model, while the experimental data of the main survey (in 2014) were utilized for the quality control of the model. In order to estimate the activity concentration in the (whole) surface of the affected area, without running the ERICA Tool, ArcGIS 10.2 software package® was applied for the interpolation of the ERICA estimated values. The simplified 1D transport model was implemented assuming a continuous point source release. This assumption approximates the discharged processes in Stratoni port, where the flotation tailings are discharged directly in the marine environment via a pipe. This type of wastes consists of a slurry mixture of finely ground solids and process water. The dispersion of the aforementioned radionuclides and the affected area estimation are depicted below, in Fig. 6.1.

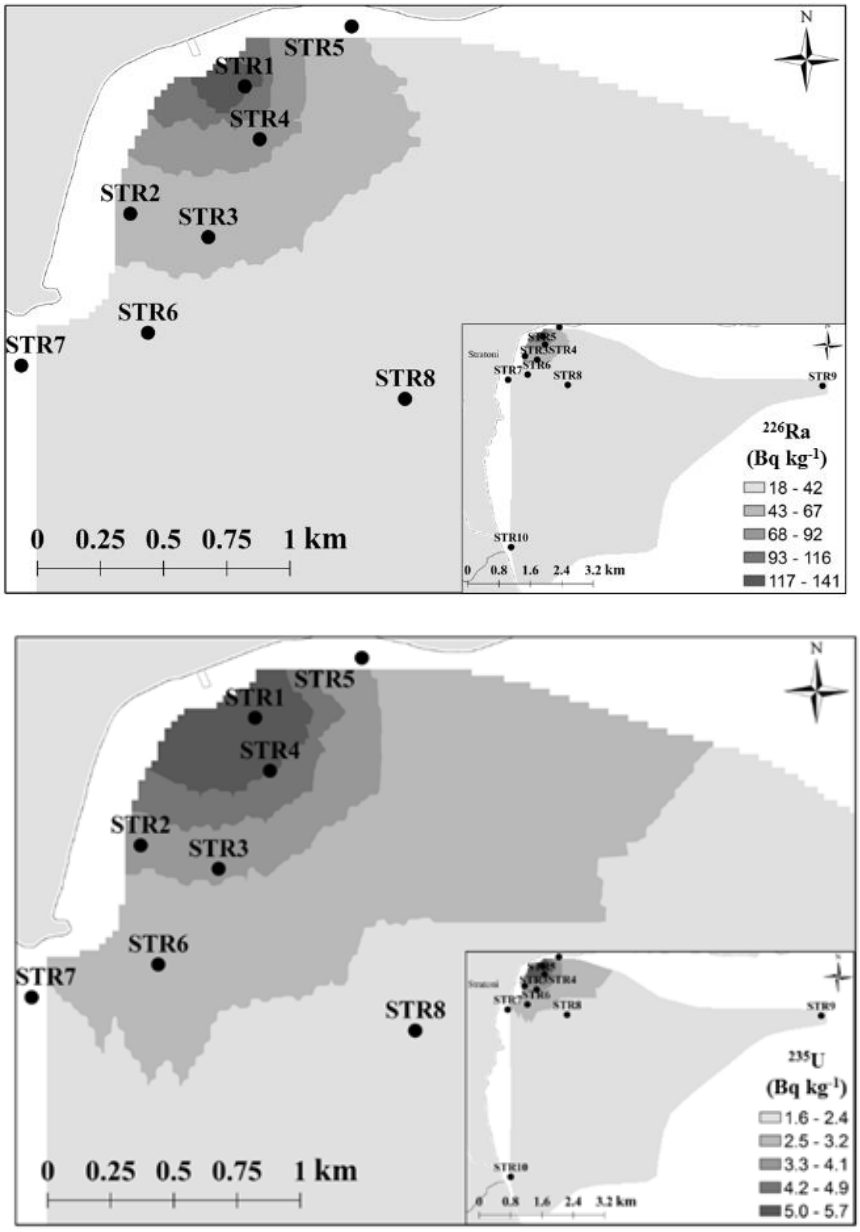

Fig. 6.1 The dispersion of ^{226}Ra (upper) and ^{235}U (lower), as well as the affected area of Ierissos Gulf due to mining activities (zoomed in figure).

The comparison between the estimated and measured activity concentrations of ^{226}Ra and ^{235}U, revealed a satisfactory agreement up to 27 % and 25%, respectively. Only in two sites (STR5 for ^{226}Ra and STR7 for ^{235}U) the measured data were not reproduced satisfactorily, wherein the estimated to measured differences exceeded 50%. This may be due to the different wind direction and current velocity values of these locations (STR5, STR7) compared to the recommended values. Especially, regarding the STR5 site, background activity concentrations were measured, indicating a negligible transfer material from the load out pier area due to the water current direction described in Chantzi (2012). However, ERICA Tool cannot reproduce this current direction as assumes an opposite one from the source (load out pier area) to the point of interest (STR5).

The model calibration using part of the experimental data provided discharge rates of 120 Bq s^{-1} and 14 Bq s^{-1} for ^{226}Ra and ^{235}U, respectively. The dispersion pattern also showed maximum activity concentrations near the load out pier area, for both radionuclides, which decreased with increasing distance. Furthermore, the shoreline values exhibited lower levels comparing with the center of Stratoni port. In the produced contours only the estimated data were utilized, thus the experimental data (e.g. STR5, STR7) are excluded. The background values, obtained at the far-located sites from the discharge point (e.g. STR9, STR10) were used for the estimation of the affected area (zoomed figures in Fig. 6.1). The affected area of both radionuclides has a semicircular pattern around the load out pier area, extended to the distant sampling points (STR9, STR10) but not to the shoreline. The negligible impact to the shoreline sampling points was verified by the low measured values at Kalatzi Lakkos (STR11) and Ierissos port (STR12). Thus, the north part of Ierissos Gulf has been affected, extending at 21 km^2. The dispersion model revealed that the affected area due to mining activities is the north part of Ierissos Gulf and reached up to the middle of the gulf. Thus, the south part of the gulf is unaffected and Ierissos city can be considered a safe region for inhabiting, tourism and fishing.

6.1.2 Comparison between 2012 and 2014 sampling surveys

The radionuclide concentrations of ^{226}Ra and ^{235}U of the preliminary survey in 2012 (Pappa et al., 2016) are depicted in the same graph - below - with those of the main survey in 2014 (present work). During the preliminary survey only the seafloor of Ierissos Gulf was studied, thus the depicted concentrations refer to the surface marine samples for the same locations. The only exception is the sample representing the load out pier area (STR1), which was not located in the same sampling point in the two surveys.

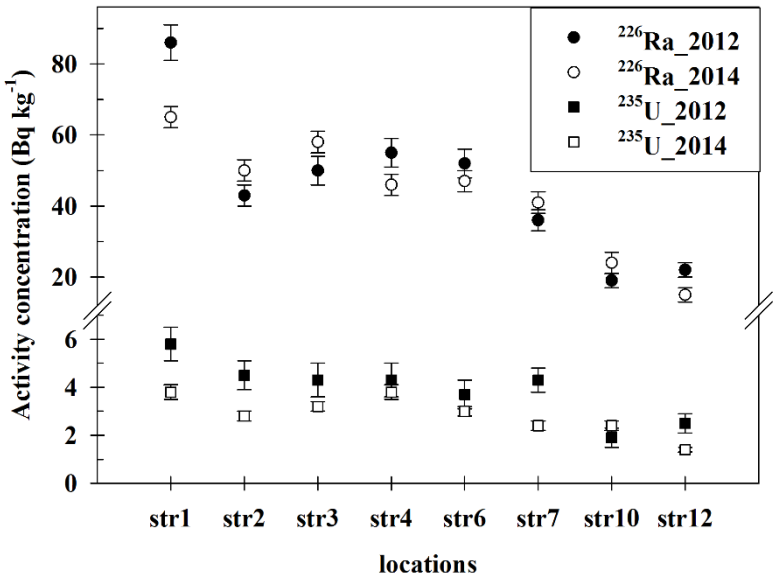

Fig. 6.2 The activity concentrations of ^{226}Ra and ^{235}U measured in the seafloor sediments of Ierissos Gulf.

Generally, the spatial distribution of the two surveys is similar, exhibiting maximum values near the load out pier and decreasing with increasing distance. Additionally, the activity concentrations are also similar, with the exception of STR1

point due to the different locations. Therefore, an almost constant situation can be observed in the seafloor status within the two sampling years. This observation is also verified by the top 2 cm of the coastal core (STR1) radionuclide profiles, wherein the concentrations are similar within uncertainties. In some cases (STR2, STR3, STR10) ^{226}Ra concentrations of 2014 survey are higher than those of 2012 survey, in contrast to the other sampling points. These "reversal concentrations" may be attributed to the water current direction in the area of these sampling points, as these sites are near the coast, meaning not deep enough and are affected by the currents and the wave height or the river discharges (STR10). Additionally, the observed differences of the uncertainties the activity concentrations between the two surveys are attributed to the detection system. The activity concentrations of 2012 were obtained via a HPGe of 50% relative efficiency, while those of 2014 were measured by a HPGe of 100% relative efficiency. Thus, the latter has lower values of uncertainty due to statistics.

6.1.3 Incidences identification with historical data

During 1908 to 1970 (core's lower part 12-27 cm) the maximum concentrations of natural radionuclides (^{226}Ra, ^{235}U, ^{40}K), trace metals (Cu, Pb, Zn) and major elements (Al, Fe) were observed. This period represents the industrial activity in the area, meaning the exploitation of mixed sulfide - manganese ores, held mainly by the Hellenic Chemical Products and Fertilizers Company (AEEHPL). The exploited ores included pyrite (FeS_2), sphalerite (ZnS) and galena (PbS), known as P.B.G. Taking into account the excess mass flux profiles of Fe (Fe_{xs}), As (As_{xs}), Zn (Zn_{xs}) and ^{226}Ra ($^{226}Ra_{xs}$), five operational periods were observed: a) 1912-1920, b) 1920-1935, c) 1935-1945, d) 1950-1970 and e) 1983-2014. The flux vertical distributions incorporating the dating model resolved efficiently the plant operation periods. However, the historical reconstruction of plant operational periods, could not be achieved solely by the metal concentration profiles.

AEEHPL Company bought Kasandra mines in 1912, so as to exploit pyrite (FeS_2) of Madem Lakkos deposit and produce sulfuric acid. Almost simultaneously, during 1920-1935, began the exploitation of P.B.G. ores. This process is depicted in the increment of Fe and As concentrations and mass fluxes, during this period, indicating a pyrite (FeS_2) and arsenopyrite (FeAsS) waste disposals. The pyrite disposal is attributed to the efficiency of the used ore-separation method, while the arsenopyrite disposal indicates a presence of this ore in the form of secondary mineral in P.B.G. ores, which was characterized by low percentage of As. The similar chemical characteristics of arsenopyrite as those of pyrite, resulted in its disposal during the separation method. During the same period (1920-1935) an increment was observed in Cu and Pb mass flux profiles, indicating the low efficiency of the ore separation, either included in the pyrite wastes or/and the P.B.G. wastes. For the same period Mn concentrations and mass fluxes exhibited low values, attributed to exploitation of pure P.B.G. ores free from impurities such as rhodochrosite ($MnCO_3$). Additionally, the elevated concentrations and mass fluxes of ^{226}Ra, during 1920-1935 have a similar trend as Fe and As. These elevated values may be correlated to Stratoni's granitoids hosting the P.B.G. ores, which consist of secondary uranium minerals (Persianis et al., 2010; Papadopoulos et al., 2013).

In the concentration and mass flux profiles of As, Fe, Zn and ^{226}Ra – and other metals - a local minimum is obtained during 1935-1945 reflecting the impact of the Second World War to mining activities. The further increment of As during 1950-1970 may be attributed to the alteration of the flotation method in order to achieve higher efficiency of P.B.G. recovery or to the exploitation of P.B.G. minerals with higher As percentage. During this period AEEHPL company abandoned the production of sulfuric acid based on FeS_2, thus the flotation method was altered. This is the reason for the observed local maximum of Fe, not as high as during 1920-1935. Moreover, the high levels of Fe in mass flux profile during 1950-1970, may be attributed to the exploitation of Mavres Petres deposit, instead of Madem Lakkos. The former is characterized by P.B.G. minerals with lower Fe percentage comparing to the latter. For the same period the lower values of ^{226}Ra concentration and mass fluxes, may reflect the different location of the P.B.G. minerals, further away from the granitoids, comparing to the P.B.G. location of 1920-1935 period.

The observed decrement of As during 1970-1975 may be attributed to the fact that arsenopyrite enriched in As was not disposed in the marine environment. This type of arsenopyrite, after its separation from the P.B.G. ores, was sent at Olymbiada's newly-built flotation plant for further exploitation, as the percentage of Au being hosted in it was significant. Therefore, the remaining arsenopyrite wastes at Stratoni's flotation plant consisted of low percentages of As. During 1983-2014, the lowest values were observed in all concentration and mass flux profiles (except from those of Mn). The minimum values represent the cessation of tailing discharge into the marine environment (Kelepertzis, 2013). Additionally, Al concentrations and mass fluxes were decreased form 1920 until 1970, which may reflect the location of the exploited P.B.G. ores. In the period between 1920 and 1935 the ore location was close to granitoids and pegmatite veins, characterized by high Al concentrations, whereas later (1950-1970) their location was further away from the pegmatite veins. The maximum values of Mn concentration and mass flux, observed during 1983-2014 show the transport processes in the coastal environment. The presence of this element in Kassandra deposits is in the form of rhodochrosite ($MnCO_3$), a light mineral which can be easily transported in the coastal environment due to the wave movements. The different type of tailing discharges can be shown by the mud content of the sediment core (core 1), where after 1965 reaches its maximum value (up to 40%).

The applied method by combining the dating models with the mass flux vertical distribution reconstructed the mine operation periods from 1908-2014. The main identified processes and periods were: the exploitation of pyrite for the production of sulfuric acid during 1912-1920, the decrease of mining activity during 1935-1945 due to the Second World War, the alteration of the exploited ores due to the type of ore exploitation and the construction and operation of Olymbiada's flotation plant during 1950-1970; and finally the end of tailing discharging into the marine environment during 1980-2010.

6.1.4 Enrichment factor and Pollution Load Index

Spatial data interpretation

The enrichment factor (EF) was estimated for the surface samples using as reference Ierissos port seafloor sampling point (STR12) and Al as normalizer.

Additionally, in this work, all the major element and the majority of trace metals showed variations in the sediment cores and surface samples. Thus, for the selection of the proper normalizing element was adopted the methodology described by Karageorgis et al. (2009). Based on this methodology Al was selected as normalizing element, as it showed the minimum coefficient of variation (V). In order to verify that Ierissos port seafloor is a pristine area and can be used as reference site, the EF of this sampling point was estimated utilizing the concentrations of the shale of the continental crust (Mn: 850 μg g^{-1}, As: 13 μg g^{-1}, Cu: 45 μg g^{-1}, Pb: 20 μg g^{-1}, Zn: 95) (Wedepohl, 1995). The EF estimation of Ierissos port revealed a pristine region with no enrichment (the EF values exhibited values of Mn: 0.2, As: 1.3, Cu: 0.2, Pb: 0.1, Zn: 0.1). The used colors depicted in the following graph, Fig. 6.3, represent the enrichment classification (Birch & Davies, 2003), where light green refers to no enrichment (EF≤ 1), green refers to moderate enrichment (1<EF≤3), blue refers to moderately severe enrichment (3<EF≤5), purple refers to moderately severe enrichment (5<EF≤10), yellow refers to severe enrichment (10<EF≤25), orange refers to very severe enrichment (25<EF≤50) and red refers to extremely severe enrichment (EF>50).

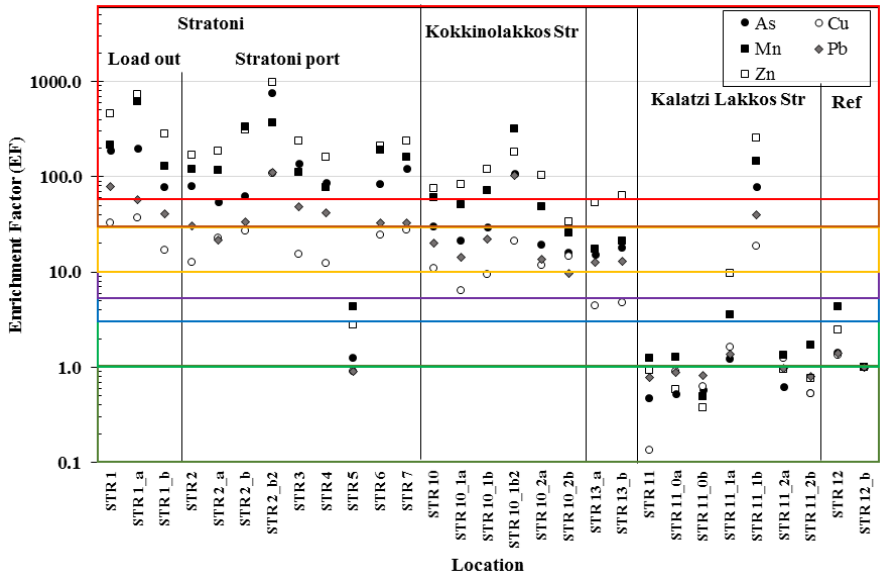

Fig. 6.3 The spatial distribution of Enrichment Factors (EFs) of As, Cu, Zn, Pb and Mn. The element of Al was used as conservative element for the estimation of EFs, as well, as the elemental concentrations of Ierissos port seafloor was utilized as reference. The light green color represents no enrichment, the green color minor enrichment, the blue moderate enrichment, the purple moderately severe enrichment, the yellow severe enrichment, the orange very severe enrichment, and the red extremely severe enrichment.

The EFs were estimated using trace metal, Mn and Al concentrations, characteristic of the study area. According to the estimated EFs, the sampling areas can be divided into different enrichment classes among extremely severe and no enrichment depending strongly on the sampling locations. It is evident that the most contaminated area is Stratoni (both marine and terrestrial parts) in Zn As and Mn, especially the load out pier area and the beach sand (STR2_b2). Even if Zn and As are trace metals, and Mn is a major element, it exhibits lower enrichment compared to Zn and As. This reveals that the disposed wastes characterizing both environments (marine and terrestrial) are due to the processed ores (e.g. P.B.G. rich in Zn followed by arsenopyrite (As)). This is also verified by the very severe enrichment in Pb at Stratoni

(another metal rich in P.B.G. ores). The different type of enrichment in Kokkinolakkos Stream e.g. extremely severe enrichment in Zn/Mn and very severe enrichment in As, may be attributed to the different metal concentrations of the disposed wastes. Kalatzi Lakkos Stream can be considered as unaffected by mining activities as exhibited minor or/and no enrichment, except from one sampling point (STR11_1b). The extremely severe enrichment of STR11_1b may be correlated with the presence of elevated values of Fe and S in this sample. As far as Cu enrichment is concerned, Stratoni and Kokkinolakkos Stream were severely enriched, while Kalatzi Lakkos and Ierissos port beach sand consisted of background levels. To summarize, the order of metal enrichment into the sediment was found to be Zn>As>Mn>Pb>Cu.

Data interpretation for STR1 (coastal) core

The enrichment factor of trace metals (As, Cu, Pb, Zn) and Mn were estimated for the coastal core (STR1). The concentration of Al was also measured only for the deepest slice of the offshore core, as it was utilized as reference sample in the enrichment factor estimation. More adequate for the estimation of the EF index are the deepest layers of an unaffected sediment core (e.g. offshore). However, as a feasibility study was estimated the EF of the background sample based on the concentrations of the continental crust. This approach is proposed not only for the verification of the correct selection of the background sample but also for providing EFs that can be compared in a global scale. Thus, the concentrations of the shale of the continental crust were also used in the EF estimated profiles. The EF estimations based on the deepest slice of STR8 core or the continental shale are depicted below, in Fig. 6.4, where colors were applied in the graph so as to describe the enrichment classification.

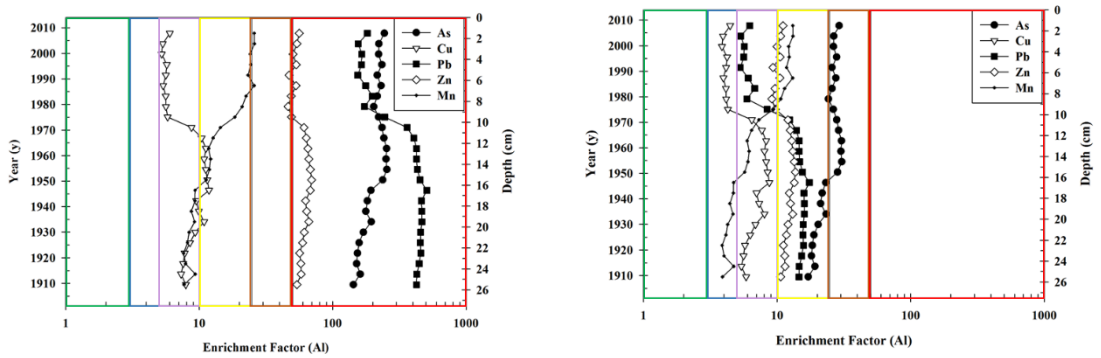

Fig. 6.4 The Enrichment Factor (EF) profiles of As, Cu, Zn, Pb and Mn. The element of Al was used for the estimation of EFs as conservative element, as well as the elemental concentrations of the shale of the continental crust (Wedepohl, 1995) (left) and of the deep pre-mine layer of STR8 core (right). The light green color represents no enrichment, the green color minor enrichment, the blue moderate enrichment, the purple moderately severe enrichment, the yellow severe enrichment, the orange very severe enrichment, and the red extremely severe enrichment.

Using the continental concentrations reference, the whole sediment core (STR1) was characterized as extremely severely enriched (EF>50) in As, Pb and Zn utilizing Birch and Davies (2003) classification. The enrichment of core's upper part (0-11cm) was found severe and moderately severe for Mn and Cu, respectively. In the lower part (12-27 cm) the enrichment was mainly moderately severe for both metals. Based on the concentrations measured in the deep pre-mine layer of STR8 core the enrichment

of STR1 core was found to be moderate, moderately severe, severe and very severe for Cu, Pb, Zn and Mn/As, respectively. In the lower part of the core the enrichment was characterized as moderate, moderately severe and severe for Mn, Cu and As/Pb/Zn, respectively. The order of the metal enrichment into the sediment using the shale as reference was Pb>As>Zn>Mn>Cu, while this order changed utilizing the STR8 deepest slice as reference to As>Zn≥Pb>Mn>Cu. Nevertheless, the classification remained almost the same for Cu and Mn with slight changes. For example the sediment core was characterized as moderately severely enriched in Cu when using the shale values, while it was characterized as moderately enriched in Cu when utilizing STR8 values. On the other hand the classification of As, Zn and Pb in the sediment core altered significantly. This difference in the classification indicate that the use of global continental crust data might not be representative for the area of study, as it represents a rough estimation and it should be used with caution and only for comparison reasons in global aspect. However, for the future a deeper layer of a more distant offshore sample could be utilized to verify the EF classification of this work, based on the ecosystem background.

Data interpretation for STR8 (offshore) core

As discussed in the result section (5.1.3) the upper part of the core may have been influenced by anthropogenic activities, however in a lesser extend as the trace metal and Mn profiles exhibited values 2 orders of magnitude lower than STR1 core. Therefore, in order to study the depth of contamination in the offshore core, a simplified index, Pollution Load Index (PLI) was determined. This index takes into account the concentrations of the metals of interest, each one normalized to the concentrations of a reference site, though it does not exclude the grain size effect. In this work, as reference sample was utilized the deepest slice of STR8 core. PLI was also applied in the STR1 (coastal) core, in order to compare the pollution in the offshore and coastal part, taking into account a conservative approach, wherein only the trace metals and Mn with highest observed concentrations were included. The results are presented in Fig. 6.5.

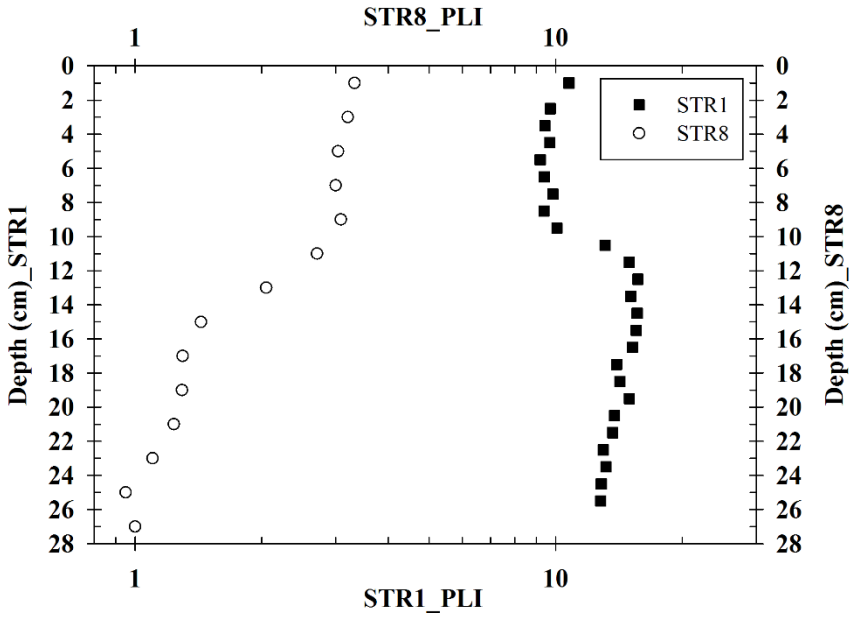

Fig. 6.5 The PLI estimation for the coastal (STR1) core and the offshore (STR8) core at Ierissos Gulf.

According to Tomlinson et al. (1980) all PLI values above 1 indicate a progressive deterioration in the area, which is the case for the whole length of both cores. However, as mentioned above the PLI estimation in this work was performed conservatively, taking into account that the lower part of STR8 core (14-27 cm) having PLI less than 2 can be considered not affected by the mining activities and is characterized by background levels. This assumption is demonstrated by the one order of magnitude lower PLI values of STR8 core comparing with STR1 core. The upper part of the core was indeed affected by anthropogenic activities as PLI exhibited a value of 4. To summarize PLI was a simplified, conservative and useful parameter so as to identify the contamination in the offshore core and estimate the depth of the contamination.

6.1.5 Statistical analysis

Spatial statistical analysis

In the present study potential statistical associations of natural radionuclides with major elements, trace metals and LOI (Loss of Ignition) were investigated. LOI is a meter of the organic content in the samples. The associations were estimated for all the surface sediments (marine and terrestrial) in order to investigate their current behavior and to obtain a significant number of samples for the statistical analysis. The statistical analysis was performed via the Spearman's rank-order (r_s) association due to significant difference from a normal distribution. For this purpose, the IBM SPSS Statistics v. 20 software package was used. The results are depicted in Table 14 and can be organized in five main groups: (a) ^{226}Ra and ^{235}U were found significantly (0.57-0.83) and moderately (0.38-0.55) positively associated with trace metals and major elements (except from Al), respectively (b) ^{228}Ac was moderately (0.44-0.53) positively associated with ^{226}Ra, ^{235}U and Al, (c) ^{40}K was significantly (0.63) positively associated with Al and moderately (0.41-0.63) negatively associated with trace metals, (d) trace metals are strongly (0.71-0.95) associated with each other, as well as with major elements and (e) Al is significantly (0.52- 0.69) non associated with trace metals and other major elements, while it was moderately and significantly (0.44-0.63) positively associated with ^{228}Ac and ^{40}K, respectively.

Group 'a' indicates the presence of radionuclides in the wastes of the P.B.G ore separation. Generally, P.B.G. ores do not contain natural radionuclides but As, Pb, Zn, Fe and S. Nevertheless they are surrounded by granitoids, which are not exploited economically (gangue) and are characterized by secondary uranium minerals. Other gangue minerals near the P.B.G. ore is rhodochrosite ($MnCO_3$), while secondary minerals such as chalcopyrite ($CuFeS_2$) are also present. Thus, the wastes of P.B.G. ore separation consist of gangue material and therefore ^{226}Ra, ^{235}U, as well as trace metals (As, Cu, Pb, Zn) and major elements (Fe, S) due to the efficiency of the method, which separates the secondary and gangue minerals. The latter explains the positive association among trace metals and major elements observed in the surface sediments (group 'd'). According to groups 'b', 'c' and 'e', it is evident that the spatial distribution of ^{228}Ac and ^{40}K is associated with Al. The negative association of Al with the wastes of the exploited ores, may indicate the absence of pegmatites (rich in K due to minerals like feldspars) in the disposed wastes in the surface of Ierissos Gulf and thus the homogeneous spatial distributions of Al and ^{228}Ac represent the mineralogy of the

study area. The non-homogeneous distribution of ^{40}K may be attributed to the different pegmatite composition between Stratoni and Ierissos regions but may also indicate dilution effects in the Stratoni port. LOI was moderate to significant positively associated with ^{226}Ra, ^{235}U, trace metals and major elements (except from Al) revealing an organic content in the samples, which partially contributes to the spatial distribution of the aforementioned elements.

Table 14 The results of statistical association (Spearman's rho (r_s)) among radionuclides, trace metals, major elements and LOI (Loss of Ignition) of the surface sediments (N=31) of Ierissos Gulf.

		^{226}Ra	**^{228}Ac**	**^{235}U**	**^{40}K**	**As**	**Cu**	**Pb**	**Zn**	**Mn**	**Fe**	**Al**	**S**	**LOI**
^{226}Ra	rs	1.000	,487**	,767**	-.090	,646**	,574**	,656**	,640**	,611**	,578**	-.273	,832**	,493**
	Sig.		.006	.000	.629	.000	.001	.000	.000	.000	.001	.152	.000	.008
^{228}Ac	rs	,487**	1.000	,527**	.186	.041	.137	.112	.038	.096	.218	,443*	-.147	.123
	Sig.	.006		.002	.316	.829	.469	.555	.840	.613	.257	.016	.514	.532
^{235}U	rs	,767**	,527**	1.000	.036	,402*	,441*	,414*	,421*	.349	,388*	-.117	,546**	,540**
	Sig.	.000	.002		.849	.028	.015	.023	.021	.059	.038	.545	.009	.003
^{40}K	rs	-.090	.186	.036	1.000	-,489**	-,489**	-,429*	-,405*	-,479**	-,630**	,634**	-.071	-.270
	Sig.	.629	.316	.849		.006	.006	.018	.026	.007	.000	.000	.755	.164
As	rs	,646**	.041	,402*	-,489**	1.000	,867**	,944**	,941**	,928**	,907**	-,678**	,867**	,671**
	Sig.	.000	.829	.028	.006		.000	.000	.000	.000	.000	.000	.000	.000
Cu	rs	,574**	.137	,441*	-,489**	,867**	1.000	,816**	,878**	,887**	,870**	-,580**	,718**	,684**
	Sig.	.001	.469	.015	.006	.000		.000	.000	.000	.000	.001	.000	.000
Pb	rs	,656**	.112	,414*	-,429*	,944**	,816**	1.000	,895**	,892**	,866**	-,595**	,730**	,571**
	Sig.	.000	.555	.023	.018	.000	.000		.000	.000	.000	.001	.000	.002
Zn	rs	,640**	.038	,421*	-,405*	,941**	,878**	,895**	1.000	,952**	,828**	-,674**	,884**	,657**
	Sig.	.000	.840	.021	.026	.000	.000	.000		.000	.000	.000	.000	.000
Mn	rs	,611**	.096	.349	-,479**	,928**	,887**	,892**	,952**	1.000	,855**	-,687**	,787**	,603**
	Sig.	.000	.613	.059	.007	.000	.000	.000	.000		.000	.000	.000	.001
Fe	rs	,578**	.218	,388*	-,630**	,907**	,870**	,866**	,828**	,855**	1.000	-,521**	,612**	,640**
	Sig.	.001	.257	.038	.000	.000	.000	.000	.000	.000		.004	.002	.000
Al	rs	-.273	,443*	-.117	,634**	-,678**	-,580**	-,595**	-,674**	-,687**	-,521**	1.000	-,685**	-.369
	Sig.	.152	.016	.545	.000	.000	.001	.001	.000	.000	.004		.000	.053
S	rs	,832**	-.147	,546**	-.071	,867**	,718**	,730**	,884**	,787**	,612**	-,685**	1.000	,498*
	Sig.	.000	.514	.009	.755	.000	.000	.000	.000	.000	.002	.000		.022
LOI	rs	,493**	.123	,540**	-.270	,671**	,684**	,571**	,657**	,603**	,640**	-.369	,498*	1.000
	Sig.	.008	.532	.003	.164	.000	.000	.002	.000	.001	.000	.053	.022	

* Spearman association is significant at the 0.05 level (2-tailed) **. Spearman association is significant at the 0.01 level (2-tailed).

Statistical analysis for STR1 (coastal) core

The statistical analysis was also performed via the Spearman's rank-order (r_s) association for the radionuclide, trace metal, major element, sand-mud percentage and LOI. Despite the discrete areas observed in the coastal core (upper and lower part) the whole core was utilized in statistical analysis to obtain a significant number of samples. The statistical analysis was performed for ^{228}Ac, but no significant associations were obtained with the aforementioned parameters and thus it was not included in the following table. Three main groups can be distinguished: (a) natural radionuclides (^{226}Ra, ^{235}U, ^{40}K) which were significantly (0.50-0.70) positively associated with Cu, Zn, Fe and strongly (0.62- 0.93) associated with Pb, Al and sand fraction, (b) trace

metals (Cu, Pb, Zn) were strongly (0.61-0.92) positively associated with each other, as well as Fe, Al and sand portion and (c) Mn which was very strongly (0.64-0.93) negatively associated with trace metals (Cu, Pb, Zn), major elements, and sand fraction, while it was found to be significantly positively associated with mud fraction.

Table 15 The results of statistical association (Spearman's rho (rs)) among radionuclides, trace metals, major elements, LOI (Loss of Ignition) and sand-mud percentage of the coastal sediment core (STR1) (N=27) of Ierissos Gulf.

		^{226}Ra	**^{235}U**	**^{40}K**	**As**	**Cu**	**Pb**	**Zn**	**Mn**	**Fe**	**Al**	**LOI**	**sand**	**mud**
^{226}Ra	r_s	1.000	,717**	,925**	-.078	,622**	,858**	,672**	-,899**	,519**	,925**	.386	,702**	-,694**
	Sig.		.000	.000	.712	.001	.000	.000	.000	.008	.000	.057	.000	.000
^{235}U	r_s	,717**	1.000	,678**	.294	,698**	,696**	,758**	-,665**	,602**	,620**	,585**	,674**	-,663**
	Sig.	.000		.000	.154	.000	.000	.000	.000	.001	.001	.002	.000	.000
^{40}K	r_s	,925**	,678**	1.000	-.065	,560**	,810**	,671**	-,863**	,499*	,877**	,400*	,736**	-,724**
	Sig.	.000	.000		.756	.004	.000	.000	.000	.011	.000	.048	.000	.000
As	r_s	-.078	.294	-.065	1.000	,591**	.008	,524**	.153	,612**	-.137	,399*	-.067	.079
	Sig.	.712	.154	.756		.002	.968	.007	.465	.001	.514	.048	.756	.713
Cu	r_s	,622**	,698**	,560**	,591**	1.000	,728**	,916**	-,636**	,899**	,624**	,623**	,429*	-,422*
	Sig.	.001	.000	.004	.002		.000	.000	.001	.000	.001	.001	.037	.040
Pb	r_s	,858**	,696**	,810**	.008	,728**	1.000	,782**	-,926**	,655**	,912**	,566**	,684**	-,675**
	Sig.	.000	.000	.000	.968	.000		.000	.000	.000	.000	.003	.000	.000
Zn	r_s	,672**	,758**	,671**	,524**	,916**	,782**	1.000	-,647**	,832**	,665**	,664**	,547**	-,535**
	Sig.	.000	.000	.000	.007	.000	.000		.000	.000	.000	.000	.006	.007
Mn	r_s	-,899**	-,665**	-,863**	.153	-,636**	-,926**	-,647**	1.000	-,573**	-,942**	-,475*	-,670**	,662**
	Sig.	.000	.000	.000	.465	.001	.000	.000		.003	.000	.016	.000	.000
Fe	r_s	,519**	,602**	,499*	,612**	,899**	,655**	,832**	-,573**	1.000	,547**	,568**	.361	-.351
	Sig.	.008	.001	.011	.001	.000	.000	.000	.003		.005	.003	.083	.093
Al	r_s	,925**	,620**	,877**	-.137	,624**	,912**	,665**	-,942**	,547**	1.000	.373	,647**	-,640**
	Sig.	.000	.001	.000	.514	.001	.000	.000	.000	.005		.066	.001	.001
LOI	r_s	.386	,585**	,400*	,399*	,623**	,566**	,664**	-,475*	,568**	.373	1.000	.241	-.224
	Sig.	.057	.002	.048	.048	.001	.003	.000	.016	.003	.066		.258	.294
sand	r_s	,702**	,674**	,736**	-.067	,429*	,684**	,547**	-,670**	.361	,647**	.241	1.000	-,999**
	Sig.	.000	.000	.000	.756	.037	.000	.006	.000	.083	.001	.258		.000
mud	r_s	-,694**	-,663**	-,724**	.079	-,422*	-,675**	-,535**	,662**	-.351	-,640**	-.224	-,999**	1.000
	Sig.	.000	.000	.000	.713	.040	.000	.007	.000	.093	.001	.294	.000	

* Spearman association is significant at the 0.05 level (2-tailed) **. Spearman association is significant at the 0.01 level (2-tailed).

Group ‘a’ indicates that the wastes disposed in the marine environment of Stratoni port consisted of granitoids and pegmatites, characterized by uranium and K minerals (e.g. feldspars), respectively. These gangue materials (granitoids and pegmatites) were located near the exploited P.B.G. ores and during separation they were disposed along with small amounts of the ore itself, thus radionuclides included in gangue minerals were associated with Cu, Pb, Zn, Fe included in P.B.G. ores. The efficiency of the separation method is also the main contributor of the high trace metal and major element concentrations, as well as for their positive association (group ‘b’). Additionally, the obtained positive association of sand with natural radionuclides, trace metals and major elements (except from Mn), reveals that these elements were adsorbed into the sandy portion of the slurry mixture waste, which was discharged through a pipeline in the marine environment. Lastly, the negative association of Mn with the aforementioned parameters, indicate a waste disposal pure from P.B.G. ores or granitoids and pegmatites and/or an additional process transferring these wastes (e.g.

waves). This can be explained by the fact that Mn is present in the Stratoni area in the form of rhodochrosite ($MnCO_3$) mineral located near the P.B.G. ores, which when disposed in the marine environment transfers by the sea currents, as Mn is a light element. The positive association of Mn with mud fraction, verifies this assumption. LOI was weakly to moderately positively associated with radionuclides, trace metals and major elements (Fe, Al) (0.40-0.66), while it was weakly negatively (0.48) associated with Mn, indicating an organic content in the P.B.G. ores, granitoids and pegmatites and not in rhodochrosite ($MnCO_3$). The organic content is a low contributor to the obtained radionuclide, minor element and major element concentrations.

6.1.6 Seawater

The mandatory limits provided by the Greek legislation (OGG, 2009), presented in Table 5, refer to the deposition of water in the aquatic environment either for water supply uses or for swimming purposes. The heavy metal concentrations (Cu, Pb, Zn, Ni, Cd) obtained in the seawater sampling points were well below these mandatory limits. Additionally, the concentrations of Cd and Ni in the seawater were well below the Environmental Quality Standards (EQS) recommended values proposed by the European Directive 2013/39/EU. However, the water concentrations of Pb at the sites STR4, STR1 (load out pier area) and STR3 were in the same level, 5 and 17 times higher than the EQS values, respectively. In all the other water sampling points, the concentration of Pb was well below the EQS thresholds. According to Paraskevopoulou et al., 2014 the risk to observe toxic effects in the organisms is high only when the metal concentrations exceed the EQS values.

6.2 Lavrio

The elaboration of results will be realized spatially and temporally, as described in the title of each subsection. The temporal elaboration will contain the time aspect using the vertical profiles of the measured data (radionuclides, trace metals, major elements and grain size distribution).

6.2.1 Estimated dispersion area

Oxygono Bay is a shallow system characterized by small surface and open mouth. The collected sampling points of Oxygono Bay are located in a special grid to cover the surface till a mean depth of 10 m. Thus, the spatial interpolation was performed in Oxygono Bay area via the empirical Bayesian Kriging (Gribov and Krivoruchko 2012) method in ArcGIS 10.2 software®, utilizing the data of the surface marine sediments during the preliminary and main surveys (2014 and 2016 sampling) and the surface sample of the coastal core (core 1). The activity concentration of natural radionuclides in Oxygono Bay revealed low radioactivity values with homogeneous spatial distribution (e.g. ^{228}Ac, ^{235}U) except from ^{226}Ra. The produced interpolated spatial distribution (see Fig. 6.6), can be considered only as an indicative picture due to the limited number of data – seven points. Three distinctive regions can be observed (a) near N5 and core 1 surface samples, (b) at the north part of Oxygono bay and (c) at the south part of the bay.

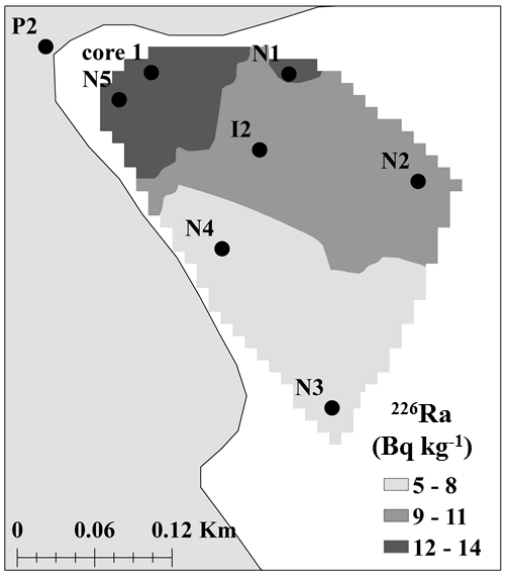

Fig. 6.6 The interpolated spatial distribution of ^{226}Ra in Oxygono Bay.

The maximum activity concentrations of ^{226}Ra was observed in the first region indicating a possible association with the elevated concentrations in the beach sand sample (P2) and a more influenced area from the mining activities. Additionally, elevated concentrations of ^{226}Ra in the northern part of Oxygono Bay, may be attributed to a) material transport enriched in radionuclides from the terrestrial part of the area and/or b) to the material transport form Thorikos Bay, in which the waste materials were disposed and they were advected to Oxygono bay due the prevailing north wind direction at the area. The minimum values were determined at the southern part of the bay, representing a less affected area. To conclude, Oxygono bay is affected by disposed wastes during the last century at Thorikos bay. The waste material is transported due to marine circulation processes and sediment transport dynamics resulting in the contamination of the continental area close to Oxygono bay.

6.2.2 Incidences identification with historical data

The vertical distribution of natural radionuclides (^{226}Ra, ^{228}Ac), trace metals (As, Cu, Pb, Zn) and major elements (Mn, Fe, Al) obtained in the coastal core (core 1) of Oxygono Bay, identified three periods of mining activities: (a) 1860-1900 (core's lower part 38-52 cm), (b) 1900-1930 (core's middle part 28-38 cm), 1930-1980 (core's upper part 12-28 cm). In these profiles it is also evident the presence of the aforementioned parameters after the cessation of the mining industry (0-12 cm) during 1980-2014 (nowadays), revealing a post-mining effect. The radionuclide, trace metal and major element profiles exhibited maximum values during 1930-2014 and minimum ones during 1860-1900. Between these periods (1900-1930) an increment was observed for some elements (e.g. ^{226}Ra, As, Mn), while a peak was obtained for others (e.g. Cu, Pb, Al) reaching the maximum value around 1920.

Lavreotiki Peninsula hosted mining activities from 3000 BC until 100 BC, generating ancient slags and wastes due to the exploitation of galena (sphalerite) for the production of Ag and Pb. During 1860-1875 minimum observed values of radionuclides and metals correspond to the presence of the ancient wastes. In 1875

Serpieris Company started to exploit these types of wastes as raw material to produce As and Pb, and expanded during 1875-1900 to the exploitation of the mixed sulfide ores (rich in Zn) also for the production of Ag, Pb.

As mentioned above around 1920 a linear increment was obtained in radionuclide and metal profiles In the following period (1920-1930) the Pb and Cu concentrations decrease drastically, while those of ^{226}Ra, As, Zn and Mn remain constant exhibiting maximum values. The observed radionuclide and metal values increment are attributed to the newly-discovered flotation method which was immediately adopted in the exploitation/ore separation activities. The good efficiency of the flotation method provided high recovery values. However the economically exploited metal was Pb and all the other recovered metals (As, Zn, Mn) were disposed. During this period the mud content increases (20%-40%) indicating the presence of finer grains in the produced tailings comparing with previous periods of operation.

However, elevated Pb concentrations were obtained in the year around 1920, despite the adaptation of the flotation method. These elevated values can be attributed to the exploitation of oxidized ores resulting in a low Pb recovery. Thus, in the following period (1920-1930) the decreasing concentrations of Pb indicate the utilization of non-oxidized ores. The exploitation of oxidized ores contributed to Cu and Al profiles as a peak is observed in each of them. These peaks are associated with the composition of the oxidized ores, containing small quantities of Cu, as well as slimes of shale enriched in Al. When the utilization of oxidized ores was abandoned, the concentrations of the aforementioned metals were reduced at the levels of pre-operational periods (around 1875). These observations regarding the exploitation of different ore types were also depicted in the peaks of Cu, Pb and Al mass flux profiles during 1900-1930.

The most important aspect of metal profiles, was that all exhibited similar values as those of 1930-1980 period, after the cessation of mining in Lavrio area (early 1980s). Thorikos Bay may be the main contributor to this post-mining effect as strong north winds and currents may transport sediment from Thorikos to Oxygono Bay after resuspension and deposition processes. Other contributors, may be processes like rain-wash, transferring material into the coast originated from the adjacent contaminated terrestrial part.

Mass flux profiles in the coastal sediment core (core 1), did not provide further information, as in the case of Stratoni, for the reconstruction of the aforementioned events. Nevertheless they can be used as baseline information of the temporal mass deposition at the study area.

To conclude the identified operational periods were the following: a) the period during 1860-1900 where the low efficiency of the applied method and the use of ancient slags as raw material are depicted in the minimum observed values regarding metals, b) the period during 1900-1930 where the improvement of the recovery method that was implemented in the mining process resulted in the increase of all metals and ^{226}Ra concentrations and c) the period during 1930-1980 where the almost constant values of metal concentrations reveal the establishment of the applied mining method and the disposal of As, Zn and Mn as elements without economical interest. The waste materials in the area are still evident during the period of 1980-2014, although the mine operations stopped in the early 80s, as demonstrated from the metal concentrations, the

metal mass flux and the EF values that remain similar compared to the previous operational mining period (1930-1980) indicating a past - mining effect for 30 years, either due to the waste distribution in the terrestrial part and/or due to the water transfer contaminants originated from the neighboring gulf of Thorikos

6.2.3 Enrichement Factor and Pollution Load Index

Spatial result interpretation

The Enrichment Factor (EF) estimation of trace metals (As, Cu, Pb, Zn) and Mn was performed for the surface sediments of Oxygono Bay and the results are presented below, in Table 16. The deepest slice of the offshore core (core 2) was utilized as reference sample. According to the adopted classification (Birch & Davies, 2003) the enrichment of Oxygono Bay can be considered extremely severe for As and Zn, very severe to extremely severe for Pb, severe to extremely severe in Mn and minor to severe for Cu. The enrichment order was found to be As>Zn>Pb>Mn>Cu. The maximum EF values were calculated in the sampling point near beach sand (N5) and the minimum ones were observed at the southern part of Oxygono Bay (N3, N4).

Table 16 Enrichment factor (EF) estimation for the surface sediments based on the elemental concentrations of offshore core's (core 2) deepest slice.

Station	**As**	**Cu**	**Pb**	**Zn**	**Mn**
N1	108	5	32	92	32
N2	151	6	52	129	35
N3	60	3	44	83	16
N4	60	3	32	68	18
N5	361	11	82	262	63

The Pollution Load Index (PLI) was also determined in Oxygono Bay and the corresponding values were interpolated spatially via ArcGIS 10.2 software®. The simplified index (PLI) indicated a progressive deterioration in the area according to Tomlinson et al. (1980), as all the PLI values were well above one. Additionally, the spatial distribution of EF was similar to PLI interpolated spatial distribution, which includes the effect of all studied trace metals (As, Cu, Pb, Zn) and Mn. The results are shown in Fig. 6.7.

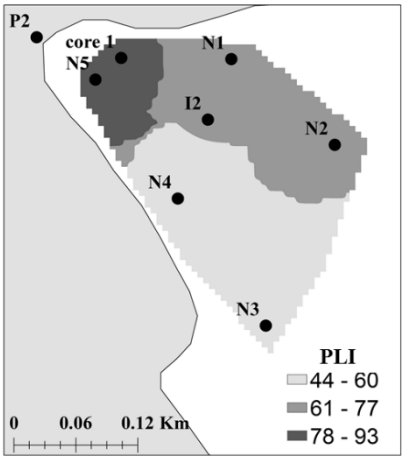

Fig. 6.7 The interpolated spatial distribution of Pollution Load Index (PLI) incorporating trace metal (As, Cu, Pb, Zn) and Mn concentrations. PLI ≤ 1 indicates no contamination or that the baseline levels of contaminants are present, while PLI > 1 indicates progressive deterioration (Tomlinson et al., 1980).

Data interpretation in core 1 (coastal)

The EF profiles of As, Cu, Pb, Zn and Mn, determined for the coastal sediment core are depicted in Fig. 6.8. Two reference values were utilized, the elemental concentrations of the shale of the continental crust and those of the deepest slice of the offshore core. The EF estimated with the first approach is presented in the left graph and the latter in the right graph. The concentrations of the continental crust for the estimation of the EF were used as a feasibility study for the selection of the background sample. According to first approach, the adopted classification revealed extremely severe enrichment in As, Pb and Zn and moderately severe enrichment in Cu for the whole core. On the other hand, the enrichment of Mn was found very severe in the upper part of the core, and severe in the middle and lower parts. The enrichment order was As>Pb>Zn>Mn>Cu. According to the second approach the calculated EF values were found up to an order of magnitude lower than those estimated with the first approach. Nevertheless, the enrichment classification did not change for As, Zn and Mn. In the cases of Pb and Cu the enrichment altered from extremely severe to very severe and from moderately to moderate severe, respectively. The new order of enrichment was As>Zn>Pb>Mn>Cu.

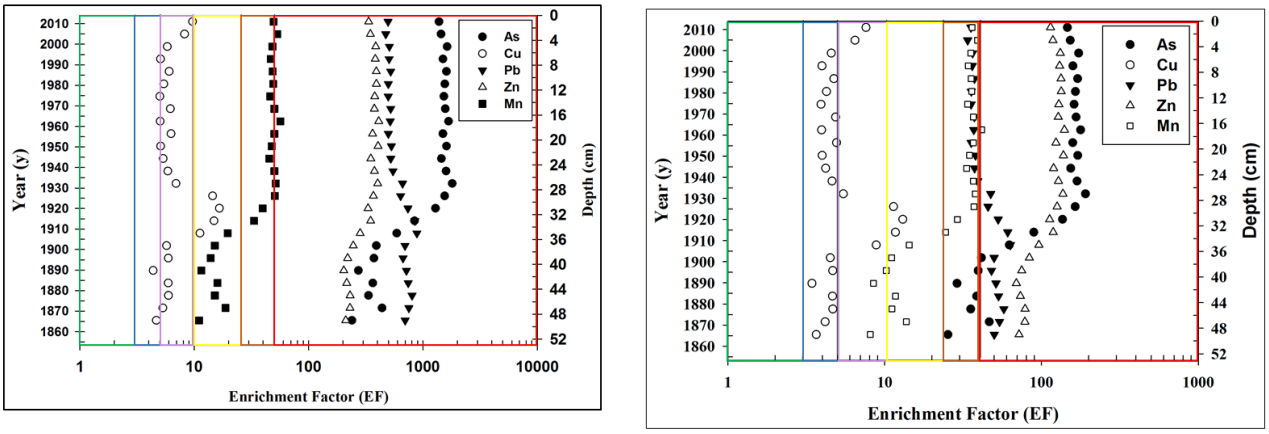

Fig. 6.8 The Enrichment Factor (EF) profiles of As, Cu, Zn, Pb and Mn. The element of Al was used for the estimation of EFs as conservative element, as well as the elemental concentrations of the shale of the continental crust (Wedepohl, 1995) (left) and of the deep pre-mine layer of STR8 core (right). The green color represents no or minor enrichment, the blue moderate enrichment, the purple moderately severe enrichment, the yellow severe enrichment, the orange very severe enrichment, and the red extremely severe enrichment.

Based on the EF classification the anthropogenic influence in the area occurred mainly during the last century (1920-2014). Additionally, during 1900-1930 the area was affected mainly by Pb and Cu concentrations, as the distinct EF peaks reveal during this period, where Cu classification altered from moderate to severe enrichment. This short term anthropogenic impact, can be attributed to the different mining methods or type of ores (e.g. oxidized) discussed in section 6.2.2.

The EF estimation is a useful parameter in order to determine the contamination and reveal the most contaminated periods. Thus in Oxygono Bay the most contaminated period regarding Pb and Cu was during 1900-1930, while concerning the other metals (As, Zn and Mn) the most contaminated period was the last 100 years. Additionally, the remaining contamination due to transport of waste material from

Thorikos Bay and/or the terrestrial part of Oxygono Bay is still evident during the last 30 years (1980-2014), after the cessation of mine exploitation in the early 1980's.

Data interpretation in core 2 (offshore)

The EF estimation was not possible for the offshore core (core 2), as major element measurements were not performed. Additionally, as discussed in the result section (5.2.3) the upper part of the core may have been influenced by anthropogenic mining activities, however in a lesser extend as the trace metal and Mn profiles exhibited values more than two (2) orders of magnitude lower than core 2. Therefore, in order to study the depth of contamination in the offshore core a simplified index, Pollution Load Index (PLI) was determined and the results are presented in Fig. 6.9. In this area, as reference sample was utilized the deepest slice of core 2. The PLI was also applied in the core 1 (coastal), so as to compare the contamination level of the two cores. As in Stratoni area only the trace metals and Mn with the highest observed concentrations were included.

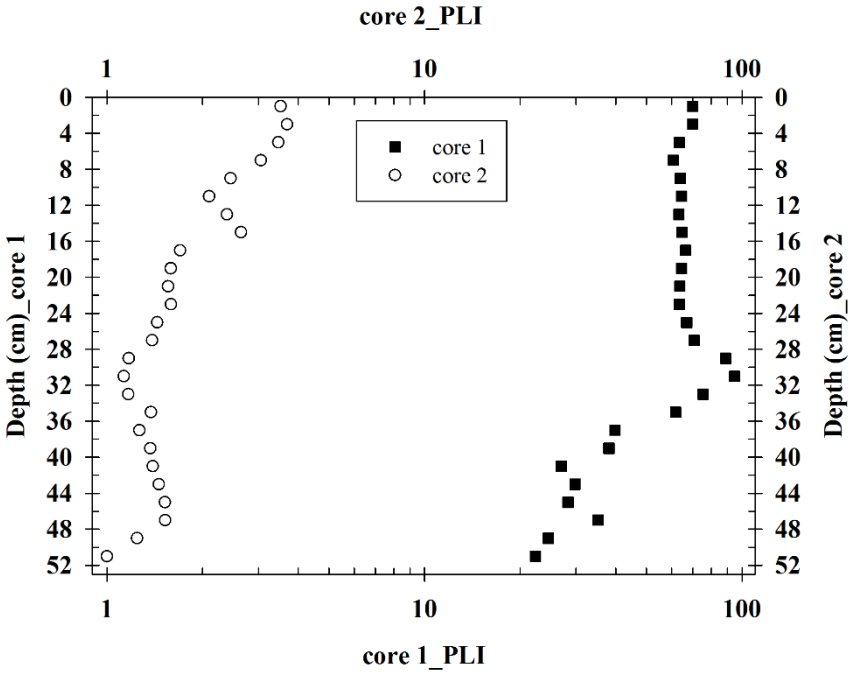

Fig. 6.9 The PLI estimation for the coastal core (core 1) at Oxygono Bay and the offshore core (core 2) at Lavreotiki Peninsula offshore area.

According to Tomlinson et al. (1980) all PLI values above one (10 indicate a progressive deterioration in the area. The middle-half of core 2 (16-52 cm) exhibited values below two (2) can be considered either no contaminated or consisted of baseline levels of contaminants. This assumption may be verified by the one order of magnitude lower PLI values of core1 comparing with core 2. The upper part of the core was indeed affected by anthropogenic activities as PLI exhibited a value above 3.

PLI exhibit significant information for studying the pollution dispersion in the coastal area of Lavreotiki since the data of core 1 and core 2 validate that path of the waste material at Thorikos bay is advected to Oxygono bay as well as to the direction of Markonisos Island via marine circulation and sediment dynamics. The PLI data at the first layer (till 16 cm) of the distant core exhibit values above the threshold ones

revealing that the area close to Makronisos Island is also affected while the deep part (below 16cm) is not affected from the mining activities.

6.2.4 Statistical analysis

The statistical analysis was performed only for the coastal core samples, so as to investigate possible associations among radionuclides, trace metals, major elements, LOI and sand-mud portion. All the samples of the core were used for the statistical analysis, in order to obtain a significant number of required data. The statistical analysis was performed for the radionuclides of ^{235}U and ^{40}K but no significant associations were obtained with the aforementioned parameters and it was not included in the following table. Four main groups of association can be observed: (a) the significant positive (0.53-0.73) association of natural radionuclides (^{226}Ra, ^{228}Ac) with trace metals and major elements (Mn, Fe), (b) the strong positive association of trace metals with each other and major elements and the significant positive association with mud content, (c) the significant positive association between Cu and Al and (d) the significant negative association of LOI and sand fraction with radionuclides, trace metals and major elements. Despite the production Pb metal from the exploited P.B.G. ores, this element was not associated with the studied parameters, only a weakly positively association (0.57) was observed with the organic content. This implies that the disposed wastes produced by the P.B.G. ore separation were clear of Pb. Additionally, the wastes were consisted of the main metals of P.B.G. ores (e.g. Zn, Fe), as well as of granitoids characterized by uranium minerals and iron-manganese ores (e.g. ankerite, rhodochrosite) surrounding or penetrating them. Thus, the good association among natural radionuclides, trace metals and major elements (group ‘a’ and ‘b’) reveals the waste nature. Additionally, the trace metal of As is also positively associated with the aforementioned parameters, since in the primary minerals of mixed sulphides, are present minerals associated with other elements such as As, Ag, Au, Bi, Cu (section 4.1.1.2). The positive association of the aforementioned parameters with the mud fractions indicates that the studied elements are adsorbed into the fine grains of wastes. The organic content or/and the sediments with coarser grains (sand) do not contribute to the elevated concentrations. Lastly, the positive association between Cu and Al, may be attributed to the utilization of oxidized ores for the Pb production, which is characterized by Cu concentrations, as well as fine grains rich in Al (slimes).

Table 17 The results of statistical association (Spearman's rho (rs)) among radionuclides, trace metals, major elements, LOI (Loss of Ignition) and sand-mud percentage of the coastal sediment core (core 1) (N=26) of Oxygono Bay.

		^{226}Ra	**^{228}Ac**	**As**	**Cu**	**Pb**	**Zn**	**Mn**	**Fe**	**Al**	**LOI**	**sand**	**mud**
^{226}Ra	rs	1.000	,765**	,739**	,527**	-,443*	,677**	,727**	,675**	.276	-,779**	-,506*	,510*
	Sig.		.000	.000	.006	.023	.000	.000	.000	.181	.000	.014	.013
^{228}Ac	rs	,765**	1.000	,793**	,577**	-.292	,753**	,738**	,654**	.300	-,644**	-,653**	,686**
	Sig.	.000		.000	.002	.148	.000	.000	.000	.146	.000	.001	.000
As	rs	,739**	,793**	1.000	,445*	-.283	,919**	,798**	,846**	.275	-,770**	-,573**	,593**
	Sig.	.000	.000		.023	.162	.000	.000	.000	.183	.000	.004	.003
Cu	rs	,527**	,577**	,445*	1.000	.199	,432*	,543**	.242	,795**	-.299	-,719**	,716**
	Sig.	.006	.002	.023		.329	.027	.004	.245	.000	.138	.000	.000
Pb	rs	-,443*	-.292	-.283	.199	1.000	-.183	-,440*	-,558**	.302	,573**	-.241	.228
	Sig.	.023	.148	.162	.329		.371	.024	.004	.143	.002	.269	.296
Zn	rs	,677**	,753**	,919**	,432*	-.183	1.000	,730**	,762**	.389	-,715**	-,631**	,653**
	Sig.	.000	.000	.000	.027	.371		.000	.000	.054	.000	.001	.001
Mn	rs	,727**	,738**	,798**	,543**	-,440*	,730**	1.000	,689**	,398*	-,659**	-,471*	,501*
	Sig.	.000	.000	.000	.004	.024	.000		.000	.049	.000	.023	.015
Fe	rs	,675**	,654**	,846**	.242	-,558**	,762**	,689**	1.000	.102	-,767**	-.402	.393
	Sig.	.000	.000	.000	.245	.004	.000	.000		.627	.000	.063	.071
Al	rs	.276	.300	.275	,795**	.302	.389	,398*	.102	1.000	-.140	-,674**	,689**
	Sig.	.181	.146	.183	.000	.143	.054	.049	.627		.504	.001	.000
LOI	rs	-,779**	-,644**	-,770**	-.299	,573**	-,715**	-,659**	-,767**	-.140	1.000	.354	-.381
	Sig.	.000	.000	.000	.138	.002	.000	.000	.000	.504		.097	.073
sand	rs	-,506*	-,653**	-,573**	-,719**	-.241	-,631**	-,471*	-.402	-,674**	.354	1.000	-,991**
	Sig.	.014	.001	.004	.000	.269	.001	.023	.063	.001	.097		.000
mud	rs	,510*	,686**	,593**	,716**	.228	,653**	,501*	.393	,689**	-.381	-,991**	1.000
	Sig.	.013	.000	.003	.000	.296	.001	.015	.071	.000	.073	.000	

* Spearman association is significant at the 0.05 level (2-tailed) **. Spearman association is significant at the 0.01 level (2-tailed).

The association of the parameters in the specific area of study provided significant information regarding the contributors (e.g. granulometry) of the elevated concentrations of radionuclides, the correlation among radionuclides and the exploited minerals, as well as the association of radionuclides and metals in the disposed wastes.

6.3 Comparison of radioactivity, trace metals and Mn concentrations with areas affected by anthropogenic activities in Mediterranean countries

In this section the concentrations of natural radionuclides, trace metals (As, Cu, Pb, Zn) and Mn obtained in the present work are compared with previous studies held near the study areas and in Mediterranean countries characterized by industrial activities. Furthermore the data of this work are compared with global values (like radionuclide world median, average value of Earth's shale and sediment quality guidelines). The compared data originate from marine environment or rivers. The data are given in the following table.

Table 18 Comparison of radioactivity, trace metals and Mn concentrations of the present work with areas affected by anthropogenic activities in Greece and Mediterranean, the world median radionuclide concentration for soil, the shale of the continental crust and sediment quality guidelines.

		Natural radioactivity				**Heavy metals**				
		^{226}Ra	**^{228}Ac**	**^{235}U**	**^{40}K**	**As**	**Cu**	**Pb**	**Zn**	**Mn**
		(Bq kg^{-1})				(μg g^{-1})				
STR1 core (coastal) [1]	min	75	30	5	570	1400	100	2500	2000	4000
	max	120	40	13	860	2200	250	4000	3000	12000
STR8 core (offshore) [1]	min	13	25	2.7	460	50	30	300	240	940
	max	30	35	4.1	650	480	80	900	630	2200
Ierissos Gulf [1] (surf)	min	10	10	0.8	350	10	1	30	5	40
	max	100	180	5.8	1200	4300	300	2500	4000	30000
core 1 (coastal core) [1]	min	4	8	1.5	130	500	40	2400	3500	1500
	max	16	16	3.5	200	5200	220	4800	9000	11000
core 2 (offshore core) [1]	min	MDA	MDA	MDA	MDA	20	8	40	40	150
	max	18	18	6.7	300	80	20	200	200	500
Oxygono B. (surf)[1]	min	5	10	1.3	111	2100	46	2300	4900	4200
	max	12	17	3.0	191	8600	102	3910	12500	11300
Oxygono B.[2]	seafloor	10	8	<2.5	180	3400	120	3300	6900	7200
	beach	20	7	<2.5	100	890	140	6000	8100	4300
Perdika B. [2]	seafloor	<2	4	<2.5	70	50	8	200	100	340
	beach	<2	<5	<2.5	80	70	15	390	180	950
Thorikos B. [2]	seafloor	8	12	<2.5	230	-*	-	-	-	-
Delenia B. [2]	seafloor	9	-	<2.5	340	35	13	120	144	330
	beach	6	9	<2.5	300	34	12	150	150	390
Previous measurements near our study areas										
Ierissos G. (Stratoni)[3]	min					-	180	1600	890	-
	max					-	206	2300	930	-
Stratoni rivers[4]	min	-	-	-	-	43	30	40	73	680
	max	-	-	-	-	2700	180	3400	4500	69400
Olympias rivers[5]	min	-	-	-	-	6	3	13	-	210
	max	-	-	-	-	1090	150	2000	-	127000
Lavreotiki P.[6]	min	-	-	-	-	6	3	20	15	-
	max	-	-	-	-	2857	270	448	5763	-
Greece (industrial areas)										
Thermaikos G.[7]	min	26	20	2	350	-	20	10	70	-
	max	70	60	7	542	-	170	220	360	-
Itea G. (bauxite)[8]	min	13	20	-	50	-	-	-	-	-
	max	70	90	-	490	-	-	-	-	-
Amvrakikos G.[9]	min	16	13	-	240	-	-	-	-	-
	max	20	40	-	870	-	-	-	-	-
Saronikos G.[10]	min	2	5	0.3	60	-	-	-	-	-
	max	60	20	6.6	380	-	-	-	-	-

Mediterranean										
Izmir B_Turkey[11]	min	10	14	-	250	-	9	<DL	17	380
	max	12	16	-	350	-	40	16	90	900
Didim B_Turkey[12]	min	9	6	-	410	-	-	-	-	-
	max	10	7	-	670	-	-	-	-	-
Izmit B_Turkey[13]	min	8	10	-	190	-	-	-	-	-
	max	30	40	-	870	-	-	-	-	-
Nador L_Morocco[14]	min	-	-	-	-	-	10	16	60	-
	max	-	-	-	-	-	400	330	1300	-
Tinto R_estuary[15]	min	14	15	-	30	-	-	-	-	-
	max	54	41	-	250	-	-	-	-	-
Odiel R_estuary[15]	min	4	16	-	20	-	-	-	-	-
	max	50	35	-	110	-	-	-	-	-
world median [16]		35	30	-	400	-	-	-	-	-
av. shale[17]		-	-	-	-	13	45	20	95	850
OMEE [18]	SEL	-	-	-	-	33	110	250	820	1100
NOAA[18]	ERM	-	-	-	-	70	270	218	410	-
FDEP[18]	PEL	-	-	-	-	64	170	160	300	-
ISQG[18]	High	-	-	-	-	70	270	220	410	-
USEPA [18]	high	-	-	-	-	33	149	128	459	-
OMEE [18]	lowest	-	-	-	-	6	16	31	120	460
NOAA[18]	ERL	-	-	-	-	8	34	47	15	-
FEDP [18]	TEL	-	-	-	-	8	28	21	68	-
ISQG[19]	low	-	-	-	-	20	80	50	200	-

Abbreviations: B: bay, G: gulf, L: lagoon, R: river, P: peninsula, MDA: Minimum Detectable Activity, DL : Detection Limit, SEL: Severe Effect Level, ERM: Effects Range-Medium, PEL: Probable Effect Level, ERL: Effects Range-Low, TEL: Threshold Effect Level

1. present work 2. (Michalopoulou, 2014) ;(Michalopoulou et al., 2015). 3. (Stamatis et al., 2002) 4. (Kelepertzis et al., 2012) 5. (Lazaridou- Dimitriadou et al., 2004) 6. (Zotiadis & Kelepertzis, 1997) 7. (Eleftheriou, 2014) for radionuclide values; (Christophordis et al., 2009) for metal values 8 (Karagiannidi et al., 2009) 9. (Papaefthymiou et al., 2013) 10. (Eleftheriou et al., 2013) 11. (Akozcan, 2012) for radionuclide values; (Akozcan & Ugur Gorgun, 2013) for metal values 12. (Akozcan, 2012) 13. (Ergul et al., 2013) 14. (Maanan et al., 2015) 15. (Hierro et al., 2012) 16. (UNSCEAR 2000) - World median of soil 17. (Wedepohl 1995) - Average continental crust (shale) concentrations (United States Environmental Protection Agency (USEPA), 2000) 18. (OMEE 1993), (USEPA 2000), (ANZECC 2000) - Sediment Quality Guidelines

* The (-) means not available data

A clear conclusion of the above table is than near industrial areas the multidisciplinary approach of studying natural radioactivity and metal concentrations is scarce, despite the fact that many industrial activities influence both parameters. Generally, the activity concentrations of all natural radionuclides (^{226}Ra, ^{235}U, ^{228}Ac, ^{40}K) obtained in Oxygono Bay or wider area of Lavrio, were lower among the other selected Greek and Mediterranean marine areas, as well as lower than the world median values. The mining activities occurred in the area enhanced NORM concentrations, but not over screening levels. On the other hand ^{226}Ra and ^{235}U in Stratoni area exhibited the highest values comparing with other Greek and Mediterranean marine areas and were found well above the world median. Additionally, ^{228}Ac values of Stratoni were characteristic of Greek radioactivity ^{228}Ac levels. The concentrations of ^{40}K in both study areas were similar with Greek and Mediterranean values, and the slightly elevated values may be attributed to the different mineralogy among the comparing areas.

Despite the low activity concentrations of natural occurring radionuclides (NORMs), especially at Oxygono Bay, the trace metal and Mn concentrations in both study areas were found much higher than in neighboring areas such as Olympias's rivers for Stratoni and Perdika Bay, Delenia Bay and Lavreotiki Peninsula for Oxygono. However, Stratoni's rivers, investigated in previous studies, exhibited similar values as those of present work collected in the terrestrial and marine area. This enforces the idea that both the terrestrial and marine parts have been affected by the waste discharges. Lastly, the trace metal and Mn concentrations of the coastal samples (surface and cores) in both study areas were orders of magnitude higher than those of the industrial areas of Greece and Mediterranean. Furthermore, the metal concentrations were higher compared to the upper threshold of sediment quality guidelines, indicating the significant impact of metallic mines in the environment of the study areas. Regarding the offshore cores, the metal concentrations in both study areas exhibited values similar to other Greek and Mediterranean industrial areas. Moreover, the high metal values of the offshore cores were found similar to the lower threshold levels of sediment quality guidelines, implying a mining impact to the offshore marine parts.

In the Mediterranean Sea, the distribution of metals is primarily controlled by the dilution process, marine circulation and surface seawater dynamics. In this work it is demonstrated that the relatively high content of these metals in Stratoni and Lavrio mine areas at the surface layer as well as at the deep layers of the cores, is due to the industrial mining activities that take place around the coasts of both areas.

Chapter 7

Conclusions

In this work the impact of metallic mining activities was investigated regarding natural radioactivity and metal concentrations in the marine sediment of two coastal areas, Stratoni and Lavrio. The study of these parameters was performed both spatially and temporally. Stratoni is a metallic mine still in operation, while Lavrio hosts the remains of an abandoned metallic mine processes. The latter area was selected so as to study the post-mining effect, as the surface and core sediments were collected almost 30 years after the cessation of the mine. Additionally, the developed and established approach in the case of the abandoned mine may be implemented in the on-going mine (Stratoni), contributing to further understanding of the mining impact and enhance protection measures (e.g. improved discharge regulations). In order to achieve an efficient description of the marine areas, targeting sampling was performed, where the surface and coastal core sediments were collected by a diver, while offshore core sediments were collected via a box-corer with the Research Vessel "Aegeao".

To summarize, in the spatial study (surface samples) of Ierissos Gulf, where the on-going mining of Stratoni occurs, the most contaminated area, regarding radionuclides and metals, revealed to be Stratoni port and especially the load out pier area of Stratoni. The radionuclide and metal contamination affected the neighboring stream (Kokkinolakos) of Stratoni until the offshore part in a lesser extent, however it did not influence the distant regions of Stratoni such as Kalatzi Lakkos stream and Ierissos city or the north part of the load out pier area. The spatial distribution of radionuclides was also verified and expanded via the radionuclide dispersion model, which estimated the radionuclide (^{226}Ra, ^{235}U) discharged rate and determined the affected area of Ierissos Gulf. According to the dispersion study the mining activities influenced the north part of the gulf and reached until the middle part of the gulf, while the south region remained unaffected. Thus, Ierissos city can be considered a safe region or residence, tourism and fishing. Despite the elevated concentrations of radionuclides, in comparizon with the world median for soil and for Ierissos port, the radiological risk for non-human biota was negligible. On the other hand the metal enrichment was found severe in many sampling points; an indicative order of enrichment in the surface samples was Zn>As>Mn>Pb>Cu.

In the marine area of Stratoni long-term monitoring data are absent. Therefore, two sediment cores were collected near the load out pier area and the offshore region (1.5 km away from the load out pier) to assess the radiological and metallic mining impact in a temporal manner. Additionally, the core of the load out pier area was utilized for the reconstruction of past events. The maximum radionuclide and metal concentrations were found between 1908 and 1970. The radionuclide ^{226}Ra concentrations were found to be above the world median for soil, however the radiological risk was negligible regarding biota. On the other hand the metal concentrations exhibited values an order of magnitude higher than the sediment quality guidelines and the enrichment was found to be severe, especially during the same period (1908-1970). An indicative order of metal enrichment in the sediment core was As>Zn≥Pb>Mn>Cu. Regarding the offshore core, the radionuclide and metal impact

reached the upper part of the core indicating an offshore influence for many years. Again the radiological risk was not significant, while an indication of metal enrichment was also verified in the upper part of the offshore core utilizing pollution load index (PLI).

The reconstruction of past events was accomplished using the radiodating methods based on ^{210}Pb and ^{137}Cs, and by combining radionuclide and metal concentrations, as well as their estimated mass fluxes. The mass flux profiles contributed to the further vertical analysis of the mining impact in a temporal aspect and the main identified processes and periods were found to be the exploitation of pyrite for the production of sulfuric acid during 1912-1920, the decrease of mining activity during 1935-1945 due to the Second World War, the alteration of the exploited ores due to the type of ore exploitation and the construction and operation of Olymbiada's flotation plant during 1950-1970; and the end of tailing discharging into the marine environment during 1980-2010.

The statistical analysis performed, revealed different associations among radionuclides and metals, in the spatial and vertical studies. Additionally, the strong association among radionuclides (^{226}Ra, ^{235}U) and metals (As, Cu, Pb, Zn, Mn), as well as taking into account the radionuclide dispersion model, may indicate an affected area due to metals. In order to investigate any possible impacts to the water column, metal concentrations were also collected in the seawater-sediment interface. According to this study, the metal concentrations for most metals were found well below the Environmental Quality Standards (EQS). Only, seawater Pb exhibited values above EQS in some sampling points, indicating that the risk to observe toxic effects in the organisms is high.

A similar approach including spatial and temporal studies in the marine environment, was incorporated in Lavrio and focused on Oxygono Bay. Lavrio is located near an abandoned mine and suffers from the post-mining impact as it is developed on top of the residuals and wastes of the mining activities. This impact is also evident in the marine part of Lavrio. Like in Stratoni case, the radionuclide concentrations had increased due to mining, both spatially and vertically, however these values were found well below Stratoni and the world median for soil. Therefore, the radiological risk is also negligible. On the other hand, the metal concentrations in Oxygono Bay exhibited values similar to those of Stratoni port and the load out pier area, again both spatially and temporally. The main difference between the two studied areas (Stratoni and Lavrio), is that mining impact in Stratoni is significant during 1908 - 1970, while at Lavrio it is significant during the last 100 y (1920-2014). Despite the cessation of mining, 30 years previously, the post-mining effect is still evident and this is due to disposed wastes during the last century at Thorikos bay. The waste material is transported due to marine circulation processes and sediment transport dynamics resulting in the contamination of the continental area close to Oxygono bay.

The spatial metal enrichment was found to be severe following an order of As>Zn>Pb>Mn>Cu. Regarding the vertical metal enrichment, the order was found similar to the spatial one (As>Zn>Pb>Mn>Cu). The most contaminated period regarding Pb and Cu was during 1900-1930, while concerning the other metals (As, Zn and Mn) the most contaminated period was during the last 100 years. Additionally, as in Stratoni case the offshore region of Lavrio has been affected, as elevated metal

values and high pollution indices were found in the upper part of the offshore core, located 1.9 km away from Oxygono Bay, indicating an influence for many years. The spatial and vertical metal studies (including both cores of Lavrio area) revealed that the path of the waste material at Thorikos bay is advected to Oxygono bay as well as towards the direction of Markonisos Island via marine circulation and sediment dynamics.

The reconstruction of past events was also achieved and was verified by historical data as in the case of Stratoni. The only difference was that the mass flux parameter did not contribute further in the temporal analysis. In the temporal analysis four operational periods were identified: a) the period during 1860-1900 where the efficiency of the applied method was low and ancient slags were used as raw materials, b) the period during 1900-1930 where the improvement of the recovery method resulted in the increase of all metals and ^{226}Ra concentrations, c) the period during 1930-1980 the establishment of the applied mining method was established and As, Zn and Mn were disposed as they were not exploited economically and d) during 1980-2014 where the post mining effect is still evident either due to the waste distribution in the terrestrial part and/or due to the water transfer contaminants originated from the neighboring gulf of Thorikos. Lastly, the statistical analysis performed on the sediment core of Oxygono Bay provided significant information regarding the contributors (e.g. granulometry) to the elevated concentrations of radionuclides, the correlation among radionuclides and the exploited minerals, as well as the association of radionuclides and metals in the disposed wastes.

As mentioned in the comparison section (6.3) in the Mediterranean Sea, the distribution of metals is primarily controlled by the dilution process, marine circulation and surface seawater dynamics. This work demonstrates that the relatively high content of these metals in the Stratoni and Lavrio mine areas at the surface layer, as well as at the deep layers of the cores, is due to the industrial mining activities that take place around the coasts of both areas.

The main achievements/conclusions of the present work are:

a) Provision of new data in the marine region.
b) Enrichment of the literature in metal (trace and major) and natural radioactivity measurements near mines.
c) Provision of baseline information regarding the marine sediment and the most contaminated regions of each area
d) Clarification of the direct disposal of wastes in the marine area
e) Determination of the sedimentation rates of both regions
f) An estimation of the radionuclide dispersion and the discharge rate of ^{226}Ra and ^{235}U
g) Determination of the affected area regarding NORM concentrations. In addition the work has proposed other interpolation methods for the estimation of metal and radionuclide spatial distribution (ERICA, ArcGIS)
h) A reconstruction of the impact of past events and verified them with historical data
i) A proposal of the metal flux estimation as an extra parameter to unfold the temporal impact
j) An assessment of the metal influence in a spatial and temporal manner (last 150 years)

k) An assessment of the radiological risk
l) An assessment of the metal influence of the offshore cores, which were characterized by incomplete datasets (no major element measurements)
m) An assessment of the metal contamination in the seawater
n) Determination of possible correlations between metals and radionuclides and
o) A proposal of some key elements for mine impact studies (^{226}Ra, ^{232}Th, As, Cu, Pb, Zn, Mn, Al and Fe).

This study will further contribute to the enrichment of the existing information concerning safety, remediation and support to national and international organizations regarding environmental protection and eventually to the design of a monitoring strategy for such areas. The information gathered will support social organizations since the study areas are well known for tourism and industrial activities, as mentioned above. The introduced methodology can be implemented in other Greek coastal regions near densely populated industrial areas such as Kavala (phosphate fertilizer industry, oil land facilities), Aliveri (lignite mining region, cement industry) and Itea (bauxite industry) or in the cases of pristine areas scheduled for future mining activities. Moreover, the model of radiological dose rate estimation and dispersion can be further developed and validated by determining site specific data or obtaining experimental dose rate values in some biota (e.g. microalgae). This work may be also implemented in other matrices, such as bio-accumulators (e.g. algae, mussels).

References

Aberg G, Charalampides G, Fosse G, Hjelmeth H, 2001. The use of Pb isotopes to differentiate between contemporary and ancient sources of pollution in Greece. *Atmospheric Environment,* pp. 35: 4609-4615.

Abrahim GMS, 2005. *Holocene sediments of Tamaki Estuary: Characterisation and impact of recent human activity on an urban estuary in Auckland, New Zealand.* Auckland, New Zealand: University of Auckland.

Abril JM, San Miguel EG, Rruiz-Canovas C, Casa-Ruiz M, Bolívar JP, 2018. From floodplain to aquatic sediments: Radiogeochronological fingerprints in a sediment core from the mining impacted Sancho Reservoir (SW Spain). *Scince of the Total Environment,* pp. 631-632: 866-878.

Akozcan S & Ugur Gorgun A, 2013. Trace metal and radionuclide pollution in marine of the Aegean Sea (Izmir Bay and Didim). *Environmental Earth Sciences,* pp. 69: 2351-2355..

Akozcan S, 2012. Distribution of natural radionuclide concentrations in sediment samples in Didim and Izmir Bay (Aegean Sea-Turkey). *Journal of Environmental Radioactivity,* pp. 112: 60-63.

Alashrah S & El-Taher A, 2018. Assessing exposure hazards and metal analysis resulting from bauxite samples collected from Saudi arabian mine. *Polish Journal of Environmental Studies,* pp. 27: 959-966.

Alexakis, D., 2011. Diagnosis of stream sediment quality and assessment of toxic element contamination sources in East Attica, Greece. *Environmental Earth Scinces,* p. 63: 1369–1383.

Allan, R., 1997. Mining and metals in the environment. *Journal of Geochemical Exploration,* pp. 58: 95-100.

Aller RC, Benninger LK, Cochran JK, 1980. Tracking particle-associated processes in nearshore environments by use of 234Th/238U disequilibrium. *Earth and Planetary Science Letters,* pp. 47:161-175.

Appleby PG & Oldfield F, 1978. The calculation of lead-210 dates assuming a constant rate of supply of unsupported 210Pb to the sediment. *Catena,* pp. 5: 1-8.

Australian and New Zealand Environment and Conservation Council (ANZECC), 2000. *Aquatic Ecosystems-Rationale and Background Information, National Water Quality Management Strategy.* s.l.:Australian and New Zealand Environment and Conservation Council , paper No 4, Vol. 2, chapter 8..

Bai H, Hu B, Wang C, Bao S, Sai G, Xu X, Zhang S, Li Y, 2017. Assessment of radioactive materials and heavy metals in the surface soil arond the Bayanwula prospective uranium mining area in China. *International Journal of Environmental Research and Public Health,* p. 14: 300.

Baskaran, M., Nix, J., Kuyper, C. & Karunakara, N., 2014. Problems with the dating of sediment core using excess 210Pb in a freshwater system impacted by large scale watershed changes. *Journal of Environmental Radioact ivity,* pp. 138: 355-363.

Batista MJ, Abreu MM, Pinto MS, 2007. Biogeochemistry in Neves Corvo mining region, Iberian pyrite belt, Portugal. *Journal of Geochemical Exploration,* pp. 92: 159-176.

Bech J, Corrales I, Tume P, Barcelo J, Duran P, Roca N, Poschenrieder C, 2012. Accumulation of antimony and other potentially toxic elements in plants around aformer antimony mine located in the Ribes Valley (Eastern Pyrenees). *J Geochem Explor,* pp. 74: 205-217.

Becker A, Klock W, Friese K, Schreck P, Treutle HC, Spetel MC, 2001. Lake Suber See as a natural sink for heavy metals from copper mining. *Journal of Geochmemical Exploration,* pp. 74: 205-217.

Beresford N, Brown JE, Copplestone D, Garnier-Laplace J, Howard B, Larsson CM, Oughton D, Prohl G, Zinger I, 2007. *D-ERICA: An Integrated Approach to the assessment and managment of environmental risks from ionising radiation,* s.l.: European Commision.

Birch GF & Davies K, 2003. *A scheme for assessing human impacts on coastal aquatic environments using sediments.* Australia, Wollongong University Papers in Center for Maritime Policy, pp. 371-380.

Brown, J. et al., 2008. The ERICA Tool. *Journal of Environmental Radioactivity,* pp. 99:1371-1383.

Brown, J. et al., 2016. A new version of the ERICA Tool to facilitate impact assessment of radioactivity on wild plants and animals. *Journal of Environmental Radioactivity,* pp. 153:141-148.

Chalupnik, S., Wysocka, M., Janson, E. & Chmielewska, I., 2017. Long term changes in the concentration of radium in discharge waters of coal mines and Upper Silecian rivers. *Journal of Environmetal Radioactivity,* pp. 171: 117-123.

Chantzi, P., 2012. *Investigation of coastal sediment transport in the Ierissos Gulf at Chalkidiki.* s.l.:Aristotle University of Thessaloniki, Master Thesis.

Charalampides, G., Arvanitidis, N., Vatalis, K. & Platia, S., 2013. Sustainability perspectives in Greece as reflected by mineral deposits exploitation. *Procedia Economics and Finance,* pp. 5: 143-151.

Christophoridis, C., Dedepsidis, D. & Fytianos, K., 2009. Occurrence and distribution of selected heavy metals in the surface sediments of Thermaikos Gulf, N. Greece. Assessment using pollution indicators. *Journal of Hazardous Materials ,* p. 168: 1082–1091.

Cochran, J., Hirschberg, D., Wang, J. & Dere, C., 1998. Atmospheric deposition of metals to coastal waters (Long Island sound, New York USA): evidence from Saltmarsh deposits. *Estuarine, Coastal and Shelf Science,* pp. 46: 503-522.

Copplestone, D., Hingston, J. & Real, A., 2008. The develpment and purpose of the FREDERICA radiation effects database. *Journal of Environmental Radioactivity,* pp. 99:1456-1463.

Demetriades, A., 2010. Medical geology in Hellas: The Lavrion environmental pollution study. *In: Medical Geology, O. Selinus et al, (eds), International Year of Planet Earth, Springer Science + Business Media B.V,* pp. 355-390.

Demetriades, A. & Vergou-Vichou, K., 1999. *General introduction: regional geology, mineralisation, mining and metallurgical activities, environmental impact, regional soil geochemistry and contamination index maps,* Athena, Hellas: A. Demetriades Geochemical atlas of the Lavrion urban area for environmental protection and planning.

Doering, C. & Bollhofer, A., 2016. A database of radionuclide activity and metal concentrations for the Alligator Rivers region uranium province. *Journal of Environmental Radioactivity,* pp. 162-163: 154-159.

Doering, C. & Bollhofer, A., 2017. Water hardness determines 226Ra uptake in the tropical freshwater mussel. *Journal of Environmental Radioactivity,* pp. 172: 96-105.

Eleftheriou, G., 2014. *Estimation and spatial-temporal dispersion of radionuclides in the aquatic environment (PhD thesis) (in Greek).* Athens: National Technical University of Athens.

Eleftheriou, G. et al., 2013. *Radionuclides and Heavy Metals Concentrations at the Seabed of NW Piraeus, Greece.* Athens, s.n.

Eleftheriou, G. et al., 2018. Radiometric dating of sediment cores from aquatic environments of north-east Mediterranean. *Journal of Radioanalytical and Nuclear Chemistry,* pp. 316: 655-671.

Ergul, H. et al., 2013. Natural and artificial radionuclide activity concentrations in surface sediments of Izmit Bay, Turkey,. *Journal of Environmental Radioactivity ,* pp. 126: 126-132.

European Commision (EC), 2003. *Effluent and dose control from European Union NORM industries-assessment of current situation and proposal for the harmonized community approach,* Luxembourg: Office for Official Publications of the European Communities.

Franke, R., 1982. Smooth Interpolation of Scattered Data by Local Thin Plate Splines. *Computer and Mathematics with Applications,* pp. 8: 273-281.

Garcia-Ordiales, E. et al., 2017. Historical accumulation of potentially toxic trace elements resulting from mining activities in estuarine salt marshes sediments of the Asturias coastline (northern Spain). *Environmental Science and Pollution Research,* pp. 1-14.

Gilg, H. & and Frei, R., 1994. Chronology of magmatism and mineralization in the Kassandra mining area, Greece: the potentials and limitations of dating hydrothermal illites. *Geochimica and Cosmochimica Acta,* pp. 58:2107-2122.

Giri, S., Singh, G. & J. V. T. R., 2011. Risk assessment due to ingestion of natural radionuclides and heavy metals in the milk samples: a case study from a proposed uranium mining area, Jharkhand. *Environmental Monitoring and Assessment,* pp. 175: 157-166.

Gomez-Gonzales, M., Garcia-Guinea, J., Laborda, F. & Garrido, F., 2015. Thallium occurrence and partitioning in soils and sediments affected by mining activities in Madrid province (Spain). *Science of the Total Environment,* pp. 536: 268-278.

Gribov, A. & Krivoruchko, K., 2012. New Flexible Non-parametric Data Transformation for Trans-Gaussian Kriging.. In: *Geostatistics Oslo 2012. Quantitative Geology and Geostatistics.* Netherlands: Springer, pp. 51-65.

group, E., 2015. *ERICA Assessment tool help function document.* [Online].

Grygar, T., Elznicova, J., Kiss, T. & Smith, H., 2016. Using sedimentary archives to reconstruct pollution history and sediment provenance: The Ohre River, Czech Republic. *Catena,* pp. 144: 109-129.

Hakanson L, 1980. An ecological risk index for aquatic pollution control- A sedimentological approach. *Water Research,* pp. 14: 975-1001.

Hierro, A., Bolivar, J., Vaca, F. & Borrego, J., 2012. Behavior of natural radionuclides in surficial sediments from an estuary impacted by acid mine discharge and industrial effluents in Southwest Spain. *Journal of Environmental Radioactivity,* pp. 110: 13-23.

Hosseini, A. et al., 2008. Transfer of radionuclides in aquatic ecosystems-Default concentration ratios for aquatic biota in the ERICA Tool. *Journal of Environmental Radioactivity,* pp. 99:1408-1429.

International Atomic Energy Agency (IAEA), 2001. *Generic models for use in assessing the impact of discharges of radioactive substances to the environment,* Vienna: International Atomic Energy Agency, TRS 19.

International Atomic Energy Agency (IAEA), 2004. *Sediment distribution coefficients and concentration factors for biota in the marine environment,* Vienna: International Atomic Energy Agency, TRS 422.

International Atomic Energy Agency, (IAEA), 2003. *Collection and preparation of bottom sediment samples for analysis of radionuclides and trace elements,* Vienna: IAEA-TECDOC-1360.

International Atomic Energy Agency, I., 1992. *Effects of ionizing radiation on plants and animals at levels implied by current radiation protection standards,* Vienna: International Atomic Energy Agency, TRS 322.

Jodlowski, P., Macuda, J., Nowak, J. & Dinh, C., 2017. Radioactivity in wastes generated from shale gas exploration and production- North Poland. *Journal of Environmental Radioactivity,* pp. 175-176: 34-38.

Kalantzi I, Zeri C, Catsiki VA, Tsangaris V, Strogyloudi E, Kaberi H, Vergopoulos N, Tsapakis M, 2016. Assessment of the use of copper alloy aquaculture nets: Potential

impacts on the marine environment and on the farmed fish. *Aquaculture,* pp. 465: 209-222.

Kalfas, C., Axiotis, M. & Tsabaris, C., 2016. SPECTRW: A software package for nuclear and atomic spectroscopy. *Nuclear Instruments and Methods in Physics Research Section A,* pp. 830:265-274.

Karageorgis, A. & Anagnostou, C., 2005. Geochemistry and mineralogy of the NW Aegean Sea surface sediments: implications for river runoff and anthropogenic impact. *Applied Geochemistry,* pp. 20:69-88.

Karageorgis, A., Katsanevakis, S. & Kaberi, H., 2009. Use of Enrichment Factors for the Assessment of Heavy Metal Contamination in the Sediments of Koumoundourou Lake, Greece. *Water Air and Soil Pollution,* pp. 204: 243-258.

Karagiannidi, T., Papaefthymiou, H. & Papatheodorou, G., 2009. Radioactive impact of a bauxite beneficiation plant in the Itea Gulf (Gulf of Corinth, Greece). *Journal of Radioanalytical and Nuclear Chemistry ,* pp. 279: 923-934.

Kelepertsis, A., Argyraki, A. & Alexakis, D., 2006. Multivariate statistics and spatial interpretation of geochemical data for assessing soil contamination by potentially toxic elements in the mining area of Stratoni, north Greece. *Geochemistry, Exploration, Environment, Analysis,* pp. 6:349-355.

Kelepertzis, E., 2013. Heavy metals baseline concentrations in soft tissues of Patella sp. from the Stratoni coastal environment, NE Greece. *Ecological Chemistry and Engineering S-Chemia,* pp. 20: 141-149.

Kelepertzis, E., Argyraki, A. & Daftsis, E., 2012. Geochemical signature of surface water and stream sediments of a mineralized drainage basin at NE Chlkidiki, Greece: a pre-mining survey. *Journal of Geochemical Exploration,* pp. 114:70-81.

Kerfoot, W. et al., 2004. Local, regional and global implications of elemental mercury in metal (copper, silver, gold and zinc) ores: insights from Lake Superior sediments. *Journal of Great Lakes Research,* pp. 30: 162-184.

Komnitsas, K., Xenidis, A. & Adam, K., 1995. Oxidation of pyrite and arsenopyrite in sulphidic spoils in Lavrion. *Minerals Engineering,* pp. 8:1443-1454.

Kontopoulos, A., Komnitsas, K., Xenidis, A. & Papassiopi, N., 1995. Environmental characterisation of the sulphidic tailings in Lavrion. *Minerals Engineering,* pp. 8: 1209-1219.

Krishnaswami S., B. L. A. R. V. D. K., 1980. Atmospherically-derived radionuclides as tracers of sediment mixing and accumulation in near-shore marine and lake sediments: evidence form 7Be, 210Pb and 239,240Pu. *Easrt and Planetary Science Letters,* pp. 47:307-318.

Krishnaswamy S, Lal D, Martin JM, Maybeck M, 1971. Geochronology of lake sediments. *Earth and Planetary Science Letters,* pp. 11:407-414.

Kusin, F. et al., 2017. The occurrence and potential ecological risk assessment of bauxite mine-impacted water and sediments in Kuantan, Pahang, Malaysia. *Environ Sci Pollut Res,* pp. 24: 1306-1321.

Larsen, T., Kristensen, J., Asmund, G. & Bjerregeerd, P., 2001. Lead and zinc in sediments and biota from Maarmorilik, west Greenland: an assessment of the environmental impact of mining wastes on an Arctic fjord system. *Environmental Pollution ,* pp. 114: 275-283.

Lazaridou-Dimitriadou, M., Koukoumides, C., Lekka, E. & Gaidagis, G., 2004. Integrative evaluation of the ecological quality of metalliferous streams (Chalkidiki, Macadonia, Hellas). *ENvironmental Monitoring and Assessment,* pp. 90: 59-86.

Liang, J. et al., 2017. Spatial variation and assessment of heavy metal and radioactive risk in Farmland around a retired uranium mine. *IOP Conference Series: Earth and Environmental Science,* p. 78: 012005.

Li, Y., Wang, Y., Gou, X. & Su, Y. W., 2006. Risk assessment of heavy metals in soils and vegetables around non-ferrous metals mining and smelting sites. *Journal of environmental sciences,* pp. 18: 1124-1134.

Li, Z. et al., 2014. A review of soil heavy metal pollution from mines in China: Pollution and health risk assessment. *Science of the Total Environment,* pp. 468-169: 843-853.

Maanan, M. et al., 2015. Environmental and ecological risk assessment of heavy metals in sediments of Nador lagoon, Morocco. *Ecological Indicators ,* pp. 48: 616-626.

Mermier, P. & Seldon, E., 1969. Physics of Nuclei and Particles. In: *Physics of Nuclei and Particles.* New York: Acadenic Press, p. 274.

Michalopoulou, V., 2014. *Study of radioactivity levels and heavy metal concentrations in coastal areas of Lavrio.* Athens: (Bachelor thesis), National Technical University of Athens.

Michalopoulou, V. et al., 2015. *Measurement of radionuclides and heavy metals concentration in surface sediments from the coastal zone of Lavreotiki peninsula.* Ioannina, s.n.

Mitas, L. & Mitasova, H., 1988. General Variational Approach to the Interpolation Problem. *Computer and Mathematics with Applications,* pp. 16:983-992.

Muller G, 1979. Schwermetalle in den Sedimenten des Rheins. *Veranderungen seit 1971. Umschau,* pp. 79:778-783.

Navarro, M. et al., 2008. Abandoned mine sites as a source of contamination by heavy metals: A case study in a semi-arid zone. *J Geochem Explor. ,* pp. 96: 183-193.

Njinga, R. & Tshivhase, V., 2017. The impact of mine tailings on the Witwatersrand and the surrounding water bodies in Gauteng Province, Soutn Africa. *Mine Water and the Environment,* pp. 36:638-643.

Noli, F. & Tsamos, P., 2018. Seasonal variations of natural radionuclides, minor and trace elements in lake sediments and water in a lignite mining area of North-Western Greece. *Environmental Science and Pollution Research,* p. 25: 12222–12233.

OMEE, O. M. o. E. a. E., 1993. *Guidelines for the Protection and Management of Aquatic Sediment Quality in Ontario.*. Ontario: Ministry of Environment and Energy. ISBN0-7778-9248-7.

Papadopoulos, A. et al., 2013. Radioactive secular equilibrium in 238U and 232Th series in granitoids from Greece. *Applied Radiation and Isotopes* , pp. 116: 22-33.

Papaefthymiou, H. et al., 2013. Uranium and other natural radionuclides in the sediments of a Mediterranean fjord-like embayment, Amvrakikos Gulf (Ioanian Sea). *Journal of Environmental Radioactivity,* pp. 122: 43-54.

Pappa, F. et al., 2016. Radioactivity and metal concentrations in marine sediments associated with mining activities in Ierissos Gulf, North Aegean Sea, Greece. *Applied Radiation and Isotopes,* pp. 116:22-33.

Pappa, F. et al., 2016. Radioactivity and metal concentrations in marine sediments associated with mining activities in Ierissos Gulf, North Aegean Sea, Greece.. *Applied Radiation and Isotopes,* pp. 116:22-33.

Pappa, F. et al., 2018. Historical trends and assessment of radionuclides and heavy metals in sediments near an abandoned mine, Lavrio, Greece. *Environmental Science and Pollution Research.*

Parliament, D. 2. o. t. E., 2013. *Official Journal of the European Union I., 226/1-17.* [Online]
Available at: http://data.europa.eu/eli/dir/2013/39/oj

Patiris, D. et al., 2016. Activity concentration and spatial distribution of radionuclides in marine sediments close to the estuary of Shatt al-Arab/Arvand Rud River, the Gulf. *Journal of Environmental Radioactivity,* pp. 157:1-15.

Pavlovic, G. et al., 2005. Use of fallout 137Cs for documenting the chronology of overbank sediments from the river Sava, Croatia, and interpreting their geochemical patterns. *Environmental Geology,* pp. 47: 475-481.

Perissoratis, C. & and Mitropoulos, D., 1989. Late quaternary evolution of the northern Aegean Shelf. *Quaternary Research,* pp. 32:36-50.

Persianis, D., Katsikis, J. & Karageorgiou, D., 2010. *The genetic hypothesis of the uraniferus mineralization, eastern Chalkidiki (Northern Greece).* Patra, Bulletin of the Geological Society of Greece.

Radakovitch O, Charmasson S, Arnaud M, Bouisset P, 1999. 210Pb and caesium accumulation in the Rhone delta sediments. *Estuarine, Coastal and Shelf Science,* pp. 48:77-92.

Razo, I., Carrizales, L., Castro, J. & Diaz-Barriga, F., 2004. Arsenic and heavy metal pollution of soil, water and sediments in a semi-arid climate mining area in Mexico. *Water, Air and Soil Pollution,* pp. 152: 129-152.

Riba, I., DelValls, T., Forja, J. & Gomez-Parra, A., 2002. Influence of the Aznalcollar mining spill on the vertical distribution of heavy metals in sediments from the Guadalquivir estuary (SW Spain). *Marine Pollution Bulletin,* pp. 44: 39-47.

Rose CL, McKay WA, Toole J, 1994. The use of the 234Th/238U disequilibrium in studying surf-zone sediment processes in the eastern Irish Sea. *Marine Environmental Research,* pp. 37:393-416.

Rose, C., McKay, A. & Toole, J., 1994. The use of the 234Th/238U disequilibrium in studying surf-zone sediment processes in the eastern Irish Sea. *Marine Environmental Research,* pp. 37: 393-416.

Rowan, J. et al., 1995. Geomorphology and pollution: the environmental impacts of lead mining, Leadhills, Scotland. *Journal of Geochemical Exploration,* pp. 52: 57-65.

Ruiz-Fernandez, A. & Hillaire-Marcel, C., 2009. 210Pb-derived ages for the reconstruction of terrestrial contaminant history into the Mexican Pacific coast: Potential and limitations.. *Marine Pollution Bulletin ,* pp. 59:134-145.

Saidu, A. & Bala, A., 2018. Assessment of the specific activity of alpha- and beta-emitting radionuclides in groundwater, Anka, Nigeria. *Iranian Journal of Medical Physics,* pp. 15: 285-294.

Sakellariadou, F., 1987. *Geochemistry of nearshore sediments from the North Aegean Sea, Greece.* s.l.:(PhD theis) Imperial College, University of London, pp.376.

Salomons W & Forstner U, 1984. *Metals in the hydrocycle.* Berlin Heidelberg: Springer-Verlag.

Salomons, W., 1995. Environmental impact of metals derived from mining activities: Processes,predictions, prevention. *Journal of Geochemical Exploration,* pp. 123: 5-23.

Sanchez-Cabeza, J. & Ruiz-Fernandez, A., 2012. 210Pb sediment radiochronology: An integrated formulation and classification of dating models. *Geochimica Cosmochimica Acta,* p. 82: 183–200.

Shepard, D., 1968. *A two-dimensional interpolation function for irregularly-spaced data.* s.l., s.n., pp. 517-524.

Shukurov, N. et al., 2014. Coupling geochemical, mineralogical and microbiological approaches to assess the health of contaminated soil around the Almalyk mining and smelter complex. *Science of the Total Environment,* pp. 476-477: 447-459.

Spencer, K., Cundy, A. & Croudace, I., 2003. Heavy metal distribution and early-diagenesis in salt marsh sediments from the Medway Estuary, Kent, UK, Estuar. *Estuarine, Coastal and Shelf Science,* pp. 57: 43-54.

Stamatis, G., Voudouris, K. & Karefilakis, F., 2001. Groundwater pollution by heavy metals in historical mining area of Lavrio, Attica, Greece. *Water Air Soil Pollut,* pp. 128: 61-83.

Stamatis, N., Ioannidou, D., Christoforidis, A. & Koutrakis, E., 2002. Sediment pollution by heavy metals in the Strymonikps and Ierissos Gulfs, North Aegean Sea, Greece. *Environmental Monitoring and Assessment,* pp. 80:33-49.

Sylaios, G., Koutrakis, E. & Kallianotis, A., 2006. Hydrographic variability, nutrient distribution and water mass dynamics in Strymonikos Gulf (Northern Greece). *Continental Shelf Research,* pp. 26:217-235.

Szarlowicz, K., Reczynski, W., Misiak, R. & Kubica, B., 2013. Radionuclides and heavy metal concentrations as complementary tools for studying the impact of industrialization on the environment. *Journal of Radioanalytical and Nuclear Chemistry* , pp. 298: 1323-1333.

Thompson PA, Kurias J, Mihok S, 2005. Derivation and use of sediment quality guidelines for ecological risk assessment of metals and radionuclides released to the environment from uranium mining and millng activities in Canada. *Environmental Monitoring and Assessment,* pp. 110: 71-85.

Tomlinson DL, Wilson JG, Harris CR, Jeffrey DW, 1980. Problems in the assessment of heavy-metal levels in estuaries and the formation of a pollution index. *Helgolander Meeresunters,* pp. 33:566-575.

Tsabaris, C. et al., 2008. An autonomous in situ detection system for radioactivity measurements in the marine environment. *Applied Radiation and Isotopes,* pp. 66: 1419-1426.

Tsabaris, C. & Ballas, D., 2005. On line gamma-ray spectrometry at open sea. *Applied Radiation and Isotopes,* pp. 62: 83-89.

Tsabaris, C. et al., 2012a. Distribution of Natural Radioactivity in sediment cores from Amvrakikos Gulf (Western Greece) as part of IAEA's campaign in Adriatic and Ionian Seas. *Radiation Protection Dosimetry,* pp. 150:474-487.

Tsabaris, C. et al., 2012b. Determination of 137Cs activities in surface sediments and derived sediment accumulation rates in Thessaloniki Gulf, Greece. *Environmental Earth Science,* pp. 67: 833-843.

Tsoulfanidis, N. & Landsberger, S., 2015. *Measurement and detection of radiation.* New York: CRC Press, Taylor and Francis Group.

Ulanovsky, A. & Prohl, G., 2006. A practical method for assessment of dose conversion coefficients for aquatic biota. *Radiation and Environmental Biophysics,* pp. 45:203-214.

Ulanovsky, A., Prohl, G. & Gomez-Ros, J., 2008. Methods for calculating dose conversion coefficients for terrestrial and aquatic biota. *Journal of Environmental Radioactivity,* pp. 99:1440-1448.

United Nations Scientific Committee on the effects of Atomic Radiation (UNSCEAR), 1996. *Sources and effects of ionising radiation,* New York: United Nations.

United Nations Scientific Committee on the effects of Atomic Radiation (UNSCEAR), 2000. *Sources and effects of ionizing radiation.* New York: Report to general assembly with scientific annexes, United Nations.

United States Environmental Protection Agency (USEPA), 1999. *The Kd model,methods of measurement and application of chemical reaction codes, Vol 1,* Washington: Office of Air and Radiation.

United States Environmental Protection Agency (USEPA), 2000. *Prediction of sediment toxicity using consensus-based freshwater sediment quality guidelines.* s.l.:EPA 905/R-00/007.

Vaalgmanaa, S. & Korhola, A., 2007. Geochemical signatures of two different coastal depositional environments within the same catchment. *Journal of Paleolimnology,* pp. 38: 241-260.

Vallete-Silver, N., 1933. The use of sediment core to reconstruct historical trends in contamination of estuarine and coastal sediments. *Estuaries,* pp. 16: 577-588.

Van Grieken RE & Markowicz AA, 2002. *Handbook of X-ray spectrometry.* New York: Marcel Dekker Inc..

Vidmar, T., 2005. EFFTRAN— a Monte Carlo efficiency transfer code for gamma-ray spectrometry.. *Nuclear Instruments and Methods A,* pp. 550: 603-608.

Vidmar, T., Kanisch, G. & Vidmar, G., 2011. Calculation of true coincidence summing corrections dor extended sources with EFFTRAN. *Applied Radiation and Isotopes,* pp. 69: 908-911.

Villa, M., Manjon, G., H. & Garcia-Tenorio, R., 2011. Uranium pollution in an estuary affected by pyrite acid mine drainage and releases of naturally occurring radioactive materials. *Marine Pollution Bulletin,* pp. 62: 1521-1529.

Wedepohl, K., 1995. The composition of the continental crust. *Geochimica Cosmochimica Acta ,* pp. 59: 1217-1232.

Wennrich R, Mattusch J, Morgenstem P, Freyer K, Treutler HC, Stark HJ, Bruggemann L, Paschke A, Daus B, Weiss H, 2004. Characterization of sediments in an abandoned mining area; a case study of Mansfeld region, Germany. *Environmental Geology,* pp. 45: 818-833.

Xenidis, A., Papassiopi, N. & Komnitsas, K., 2003. Carbonate-rich mining tailings in Lavrion: risk assessment and proposed rehabilitation schemes. *Advances in Environmental Research,* pp. 7: 479-494.

Yellishetty, M., Ranjith, P. & Kumar, D., 2009. Metal concentrations and metal mobility in saturated mine wastes in mining areas of Goa, India. *Resources, Conservation and Recycling,* pp. 53: 379-385.

Zotiadis, V. & Kelepertzis, A., 1997. *Pollution of bottom sediments from the Aegean region south-eat of the Lavreotiki Peninsula, as an impact of the mining activity of Lavrion sulfide deposits, Greece.* Balkema, Rotterdam, Marinos, Koukis, Tsiambaos & Stoumaras (eds).

Annexes

I. Quality Assurance and Quality Control (metals)

Metal measurements

The measurement validation for trace metal and major element concentrations was performed by the reference materials MESS-2 and PACS-2 provided by the National Research Council of Canada. Table I-1 presents the differences between the measured (HCMR lab) and reference values of PACS-2 for some of the elements of interest.

Table I-1 The comparison between the measured and certified values, verifying the quality of the measurement with the XRF system of HCMR.

Trace metal concentrations (μg g^{-1})					
	Measured value	**Uncertainty***	**Reference value**	**Uncertainty**	**|z| score**
As	27.0	1.4	26.2	1.5	0.4
Co	11.0	0.6	11.5	0.3	0.8
Cr	94	3	90.7	4.6	0.6
Cu	291	4	310	12	1.5
Mn	432	5	440	19	0.4
Mo	6.0	0.2	5.43	0.2	1.9
Ni	39.0	1.3	39.5	2.3	0.2
Pb	172	3	183	8	1.3
Sb	11.0	0.6	11.3	2.6	0.1
Sn	21.0	1.1	19.8	2.5	0.4
Sr	265	2	276	30	0.4
V	130	2	133	5	0.6
Zn	354	6	364	23	0.4
Major element concentrations (%)					
	Measured value	**Uncertainty***	**Reference value**	**Uncertainty**	**|z| score**
Fe_2O_3	5.66	0.05	5.85	0.08	2.0
CaO	3.04	0.03	2.8	0.3	1.2
Ti_2O	0.693	0.009	0.74	0.05	0.9
Al_2O_3	12.39	0.12	12.5	0.6	0.2
K_2O	1.40	0.04	1.49	0.06	1.2
MgO	2.39	0.04	2.4	0.2	0.2
Na_2O	4.3	0.4	5.0	0.3	1.5
P_2O_5	0.203	0.005	0.22	0.01	1.5
SO_3	2.72	0.12	3.2	0.3	1.5
Si_2O	99.5	0.2	99.8	0.2	1.2

*The uncertainty of the measured values is the standard deviation of the method and laboratory reproducibility

II. Full Energy Peak Efficiency (FEPE) Values

The FEPE values for all the detection systems (HCMR, NTUA and NSCR) are presented below in Table II-1. The values were corrected regarding True Coincidence Summing (TCS) and self-attenuation effects. The final values describe a source of big geometry (65 cm^3), filled with a sediment-like sample of 1.2 g cm^{-3}.

Table II-1 The corrected FEPE values for True Coincidence Summing and self-attenuations effects for all utilized detection systems.

		HCMR_3700V				HCMR_2700 V				NTUA_3500 V				NCSR_5000 V			
			corrections				corrections				corrections				corrections		
Radionuclide	Energy (keV)	FEPE	TCS	EF	final	FEPE	TCS	EF	final	FEPE	TCS	EF	final	FEPE	TCS	EF	final
^{231}Th	**25.6**	0.0361	1.0000	1.1295	0.0407	-	-	-	-	-	-	-	-	-	-	-	-
^{152}Eu	**45.5**	0.0643	1.0000	0.5684	0.0365	0.0959	1.0000	0.5683	0.0545	-	-	-	-	0.0778	1.0000	0.5993	0.0466
^{210}Pb	**46.5**	0.0702	1.0000	1.0590	0.0743	0.0873	1.0000	0.9669	0.0844	-	-	-	-	0.0824	1.0000	1.0593	0.0873
^{234}Th	**63.3**	0.0815	1.0338	1.0348	0.0872	0.1193	1.0348	0.9732	0.1202	0.0071	1.0000	1.0642	0.0076	0.1238	1.0000	1.0354	0.1282
^{234}Th	**92.5**	0.1082	1.0016	1.0210	0.1107	0.1079	1.0016	0.9767	0.1056	0.0457	1.0000	1.0468	0.0478	0.1101	1.0000	1.0208	0.1124
^{152}Eu	**121.8**	0.1061	1.4204	0.8112	0.1222	0.1054	1.4169	0.8115	0.1212	0.0680	1.1440	0.8201	0.0638	0.1267	1.1631	0.8202	0.1208
^{235}U	**143.8**	0.0984	1.0659	1.0139	0.1063	0.1478	1.0679	0.9781	0.1544	0.0572	1.0079	1.0375	0.0598	0.1233	1.0083	1.0129	0.1260
^{235}U	**163.3**	0.0965	1.0341	1.0124	0.1010	0.1263	1.0353	0.9784	0.1280	0.0705	1.0029	1.0356	0.0732	0.1421	1.0031	1.0113	0.1441
^{235}U	**185.7**	0.0872	1.0380	1.0111	0.0915	0.1083	1.0389	0.9786	0.1102	0.0608	1.0079	1.0337	0.0633	0.1234	1.0083	1.0099	0.1256
^{235}U	**205.3**	0.0871	0.9937	1.0101	0.0874	0.1275	0.9936	0.9787	0.1240	0.0712	1.0018	1.0325	0.0736	0.1172	1.0020	1.0088	0.1185
^{227}Th	**236.0**	0.0644	1.1547	1.0088	0.0750	0.1001	1.1556	0.9789	0.1132	0.0711	1.0095	1.0308	0.0740	0.1164	1.0105	1.0075	0.1185
^{152}Eu	**244.7**	0.0527	1.6635	0.8570	0.0752	0.0565	1.6610	0.8573	0.0804	0.0544	1.1963	0.8633	0.0562	0.0699	1.2180	0.8626	0.0734
^{152}Eu	**344.3**	0.0531	1.1250	0.8735	0.0522	0.0558	1.1229	0.8738	0.0548	0.0467	1.0958	0.8793	0.0450	0.0814	1.1080	0.8786	0.0793
^{152}Eu	**778.9**	0.0242	1.1977	0.9087	0.0264	0.0247	1.1952	0.9090	0.0269	0.0240	1.1336	0.9133	0.0249	0.0424	1.1488	0.9128	0.0445
^{152}Eu	**867.4**	0.0146	1.7817	0.9130	0.0238	0.0161	1.7804	0.9133	0.0261	0.0212	1.2218	0.9174	0.0238	0.0269	1.2423	0.9169	0.0307
^{152}Eu	**964.1**	0.0161	1.4700	0.9170	0.0217	0.0169	1.4711	0.9173	0.0228	0.0217	1.0845	0.9214	0.0217	0.0309	1.0905	0.9208	0.0311
^{234}Th	**1001.0**	0.0186	1.0261	0.9977	0.0190	-	-	-	-	0.0293	0.9945	1.0168	0.0297	0.0404	0.9939	0.9969	0.0400
^{152}Eu	**1085.8**	0.0175	1.0714	0.9215	0.0173	0.0202	1.0721	0.9219	0.0200	0.0229	0.9386	0.9257	0.0199	0.0398	0.9371	0.9253	0.0345
^{152}Eu	**1112.1**	0.0142	1.3881	0.9225	0.0182	0.0159	1.3901	0.9228	0.0204	0.0205	1.0397	0.9265	0.0198	0.0308	1.0406	0.9260	0.0297
^{152}Eu	**1408.0**	0.0110	1.4189	0.9309	0.0145	0.0126	1.4208	0.9312	0.0167	0.0166	1.0589	0.9346	0.0164	0.0247	1.0615	0.9342	0.0245
^{40}K	**1460.8**	0.0128	1.0081	0.9715	0.0125	0.0157	1.0126	0.9716	0.0154	0.0160	1.0000	0.9733	0.0155	0.0323	1.0000	0.9731	0.0314

III. Quality Assurance and Quality Control (radionuclides)

The measurement validation for activity concentrations was performed by the reference material IAEA-385 provided by the International Atomic Energy Agency. Table III-1 presents the differences between the measured (HCMR lab) and reference values of IAEA-385 for some of the elements of interest

Radionuclide measurements

Table III-1 The comparison between the measured and certified values, verifying the quality of the measurement with the HPGe system of HCMR.

Radionuclide	**Measured value**	**Uncertainty**	**Reference value**	**Uncertainty**	**|z| score**
^{40}K	591.1	5.3	611	11	1.6
^{137}Cs	27.8	0.4	26.54	1	1.1
^{208}Tl	10.7	0.3	11.6	2.1	0.4
^{212}Bi	36.0	0.9	34.2	3.1	0.6
^{212}Pb	35.1	0.6	37.3	3	0.7
^{214}Bi	18.7	0.3	19.6	1.1	0.8
^{214}Pb	18.4	0.3	21.6	1.2	2.6
^{226}Ra	23.3	1.9	22.7	1.1	0.3
^{228}Ac	35.3	0.4	31.5	1.4	2.6
^{235}U	1.5	0.2	1.36	0.14	0.3

IV. Minimum Detectable Activity Codes (MDA)

The graphs of Mininimum Detectable Activity (MDA), for all the used detection systems (see Fig. 4.7) were calculated as shown below. The utilized columns were: col(1) the number of channels, col(2) the calculated energies (in keV), col(3) the counts of each channel, col(4) the determined efficiency for each channel and col(5) the estimated FWHM for each energy peak.

	Energy Calibrat.	**FWHM**	**FEPE**	**MDA**

HCMR 2700 V	a=8.796
	b=0.4311
	c=-4.35e-10
	x=col(1)
	y=a+b*x+c*x^2
	put y into col(2)
		a=1.1376
		b=0.0006
		x=col(2)
		y=a+b*x
		put y into col(5)
			a=19.93522
			b=2.051604
			c=524.6653
			d=3.03268
			x=col(2)
			y=a*x^b/(1000*c+x^d)
			put y into col(4)
				calib=0.4311 'calibr. constant
				time=79200 'measurement time
				mass=0.075 'kg bgr sample mass
				for i = 2 to 4095 do
				de(i)=cell(5,i)*3
				N(i)=de(i)/calib
				sum1=cell(3,i-1)
				sum2=cell(3,i+1)
				bgr=(sum1+sum2)*N(i)/2
				mda1=2.71+4.65*sqrt(bgr)
				mda=mda1/(cell(4,i)*time)
				cell(6,i)=mda/mass
				end for

HCMR 3700 V	a=11,182
	b=0,3635
	c=-6e-8
	x=col(1)
	y=a+b*x+c*x^2
	put y into col(2)
		a=2.7649
		b=0.0006
		x=col(2)
		y=a+b*x
		put y into col(5)
			a=22.6363
			b=1.57882
			c=137.06339
			d=2.59988
			x=col(2)
			y=a*x^b/(1000*c+x^d)
			put y into col(4)
				calib=0,3635'calibr. constant
				time=86400 'measurement time
				mass=0,075 'kg bgr sample mass
				for i = 2 to 4095 do
				de(i)=cell(5;i)*3
				N(i)=de(i)/calib
				sum1=cell(3;i-1)
				sum2=cell(3;i+1)
				bgr=(sum1+sum2)*N(i)/2
				mda1=2.71+4.65*sqrt(bgr)
				mda=mda1/(cell(4;i)*time)
				cell(7;i)=mda/mass
				end for

	Energy Calibrat.	FWHM	FEPE	MDA

NTUA 3500 V	a=6.6055
	b=0.4355
	c=-7.08e-8
	x=col(1)
	y=a+b*x+c*x^2
	put y into col(2)
		a=1.2595
		b=0.0018
		x=col(2)
		y=a+b*x
		put y into col(5)
			a=0.00291
			b=20.20692
			c=-1973.55688
			d=45147.20677
			x=col(2)
			y=a+(b/x)+(c/x^2)+(d/x^3)
			put y into col(4)
				calib=0.4355 'calibr. constant
				time=90000 'measurement time
				mass=0.075 'kg bgr sample mass
				for i = 2 to 4095 do
				de(i)=cell(5,i)*3
				N(i)=de(i)/calib
				sum1=cell(3,i-1)
				sum2=cell(3,i+1)
				bgr=(sum1+sum2)*N(i)/2
				mda1=2.71+4.65*sqrt(bgr)
				mda=mda1/(cell(4,i)*time)
				cell(6,i)=mda/mass
				end for

NCSR 5000 V	a=1.2705
	b=0.5256
	c=-2e-18
	x=col(1)
	y=a+b*x+c*x^2
	put y into col(2)
		a=1.4426
		b=0.0009
		x=col(2)
		y=a+b*x
		put y into col(5)
			a=5.007296
			b=2.099415
			c=100
			d=2.817371
			x=col(2)
			y=a*x^b/(1000*c+x^d)
			put y into col(4)
				calib=0.5256 'calibr. constant
				time=86400 'measurement time
				mass=0.075 'kg bgr sample mass
				for i = 2 to 4095 do
				de(i)=cell(5,i)*3
				N(i)=de(i)/calib
				sum1=cell(3,i-1)
				sum2=cell(3,i+1)
				bgr=(sum1+sum2)*N(i)/2
				mda1=2.71+4.65*sqrt(bgr)
				mda=mda1/(cell(4,i)*time)
				cell(6,i)=mda/mass
				end for

AUTH 3100 V	a=3.1675
	b=0.1954
	c=-5e-6
	x=col(1)
	y=a+b*x+c*x^2
	put y into col(2)
		a=0.4578
		b=0.0025
		x=col(2)
		y=a+b*x
		put y into col(5)
			a=0.0409
			b=0.0006
			c=-0.000002
			x=col(2)
			y=a+b*x+c*x^2
			put y into col(4)
				calib=0.1954 'calibr. constant
				time=253030 'measurement time
				mass=0.075 'kg bgr sample mass
				for i = 2 to 2014 do
				de(i)=cell(5,i)*3
				N(i)=de(i)/calib
				sum1=cell(3,i-1)
				sum2=cell(3,i+1)
				bgr=(sum1+sum2)*N(i)/2
				mda1=2.71+4.65*sqrt(bgr)
				mda=mda1/(cell(4,i)*time)
				cell(6,i)=mda/mass
				end for

V. Relative uncertainty values

The relative uncertainties of radioactivity, trace metal and major element concentrations for all the measured samples are presented in Table V-1. The differences in the relative uncertainties of radioactivity measurement are attributed to the different relative efficiencies of the detection systems, the shielding sourrounding them and the masses of the samples (e.g. the sediment samples of core 2 were of "small" geometry, meaning ~9 gr).

Table V-1. The relative uncertainties (%) of radioactivity, trace metal and major element concentrations. The title "surface" refer to surface seafloor samples, while STR 1, STR 8, core 1 and core 2 refer to core sediments of Stratoni and Lavrio.

		Ierissos Gulf			**Lavrio**		
		surface	**STR 1**	**STR 8**	**surface**	**core 1**	**core 2**
Radioactivity	^{210}Pb	20	12	-	10	24	-
	^{234}Th	7	-	-	13	-	27
	^{226}Ra	6	2	7	7	9	18
	^{214}Pb	8	4	9	6	12	31
	^{214}Bi	8	5	11	11	16	14
	^{228}Ac	7	12	11	9	16	30
	^{212}Pb	11	15	14	11	20	-
	^{212}Bi	18	25	23	16	28	-
	^{208}Tl	13	17	17	9	20	32
	^{235}U	9	13	10	13	21	-
	^{137}Cs	21	29	20	21	22	-
	^{40}K	9	6	11	7	11	6
Trace metals	As	12					
	Cu	9					
	Pb	5					
	Zn	5					
Major elements	Mn	5					
	Fe	5					
	Al	5					

VI. Measured data of all trace metals and major elements

The values of all measured trace metals in the surface samples of Ierissos Gulf are presented in Table VI-1.

Table VI-1 The trace metal concentrations in the surface sediments of Ierissos Gulf.

Sample name	As	Ba	Bi	Br	Ce	Cr	Cu	Hf	La	Mo	Nd	Ni	Pb	Rb	Sb	Sc	Sr	Th	V	Y	Zn	Zr
	($\mu g\ g^{-1}$)																					
STR 1	1696	447	-	20.0	86	70	145	20	22.0	3.7	19	20	1945	102	43	11	165	7	83	20	2853	90
STR 1_a	1512	376	15.8	19.3	962	70	138	24.8	21.9	3.9	57	25	1221	95	59	13	119	13	58	16	3855	50
STR 1_b	798	461	9.7	2.0	280	54	83	11.6	23.5	3.4	18	16	1139	122	49	11	159	10	56	14	1949	72
STR 2	928	425	11.8	20.4	425	61	71	10.6	20.6	3.7	48	23	957	118	42	12	245	17	81	14	1328	70
STR 2_a	533	434	14.4	6.9	168	62	110	11.9	20.5	3.2	27	25	597	120	35	6	145	10	36	10	1268	63
STR 2_b	573	351	15.5	6.7	439	63	119	14.5	12.7	4.0	38	26	828	112	40	9	125	11	49	12	1903	61
STR 2_b2	4289	344	31.8	3.4	2269	85	304	24.9	22.6	4.9	49	16	1752	72	58	12	97	7	70	14	3838	76
STR 3	1349	435	11	20.0	106	59	73	16.6	10.5	3.5	8	6	1295	101	35	11	179	9	57	15	1592	74
STR 4	920	428	7.7	38.0	258	58	66	8.6	14.8	4.2	27	21	1231	101	31	12	202	10	68	15	1192	60
STR 5	15	323	1.8	20.4	27	75	5	6.2	10.3	0.5	15	41	29	72	4	7	383	14	37	11	22	46
STR 6	814	365	11.9	20.8	75	64	115	15.1	6.1	3.4	10	18	884	110	31	9	170	14	69	13	1375	59
STR 7	1074	321	14.8	20.4	77	180	121	17.3	11.5	3.2	18	47	813	81	37	18	158	16	117	14	1454	68
STR 10	393	255	5.9	22.1	70	280	71	13.8	21.4	4.1	24	126	723	70	44	19	134	13	147	28	673	140
STR 10_1a	219	250	2.1	3.6	35	143	32	8.2	4.7	1.7	9	62	395	67	26	7	90	9	63	11	571	60
STR 10_1b	318	282	2.3	2.7	47	196	50	12.7	11.8	2.3	11	85	654	70	42	13	108	10	97	16	888	73
STr 10_1b2	979	278	6.1	1.8	96	423	94	12.1	16.9	3.2	15	89	2579	57	163	16	140	7	144	30	1142	68
STr 10_2a	264	318	2.1	4.9	66	475	79	10.5	15.6	2.3	22	279	511	84	29	17	109	11	124	22	953	92
STR 10_2b	295	339	4	14.6	83	806	132	9.3	30.6	1.8	34	525	496	99	27	25	82	13	160	30	420	84
STR 13_a	111	212	2.7	7.1	23	93	16	7.6	3.8	1.3	10	39	252	56	13	7	84	11	51	10	266	51
STR 13_b	140	201	3.1	4.8	28	114	18	4.5	9.9	1.3	12	46	279	55	16	6	89	8	61	12	336	55
STR 11	8	353	4.3	21.4	18	21	1	4.3	9.2	0.5	8	7	36	108	3	4	385	14	13	7	10	71
STR 11_0a	8	536	1.7	15.2	76	21	7	3.8	4.9	-	27	8	38	108	2	2	392	30	0	7	6	83
STR 11_0b	8	593	2.8	4.0	29	-2	4	6.4	1.8	-	-	5	32	106	2	1	340	9	4	2	4	33
STR 11_1a	18	528	2.7	11.3	43	30	11	4.6	13.4	0.9	13	17	54	103	2	4	358	18	16	6	96	62
STR 11_1b	783	427	10	2.6	586	53	91	15.5	14.3	3.8	55	28	1102	120	44	10	159	10	47	12	1762	59
STR 11_2a	10	541	3.4	2.5	20	8	9	6.2	-	-	9	13	41	111	3	2	370	12	6	3	10	36
STR 11_2b	9	505	2.2	1.8	29	8	4	7.3	7.8	-	9	9	36	111	2	0	371	10	6	3	8	33
STR 12	14	240	2.7	20.1	65	39	6	4.6	13.6	1.2	25	8	38	56	3	5	300	14	8	11	17	57
STR 12_b	12	617	2.6	3.5	33	9	6	3.5	6.5	-	-	6	33	90	3	4	322	9	-	4	8	32

The values of all measured major elements in the surface samples of Ierissos Gulf are presented in Table VI-2.

Table VI-2 The major element concentrations in the surface sediments of Ierissos Gulf.

Sample name	L.O.I.	Al	Si	P	K	Ca	Ti	Fe	Na	Mg	S	Mn
	(%)											
STR 1	8.6	4.27	20.9	0.08	1.86	6.76	0.22	7.52	1.64	1.79	3.60	1.06
STR 1_a	12.5	3.63	20.1	0.04	1.54	6.64	0.18	8.19	0.81	1.78	2.59	2.65
STR 1_b	6.6	4.79	28.4	0.04	2.28	4.63	0.16	4.11	0.62	1.18	1.60	0.92
STR 2	7.0	5.43	25.7	0.05	2.13	5.18	0.24	4.86	0.99	1.51	2.00	1.07
STR 2_a	4.2	4.71	30.8	0.04	2.34	3.18	0.16	3.81	0.64	1.07	1.52	0.80
STR 2_b	7.8	4.28	26.0	0.04	1.97	5.38	0.17	4.55	0.55	1.76	2.24	1.72
STR 2_b2	20.8	2.70	14.4	0.03	1.09	2.90	0.15	20.03	0.70	1.03	2.00	0.84
STR 3	7.4	4.62	24.0	0.05	1.95	6.03	0.20	5.77	0.91	1.67	3.20	0.71
STR 4	11.2	5.10	24.8	0.05	2.02	6.28	0.19	4.77	1.16	1.61	1.00	0.58
STR 5	3.2	5.52	33.8	0.04	2.06	3.08	0.23	1.77	1.54	1.16	0.03	0.04
STR 6	8.5	4.60	26.4	0.04	2.09	5.97	0.18	4.05	0.83	1.62	1.64	1.07
STR 7	8.3	4.23	22.9	0.05	1.46	6.70	0.27	7.88	0.93	2.22	2.32	0.76
STR 10	4.1	6.23	29.9	0.06	1.39	2.13	0.64	5.83	1.24	1.94	0.12	0.46
STR 10_1a	2.0	4.80	36.5	0.03	1.44	0.86	0.25	3.00	0.66	0.95	0.03	0.35
STR 10_1b	2.7	5.11	34.6	0.03	1.48	1.28	0.31	3.99	0.69	1.20	0.03	0.58
STR 10_1b2	3.2	4.35	30.6	0.04	1.04	2.35	0.43	8.62	0.65	1.17	0.10	1.93
STR10_2a	5.9	6.43	30.3	0.04	1.60	1.64	0.35	4.75	0.79	2.33	0.03	0.38
STR 10_2b	13.0	8.73	22.0	0.06	1.47	2.27	0.42	7.11	0.48	3.76	0.05	0.27
STR 13_a	1.5	3.43	39.3	0.02	1.27	0.87	0.16	1.72	0.64	0.72	-	0.07
STR 13_b	1.6	3.69	38.6	0.02	1.25	0.96	0.20	2.12	0.68	0.84	-	0.09
STR 11	1.3	7.86	34.3	0.03	3.09	1.40	0.13	0.55	2.54	0.15	0.01	0.01
STR 11_0a	1.1	7.29	35.2	0.02	3.36	1.32	0.08	0.37	2.26	0.10	-	0.02
STR 11_0b	0.5	6.65	36.7	0.01	3.40	0.87	0.03	0.25	1.82	0.04	-	0.01
STR 11_1a	11.6	6.85	29.9	0.19	2.65	1.73	0.11	0.97	1.86	0.32	0.17	0.03
STR 11_1b	7.1	4.75	28.6	0.04	2.23	4.70	0.16	4.18	0.67	1.24	1.20	0.90
STR 11_2a	0.5	7.32	35.8	0.02	3.45	1.06	0.05	0.24	2.05	0.06	-	0.01
STR 11_2b	0.7	7.59	35.4	0.02	3.46	1.06	0.05	0.23	2.12	0.07	-	0.01
STR 12	9.3	4.66	30.1	0.03	1.73	7.46	0.17	0.66	1.56	0.79	0.01	0.04
STR 12_b	4.1	5.62	34.5	0.01	2.96	3.43	0.03	0.13	1.51	0.36	-	0.01

LOI: Loss Of Ignition

The values of all measured trace metals in the coastal sediment (STR 1) samples of Ierissos Gulf are presented in Table VI-3.

Table VI-3 The trace metal concentrations at the coastal sediment (STR 1) samples of Ierissos Gulf.

Depth (cm)	As	Ba	Br	Ce	Co	Cr	Cu	Hf	La	Mo	Nb	Nd	Ni	Pb	Rb	Sb	Sc	Se	Sr	Te	Th	V	Y	Zn	Zr
	($\mu g\ g^{-1}$)																								
1.0	1696	447	20	86	4.7	70	145	20	22	3.7	4	19	20	1945	102	43	11	7	165	4	7	83	20	2853	90
2.5	1512	451	19	74	4.8	62	125	21	16	4.0	5	6	19	1630	96	37	9	5	160	6	10	74	18	2688	82
3.5	1491	428	24	74	3.8	61	122	16	0	3.3	5	14	18	1717	96	37	11	6	155	3	9	73	18	2489	76
4.5	1554	475	15	85	2.7	64	131	17	10	3.5	6	19	19	1682	98	37	13	5	157	3	9	76	19	2595	91
5.5	1455	471	8	70	4.0	65	131	18	12	3.3	5	17	17	1601	96	38	13	4	155	6	9	72	17	2324	76
6.5	1475	457	17	75	3.8	58	119	18	12	2.9	4	14	19	1742	97	37	10	6	155	5	7	72	19	2487	90
7.5	1486	459	19	74	4.8	70	133	11	18	3.4	4	7	18	2099	99	41	9	5	151	4	7	71	19	2456	70
8.5	1415	432	21	85	2.7	63	136	17	17	3.2	4	15	19	1859	102	39	11	5	155	5	6	77	17	2361	74
9.5	1527	503	18	78	6.5	61	139	19	12	3.3	4	10	18	2610	101	42	13	7	143	4	9	70	21	2482	80
10.5	1788	497	23	105	4.1	60	231	17	9	2.6	3	12	16	4250	115	57	12	12	126	3	-	70	26	3408	72
11.5	2009	519	20	103	5.4	67	299	10	13	2.4	3	17	19	5189	125	61	13	12	119	10	-	73	29	3859	66
12.5	2159	505	20	136	5.6	65	330	15	13	2.7	2	29	18	5579	130	64	16	11	115	10	-	74	31	4052	67
13.5	2051	516	17	112	5.6	61	307	18	4	2.4	2	14	19	5338	125	57	14	12	114	-	-	69	31	3947	67
14.5	2130	523	21	115	6.2	58	323	19	9	3.0	3	24	18	5538	128	61	11	13	113	4	-	72	32	4159	65
15.5	1985	532	22	129	3.2	64	332	23	7	2.3	1	26	20	5822	127	66	15	12	115	6	-	69	32	4248	65
16.5	1673	569	26	119	6.9	61	354	19	18	1.7	1	32	17	6764	134	66	14	17	116	3	-	72	35	4297	67
17.5	1584	575	23	114	2.7	58	286	15	8	2.1	2	12	17	6193	133	102	16	15	117	6	-	66	33	3981	73
18.5	1575	593	24	108	4.3	60	305	11	20	1.5	1	16	18	6369	137	60	10	14	118	4	-	74	34	4148	69
19.5	1724	554	25	117	4.1	64	333	8	19	2.2	1	23	19	6351	135	67	15	15	116	6	-	70	34	4290	70
20.5	1528	564	29	106	3.4	55	290	13	5	2.2	2	22	19	6322	136	60	13	13	115	9	-	69	34	4020	68
21.5	1469	611	27	107	5.2	60	274	11	6	2.2	3	23	19	6518	140	63	14	15	119	10	-	72	34	4047	70
22.5	1420	576	25	91	6.2	59	249	8	11	1.9	1	19	17	6526	135	55	14	13	114	5	-	70	34	3820	70
23.5	1424	619	28	108	4.1	68	247	13	8	1.6	2	26	20	6450	145	59	13	16	123	2	-	73	34	3977	75
24.5	1431	568	25	106	5.6	61	225	12	14	2.0	3	20	18	5852	132	56	12	14	120	4	-	70	32	3781	73
25.5	1349	593	27	79	5.2	69	259	11	17	1.9	1	19	21	6176	141	55	14	11	118	8	-	71	33	3716	75

The values of all measured major elements in the coastal sediment (STR 1) samples of Ierissos Gulf are presented in Table VI-4.

Table VI-4 The major element concentrations at the coastal sediment (STR 1) samples of Ierissos Gulf.

Depth	**L.O.I**	**Al**	**Si**	**P**	**K**	**Ca**	**Ti**	**Fe**	**Na**	**Mg**	**S**	**Mn**
(cm)	**(%)**											
1.0	8.62	4.27	20.9	0.08	1.86	6.76	0.22	7.52	1.64	1.79	3.60	1.06
2.5	8.86	4.19	21.4	0.07	1.82	7.45	0.22	6.97	1.50	1.82	3.18	1.05
3.5	11.33	4.15	20.9	0.07	1.80	7.51	0.21	7.44	1.41	1.82	2.36	1.00
4.5	10.05	4.09	21.0	0.07	1.80	7.06	0.22	7.43	1.26	1.79	3.20	0.98
5.5	9.87	4.15	21.2	0.08	1.82	6.86	0.21	7.54	1.21	1.79	3.16	0.98
6.5	19.90	3.93	20.8	0.07	1.51	6.14	0.22	6.63	0.83	1.79	1.20	0.55
7.5	11.61	4.23	21.1	0.07	1.82	6.83	0.20	7.26	1.04	1.83	2.80	0.93
8.5	8.75	4.29	20.9	0.07	1.86	6.74	0.21	7.34	2.06	1.79	3.20	0.95
9.5	11.00	4.25	20.4	0.07	1.85	6.30	0.20	8.42	1.57	1.77	3.08	0.74
10.5	14.18	4.70	19.5	0.06	2.05	6.26	0.19	8.55	1.47	1.85	2.08	0.64
11.5	15.44	5.11	18.9	0.06	2.16	6.19	0.17	8.55	1.32	1.92	1.60	0.58
12.5	16.51	5.23	18.4	0.06	2.18	6.22	0.17	8.64	1.28	1.98	1.68	0.55
13.5	16.71	5.02	18.7	0.06	2.16	6.33	0.18	8.67	1.23	1.94	1.60	0.57
14.5	13.89	5.14	18.2	0.05	2.14	6.26	0.17	8.60	0.97	1.96	3.20	0.54
15.5	15.64	5.15	18.2	0.05	2.18	6.34	0.17	8.80	1.03	2.00	2.32	0.52
16.5	17.02	5.32	18.0	0.05	2.22	5.78	0.16	8.75	0.91	1.94	2.24	0.44
17.5	16.45	5.35	18.7	0.05	2.28	5.59	0.16	8.55	1.10	1.84	2.00	0.44
18.5	16.23	5.47	18.6	0.05	2.31	5.52	0.16	7.91	1.09	1.83	2.40	0.43
19.5	14.27	5.45	18.4	0.05	2.29	5.81	0.16	8.84	1.00	1.91	2.80	0.46
20.5	15.38	5.53	18.7	0.05	2.36	5.35	0.16	8.73	0.92	1.80	2.36	0.45
21.5	15.48	5.72	19.2	0.05	2.41	5.31	0.16	8.43	1.02	1.81	1.80	0.43
22.5	13.72	5.69	19.3	0.05	2.39	5.37	0.16	8.43	0.95	1.80	2.60	0.42
23.5	15.05	5.79	19.6	0.05	2.43	5.28	0.16	8.26	1.18	1.77	1.72	0.42
24.5	13.42	5.47	19.7	0.05	2.30	5.47	0.17	8.05	0.87	1.76	2.81	0.50
25.5	13.83	5.81	19.5	0.05	2.46	5.31	0.17	8.05	1.11	1.78	2.45	0.42

LOI: Loss Of Ignition

The values of all measured major elements in the offshore sediment (STR 8) samples of Ierissos Gulf are presented in Table VI-5.

Table VI-5 The trace element concentrations at the offshore sediment (STR 8) samples of Ierissos Gulf.

Depth	As	Ba	Bi	Br	Ce	Co	Cr	Cu	Hf	I	La	Mo	Nd	Ni	Pb	Rb	Sb	Sc	Se	Sr	Th	V	Y	Zn	Zr
(cm)	($\mu g\ g^{-1}$)																								
1	482	287	12.0	48	69	14.7	132	76	7	54	30	2.1	18	54	870	79	17	13	2.1	483	19	113	18	628	64
3	440	297	9.0	42	79	11.2	132	78	11	43	14	2.5	22	54	849	79	17	15	3.3	501	18	111	16	621	62
5	404	273	11.6	36	77	11.5	119	72	10	31	13	1.8	17	49	798	76	14	14	2.8	584	18	104	15	599	53
7	381	277	11.1	38	76	12.0	121	77	8	32	18	1.7	24	47	781	74	16	16	2.9	576	18	103	16	583	57
9	372	300	12.3	41	71	13.3	118	80	12	31	19	2.2	17	51	817	78	19	16	3.0	639	20	104	17	610	57
11	311	284	12.2	38	73	13.6	114	70	6	27	25	2.2	22	45	726	75	17	12	3.7	653	21	93	17	543	59
13	190	279	8.8	33	58	12.7	127	55	10	24	24	1.7	20	49	543	73	14	15	3.7	730	24	90	16	447	54
15	94	255	8.0	35	63	12.5	113	41	6	15	23	1.7	19	51	400	70	12	16	0.7	778	26	83	16	351	50
17	84	263	4.9	34	118	11.2	103	32	8	20	24	1.6	42	53	402	66	11	11	2.7	825	24	70	14	344	49
19	86	251	7.2	35	119	12.9	94	34	7	17	16	1.6	29	51	387	64	12	15	3.2	855	25	66	14	327	49
21	81	261	2.8	35	127	0.7	111	30	6	13	13	1.6	37	50	379	67	12	17	2.5	811	26	69	16	324	54
23	66	271	5.7	34	108	16.0	99	32	4	12	19	1.6	30	52	309	66	10	14	2.2	850	23	70	16	274	54
25	51	253	6.1	31	90	15.1	96	26	11	11	17	1.8	32	55	279	64	10	15	1.5	867	24	59	15	245	49
26.5	54	244	4.6	31	92	7.9	109	30	5	16	26	1.0	21	60	291	67	10	14	1.9	801	25	71	15	241	58

The values of all measured trace metals and major elements at the surface samples of Lavrio coast are presented in Table VI-6.

Table VI-6 The trace metal and major element concentrations at the surface sediments of Lavrio.

Trace metals

Sample	As	Ba	Br	Ce	Co	Cr	Cu	Hf	I	La	Mo	Nd	Ni	Pb	Rb	Sb	Sc	Sn	Sr	Te	Th	V	Y	Yb	Zn	Zr
	($\mu g\ g^{-1}$)																									
I1	53	140	31	15	3	59	8	nM	9	4	1.3	8	20	201	15	3	9	nM	859	nM	18	39	11	nM	97	5
P1	69	155	9	14	4	58	15	nM	5	6	1.4	9	24	391	22	4	12	nM	1068	nM	19	35	13	nM	181	5
I2	3382	551	38	127	10	105	121	nM	25	11	2.9	23	52	3328	34	59	17	nM	450	nM	1	152	26	nM	6944	49
P2	885	1071	-	71	13	140	117	nM	3	10	0.7	24	60	5986	25	100	13	nM	224	nM	-	83	34	nM	8077	34
I4	35	144	30	33	5	62	13	nM	7	18	2.9	19	21	122	59	2	14	nM	835	nM	17	79	15	nM	144	79
P4	34	163	5	26	5	52	12	nM	0	10	2.3	17	19	146	59	3	11	nM	636	nM	17	71	13	nM	147	70
N1	4177	553	79	71	23	92	70	137	-	10	3.5	16	22	2520	26	63	61	19	229	45	21	152	194	23	7151	13
N2	4315	465	105	72	27	109	74	121	18	25	2.7	14	29	2940	37	65	59	18	322	49	23	170	216	20	7362	5
N3	2061	353	109	47	15	89	46	103	19	40	1.8	18	21	3000	34	42	70	26	887	43	112	131	222	18	5659	-
N4	2138	432	70	42	17	97	50	87	4	12	2.4	15	24	2299	32	46	58	30	352	55	48	149	171	24	4911	5
N5	8625	1428	74	101	50	103	102	149	-	-	-	35	29	3909	23	97	57	13	136	53	-	262	283	30	12542	13

Major elements

Sample	Al	Si	P	K	Ca	Ti	Fe	Na	Mg	S	Mn
	(%)										
I4	5.05	24.8	0.01	1.47	11.0	0.31	2.4	1.81	0.93	0.16	0.03
N1	2.33	12.6	0.04	0.62	15.2	0.19	12.7	0.79	1.32	4.16	0.93
N2	1.72	12.3	0.04	0.64	15.9	0.16	12.4	1.12	1.44	3.04	0.75
N3	2.05	11.4	0.03	0.51	21.4	0.16	7.8	1.22	1.45	0.00	0.42
N4	2.16	17.5	0.03	0.77	16.3	0.17	8.0	0.76	1.16	0.72	0.50
N5	1.44	8.8	0.05	0.42	11.6	0.16	20.6	0.79	1.40	6.21	1.13

Some trace metals were measured only at samples of the second survey (code: N#), thus the "nM" describe the non-measured metals for those elements.

The values of all measured trace metals at the coastal core (core 1) sediments of Lavrio are presented in Table VI-7.

Table VI-7 The trace metal concentrations at the coastal core (core1) sediments of Lavrio.

Depth	As	Ba	Br	Ce	Cr	Cu	Hf	I	La	Mo	Nb	Nd	Ni	Pb	Rb	Sb	Sc	Se	Sr	Ta	Te	Th	V	Y	Zn	Zr
(cm)	($\mu g\ g^{-1}$)																									
1	4316	926	18.2	139	92	104	41	3.5	8		4.8	15	51	2382	34	62	18.9	4.1	249	4.1	2.5	1.2	147	25	7650	49
3	4540	712	12.5	134	107	90	45	1.6	17	0.9	4.7	8	47	2293	34	63	9	3.6	217	2.1	3.2	-	171	23	7984	53
5	4794	907	11.8	2111	90	59	41	4.1	22	0.8	4.4	69	27	2302	33	68	6	3.4	205	15.7	3.1	1.5	163	24	8307	52
7	4464	1080	13.4	710	98	52	40	6.9	24		4.4	23	26	2318	33	63	14.3	5.7	241	10.7	5.9	-	169	25	8327	51
9	4707	956	15.9	1178	88	61	47	0.2	11	0.9	5	33	166	2353	33	64	8.4	3	242	6.1	0.2	-	175	25	8370	54
11	4759	1128	13.7	2071	80	57	45	6.9	8		4.3	69	30	2348	35	65	16.1	3	241	20.4	5.6	-	173	23	8760	52
13	4756	1318	12.2	526	99	54	46	4.6	29		3.3	52	28	2387	35	64	21.9	4.8	253	16.4	1.4	-	170	24	8625	52
15	4658	833	18.6	2036	89	63	41	3.4	19	1.1	3.3	69	28	2382	32	68	13.6	3.3	196	16.5	4.9	0.4	161	25	8135	51
17	5042	803	15.3	2138	93	52	45	0.9	19	1.9	4.1	93	30	2394	33	71	14.5	4.4	190	17	6.1	0.1	187	24	9018	57
19	4530	763	11.3	1827	95	66	37	1.3	4	1.3	4.5	54	31	2322	33	67	11.3	2.1	212	15.7	1.8	5	154	24	8030	54
21	4828	1033	13.1	2043	96	53	49	4	22	0.9	4.6	69	28	2449	35	67	15.7	4.9	210	17.1	6.9	0.8	166	22	8879	62
23	4573	566	21.3	724	78	58	47	5.5	18	2.2	3.8	15	29	2534	34	65	14.4	3.7	224	11	-	3.8	168	24	8054	52
25	4881	691	15.5	1921	107	62	41	3.1	15	1.8	4.8	71	21	2581	32	70	13.2	6.4	219	12.5	3.6	1.4	163	24	8430	56
27	5200	816	17.2	1703	92	69	42	0.5	8	0.3	4.4	65	29	2945	35	73	15.5	4.9	239	23.8	3.8	-	154	26	8467	49
29	5141	577	18.9	158	85	166	48	6.6	32	1.2	4.1	29	56	3254	35	75	15.9	6.6	190	2.6	4.9	-	145	28	8943	55
31	4785	619	23.3	151	95	213	42	9.5	13	2.6	4.6	23	55	4230	34	83	17.8	6.6	185	2.2	-	-	122	32	8991	71
33	2767	420	32.7	117	100	169	43	12.4	13	2.4	2.8	26	48	4290	31	67	10.3	10.2	272	2.8	-	1.9	119	31	8343	50
35	2073	474	28.1	103	107	136	33	16.4	4	4	1.7	23	50	4785	34	77	14.3	9.3	345	0.2	1.5	-	98	32	7248	47
37	1250	367	28.1	77	103	63	34	5.6	16	7.4	3.1	27	45	3427	32	50	11.4	7.2	466	2.9	4.6	4.9	95	28	5740	34
39	1199	449	31.4	75	102	66	23	5.9	15	4.4	2.2	21	48	3316	31	43	13.3	7.9	585	2.4	2.1	6.3	87	28	5161	29
41	731	401	40.7	70	95	40	20	7.8	3	3.2	1.7	16	37	2949	29	33	12.9	5.2	627	3.6	7.4	9.4	73	25	3968	22
43	882	406	32.1	56	98	49	23	4.8	12	2.1	1.2	13	38	2769	28	31	10.5	7.5	630	1.2	3.5	9.4	75	25	3805	27
45	766	326	46.0	59	95	47	20	4.8	2	3.5	1.9	23	35	2835	28	29	11.1	5.9	630	2.2	0	9.8	75	25	3860	25
47	1176	471	29.1	71	96	49	25	3.8	5	0.8	1.9	20	37	3108	29	34	8.9	5.3	626	1.2	1.1	8.3	85	27	4501	28
49	595	357	36.3	48	91	40	21	8.2	27	2	1.4	11	37	2674	28	30	11.5	5.2	663	3.2	10.3	8	72	24	3833	23
51	497	280	35.3	59	98	36	16	8.2	13	2.2	1.6	16	38	2883	28	26	8.3	5.7	698	2.7	4.2	11	70	25	3471	24

The values of all measured major elements at the coastal core (core 1) sediments of Lavrio are presented in Table VI-8.

Table VI-8 The major elements concentrations of coastal core (core 1) sediments of Lavrio

Depth	**L.O.I**	**Al**	**Si**	**P**	**K**	**Ca**	**Ti**	**Fe**	**Na**	**Mg**	**S**	**Mn**
(cm)	**(%)**											
1	14.04	1.9	13.0	0.05	0.59	12.2	0.19	12.6	0.76	1.21	5.41	0.80
3	15.38	1.9	13.3	0.05	0.62	12.2	0.19	12.8	1.36	1.21	4.14	0.87
5	13.30	1.8	12.0	0.05	0.53	11.3	0.18	14.8	0.57	1.26	5.85	0.90
7	13.87	1.8	12.5	0.04	0.57	12.3	0.19	13.2	0.57	1.21	5.85	0.81
9	14.28	1.8	12.1	0.05	0.55	12.3	0.18	13.5	0.73	1.22	5.83	0.83
11	11.86	1.9	12.6	0.05	0.57	12.2	0.19	13.1	0.64	1.22	6.61	0.80
13	11.32	1.9	12.7	0.05	0.55	12.1	0.19	13.2	0.63	1.27	6.65	0.80
15	13.04	1.8	13.0	0.05	0.57	11.9	0.19	13.1	0.67	1.20	6.05	0.82
17	14.38	1.8	12.4	0.05	0.56	11.3	0.19	14.6	1.06	1.26	5.33	0.91
19	14.07	1.9	12.5	0.05	0.57	11.5	0.19	13.8	0.94	1.22	4.99	0.85
21	13.70	1.8	12.7	0.05	0.58	11.8	0.19	13.3	0.97	1.21	5.80	0.82
23	14.20	1.9	13.0	0.05	0.58	12.2	0.18	12.5	0.59	1.22	5.61	0.79
25	14.00	1.9	12.8	0.05	0.55	11.8	0.19	13.3	0.63	1.22	5.53	0.84
27	13.84	1.8	12.2	0.05	0.55	12.2	0.18	13.3	0.58	1.22	6.01	0.81
29	14.32	2.0	12.4	0.05	0.58	12.1	0.17	13.2	0.53	1.24	5.84	0.81
31	14.64	2.3	11.8	0.05	0.62	12.3	0.18	12.7	0.80	1.28	6.01	0.74
33	15.76	2.0	14.0	0.04	0.63	13.8	0.17	9.1	0.88	1.15	5.01	0.51
35	17.27	2.2	14.4	0.04	0.60	14.0	0.17	7.5	0.84	1.12	5.01	0.37
37	20.38	2.0	16.0	0.03	0.63	16.3	0.19	4.9	0.80	1.09	2.72	0.22
39	22.49	2.0	15.8	0.03	0.63	20.0	0.18	4.7	1.00	1.21	0.08	0.22
41	25.09	1.6	14.5	0.03	0.57	18.8	0.16	3.8	1.22	1.10	1.58	0.17
43	24.31	1.5	14.0	0.03	0.52	20.3	0.15	3.0	0.82	1.03	2.53	0.13
45	27.11	1.4	13.2	0.02	0.51	20.9	0.15	2.4	1.21	1.08	1.76	0.09
47	25.18	1.6	13.8	0.03	0.56	19.8	0.18	3.5	0.99	1.08	1.90	0.16
49	25.67	1.5	14.7	0.03	0.54	20.1	0.16	2.6	0.92	1.05	1.52	0.09

LOI: Loss Of Ignition

The values of all measured trace metals at the offshore core (core 2) sediments of Lavrio are presented in Table VI-9.

Table VI-9 The trace metal concentrations at the offshore core (core2) sediments of Lavrio.

Depth	As	Ba	Bi	Br	Ce	Co	Cr	Cu	Hf	I	La	Mn	Nd	Ni	Pb	Rb	Sb	Sc	Se	Sr	Th	V	Y	Zn
(cm)	($\mu g\ g^{-1}$)																							
1	70	42	7	81	21	4	68	19	9	47	3	443	8	33	198	28	7	11	3	2714	52	36	9	229
3	80	49	5	61	23	4	62	15	15	36	8	483	10	30	227	25	6	11	4	2704	52	29	11	255
5	69	43	7	64	15	4	61	16	14	41	-	465	13	28	213	25	6	11	2	2751	52	30	11	232
7	60	60	5	63	25	3	67	16	5	38	7	398	14	29	173	25	6	9	4	2692	54	28	12	196
9	50	36	5	60	20	3	61	14	8	35	13	318	4	26	139	24	4	8	2	2920	58	27	9	141
11	46	21	7	54	32	5	46	12	14	32	11	252	4	20	131	23	6	6	2	2997	60	21	9	114
13	42	51	5	71	25	6	66	15	13	46	4	329	10	33	126	26	6	8	3	2765	58	31	11	146
15	47	57	3	72	13	5	73	15	12	47	8	367	15	36	148	28	7	11	3	2725	54	33	10	169
17	31	40	3	69	18	6	59	6	12	32	-	256	8	29	122	27	5	8	4	2793	56	25	11	112
19	26	55	6	68	5	3	59	12	13	40	10	223	6	30	91	28	6	9	3	2768	56	28	10	78
21	29	49	7	63	6	4	56	12	12	34	19	201	8	28	94	26	7	7	3	2872	55	25	11	68
23	22	50	3	67	27	5	65	11	12	40	6	232	11	34	92	27	5	6	3	2740	55	33	10	93
25	26	35	3	58	14	4	51	9	12	37	12	200	3	25	88	24	5	7	4	2871	53	22	14	71
27	27	32	4	55	28	4	53	9	16	27	6	203	11	26	78	23	5	9	2	2829	54	25	9	67
29	20	41	5	60	13	3	63	9	8	27	5	178	12	28	64	25	5	7	4	2784	56	24	9	51
31	17	36	6	60	24	6	61	9	12	29	14	179	9	29	62	27	4	7	1	2754	57	27	11	55
33	25	38	7	60	20	4	58	7	7	27	11	176	10	31	64	25	3	9	4	2774	57	29	10	52
35	23	57	3	66	5	6	61	11	6	32	1	189	5	33	72	27	5	10	3	2751	53	38	10	70
37	19	40	6	68	9	6	61	11	13	32	15	176	7	33	70	29	5	8	3	2820	58	36	9	63
39	19	45	4	62	30	6	58	11	7	36	-	190	13	30	76	25	7	7	3	2867	55	30	9	75
41	19	48	4	45	9	4	69	16	10	34	14	192	8	35	68	28	4	11	3	2747	54	36	10	64
43	22	52	2	38	18	5	81	14	10	43	17	212	7	41	69	31	4	10	2	2640	55	36	10	72
45	22	52	5	41	8	5	81	14	8	41	17	224	8	38	72	29	4	11	2	2713	52	35	10	78
47	23	61	7	43	18	3	72	15	9	39	5	212	13	37	69	28	6	14	2	2736	54	35	10	77
49	21	41	6	46	29	2	65	13	6	29	8	193	13	35	52	27	5	9	5	2806	58	37	9	56
51	19	49	7	47	14	6	60	9	10	26	15	174	5	34	42	25	5	11	5	2747	54	46	10	42

Publications

Peer review international journals:

1. **Dispersion pattern of ^{226}Ra and ^{235}U using the ERICA Tool in the coastal mining area, Ierissos Gulf, Greece**, F.K. Pappa, C. Tsabaris, D.L. Patiris, E.G. Androulakaki, A. Ioannidou, G. Eleftheriou, M. Kokkoris, R. Vlastou, Applied Radiation and Isotopes (submitted).

2. **Historical trends and assessment of radionuclides and heavy metals in sediments near an abandoned mine, Lavrio, Greece,** F.K. Pappa, C. Tsabaris, D.L. Patiris, E.G. Androulakaki, G. Eleftheriou, C. Betsou, V. Michalopoulou, M. Kokkoris, R. Vlastou, Environmental Science and Pollution Research, 25, 30084-30100 (2018).

3. **A methodology for expanding the use of NaI(Tl) based spectrometry environmental radioactivity measurements**, M. Pilakouta, F.K. Pappa, D.L. Patiris, C.A. Kalfas, *Applied Radiation and Isotopes* 139, 159-168 (2018)

4. **Metal concentrations and radioactivity in sediments at the northern coastal zone of Ikaria Island, eastern Mediterranean, Greece**, F. Fouskas, A. Godelitsas, A. Argyraki, F.K. Pappa, C. Tsabaris, *Journal of Radioanalytical and Nuclear Chemistry*, 317, 55-68 (2018).

5. **Radiometric dating of sediment cores from aquatic environments of north-east Mediterranean**, G. Eleftheriou, C. Tsabaris, D.K. Papageorgiou, D.L. Patiris, E.G. Androulakaki, F.K. Pappa, *Journal of Radioanalytical and Nuclear Chemistry*, 1-17 (2018)

6. **Radioactivity and metal concentrations in marine sediments associated with mining activities in Ierissos Gulf, North Aegean Sea, Greece**, F.K. Pappa, C. Tsabaris, A. Ioannidou, D.L. Patiris, H. Kaberi, I. Pashalidis, G. Eleftheriou, E.G. Androulakaki, R. Vlastou, *Applied Radiation and Isotopes* 116, 22-33 (2016).

7. **Activity concentration and spatial distribution of radionuclides in marine sediments close to the estuary of Shatt al-Arab/Arvand Rud River, the Gulf**, D.L. Patiris, C. Tsabaris, C.L. Anagnostou, E.G. Androulakaki, F.K. Pappa, G. Eleftheriou, G. Sgouros, *Journal of Environmental Radioactivity* 157, 1-15 (2016).

8. **Efficiency calibration for in situ γ-ray measurements on the seabed using Monte Carlo simulations: Application in two different marine environments**, E.G. Androulakaki, C. Tsabaris, G. Eleftheriou, M. Kokkoris, D.L. Patiris, F.K. Pappa, R. Vlastou, *Journal of Environmental Radioactivity* 164, 47-59 (2016).

9. **In situ γ-ray spectrometry in the marine environment using full spectrum analysis for natural radionuclides**, E.G. Androulakaki, M. Kokkoris, C. Tsabaris, G. Eleftheriou, D.L. Patiris, F.K. Pappa, R. Vlastou, *Applied Radiation and Isotopes* 114, 76-86 (2016).

10. **Vertical distribution of ^{137}Cs activity concentration in marine sediments at the Amvrakikos Gulf, Western of Greece**, C.Tsabaris, D.L. Patiris, E. Fillis-Tsirakis, V. Kapsimalis, M. Pilakouta, F.K. Pappa, R. Vlastou, *Journal of Environmental Radioactivity* 14, 1-8 (2015).

Contribution to conference proccedings

1. **Application of radio-dating methods in marine areas of Greece**, F.K. Pappa, C. Tsabaris, D.L. Patiris, E.G. Androulakaki, G. Eleftheriou, M. Kokkoris, R. Vlastou, Proceedings of 27th Symposium of the Hellenic Nuclear Physics Society, 8-9 June 2018, Athens, Greece (in press).

2. **Simplified natural radioactivity dispersion model application in a coastal area**, F.K. Pappa, C. Tsabaris, D.L. Patiris, E.G. Androulakaki, G. Eleftheriou, R. Vlastou, M. Kokkoris, 12th Panhellenic Symposium on Oceanography and Fisheries, Corfu island, Greece, 31 May-3 June 2018.

3. **Efficiency calibration of a medium resolution subsea detection system for sediment extended samples**, F. Maragos, C. Tsabaris, E.G. Androulakaki, M. Kokkoris, F.K. Pappa, D.L. Patiris, R. Vlastou, Proceedings of 26th Symposium of the Hellenic Nuclear Physics Society, 9-10 June 2017, Athens, Greece (in press).

4. **Radioactivity measurements in granite samples using NaI(Tl) spectrometry**, M. Pilakouta, F.K. Pappa, D.L. Patiris, C. Tsabaris, Proceedings of 26th Symposium of the Hellenic Nuclear Physics Society, 9-10 June 2017, Athens, Greece (in press).

5. **Chronological records of metal contamination in an abandoned mine (Lavrio, Greece), using sediment profiles**, F.K. Pappa, C. Tsabaris, D.L. Patiris, E.G. Androulakaki, G. Elefteriou, A. Ioannidou, M., Kokkoris, R. Vlastou, Proceedings of 26th Symposium of the Hellenic Nuclear Physics Society, 9-10 June 2017, Athens, Greece (in press).

6. **The use of natural and anthropogenic radionuclides in calculating the recent sedimentation rates in the marine environment**, H. Kaberi, S. Iliakis, F.K. Pappa, C. Tsabaris, Proceedings of 26th Symposium of the Hellenic Nuclear Physics Society, 9-10 June 2017, Athens, Greece (in press).

7. **Chronological records of metal contamination at two mining areas using sediment profiles,** F.K. Pappa, C. Tsabaris, D.L. Patiris, E.G. Androulakaki, A. Ioannidou, M. Kokkoris, R. Vlastou, International Conference Environmental Radioactivity, 29 May-2 June 2017, Vilnius, Lithuania.

8. **Comparison of MCNP and ERICA codes in two different marine areas**, F.K. Pappa, C.Tsabaris, D.L. Patiris, G. Eleftheriou, E.G. Androulakaki, M. Kokkoris, R. Vlastou, Proceedings of 25th Symposium of the Hellenic Nuclear Physics Society, 3-4 June 2016, Athens, Greece.

9. **NORM measurements at the beach sand and coastal sediments near a mining area, Ierissos Gulf, Greece**, F.K. Pappa, C.Tsabaris, D.L. Patiris, H. Kaberi, E.G.. Androulakaki, G. Eleftheriou, M. Kokkoris, R. Vlastou, A. Ioannidou, International Conference Environmental Radioactivity, 21-25 September 2015, Thessaloniki, Greece.

10. **Temporal variation of ^{137}Cs profiles in Lemnos deep basin, North Aegean Sea, Greece**, F.K. Pappa, G.A. Kyriakidis, C. Tsabaris, D.L. Patiris, E.G. Androulakaki, H. Kaberi, V. Zervakis, M. Kokkoris, R. Vlastou, E. Krasakopoulou, Proceedings of 24th Symposium of the Hellenic Nuclear Physics Society, University of Ioannina 2015 (in press).

11. **Measurement of Radionuclides and Toxic Metals Concentrations in Sediments due to Mining Activities, Ierissos Gulf**, Chalkidiki, F.K. Pappa, C. Tsabaris, H. Kaberi, C. Zeri, I. Pashalidis, A. Ioannidou, D.L. Patiris, E.G. Androulakaki, G. Eleftheriou, M. Kokkoris, R. Vlastou, 11th Panhellenic Symposium on Oceanography and Fisheries, Mytilene, Lesvos island, Greece, May 2015

12. **Radiotoxic metals concentration measurement in sediments due to gold mining activities**, Chalkidiki, F.K. Pappa, C. Tsabaris, H. Kaberi, C. Zeri, I. Pashalidis, A. Ioannidou, E.G. Androulakaki, G. Eleftheriou, D.L. Patiris, M. Kokkoris, R. Vlastou, Proceedings of 23rd Symposium of the Hellenic Nuclear Physics Society, Aristotle University of Thessaloniki, Thessaloniki 2014.

13. **Sediment pollution by radionuclides and toxic metals in the Ierissos Gulf, North Aegean Sea, Greece**, F.K. Pappa, C. Tsabaris, H. Kaberi, C.Zeri, E. Androulakaki, I. Pashalidis, A. Ioannidou, M. Kokkoris, G. Eleftheriou, D.L. Patiris, R. Vlastou, Proceedings of 22nd Symposium of the Hellenic Nuclear Physics Society, University of Athens, Athens 2013.

14. **Localization of a submarine groundwater source of eastern coast of Back Sea-Georgia, using radiotracing techniques**, D.L. Patiris, M. Schübert, G. Eleftheriou, E.G. Androulakaki, F.K. Pappa, G., Melikadze and C. Tsabaris, Proceedings of 22nd Symposium of the Hellenic Nuclear Physics Society, University of Athens, Athens 2013.

15. **Radionuclides and heavy metals concentrations at the seabed of NW Piraeus, Greece,** G. Eleftheriou, C. Tsabaris, V. Kapsimalis, D.L. Patiris, E.G. Androulakaki, F.K. Pappa, M. Kokkoris, R. Vlastou, Proceedings of 22nd Symposium of the Hellenic Nuclear Physics Society, University of Athens, Athens 2013.

16. **Progress in radionuclide characterisation in the marine sediment using an underwater gamma-ray spectrometer in 2π geometry**, E.G. Androulakaki, C. Tsabaris, M. Kokkoris, G. Elaftheriou, D.L. Patiris, D. Papageorgiou, F.K. Pappa, R. Vlastou, Proceedings of 22nd Symposium of the Hellenic Nuclear Physics Society, University of Athens, Athens 2013.

17. **A theoretical study for the development of a deep sub-sea radioactivity system**, C. Tsabaris, E.G. Androulakaki, M. Kokkoris, G. Eleftheriou, D.L. Patiris, F.K. Pappa, S. Alexakis, R. Vlastou, Proceedings of 22nd Symposium of the Hellenic Nuclear Physics Society, University of Athens, Athens 2013.

18. **Sediment measurements of samples from Tigris and Euphrates estuary by means of gamma-ray spectroscopy**, D.L. Patiris, C. Tsabaris, E. Androulakaki, G. Eleftheriou, D. Papageorgiou, F. Pappa, G. Sgouros, C. Anagnostou, Proceedings of 21st Symposium of the Hellenic Nuclear Physics Society, National Centre for Scientific Research "Demokritos", Athens 2012.

19. **Experimental set up for the determination of Natural radionuclides in formation waters produced in oil and gas exploration fields,** C. Tsabaris, D.L. Patiris, G. Eleftheriou, E. Androulakaki, A. Prospathopoulos, M. Kokkoris, F.K. Pappa, S. Alexakis, R. Vlastou, C.A. Kalfas, Proceedings of 21st Symposium of the Hellenic Nuclear Physics Society, National Centre for Scientific Research "Demokritos", Athens 2012.

20. **Dispersion of ^{137}Cs concentration in the basins of the Aegean Sea**, F.K. Pappa, D.L. Patiris, G. Eleftheriou, C. Tsabaris, M. Kokkoris, R. Vlastou, H., Kaberi, Proceedings of 20th Symposium of the Hellenic Nuclear Physics Society, National Technical University of Athens, Athens 2011

Conference presentations (orals and posters)

Poster presentations:

1. Poster presentation at 20th Symposium of the Hellenic Nuclear Physics Society, 2011: **Dispersion of ^{137}Cs concentration in the basins of the Aegean Sea,** F.K. Pappa, D.L. Patiris, G. Eleftheriou, C. Tsabaris, M. Kokkoris, R. Vlastou, H., Kaberi, Athens, May 26-27, 2011
2. Poster presentation at 22nd Symposium of the Hellenic Nuclear Physics Society, 2013: **Sediment pollution by radionuclides and toxic metals in the Ierissos Gulf, North Aegean Sea, Greece**, F.K. Pappa, C. Tsabaris, H. Kaberi, C.Zeri, E. Androulakaki, I. Pashalidis, A. Ioannidou, M. Kokkoris, G. Eleftheriou, D.L. Patiris, R. Vlastou, Athens, May 30-31, 2013.

Oral presentations:

1. Oral presentation at 27th Symposium of the Hellenic Nuclear Physics Society: **Application of radio-dating methods in marine areas of Greece**, F.K. Pappa, C. Tsabaris, D.L. Patiris, E.G. Androulakaki, G. Eleftheriou, M. Kokkoris, R. Vlastou, Athens 8-9 June 2018

2. Oral presentation at 12th Panhellenic Symposium on Oceanography and Fisheries: **Simplified natural radioactivity dispersion model application in a coastal area**, F.K. Pappa, C. Tsabaris, D.L. Patiris, E.G. Androulakaki, G. Eleftheriou, R. Vlastou, M. Kokkoris, Corfu, 31 May-3 June 2018.

3. Oral presentation at 26th Symposium of the Hellenic Nuclear Physics Society: **Chronological records of metal contamination in an abandoned mine (Lavrio, Greece), using sediment profiles**, F.K. Pappa, C. Tsabaris, D.L.

Patiris, E.G. Androulakaki, G. Elefteriou, A. Ioannidou, M., Kokkoris, R. Vlastou, Athens, 9-10 June 2017.

4. Oral presentation at 4th International Conference Environmental Radioactivity: **Chronological records of metal contamination at two mining areas using sediment profiles,** F.K. Pappa, C. Tsabaris, D.L. Patiris, E.G. Androulakaki, A. Ioannidou, M. Kokkoris, R. Vlastou, Vilnius, Lithuania, 29 May-2 June 2017.

5. Oral presentation at 25th Symposium of the Hellenic Nuclear Physics Society: **Comparison of MCNP and ERICA codes in two different marine areas**, F.K. Pappa, C.Tsabaris, D.L. Patiris, G. Eleftheriou, E.G. Androulakaki, M. Kokkoris, R. Vlastou, Athens, 3-4 June 2016.

6. Oral presentation at 3rd International Conference Environmental Radioactivity: **NORM measurements at the beach sand and coastal sediments near a mining area, Ierissos Gulf, Greece**, F.K. Pappa, C.Tsabaris, D.L. Patiris, H. Kaberi, E.G.. Androulakaki, G. Eleftheriou, M. Kokkoris, R. Vlastou, A. Ioannidou, Thessaloniki, 21-25 September 2015.

7. Oral presentation at 24th Symposium of the Hellenic Nuclear Physics Society: **Temporal variation of ^{137}Cs profiles in Lemnos deep basin, North Aegean Sea, Greece**, F.K. Pappa, G.A. Kyriakidis, C. Tsabaris, D.L. Patiris, E.G. Androulakaki, H. Kaberi, V. Zervakis, M. Kokkoris, R. Vlastou, E. Krasakopoulou, Ioannina, 22-23 May 2015.

8. Oral presentation at 11th Panhellenic Symposium on Oceanography and Fisheries: **Measurement of Radionuclides and Toxic Metals Concentrations in Sediments due to Mining Activities, Ierissos Gulf**, Chalkidiki, F.K. Pappa, C. Tsabaris, H. Kaberi, C. Zeri, I. Pashalidis, A. Ioannidou, D.L. Patiris, E.G. Androulakaki, G. Eleftheriou, M. Kokkoris, R. Vlastou, Mytilene, Lesvos island, 13-17 May 2015

9. Oral presentation at 23th Symposium of the Hellenic Nuclear Physics Society: **Radiotoxic metals concentration measurement in sediments due to gold mining activitie**s, **Chalkidiki**, F.K. Pappa, C. Tsabaris, H. Kaberi, C. Zeri, I. Pashalidis, A. Ioannidou, E.G. Androulakaki, G. Eleftheriou, D.L. Patiris, M. Kokkoris, R. Vlastou, Thessaloniki, 20-21 June 2014.